Gamma delta T cell immunotherapy against breast cancer and overcoming mechanisms of immune evasion

by

Indrani Dutta

A thesis submitted in partial fulfillment of the requirements for the degree of

Doctor of Philosophy

in

Cancer Sciences

Department of Oncology
University of Alberta

Abstract

Gamma delta T cells (γδTc) are immunosurveillance cells garnering great interest for their anti-tumoral activity. Target cell recognition is mediated by the T cell antigen receptor (TCR) and/or the natural killer receptor NKG2D, whose ligands are upregulated on cancer cells. Tumor cell lysis is mediated in part by Fas ligand (FasL) and Tumor necrosis factor-related apoptosis-inducing ligand (TRAIL), which induce apoptosis in target cells. Clinical trials have proven the safety of γδTc immunotherapy and increased circulating γδTc levels correlate with improved patient outcome. We investigated the impact of hypoxia on γδTc and target breast cancer cells. We also investigated the efficacy of γδTc against breast cancer stem-like cells (BCSC). Hypoxia and BCSC are two major factors associated with therapy resistance and cancer recurrence. Firstly, we discovered that using blocking antibodies to the γδ TCR induces γδTc apoptosis. Blocking assays require the use of antibodies against specific receptors and ligands in cytotoxicity assays. Gamma delta T cell apoptosis was further increased in the presence of IL-2, which is often included in cytotoxicity assays. However, we found that adding IL-2 does not significantly contribute to γδTc cytotoxicity against breast cancer cells. These findings informed us to not use IL-2 in our cytotoxicity assays and to test γδTc viability when using blocking antibodies in parallel with blocking cytotoxicity assays. Secondly, we investigated the impact of hypoxia on γδTc cytotoxicity. Hypoxia or low oxygen levels are characteristic of the breast cancer micro-environment and can promote therapy resistance by inducing cellular plasticity. We found that hypoxia activated γδTc and enhanced their ability to kill breast cancer cells. However, hypoxia also resulted in breast cancer cell resistance to γδTc killing by increased MICA shedding. Soluble MICA can bind to the NKG2D receptor on γδTc and competitively block its interaction with

NKG2D ligands on the target cell surface. This can reduce NKG2D-mediated target recognition by γδTc, ultimately reducing γδTc cytotoxicity.

Hypoxia is known to promote cellular plasticity and BCSC generation. Hence, finally, we investigated whether γδTc can target BCSC. BCSC are a small population of cancer cells that are highly tumorigenic and can self-renew as well as differentiate into multiple lineages. Our study demonstrated that BCSC are less sensitive to γδTc cytotoxicity than non-stem cells (NSC). We explored several mechanisms that could orchestrate this resistance. The most compelling results were the expression and shedding of NKG2D ligand MICA. The BCSC exhibited lower surface expression of MICA and higher MICA shedding than NSC. Mass spectrometry analysis, which indicated global differences in BCSC and NSC secretomes, also confirmed enhanced MICA shedding by BCSC. Accordingly, we demonstrated that blocking MICA shedding using inhibitors against proteases ADAM10 and ADAM17 lead to significantly enhanced cytotoxicity of γδTc against BCSC. Notably, we observed that treatment with ADAM inhibitors brought breast cancer stem cell lysis by γδTc to the same level as NSC killing by γδTc alone without inhibitors. This suggests a complete reversal of BCSC resistance. Moreover, γδTc killing of NSC was further enhanced using the ADAM inhibitor in combination compared to γδTc alone. Hence, we concluded that a combination of γδTc and the ADAM inhibitor GW280264X is an effective strategy to target resistant BCSC. In summary, we discovered that hypoxia and BCSC population can lead to breast cancer resistance against γδTc and determining how these target cells evade γδTc killing and devising strategies to overcome this resistance will improve γδTc immunotherapy for cancer.

Preface

The research in this thesis was conducted with assistance or in collaboration, as noted below.

Chapter 2 of this thesis has been published as **Indrani Dutta**, Lynne-Marie Postovit, Gabrielle M. Siegers. (2017). "**Apoptosis Induced via Gamma Delta T Cell Antigen Receptor "Blocking" Antibodies: A Cautionary Tale.***" Frontiers in Immunology***.** 8:776 doi10.3389/fimmu.2017.00776.

I was responsible for study and experimental design, conducting experiments and data analysis. Dr. Gabrielle Siegers is my supervisor and was involved in all stages of the project, including study and experimental design, analysis and writing the manuscript. Dr. Lynne-Marie Postovit co-supervised the study and edited the manuscript.

Chapter 3 of this thesis has been published as Gabrielle M. Siegers, **Indrani Dutta**, Raymond Lai and Lynne-Marie Postovit. (2018). "**Functional Plasticity of** γδ T **Cells and Breast Tumor Targets in Hypoxia**." ***Frontiers in Immunology***. 9:1367 doi 10.3389/fimmu.2018.01367. I assisted with experimental design, conducting the experiments and data analysis. Dr. Gabrielle Siegers was involved at all stages of the project, including study and experimental design, performing experiments, analyzing data and writing the manuscript. I did some of the western blots and all of the blocking assays; the cytotoxicity assays in figure 5 were done by Dr. Gabrielle Siegers and me together in parallel. Dr. Raymond Lai scored immunohistochemistry (IHC) slides in figure 1. Dr. Lynne-Marie Postovit supervised this study, contributing to conception, study design and manuscript editing prior to publication.

Chapter 4 of this thesis has been published as **Indrani Dutta**, Dylan Dieters-Castator, James W. Papatzimas, Anais Medina, Julia Schueler, Darren J. Derksen, Gilles Lajoie, Lynne-

Marie Postovit and Gabrielle M. Siegers. "**ADAM protease inhibition overcomes resistance of breast cancer stem-like cells to γδ T cell immunotherapy**." ***Cancer Letters***. (First author). I was responsible for study and experimental design, data analysis, and writing the manuscript. I performed all the experiments, unless stated otherwise. Dr. Gabrielle Siegers supervised the study and was involved at all stages of the project, including study and experimental design, data analysis, and writing the manuscript. We performed the *in vivo* experiments together. Dr. Lynne-Marie Postovit co-supervised the study and was involved in concept formation, study design and manuscript editing. Dr. Dylan Dieters-Castator conducted all the mass spectrometry experiments and analysis. Dr. James Papatzimas and Dr. Darren Derksen developed and provided the MCL-1 degrader dMCL1-2. Dr. Anais Medina made the original observation that our panel of breast cancer cell lines had varying percentages of BCSC and we chose the cell line models based on her results. Dr. Julia Schueler provided the PDX401 cell line. Dr. Gilles Lajoie contributed to the design of mass spectrometry experiments.

All the studies were conducted in compliance with the recommendations of the Research Ethics Guidelines, Health Research Ethics Board of Alberta—Cancer Committee with written informed consent from all participants in accordance to the Declaration of Helsinki. The in vivo experiment protocol in chapter 4 was approved by the Animal Use Subcommittee at the University of Alberta (AUP00001288).

Acknowledgements

This work would never have been possible without the help and support of many people. First, I would like to express my deepest gratitude to my supervisor Dr. Gabrielle Siegers. You have educated and motivated me throughout this journey. You have taught me how to slow down and do science the right way, how to dig deeper and be thorough. You have been steady support through this struggle. You are an amazing mentor who has persistently provided me with vision, constructive criticism and encouragement without which this dissertation would not be possible. I am also deeply indebted to Dr. Lynne Postovit, my co-supervisor. You are an inspiration to not just me but any young women in science. You have spanned the whole country in pursuit of knowledge. Your generosity and support have been incredible, and it has been an honour to be under your tutelage.

To my family, everything I am today, I am because of your love and support. Your constant words of encouragement and support from halfway across the world have fueled my deep desire to work hard and pursue my dreams. Baba, your passion for science and thirst for knowledge, even at this age, is an immense source of inspiration. You have taught me to be brave, taught me there is nothing I cannot do, once I put my mind to it. Ma, your ability to work tirelessly, love boundlessly, and your generosity of spirit are aspirational. Every day, I try to emulate that. I am proud to be your daughter. To my sister, you have always been my best friend and my confidante, a constant source of light and encouragement in my life.

There are no words to express my gratitude for my husband, Saket. Your hard work, passion and dedication to science are beyond compare. You have taught me it is never an option to give up. It has been an honour to see you rise from your struggles, unfazed and triumphant. You are a wonderful human being with the biggest heart, and each day, I strive to be a little more like you.

To all my friends in Edmonton, you have been a pillar of support through these years. You have stood by me through thick and thin making it so easy to start my new life here in a completely new country. In you, I found a home so far away from home.

Table of Contents

List of Figures

List of Tables

List of Abbreviations

ABC	ammonium bicarbonate
αβTc	αβ T cells
ADAM	a disintegrin and metalloproteinase
ADCC	antibody-dependant cellular cytotoxicity
ADP	adenosine diphosphate
AF	alexa fluor
AICD	activation-induced cell death
ALDH	aldehyde dehydrogenases
AML	acute myeloid leukemia
AnnV	annexin V
ANOVA	analysis of variance
AP-1	activating protein-1
APC	allophycocyanin
ARG	arginase
ATCC	American type culture collection
ATP	adenosine triphosphate
BAK	BCL-2-antagonist/killer
BAX	BCL-2-associated X protein
BCL-2	B-cell lymphoma 2
BCL-xL	B-cell lymphoma-extra large
BCSC	breast cancer stem cell
BRCA1	breast cancer-1
c-FLIP	cellular FLICE (FADD-like IL-1β-converting enzyme) inhibitory protein
CA	carbonic anhydrase
CAFs	cancer-associated fibroblast
CalAM	calcein AM
cAMPs	cyclic adenosine monophosphate
CAR-T	chimeric antigen receptor T cells
CCL	chemokine (C-C motif) ligand
CD	cluster of differentiation
CEACAM-1	carcinoembryonic antigen cell adhesion molecule 1
CM	conditioned media
COX2	cyclooxygenase-2
CR	complete response
CRS	cytokine release syndrome
CSC	cancer stem cell
CTL	cytotoxic T lymphocytes
CTLA-4	cytotoxic T-lymphocyte-associated protein
DAMPs	damage-associated molecular patterns
DC	dendritic cell
DDR	DNA damage response
DMSO	dimethyl sulfoxide
DNA	deoxyribonucleic acid

DNAM-1	DNAX accessory molecule-1
DR5	death receptor 5
DTT	dithiothreitol
E:T	effector:target
ECL	enhanced chemiluminescence
ECM	extra-cellular matrix
EDTA	ethylenediaminetetraacetic acid
ELISA	enzyme-linked immunosorbent assay
EMRA	effector memory RA+
EMT	epithelial–mesenchymal transition
EpCAM	epithelial cell adhesion molecule
ER	estrogen receptor
FA	formic acid
FACS	fluorescence-activated cell sorting
FADD	fas-associated protein with death domain
FBS	fetal bovine serum
FDA	food and drug administration
FITC	fluorescein isothiocyanate
FMO	fluorescence minus one
GAL	galectin
γδTc	γδ T cells
GM-CSF	granulocyte-macrophage colony-stimulating factor
GMP	good manufacturing practice
GvHD	graft-versus-host disease
HCL	hydrochloric acid
HeLa	Henrietta Lacks
HEPES	4-(2-hydroxyethyl)-1-piperazineethanesulfonic acid
HER	human epidermal growth factor receptor
HIF	hypoxia-inducible factor
HMB-PP	(E)- 4-hydroxy-3-methyl-but-2-enyl pyrophosphate
HMGB1	high-mobility group protein B1
hMSH2	human MutS homologues
HRE	hypoxia-response element
HRP	horseradish peroxidase
IDO	indoleamine-pyrrole 2,3-dioxygenase
IFN	interferon
IgG	immunoglobulins
IL	interleukin
IPP	isopentenyl pyrophosphate (IPP)
ITIM	immunoreceptor tyrosine-based inhibition motif
KEGG	Kyoto encyclopedia of genes and genomes
KLF4	Kruppel-like factor 4
LAG-3	lymphocyte-activation gene 3
LC-MS	liquid chromatography–mass spectrometry
M-PER	mammalian protein extraction reagent
mAb	monoclonal antibodies
MART	melanoma antigen recognized by T cells

MCF-7	Michigan cancer foundation-7
MCL-1	myeloid cell leukemia 1
MDR	multi-drug-resistant
MDSC	myeloid-derived suppressor cells
MEM	minimum essential medium
MFI	median fluorescence intensity
MHC	major histocompatibility complex
MICA	MHC class I polypeptide–related sequence A
MIP-1α	macrophage inflammatory protein 1-alpha
MSC	mesenchymal stem cell
MUC	mucin
N-bis	aminobisphosphonates
NEAA	non-essential amino acid
NF-κB	nuclear factor κB
NK	natural killer
NKG2	natural killer group 2
NKp30	natural killer cell p30-related protein
NKR	NK cell receptor
NOD/SCID	nonobese diabetic/severe combined immunodeficiency
NSC	non-stem cell
NSG	NOD.Cg-Prkdc^{scid} Il2rg^{tm1Wjl}/SzJ
OCT4	octamer-binding transcription factor 4
OR	objective response
pAgs	phosphoantigens
PARP	poly ADP ribose polymerase
PBMC	peripheral blood mononuclear cell
PBS	phosphate-buffered saline
PD-1	programmed cell death protein 1
PD-L1	programmed death-ligand 1
PDX	patient derived xenografts
PE	phycoerythrin
PerCP	peridinin-chlorophyll-protein
PFA	paraformaldehyde
PGE2	prostaglandin E_2
PHD	propyl hydroxylase domain enzymes
PMA	phorbol myristate acetate
PR	progesterone receptor
PS	phosphatidylserine
pVHL	Von Hippel-Lindau tumor suppressor protein
Rag	recombination-activating genes
RANTES	regulated on activation, normal T cell expressed and secreted
ROS	reactive oxygen species
RPMI	Roswell park memorial institute medium
SDS-PAGE	sodium dodecyl sulfate polyacrylamide gel electrophoresis
SOX	SRY (sex determining region Y)-box
STAT	signal transducer and activator of transcription
sTRAIL	soluble TRAIL

TAA	tumor-associated antigens
TAM	tumor-associated macrophages
TBST	tris-buffered saline (TBS) and Tween 20
TCR	T cell antigen receptor
TEGs	T cells engineered with defined gamma delta TCRs
TGF	transforming growth factor beta
Th1	Type 1 T helper
TIGIT	T cell immunoreceptor with Ig and ITIM domains
TIL	tumor-infiltrating lymphocytes
TIM-3	T-cell immunoglobulin and mucin-domain containing-3
TLRs	toll-like receptors
TME	tumor microenvironment
TNBC	triple-negative breast cancer
TNF	tumor necrosis factor
TRAIL	TNF-related apoptosis-inducing ligand
Tregs	regulatory T cells
TSST-1	toxic shock syndrome toxin 1
ULBP	UL16-binding proteins
UPLC	ultra-performance liquid chromatography
VEGF	vascular endothelial growth factor
Vδ	variable delta
Vγ	variable gamma
ZA	zombie aqua
ZNIR	zombie near-infrared

Chapter 1- Introduction

1.1 Breast cancer

Breast cancer is the most common malignancy in women and the second leading cause of their cancer-related death worldwide[1]. Over the past decade, significant advancements in the diagnosis and treatment of breast cancer have resulted in a considerably improved mortality rate. However, metastatic disease treatment is currently ineffective, leaving most advanced breast cancers incurable with presently available therapies[2].

The principal treatment for breast cancer is surgical resection and often systemic chemotherapy. Systemic therapy can be given before surgery (neoadjuvant) in women with large tumors to reduce the tumor burden, or it can be given be given after surgery. Additionally, post-operative radiation therapy is common and improves disease-free and overall survival for a patient with early breast cancer[2]. For targeted treatment, breast cancer has been clinically classified into five molecular subtypes, each with a unique expression pattern: (i) normal-like, (ii) luminal A and B (expressing oestrogen receptor (ER)), (iii) basal-like and human epidermal growth factor receptor 2 (HER2)- enriched (no ER expression), (iv) triple-negative breast cancer (TNBCs) lacking expression of ER, progesterone receptor (PR), and (v) TNBC claudin-low[3]. Typically, luminal A is the most common and has the best prognosis[4]. Luminal B tumors have a higher proliferation index and are more aggressive. All luminal tumors are given endocrine therapy, such as tamoxifen or aromatase inhibitors. Normal-like tumors have a low proliferation index, but poorer outcomes compared to luminal A. Although HER2+ breast cancers present with an advanced tumor grade and have lymph node seeding, the prognosis has drastically improved since the discovery of Trastuzumab (Herceptin), an anti-HER2 antibody[4]. Neoadjuvant chemotherapy, such as anthracycline-taxane or carboplatin, together with anti-HER2 therapy, has become the standard of care for HER-2 positive breast cancers. The most aggressive breast cancers are TNBCs that

constitute about 20% of all breast cancer diagnoses and have a poor prognosis and lack targeted therapies. For TNBCs, the standard of care is anthracycline and taxane or docetaxel and cyclophosphamide administered in combination[2]. Recently, poly (ADP-ribose) polymerase (PARP) inhibitors against BRCA1-mutant TNBC tumors have also shown some promise[5]. Unfortunately, approximately 40% of TNBC patients still experience resistance and relapse[6].

1.1.1 Tumor heterogeneity and plasticity

Breast tumors are characterized by the co-existence of subpopulations of cells that differ in their stromal composition, genomic landscape and behavioral traits, which creates a major challenge for therapies as they must effectively target several phenotypes. Several genetic, epigenetic and environmental factors can give rise to further tumor variability[7]. At the same time, cancer stem cells (CSC) display a high degree of plasticity, which results in the generation of cells with a wide range of phenotypic, functional, and metabolic features[8,9]. Hence, CSC represent a significant source of tumor heterogeneity.

In general, CSC are defined as a small population of cells that can self-renew, as well as differentiate into multiple lineages[10]. Dick *et al*., was the first to demonstrate that only a few rare cells of mouse AML(CD34+CD38-) could initiate leukemia in other mice[11]. Two models that explain the genesis of CSC and intra-tumor heterogeneity are the "clonal evolution" and the "cancer stem cell model." Both models propose that tumors originate from single cells that acquire unrestricted proliferative potential, ultimately leading to the ability to metastasize, through multiple molecular modifications. The clonal evolution or stochastic model, however, hypothesizes that this phenomenon is driven by a clone that acquires the highest degree of "fitness" through the accumulation of random genetic and epigenetic alterations[12]. According to this model, the therapy-resistant tumor clones emerge as a consequence of stochastic modifications that confer a selective

growth advantage to specific clones in response to environmental pressures, such as therapy. Therefore the stochastic model suggests that cancer can only be eradicated once every population of tumor cells is eliminated, considering they all display an equal degree of "fitness"[13]. By contrast, the cancer stem cell or hierarchical model postulates that CSC are at the apex of the tumor cell hierarchy, endowed with unlimited self-renewal ability and tumorigenic potential[14]. This theory implies that the cancer will cured once the CSC are eradicated.

Both models are not mutually exclusive. Advancements in deep and single-cell sequencing have revealed both stochastic accumulation of mutations and hierarchy playing significant roles in the establishment of CSC[15,16]. While it is established that CSC can recapitulate the entire phenotypic heterogeneity of the tumor[17-19], several studies have shown that differentiated non-stem cells (NSC) can also de-differentiate under certain conditions. This led to a fluid CSC model proposal where the hierarchy of cells is more plastic and transient than previously suggested[20,21]. These data established the concept of dynamic entities, which are being continually shaped by micro-environmental features such as hypoxia[22] or soluble factors like IL-6[23] and transforming growth factor- β (TGF-β)[21]. Intrinsic factors such as chromatin configuration[21], and epigenetic reprogramming[24] also play a crucial role. Hence, integrating these different models may provide a more comprehensive understanding of tumorigenesis and tumor heterogeneity.

1.1.2 Breast cancer stem cells (BCSC)

Breast cancer stem-like cells (BCSC) were the first CSC identified in a solid tumor. In 2003, Al-Hajj and colleagues found that cells with the surface marker profile $CD44^+CD24^-$ from breast cancer patients formed tumors in immunodeficient NOD/SCID mice with as few as 100 cells, whereas tens of thousands of $CD44^+CD24^+$ cells failed to form tumors. Also, the tumors formed by the $CD44^+CD24^-$ cells could be passaged serially (self-renew), and could also reproduce

the tumor heterogeneity found in the original tumor (differentiation)[18]. This is the gold standard test for CSC. However, due to the cost and time-consuming nature of these experiments, surrogate experiments such as sphere formation assays, cell surface markers, or gene expression are often employed[25].

CD24 and CD44 adhesion molecules facilitated the identification of BCSC that possess a greater tumor initiation capability. CD44 is a transmembrane glycoprotein involved in cell-cell adhesion, interaction, and migration[26]. CD24 is also a cell surface glycoprotein. $CD24^{high}$ expression in the normal human mammary gland and breast tumor correlates with a differentiated gene expression signature, and $CD44^{high}$ cells exhibit a more "stem-like" gene expression signature[27]. Aldehyde dehydrogenase (ALDH) activity is another widely-used marker for the identification and isolation of normal and malignant human breast cells[19]. ALDH is an enzyme involved with cell detoxification machinery enabling enhanced DNA damage checkpoint response and DNA repair capacity, allowing cancer cells to evade genotoxic treatments[19]. Other markers that are less widely used include side population, CD133 and CD61[28].

Several embryonic signaling pathways such as Wnt, Hedgehog, and Notch, are dysregulated in BCSC and promote plasticity and self-renewal. Treatment strategies targeting these pathways to eradicate CSC are being explored[29]. Additionally, transcription factors such as SOX2, OCT4, NANOG, KLF4, Nestin, and c-MYC are also crucial for CSC and their ability to self-renew, and are potential targets for cancer therapies[30].

1.1.3 Tumorigenic behavior of BCSC

Studies have also shown that CSC are correlated with poor clinical outcomes in various cancers[31]. In the case of BCSC, their frequency was associated with the aggressiveness of the primary breast cancer[9]. Accumulating evidence suggests that BCSC cause the failure of traditional

therapies[31-34]. This could result from CSC being highly resistant to conventional chemotherapy, radiotherapy and, to some extent immunotherapy, which leads to relapse and recurrence in patients[35]. The expression of multidrug resistance (MDR) transporters increases drug efflux and makes the cells resistant to chemotherapy[36]. In particular, the ABC transporter, ABCB1, is over-expressed in BCSC, leading to resistance against doxorubicin and paclitaxel[37]. Studies have shown that there is activation of DNA damage responses (DDR) and superior DNA repair capacity in CSC, which protects them from several cytotoxic drugs. CSC also seem to upregulate free radical scavengers, which may protect them from DNA damage caused by reactive oxygen species (ROS) and explain their resistance to radiation treatment[38,39]. Moreover, CSC can remain quiescent, which shelters them from radiation and other anticancer agents targeting highly proliferative cells[40]. CSC have been found to over-express anti-apoptotic proteins such as B-cell lymphoma 2 (BCL-2), Myeloid cell leukemia-1 (MCL-1), Survivin, and FADD-like IL-1β-converting enzyme-inhibitory protein (c-FLIP), which can make them more refractory to chemo- and radio- therapeutics[41].

It is also well established that these highly resilient cells play a key role during cancer metastasis[42-45]. $CD44^{+}CD24^{-}$ BCSC overexpress epithelial-mesenchymal transition (EMT) markers and enhance the incidence of metastasis when administered through mice tail veins[46]. A higher percentage of $CD44^{+}CD24^{-}$ cells in the primary tumors correlated with the presence of distant metastases[47]. A majority of tumor cells in early metastases of the bone marrow as well as pleural metastases expressed the $CD44^{+}CD24^{-}$ signature[34,48]. Some studies have revealed that there is a subpopulation of circulating tumor cells from metastatic breast cancer patients that express stem cell markers[49,50]. Additionally, evidence suggests that CSC are involved in angiogenesis or *de novo* vessel formation, which helps supply nutrients to the tumor site[51]. Hence it is imperative to develop therapeutic strategies to target these cells. Recently, immunotherapy has become an established pillar of cancer therapy, improving the prognosis of a broad variety of cancers[52]. For

our study, we are trying to target BCSC by employing gamma delta T cells (γδTc) of the immune system. To understand how cancer immunotherapy functions, it is important to first determine the relationship and crosstalk between the tumor and the immune cells.

1.2 Cancer immunosurveillance

In the early 1900s, Paul Enrlich was the first to propose that the immune system could eliminate cancer[53]. However, due to the limited knowledge of the immune system at the time, it was impossible to validate his prediction. Ehrlich's proposal was revisited after the maturation and development of the field of immunology. Interest in tumor immunology was rekindled in the mid-1900s, largely due to improved understanding of the immune system and the discovery of tumor antigens[54]. Moreover, the idea that tumors were immunologically distinct from normal cells could be critically tested with the accessibility of inbred mice strains[55]. In 2001 it was discovered that the immune system could control the tumor quantity and tumor quality (immunogenicity)[56-58]. The study showed that tumors in mice that are immune deficient were more immunogenic (classified as "unedited") than tumors from immunocompetent mice (termed "edited"). This illustrated that the immune system not only protects the host against tumor formation, but also shapes tumor immunogenicity. Cancer immunoediting, in its most evolved incarnation, is a dynamic process that proceeds through three distinct phases: elimination, equilibrium, and escape[58,59] (Fig. 1.1).

Elimination: This is the phase where the innate and adaptive immune system detect pre-malignant signals and eliminates them before they become clinically apparent. During tumor development, dying cells, stressed cells, and damaged tissues release cytokines, damage-associated molecular pattern molecules (DAMPs) or stress ligands, also known as natural killer group 2D (NKG2D) ligands[60,61]. These signals activate the innate immune system that presents antigens to the adaptive lymphocytes and releases immunomodulatory cytokines, enabling the development of a tumor-

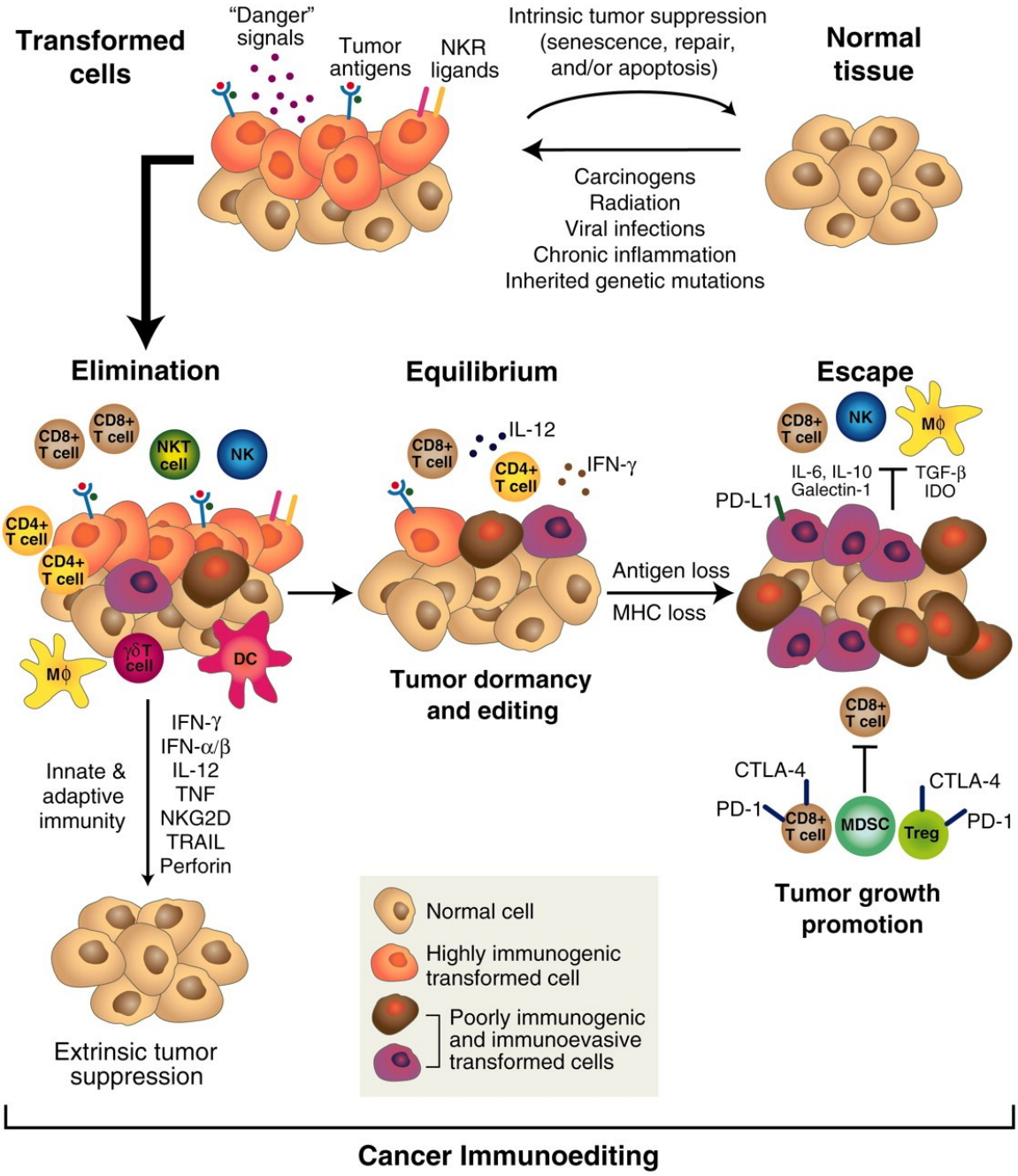

Figure 1.1 Theory of cancer immunoediting
Cancer immunoediting consists of three phases, elimination, equilibrium and escape. In the elimination phase, innate and adaptive immune system work in concert to prevent cancer growth. If tumor cells escape the elimination phase, they may enter the equilibrium phase where tumor outgrowth is contained by immunologic mechanisms. Tumor cells are maintained in a state of functional dormancy and are continually being immunoedited. As a consequence of constant immune selection pressure on tumor cells, tumor variants escape the equilibrium phase and enter the escape phase where they are resistant to the anti-tumor immune response. These tumor cells further induce an immune suppressive state within the tumor microenvironment. Adapted with permission from American Association for the Advancement of Science. (Schreiber *et al*., 2011)

specific adaptive immune response[60]. This phase has not been directly observed *in vivo*, but greater penetrance and earlier onset of neoplasia in immunodeficient mice indicated the presence of immune system-mediated elimination[60]. Lymphocyte-deficient mice (*Rag1*$^{-/-}$ and *Rag2*$^{-/-}$), severe combined immunodeficient (SCID), and nude (αβ or γδTc deficient) mice displayed increased susceptibility to the induction of a tumor[60,62,63].

Equilibrium: Certain tumor clones can overcome the elimination phase and enter what is known as the equilibrium phase, during which the immune cells and the tumor cells enter a dynamic balance. The immune cells restrict outgrowth of the tumor cells, but they do not completely eradicate them, whereas tumor cells are maintained in a state of functional dormancy[64]. This phase represents a constantly evolving interplay between the tumor cells and the immune compartment, where the tumor immunogenicity is being edited continuously. Evidence for this phase can be found in experiments done in immunocompetent mice that were treated with low-dose carcinogens[65]. These mice did not develop an observable tumor for extended periods[65]. However, when the immune system was eliminated in these mice, by depleting T cells and IFNγ, many of the mice then developed a tumor at the original injection site[66]. The equilibrium phase provides selective pressure that leads to the outgrowth of tumor cells that have acquired the most immune-evasive modifications[65].

Escape: In this phase, the cancer cells are constantly undergoing stochastic genetic and epigenetic modifications to acquire the critical changes necessary to circumvent the immune system and to establish a full-blown malignancy[59]. Concurrently, the host immune system itself is suppressed by the tumor micro-environment. This dynamic interplay between the changing cancer cells and the immunological pressure leads to the Darwinian selection of the most competent tumor cells, leading to tumorigenesis[59,67]. The various mechanisms of immune evasion are discussed in greater

detail later.

1.2.1 Breast cancer immune contexture

There is strong evidence suggesting that the breast tumor micro-environment (TME) and infiltrating immune cells are involved in the initiation and progression of tumors and metastasis[68,69]. Typically, immune cells such as tumor-associated macrophages (TAMs), myeloid-derived suppressive cells (MDSCs) and regulatory T cells (Tregs) promote tumor growth whereas. Resident features of the breast TME include tumor-infiltrating lymphocytes (TILs), TAMs, cancer-associated fibroblasts (CAFs), endothelial cells, pericytes, cytokine milieu and the extracellular matrix (ECM). The cancer cells not only escape elimination by the host immune system but also effectively modify the function of the infiltrating immune cells and thus create a more favourable TME[70]. Cancer cells recruit immune, stromal, and vascular cells by secreting cytokines, chemokines, and growth factors. Subsequently, all these cells build the TME by releasing more growth-promoting signals and metabolites. They also remodel tissue structure. The TME plays a crucial role in modulating proliferation as well as metastasis[71-73].

Predominantly, breast cancers have been classified as immunologically "silent" or "cold" tumors, characterized by low mutation rates, and therefore low neo-antigen burden, and consequently fewer effector TILs[74]. However, the immunogenicity of breast cancer varies based largely on the subtype. ER+ luminal cancers have a much lower mutational load, while TNBC have the highest[75]. There is evidence that TIL infiltration increases paralleling disease progression suggesting underlying interactions of the tumor and immune cells[76]. In breast cancer patients, prior to surgery and adjuvant therapy, an overall immune dysfunction and suppression were seen with a lower percentage of CD8+ and Th1 CD4+ mediators of an anti-tumor response[77]. Some studies also discovered natural killer (NK) cell impairment in the breast TME that played a role in the

initial stages of tumorigenesis[78,79]. Under normal conditions, NK cells are members of innate immunity that play an essential role in eliminating cancer or virally infected cells[80]. In a study with breast cancer patients, expression of activating receptors, such as NKG2D and NKp30, was reduced while the expression of the inhibitory receptor NKG2A was enhanced, reducing NK cell cytotoxicity[81]. Dendritic cells (DC) predominantly responsible for antigen presentation and T cell activation were also found to be impaired and skewed towards promoting tumor growth[82]. Moreover, immune-suppressive cells such as Tregs and MDSCs were found in abundance in the breast cancer TME, impeding an effective immune response. The depletion of Tregs was able to elicit an effective anti-tumor immune response even without additional immunotherapy[83]. MDSCs promote immune suppression by producing the enzymes indoleamine 2,3-dioxygenase (IDO) and arginase 1 (ARG1), which catabolize nutrients essential for T cell activation and function, leading to T cell inhibition and apoptosis [84,85].

Moreover, tumor cells often downregulate the major histocompatibility complex (MHC) and antigen expression[86]. They also tend to upregulate inhibitory signals such as programmed death-ligand-1 (PD-L1) to escape immune attack[87]. TNBC patients and basal cell lines have shown upregulation of PD-L1 compared to luminal breast cancers[88,89]. CD8+ T cells in breast cancer tumors also exhibited higher expression of inhibitory receptors such as T cell immunoglobulin- and mucin-domain-containing molecule (TIM-3) and lymphocyte activation gene 3 (LAG-3)[90,91]. In fact, a major proportion of the TILs showed co-expression of PD-1 or PD-L1 with LAG-3[90,91]. Another study revealed that tumor cells and stromal cells in the TME secreted many suppressive cytokines such as vascular endothelial growth factor (VEGF), IL-10 and TGF- β[92,93].

The immune contexture also has shown a powerful prognostic value. TNBC and HER2+ breast cancer patients showed a significant correlation between TILs at time of diagnosis and their overall survival[94,95]. CD8+ T cells and activated memory T cells were associated with a reduction

in the risk of relapse in ER- cancers, while the presence of Tregs was mostly associated with poor prognosis[96]. Mature DCs in the tumor site were found to be associated with fewer metastases and a better clinical outcome[97]. Additionally, TAMs were found to be associated with an unfavourable prognosis in basal cancer subtypes[98]. Immune infiltrates in the tumor before treatment can enhance response to certain chemotherapeutic drugs because of their ability to elicit an anti-tumor immune response against the dying cells. High TIL infiltration in TNBC was positively correlated with complete response to chemotherapeutic agents[99,100]. Also, patients that responded poorly to chemotherapy also showed a significant reduction in NK cell cytotoxicity[101]. Therapeutic strategies to modulate and harness the power of the anti-tumor immune system are now being investigated for treating breast cancer.

Immunotherapy has been effective in targeting cancers like melanoma and lung cancer, which have a very high mutational load that makes it easier for the immune system to recognize them[102,103]. As mentioned earlier, mutations are much lower in breast cancers[74]. TNBC have the highest rate of mutation and immune cell infiltration between all the subtypes, and hence, most current work relating to immunotherapy have focused on TNBC[75]. Most relevant strategies include checkpoint inhibitors, Chimeric antigen receptor (CAR) T cell therapy and cancer vaccines. Checkpoint blockade is discussed in more detail later. CAR T cells have also been successful in breast cancer[104,105]. CAR T cells involve genetically modifying the patient's own T cells to express a chimeric antigen receptor that can target specific proteins[104,105]. Various early phase I studies are assessing the safety and tolerability of CAR T cells against different tumor antigens in breast cancer patients[106]. Another way to harness the tumor killing power of the immune system is through cancer vaccines. Vaccines can sensitize a patient's immune system to specific tumor-associated antigens (TAA), thus allowing specific targeting and elimination of tumor. Additionally, vaccines can enable the release of additional cytokines and antigens that boost and focus the immune response

for a more sustained protective response[107]. There is an ongoing phase III clinical trial with a HER2[107,108] (NCT01479244) peptide vaccine and a phase I clinical trial with Mucin 1 (MUC1) (NCT00986609)[109] vaccines against TNBC. MUC1 is a transmembrane glycoprotein that is abnormally expressed in breast cancers[110]. Adoptive transfer of γδTc have also shown promising results against breast cancer[111].

1.3 Gamma Delta T cells (γδTc)

T cells are a crucial part of the TME, and their therapeutic manipulations, be it with adoptive cell transfer or with checkpoint blocking, have been some of the most relevant breakthroughs made in the field of cancer immunotherapy. While most of the studies and clinical applications have focused on conventional αβTc, a second type of T cells, γδTc, also play an important role in cancer immunity[112].

αβTc have TCR composed of two glycoprotein chains, the α and β TCR chains. A third chain (γ chain) was accidentally discovered and cloned in 1984, which finally led to the discovery of this small subset of T cells in 1987[113,114]. In contrast to αβTc, γδTc TCR express one γ chain and one δ chain on their surface and comprise only 2-5% of circulating lymphocytes, but predominate in several anatomic sites such as the skin, intestine, and lungs[115-117].

In general, activation of γδTc does not require antigens to be processed and presented by antigen-presenting cells (APCs). This boosts interest in their use as a therapy due to their ease of activation and lack of alloreactivity[115,118]. However, there are exceptions, for instance, γδTc can recognize the melanoma-associated antigens, MART-1 and gp-100 in an MHC-restricted manner[119]. γδTc can rapidly recognize exogenous pathogens and endogenous ligands induced by stress, infection, or transformation and initiate an adaptive immune response contributing to the

first line of defense[120]. γδTc target recognition is discussed in more detail in the following sections. Following γδTc target recognition, activated γδTc express markers reminiscent of CD8+ cytotoxic T lymphocytes (CTL) and NK cells, allowing them to target and kill cells *via* a range of mechanisms. These mechanisms include the release of perforins and granzymes as well as expression of ligands such as Fas ligand (FasL) and TNF-related apoptosis-inducing ligand (TRAIL). Perforins disrupt the target cell membrane, while granzymes induce apoptosis. γδTc can also release TRAIL and FasL, which bind to TRAIL receptors and Fas, respectively on the target cell surface and induce target cells apoptosis[121] (Fig. 1.2). Similar to NK cells, γδTc can upregulate CD16 (FcγRIIIa) that can induce antibody-dependant cellular cytotoxicity (ADCC) on targets that have antibodies bound to them[122]. Upon activation γδTc secrete high levels of pro-inflammatory cytokines such as IFNγ or Tumor Necrosis Factor-α (TNFα) that help stimulate and regulate the function of other immune cells like DC or cytotoxic effector CD8+ T cells[123-127]. γδTc also exhibit antigen-presenting functions and regulatory abilities[128-131]. Additionally, chemokines secreted by γδTc are involved in recruiting other immune cells such as macrophages, NK cells, B cells and T cells[115]. Studies have also highlighted the interaction between γδTc and both DC and B cells[115]. These properties enable them to participate in, and respond to various diseases, including infection, allergy, autoimmunity, and cancer[132-134].

1.3.1 γδTc subsets

The are two major subsets of γδTc in humans are differentiated based on the δ chain on their TCR: Vδ1 and Vδ2[135]. The Vδ1 gene is predominantly paired with the gene family Vγ2/3/4/5/8 while the Vδ2 gene is paired with the Vγ chain (Vγ9)[135]. The Vδ3 and Vδ5 subsets make up minor populations that are not discussed here. Each subset exhibits unique developmental

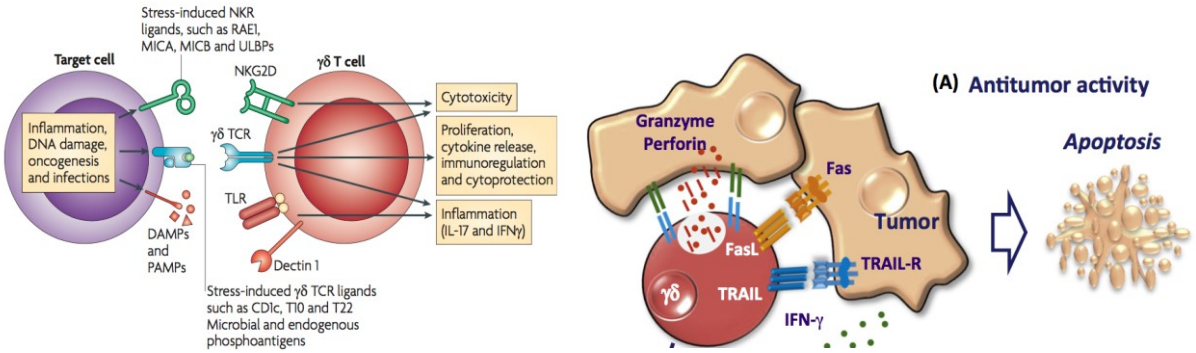

Figure 1.2 γδ T cell recognition and targeting.
γδTc recognize target cells using γδ TCR and NKG2D receptors that recognize stress ligands such as MICA/B and ULBP-2-6. Following recognition, γδTc release TRAIL and FasL that bind to TRAIL receptor and Fas on targets and induce apoptosis in the targets. γδTc also release perforin and granzymes that also mediate apoptosis in target cells. Adapted with permission from Springer Nature and Elsevier. (Bonneville *et al*., 2010 and Chitadze *et al*., 2017)

characteristics, anatomical localization and differentially targets malignancies[115,136,137].

1.3.1.1 Vγ9Vδ2 γδT cells

In human, Vδ2 chain, in most cases, pairs with the Vγ9 chain and is hence termed Vγ9Vδ2 γδTc cell (Vδ2). They are predominantly found in peripheral blood (>70% of γδTc)[135]. Typically, these cells are activated by phospho-antigens (pAgs) that are produced by foreign microbes and transformed cells. For instance, (E)-4-Hydroxy-3-methyl-but-2-enyl pyrophosphate (HMB-PP) is an intermediate metabolite of isoprenoid biosynthesis in microbes and causes Vδ2 activation. Isopentenyl pyrophosphate (IPP) is generated by mammalian transformed cells through the mevalonate pathway, which also activates Vδ2. For example, studies have shown malignancies with p53 mutations that significantly upregulated the mevalonate pathway[138]. Exposure to these two intermediates leads to the activation of Vδ2 in a TCR-dependent manner[139,140]. Moreover, *in vitro*, Vδ2 can be activated and expanded selectively using aminobisphosphonates (N-bis) like zoledronic acid in combination with low-dose IL-2[141]. Studies suggest that IPP and HMBPP activate the T cells by forming complexes with devoted antigen-presenting molecules (APMs). pAg interact with proteins like F1-ATPase expressed by tumor cells, which helps them activate the TCR[142]. Another essential pAgs presenting modality of Vδ2 activation is Butyrophilin3A, a subfamily of proteins. They belong to the B7 co-stimulatory family and might present pAgs directly to Vδ2[143-145]. Moreover, human Vδ2 recognize stress ligands *via* the natural killer receptor, NKG2D. NKG2D ligands include UL16-binding proteins (ULBP) 1–6 and major histocompatibility-like proteins MICA and MICB, which are often upregulated on transformed cells and mostly absent in normal cells[125,146-149]. These NKG2D ligands are discussed in more detail later. Other receptors like Toll-like receptors (TLRs) and natural killer receptors (NKRs) have also

been reported to co-stimulate human Vδ2 in concert with TCR stimulation[125,150]. Other reported ligands for Vδ2 include ectopically expressed DNA mismatched repair protein MutS homologue 2 (hMSH2)[151], superantigens such as staphylococcal enterotoxins (SEs) and toxic shock syndrome toxin (TSST)-1 or nectin-like-5, which is expressed on tumor cells, and recognized by a NKR, DNAM-1.

1.3.1.2 Vδ1 γδT cells (Vδ1)

Human Vδ1 γδTc cells (Vδ1) are predominantly found in the gut epithelia, dermis, spleen and liver. They are involved in maintaining epithelial tissue integrity[115,127]. Recently, there has been new interest in determining the protective role of Vδ1 against human cancers[115,152]. Vδ1 ligand recognition is not well characterized, apart from a few studies. Studies have illustrated that like Vδ2, Vδ1 cells respond to cancer cells that overexpress MICA/B and ULBPs[153,154]. Vδ1 also recognize B7 family members over-expressed on cancer cells using NKp30 receptors, which can be expressed by Vδ1 depending on the expansion protocol used[155]. Moreover, microbial and self-lipids bound to non-classical MHC protein, CD1d, can be recognized by Vδ1[156]. In contrast to Vδ2, Vδ1 are not susceptible to activation-induced cell death (AICD). Vδ1can persist in the circulation for several years[157,158]. Therefore, understanding subset-specific tumor responses is key to rationally exploit the anti-tumor capabilities of γδTc.

1.3.2 NKG2D receptors and ligands

The NKG2D receptor plays a crucial role in the cytotoxic response, particularly in the anti-tumor response of γδTc, NK cells and NK T cells[149]. NKG2D ligands, MICA/B and ULBPs, are not expressed by normal tissues but they are upregulated on transformed and stressed cells[159]. MICA/B is expressed by breast cancer cells and is implicated in γδTc cytotoxicity[127,146,160,161]. This

stress-induced upregulation of ligands can occur during the DNA repair response pathways, during osmotic shock and/or oxidative stress *via* EGFR signaling[162]. Other NK receptors such as NKp30, NKp44, and DNAM-1 (CD226) can also be expressed on γδTc, albeit in varying levels depending on the expansion protocol of γδTc[130]. These studies demonstrate that γδTc are uniquely armed with two independent recognition pathways to sense infected, stressed, or transformed cells.

However, NKG2D ligands are not always uniformly expressed; for example, leukemia stem cells showed an absence of NKG2D ligand expression, which made them less susceptible to γδTc recognition and targeting[163]. Another study has shown that reduced expression of MICA/B on BCSC makes them less susceptible to NK cell killing[164]. Research from our lab has demonstrated that TME factors, such as hypoxia (chapter 3) and the embryonic protein NODAL, are associated with reduced surface expression and increased shedding of MICA by breast cancer cells, which reduces their susceptibility to γδTc cytotoxicity[165,166]. Apart from reduced recognition by γδTc, shed ligand may interact with NKG2D on the surface of γδTc that ultimately inhibits their ability to interact with target cells. Moreover, soluble NKG2D ligand binding can cause the downregulation of NKG2D receptors from the cell surface of effector cells[167,168]. The ADAM (a disintegrin and metalloproteinase) proteases, ADAM10 and ADAM17, have been implicated in NKG2D ligand cleavage[169-172]. In summary, the NKG2D/NKG2DL pathway plays a crucial role in anti-tumor immune response and has potential clinical applications for cancer immunotherapy.

1.3.3 γδTc and cancer

In the last few decades, there have been major advancements made in cancer-associated γδTc research, unravelling their critical influence and contributions to anti-tumor immunity[173]. A striking phenotype of mice lacking γδTc was that they showed a significantly higher occurrence of

papillomas, which then developed into carcinomas in a model of chemically induced skin cancer [63]. γδTc are involved in the immune response against many tumors, including breast cancer[112]. γδTc infiltration has been reported in different types of cancers, such as melanoma, breast, ovarian and lung tumors[174-177]. Recently, a study in 2015 demonstrated intra-tumoral γδTc to be the most significant predictor of favourable survival across various cancer types[178]. However, technical limitations of this study design were later noted as the distinction between γδTc and other subsets of T cells and NK cells was not done appropriately. Tosolini and co-workers improved the identification of γδTc using machine-learning methods and found more variability between individuals and different types of cancers. Overall, the abundance of Vδ2 TILs in this study was associated with favourable outcomes in several different cancers[179]. Some studies arrived at a contradictory conclusion. These studies demonstrate that γδTc are immune suppressive and pro-tumorigenic. The role of γδTc are seemingly context and TME dependant, the intricacies of which are reviewed well in[131,180]. Several clinical trials have been conducted with γδTc in adoptive cell therapy against cancers[111,181-184]. The majority of the trials have found them to be safe and well tolerated[185,186]. Further research is needed to determine how the cells react to tumor over the course of tumor development and how these cells can be best utilized therapeutically.

1.3.4 γδTc and breast cancer

Early evidence demonstrated the ability of γδTc to target breast cancer cells. In 1993, Bank *et al*., were the first to report that Vδ2 could target MCF-7, a luminal A breast cancer cell line[187]. Following that, Guo *et al*., showed that γδTc could also target the luminal A T47D line and the TNBC MDA-MB-231 line[188]. Another study showed the downregulation of MICA/B on the resistant tumor cells, suggesting their role in γδTc cytotoxicity[189]. *In vivo* studies also showed

localization of γδTc to the tumor and exhibited an inhibition of tumor growth by γδTc[171,189]. Migration of infused γδTc to breast tumors and metastatic lesions was also demonstrated in patients[190]. Yet another study showed that γδTc pre-treated with zoledronate could crawl over the surface of untreated breast cancer cells, form strong conjugates, and lyse them[191].

γδTc TILs were identified in breast tumors with the predominant subtype being Vδ1, which makes up 7.2-75.7% of T cell population in breast tumor[192]. A study in mice showed that splenic-derived γδTc secreted IL-17A, which creates an immune-suppressive micro-environment by recruiting suppressive neutrophils[193]. Studies have also suggested that γδTc serve as an important source of IL-17 promoting tumor growth[194]. However, while IL-17A-secreting lymphocytes are common in mice, they are extremely rare in humans and require a highly inflammatory milieu to polarize to an IL-17-secreting phenotype[186,195]. Hence, both *in vitro* and *in vivo* studies suggest that γδTc could have opposing roles in breast cancer tumor growth, which may depend on various factors such as the breast cancer subtype and TME[131].

There are contradictory reports regarding γδTc infiltrating breast tumors. A few earlier studies showed lower circulating γδTc in breast cancer patients than healthy controls, and the number was lower still in higher grade tumors[196,197]. They also found that γδTc expanded from the cancer patients had less granzyme B production compared to γδTc from healthy controls[197]. Another study found that the number of γδTc positively correlated with a higher grade of breast carcinoma, which also positively correlated with a worse prognosis[175]. However, they did not confirm causality. Moreover, the interpretation in this study is questionable as the study was not powered appropriately. A more recent study also identified CD73-expressing Vδ1 that were more prevalent in higher-grade tumors and were found to reduce the proliferation of αβTc *in vitro*[198]. Another study showed higher infiltration of γδTc in TNBC compared to normal breast tissue[199].

Even more confounding, other researchers showed that γδTc were found in more abundance in remission cases compared to relapse cases[200]. Aditionally, using an unbiased *in silico* techniques, others found that a higher fraction of γδTc was associated with a higher pathological complete response(CR)[201] in breast cancer patients. More recent studies also revealed that infiltrating γδTc cells in breast tumors were reactive against the tumor[202]. Adrian Hayday's lab also very recently identified an innate-like γδTc in both the healthy human breast as well as breast tumors that were equally functionally competent and responded *via* NKG2D engagement and were able to lyse breast cancer cells[200]. As evidence suggests, γδTc display a degree of functional plasticity and can be polarized to different subtypes depending on the stimulus of various cytokines and the TME[131,186]. A clearer understanding of these processes will enable us to manipulate γδTc plasticity and ensure optimal efficacy against cancer.

1.3.5 Clinical application of γδTc

In recent years, γδTc have emerged as a novel immunotherapeutic approach for different malignancies. Apart from their potent anti-tumor immune response and excellent safety profile[203], they have several notable advantages. The two major immune evasion mechanisms employed by tumor cells against αβTc therapy are the downregulation of MHC and the loss of antigens that are αβTc -specific and expressed by tumor cells. The selective pressure of therapy drives the evolution of cancer cells to escape recognition by epitope mutation, making them devoid of MHC or the tumor-specific antigen being targeted by the therapy[86,204]. MHC downregulation does not impact γδTc therapy as it is typically MHC- independent and can therefore recognize tumors lacking MHC[115]. Their typical MHC-independent activation means that they do not cause graft-versus-host disease, they are not impacted by peptide-MHC antigen loss, and their kinetics in response to stress

signals are faster than αβTc[115]. Moreover, γδTc do not typically recognize a single antigen as with αβTc, but rather a broad range of stress signals expressed by transformed cells and are therefore not subject to these limitations. Upon stimulation, γδTc can acquire antigen-presenting functions and mediate a robust cross-presentation of extracellular antigens[205], making them a valuable candidate for cellular vaccines that goes beyond their cytotoxic function[129]. Improved and efficient expansion protocols of γδTc *ex vivo* have further bolstered its success as a therapy[206-211].

Clinical trials have been done using either the bulk γδTc population or specific subsets. There have been two main approaches using Vδ2 cells. The first is to activate and expand Vδ2 directly *in vivo* using pAgs or N-bis, such as zoledronate along with IL-2. This strategy has been tested in eight different phase 1 clinical trials. The main goal of Phase 1 is to determine the safety and not efficacy, and most patients enrolled are late stage. This therapy was found to be safe and resulted in a robust expansion of IFNγ-producing Vδ2 *in vivo*[203]. The second strategy is to adoptively transfer Vδ2 that have been expanded *ex vivo* again using pAgs or N-bis alone with IL-2. This strategy has been used in nine clinical trials with 86 patients in total and it was well tolerated[203].

Concerning breast cancer, a clinical trial involving ten metastatic and treatment refractory breast cancer patients were administered zoledronate and IL-2 for *in vivo* expansion of Vδ2. They found that three-quarters of the patients survived past 12 months with a robust expansion of Vδ2, while the remaining three patients died between three to eleven months after a decline in their Vδ2 numbers[111]. Given that all the patients were in advanced stage cancers and refractory to other treatments, these results look encouraging. An ongoing phase III clinical trial (NCT00171314) is determining the effect of a single dose of zoledronate with pre-operative letrozole (aromatase inhibitor, used in breast cancer treatment to block the conversion of androgen to oestrogens in post-

menopausal women) in ER+ HER2- breast cancer patients[212]. This study also aims to determine the efficiency of Vδ2 expansion with zoledronate and assess if a higher level of pre-treatment peripheral Vδ2 are predictive of prognosis[212].

Trial results from various cancers demonstrates that γδTc therapy is safe and well-tolerated, with no evidence of graft versus host disease (GvHD). However, efficacy and anti-tumor responses are highly variable. This variation can be explained by the late stage, as often phase I trials only enroll metastatic patients. It could also be attributed to the variability in the expansion protocol both *in vivo or ex vivo* and even on the variability of the treatment regimens applied in the different trials. For instance, one study revealed that multiple doses of zoledronate led to a progressive reduction in peripheral Vδ2[196] and they suggest that perhaps less frequent zoledronate administration is more efficient in expanding Vδ2[196]. Moreover, in some cancer patients, the Vδ2 were dysfunctional or susceptible to activation-induced anergy. Therefore, repeated stimulation of Vδ2 with multiple doses of pAgs or N-bis may result in terminal differentiation and exhaustion[213-215]. Thereby, the adoptive transfer of Vδ2 expanded *ex vivo* seems to be a more effective approach. It is promising that treatment with allogeneic Vδ2 from healthy donors does not seem to cause GvHD, and that cells from a single donor can be expanded to large batches of cells. Although the number of patients treated with allogeneic cells is too few to draw any conclusions, these results are an indication that cells expanded from healthy allogeneic donors have a functionally superior phenotype compared with patient-derived autologous Vδ2[216].

1.3.6 Challenges in the development of γδ T Cell Immunotherapy

The major impediments in the road for γδTc therapy are γδTc anergy, reductions in the number of peripheral γδTc after infusion and suppressive TME, which limit the anti-tumor

functions of γδTc. γδTc cytotoxicity against carcinoma was diminished by soluble factors such as soluble MICA/B[217,218], several cytokines like IL-23, IL-15, IL-17, IL-4, TGF-β, factors such as prostaglandins, kynurenins and immune cells such as neutrophils largely influence γδTc polarization, which may, in turn, result in a reduction in their number[186,218,219]. Neutrophils can produce hydrogen peroxide that inhibits T cell proliferation[220]. Lack of clinical response was also associated with increased pre-treatment serum levels of VEGF, which was further increased with zoledronate and IL-2 injections[221]. Thus far, only a few clinical trials have evaluated the patients' immune status prior to γδTc immunotherapy, which can limit the likelihood of failure and provide appropriate treatment options to patients. Another factor influencing Vδ2 *in vivo* expansion with zoledronate is poor systemic availability of N-bis, which is eliminated rapidly by renal excretion[222]. Several of these pitfalls may be overcome using adoptive cell transfer, which appears to be more effective.

1.3.7 Improving γδ T cell Immunotherapy

Studies are now focussing on improving γδTc therapy. One such approach is redirecting γδTc to specific antigens using bispecific antibodies, in which one of the binding sites recognizes a tumor-specific molecule such as HER2 or EpCAM, and the other binds to the Vγ9 chain of Vδ2 or CD3 or CD16 antigen on γδTc. Preclinical models using such bispecific antibodies have shown encouraging results[223-225]. Another study developed recombinant immunoligands that consist of CD20 single-chain variant fragment, which is further linked to MICA or ULBP2, which enhanced the cytotoxicity of expanded γδTc against CD20-positive lymphoma cells by engaging the NKG2D receptor[226]. Yet another approach is developing CAR for γδTc. Deniger *et al*. transduced polyclonal γδTc with CD19-specific CAR, which could target and efficiently kill $CD19^+$ leukemia cells both

in vitro and *in vivo* in mouse models[227]. The transduction of high-affinity Vδ2 TCR into αβTc is another strategy currently under clinical development. This transduction is designed to overcome low persistence of hyporesponsive Vδ2 in patients with advanced cancer. These transduced αβTc are expected to develop durable, memory-based responses under particular settings such as immune checkpoint inhibition. These hybrid T cells, named T cells engineered with defined gamma delta TCRs (TEGs), were responsive against multiple tumors[228], can be produced under good manufacturing practice (GMP) conditions[229] and are currently being tested in phase I clinical trial in patients with hematological malignancies[230]. Combinations of γδTc with other agents have also been investigated. One study demonstrated that the treatment of HER2 positive cell lines with γδTc in combination with trastuzumab led to increased efficacy compared to either therapy alone[231].

Finally, clinical trials with γδTc have heavily relied on Vδ2, and more recent studies have shown that Vδ1 are less susceptible to activation-induced exhaustion. They seem to also last longer after an adoptive transfer, which can provide a more durable anti-tumor response[152,232,233]. Recently, two groups (Bruno Silva-Santos and Adrian Hayday) have developed protocols to selectively expand Vδ1 from blood and skin, respectively. Both protocols successfully expanded and activated Vδ1 that produced abundant IFNγ and TNFα and were cytotoxic against various cancers[209,234]. The safety and efficacy of autologous or allogeneic Vδ1 are yet to be determined in human clinical studies. However, adoptive transfer of autologous TILs has shown exciting clinical results in patients with metastatic melanoma[235,236] where Vδ1 represent the major TIL subset (~50% of the total $CD3^+$ population)[174]. In our study, we expand and employ both Vδ1 and Vδ2 subsets to target breast cancer cells. Another avenue to investigate is combination of γδTc with neutralizing antibodies against suppressive cytokines such as IL-10, soluble factors such as soluble MICA and with immune checkpoint blockade targeting PD-1 and cytotoxic T- lymphocyte

associated protein-4 (CTLA-4) to counteract immune suppression and exhaustion *in vivo*. Hence with the different approaches being tested in clinical trials over the coming years, it is exciting to see γδTc transform into a safe and powerful tool for cancer immunotherapy. Although γδTc immunotherapy shows promise, how well the γδTc can target CSC is largely unknown. Thus far, only a few studies have reported the ability of γδTc to target CSC (colon cancer, ovarian and neuroblastoma)[237-239]. These studies did not compare γδTc cytotoxicity against CSC to that against NSC to get a complete picture. Also, they included just Vδ2 in their study. Our study employs both subsets of γδTc and we examine the ability of these cells to target both BCSC and NSC. Cancer cells can utilize several different mechanisms to evade immune targeting, and a more in-depth understanding of the different mechanisms is pertinent to develop successful therapy.

1.4 Immune Evasion

There are several mechanisms of immune evasion employed by tumor cells. Tumor cells may (i) produce immune-suppressive cytokines[59,67], (ii) recruit immune-suppressive cells[59], (iii) evade immune recognition by down-regulating their tumor surface antigens and/or MHC II proteins, or acquire mutations that disrupt the antigen presentation and processing machinery[58,67], (iv) increase resistance to cytotoxic effects of immunity by upregulating anti-apoptotic proteins or mutation in death receptors like TRAIL, Fas, DR5[60] , and (v) express immune-inhibitory ligands[240]. Immune evasion is not only an important step in the development of cancer but also exists as a potential obstacle to immunotherapies.

1.4.1 Tumor secretions of immune suppressive factors

Several soluble factors are released by tumor cells or stromal cells that can exert suppressive and dampening effects on immune cells. Suppressive cytokines like IL-10 are released by tumor

cells, especially CSC[241] and other stromal cells that can inhibit T cell cytotoxicity and effector functions. Lipids like Prostaglandin E2 (PGE2) are overproduced in the TME by CSC due to the upregulation of the enzyme cyclooxygenase-2 (COX 2)[242-244]. A study showed that PGE2 released by mesenchymal stem cells (MSC) of bone marrow donors could block the function of Vδ2[245,246]. Furthermore, studies have illustrated the immune-suppressive role of metabolites, such as adenosine, that are elevated in response to tissue hypoxia or acute inflammation[247]. Adenosine binds to adenosine receptors and disrupts T cell effector responses[248]. Tumor-derived adenosine can also inhibit tumor cell destruction by Vδ2[245,249]. Galectins are a family of evolutionarily conserved glycan-binding proteins whose family members are upregulated in the TME and involved in immune-suppressive functions[250]. They are also upregulated by the CSC in several tumors[251]. Gal-3, a member of the galectin family, was reported to inhibit γδTc proliferation but not impact their cytotoxicity[252]. Hence, a better understanding and characterization of the different secreted factors impacting γδTc is warranted. In summary, all these data indicate that cancer cells, and especially CSC, can suppress the impact of immune cells and create an immune-suppressive microenvironment.

1.4.2 Dysregulated Anti-Apoptotic Proteins in CSC

Circumvention of apoptosis is a critical hallmark of cancer. Multiple reports suggest that aberrant expression and ratio of apoptotic and anti-apoptotic proteins contribute to survival of CSC. The cell death regulating BCL-2 family proteins, MCL-1 and BCL-XL were found to be over-expressed in BCSC and played a crucial role in their survival[253,254]. High levels of BCL-2, BCL-XL and MCL-1 have been described in glioblastoma stem cells (GSC) and leukemia stem cells (LSC) that were also associated with their resistance to chemotherapy. To address this adaptation, significant efforts are being made. Several studies are focusing on developing therapeutic

interventions to eliminate CSC using inhibitors of the BCL-2 family of proteins[254-256]. Another anti-apoptotic protein, survivin, was preferentially expressed by BCSC and played a role in their survival[257]. Survivin is also associated with chemoresistance of colon cancer stem-like cells[258].

1.4.3 MCL-1

While several anti-apoptotic proteins have been implicated in cancer therapy resistance, our study focuses on MCL-1. MCL-1 function is essential to cell survival and homeostasis and in determining the fate of a cell. MCL-1 sequesters the pro-apoptotic proteins BAK/BAX. Activated and exposed BAX and BAK form pores in the mitochondrial outer membrane causing cytochrome c and other apoptotic proteins to leak into the cytosol, which leads to the formation of apoptosomes, the activation of caspases, finally leading to the cleavage of cellular proteins and cell death[259]. Hence the MCL-1:BAK/BAX complex retains BAK/BAX in an inactive state, preventing them from inducing apoptotic pathways and preserving mitochondrial membrane integrity[260]. MCL-1 amplification and overexpression have been reported in several human tumors, including breast cancer[260-262]. This overexpression was also associated with poor prognosis and resistance to anticancer drugs such as taxol, cisplatin, erlotinib and other standard anticancer drugs. MCL-1 knockdown increased cancer sensitivity to these drugs[260]. In a cohort of breast cancer PDX models, it was found that TNBC had the highest amount of MCL-1 RNA and protein compared to other subtypes[263]. Other studies showed that MCL-1 expression levels correlated with high tumor grade and poor prognosis in patients[264,265].

Hence inhibition of MCL-1 and other anti-apoptotic proteins could be a successful approach to trigger apoptosis and cell death in transformed cells, especially CSCs[266]. One vital point to keep in mind when considering MCL-1 inhibitors for therapy is that MCL-1 is ubiquitously expressed and is essential for embryonic development, so MCL-1 inhibitors can affect normal cells

as well[267]. However, since cancer cells express the protein in much higher abundance, the effects might be mitigated by careful dosing. Over the past few years, significant progress has been made in discovering potent and specific MCL-1 inhibitors[266,268]. Although there is an improved anti-tumoral effect with these inhibitors as a single agent, using these drugs in combination with targeted therapies has enhanced the impact and durability of response and has even shown response in preclinical models where monotherapy has failed[269-273]. Hence, exploring the effects of MCL-1 inhibitors in combination with other forms of therapy may prove to be a fruitful avenue to pursue. We used an MCL-1 degrader that targets MCL-1 using the proteolysis targeting chimera (PROTAC). PROTACS are small molecules that tether target proteins to E3 ligases inducing ubiquitination and tag proteins for proteasomal degradation[268]. Thus, MCL-1 inhibition in combination with chemotherapy or immunotherapy to ensure apoptosis of target cells is an attractive strategy.

1.4.4 NKG2D shedding ADAM proteases

ADAM proteins involved in proteolytic cleavage of MICA/B are a family of membrane-anchored zinc proteases that can convert nearby membrane-anchored proteins into their soluble forms. These soluble forms can function as activators or inhibitors of protein function. In many cases, they cleave membrane-bound cytokine precursors into soluble bioactive mediators[274,275]. The best-known example of this is the cleavage of membrane-bound tumor necrosis factor (TNF) to its soluble form (sTNF) by ADAM17, which is why it was originally named TNF-α converting enzyme (TACE)[276]. ADAM family proteases are involved in various body functions and developmental processes. Apart from NKG2D ligands, some relevant examples would be LAG-3[265], IL-6 receptor (IL-6R)[277] cleaved by ADAM17; TIM-3[278], HER2[279], CD44[280] cleaved by ADAM10; Notch[281], PD-L1[282], FasL[283] cleaved by both ADAM10 and 17.

In recent years, ADAM proteases have been implicated in various tumor processes such as cancer initiation, progression and resistance to specific therapies[284,285]. ADAM17 is the most widely studied of the ADAM proteases. High levels of ADAM17 have been found in different cancers, and higher ADAM17 was associated with poor prognosis[286]. Additionally, *in vitro* inhibition of ADAM10 in various cancers led to decreased cell migration, invasion and cell proliferation[287]. ADAM10 is structurally and functionally similar to ADAM17[284] and can cleave the same substrates in some cases[288]. Several different inhibitors for ADAM10 and 17 have been developed and tested in preclinical and clinical trial settings against various types of cancers, and they are reviewed in detail in[287]. Small molecular inhibitors, monoclonal antibodies and even ADAM pro-domain peptide-based therapeutics to competitively inhibit ADAM are under investigation[287]. However, the success obtained with these inhibitors in the preclinical setting has not yet been recapitulated in clinical trials, partly due to adverse side effects or due to poor efficacy[289]. Therefore, optimization of ADAM inhibitors will allow for more specific and fine-tuned modulation of ADAM proteolytic activity, which is crucial for their development into useful drugs.

1.4.5 Checkpoint inhibitors

Immune checkpoint pathways or co-inhibitory pathways play a critical role in maintaining and modulating the immune response. Under normal circumstances, the checkpoint pathways act as the brakes to the immune response. There is an intricate balance between them and the activating pathways that creates tight control of immune activation. Checkpoint pathways control the strength and duration of the immune responses, thereby avoiding excessive activation and limit immune-mediated tissue damage, controlling the resolution of inflammation and maintaining tolerance to prevent autoimmunity. However, tumor cells can induce different immune checkpoint pathways to

harbour immunosuppressive functions. In this section, we will mainly focus on PD-1 and CTLA-4, which are the most well studied, along with LAG-3 and TIM-3.

1.4.5.1 PD-1 and its ligands

PD-1 belongs to the B7-CD28 superfamily expressed on T cells, B cells, NK cells, DC and activated monocytes. PD-1 ligands, PD-L1 and PD-L2, are expressed by several tumor cells and also by activated B cells and T cells, dendritic cells, macrophages, and fibroblasts[290]. In normal cells, PD-1 functions as a major negative immune regulator[291]. It appears within 24h of activation and declines with the clearance of the antigens[291]. Cancer exploits the PD-1/PD-L1 ligand pathway to evade the host immune response. Binding of PD-1 on immune cells to its ligand cancer cells can result in attenuated TCR stimulation, impairment of T cell proliferation and cytokine production and decreased expression of pro-survival factor Bcl-XL in the T cells[292,293]. Chronic PD-1 signaling plays a critical role in the induction of anergy, exhaustion and development of induced Tregs (iTregs), facilitating tumor immune escape[293-295].

In 1992, PD-1 was identified by the Honjo lab as a gene upregulated and strongly induced in T cell hybridomas undergoing apoptosis[296]. He, and Jim Allison, who discovered the inhibitory role of CTLA-4, were awarded the Nobel prize in Physiology and Medicine in 2018 for their breakthrough contribution in the field of cancer immunotherapy. In cancer, over-expression of the c-FOS subunit of transcription factor AP1 or nuclear factor κB (NF-κB) can increase the expression of PD-1[297,298]. Cytokines such as IL-6, IL-12 and VEGF can enhance PD-1 expression[299,300].

In cancer, PD-L1 expression is driven principally by transcription upregulation. Several transcription factors are involved, including hypoxia-inducible factor (HIF)-1α, STAT3, and NF-κB[301]. Higher levels of HIF-1 α are correlated with PD-L1 expression and with T-cell function downregulation. HIF-1α regulates PD-L1 by binding to a hypoxia response element in the PD-L1

promoter to induce PD-L1 transcription[302].

PD-L2 has a higher affinity for PD-1 than PD-L1. However, PD-1–PD-L2 interaction is much less functionally relevant than the PD-1–PD-L1 interaction due to the low expression of PD-L2. PD-1–PD-L1 interaction is sensitive to PD-L2 competition only when PD-L2 levels are very high[303]. Moreover, several reports show that PD-1-PD-L1, but not PD-L2, was involved in T cell tolerance and apoptosis[304]. This indicates that PD-1's suppressive function is largely mediated by PD-L1 but not PD-L2. The roles of PD-L2 have been controversial in the literature. Some reports suggest that PD-L2 is an inhibitory co-stimulator, whereas others indicate that it can also act as a positive co-stimulator and exerts its function through receptors other than PD-1[304].

PD-L1 expression has been reported *in situ* in various malignancies, including breast, lung, ovarian and colorectal cancer as well as melanoma and gliomas. In many cases, higher expression of PD-1 is inversely correlated with survival[305-311]. PD-1 expression is upregulated on TILs[312-315], and several meta-analyses have revealed that PD-L1 overexpression signified a poor prognosis in many cancer types[316-319]. At least 500 clinical trials targeting PD-1 signaling have been conducted to date, applying nine types of antibodies on at least 20 kinds of malignancies[320]. Five inhibitors of PD-1/PD-L1 have been approved by the FDA for various cancers[321]. In March 2019, the FDA approved the first checkpoint inhibitor immunotherapy drug, the anti-PD-L1 antibody atezolizumab (Tecentriq®), combined with chemotherapy (Abraxane®) for TNBC patients who are positive for PD-L1 protein expression[322]. However, the response rates are modest and adverse side effects can cause treatment discontinuation.

1.4.5.2 CTLA-4

Anti-CTLA-4 antibodies were the first immune checkpoint blockade approaches that were clinically validated[323]. CTLA-4 is a central inhibitory regulator of T-cell proliferation, expansion and activation[324-328]. CTLA-4 and CD28 are homologous receptors (with 30% sequence homology) expressed by lymphocytes ($CD8^+$, $CD4^+$T cells, γδTc, NK cells), which mediate antagonistic effects in T cell activation. Both CTLA-4 and CD28 bind to the same ligands, CD80 (B7-1) and CD86 (B7-2)[326]. These ligands are expressed predominantly on the surface of APCs and in some cases on tumor cells. However, CTLA-4 binds to them with higher affinity, thus can act as an antagonist to CD28. Ligation of CD28 to CD80 and CD86 mediates T-cell co-stimulation in combination with TCR signals. In contrast, when CTLA-4 binds to these ligands, it serves to inhibit T-cell responses[326].

Despite the immunosuppressive function of CTLA-4, their association with disease prognosis is not clear. However, a study showed that CTLA-4 is overexpressed in more than 50% of breast carcinomas[329]. There are five ongoing clinical trials of anti-CTLA-4 antibodies for breast cancer[330]. Combined blockade of PD-1 and CTLA-4 can play a synergistic role; CTLA-4 is responsible for inhibiting early stages of T cell activation and PD-1 for inhibiting T cells in peripheral tissues. This combination has been approved for metastatic melanoma, mismatch repair-deficient microsatellite instability-high metastatic colorectal cancer, and advanced renal cell carcinoma[331].

1.4.5.3 TIM-3

TIM-3 is expressed by many T cell populations (Th1 cells, $CD8^+$T cells, and Tregs), NK cells, NKT cells, and APCs such as dendritic cells and macrophages. TIM-3 has four known ligands, phosphatidylserine (PS), galectin-9 (GAL-9), high-mobility group protein B1 (HMGB1),

and carcinoembryonic antigen cell adhesion molecule 1 (CEACAM-1)[290]. TIM-3 is reported to induce immunological tolerance. It has been associated with asthma, food allergy and autoimmune diseases, including multiple sclerosis and rheumatoid arthritis[332]. TIM-3 is also often associated with immune exhaustion during chronic viral infection[333] and cancer. In a breast cancer model, blocking TIM-3 improved response to paclitaxel chemotherapy[334]. Reports suggested co-expression of TIM-3 and PD-1 resulted in highly dysfunctional $CD8^+$T cells in cancer[335-338]. Reports also indicated the upregulation of TIM-3 expression in tumors treated with PD-1 antibodies, which might be a mechanism of resistance to PD-1 therapy. Hence, a combination of TIM-3 and PD-1 blockade might be more effective than monotherapy[335,337,339-343]. Several clinical trials are focusing on TIM-3 as a new approach for immunotherapy with promising results[333].

1.4.5.4 LAG-3

LAG-3 or CD223 is a structural homolog of CD4, which binds to MHC-II and transmits inhibitory signals to reduce proliferation and effector function, T-cell activation and cytokine secretion[344-347]. LAG-3 is expressed on activated T cells, Tregs, B cells, NK cells and DCs[290]. Several reports suggest that following antigen stimulation, LAG-3 can negatively regulate $CD8^+$T cell activity [347-349]. Many reports show over-expression of LAG-3 on tumor infiltrating $CD8^+$T cells in various cancer types, including breast cancer[91,350]. In breast cancer, PD-1 and LAG-3 are also co-expressed on the tumor infiltrating $CD8^+$T cells[91]. Combined blocking of both receptors in tumor models also has a greater therapeutic benefit than blockade of either alone[351-353]. In summary, checkpoint blockade plays key role in most cancers and targeting them is both a challenge and an opportunity for cancer treatment.

1.4.5.5 Checkpoint pathways and γδTc

It has previously been shown that γδTc can express PD-1 molecules[354], which may control T cell proliferation[355] and the production of anti-tumor cytokines[356]. Treatment with Pembrolizumab (PD-1 blocking antibody) boosted IFNγ in zoledronate-stimulated γδTc and improved their cytotoxicity against leukemia cell lines[357]. Additionally, FOXP3^{+}Treg-like Vδ2 had increased expression of CTLA-4 molecules. These Tregs-like Vδ2 displayed inhibitory effects such as the inhibition of PBMC proliferation[358]. A recent study in 2018 found that the percentage of γδTc expressing TIM-3, LAG-3, CTLA-4 and PD-1 was significantly upregulated in virus and *Plasmodium vivax*-infected patients[359]. Multivariate computational analysis also revealed that HIV+ patients expressed significantly higher frequencies of TIGIT, TIM-3 and CD160 than controls[360]. The presence of checkpoint receptors on γδTc and their impact on γδTc function needs to be examined in greater detail to design interventions that can boost the immune potency of γδTc therapy. TME factors such as hypoxia can also play a crucial role in mediating the upregulation of checkpoint pathways and immune escape.

1.5 Hypoxia

Due to the rapid growth and proliferation of the tumor cells, tumors quickly outgrow their blood supply, leaving areas within the tumor where the oxygen concentration and nutrient supply are significantly lower than in normal tissues. At the core, the cellular response to hypoxia is mediated by two master regulators that form a heterodimeric complex. They are the constitutively expressed nuclear HIF-1β and the cytoplasmic oxygen-dependent HIF-α (HIF-1α, HIF-2α, HIF-3α). This complex is further stabilized by a group of oxygen- and iron-dependent enzymes called HIF-propyl hydroxylase domain enzymes (PHD1-3). Under normoxic conditions, PHDs

hydroxylate two conserved proline residues on HIF-α subunit, allowing their recognition and initiating binding of the Von Hippel-Lindau tumor suppressor protein (pVHL) and subsequent ubiquitination and proteasomal degradation[361]. However, under hypoxic conditions, PHDs are suppressed as they require oxygen as a co-substrate[362]. This releases the HIF-1α subunit, which then translocates into the nucleus and binds to HIF-1β. The heterodimeric HIF-1α:HIF-1β complex then moves to the hypoxia-responsive elements (HREs) of the target genes resulting in transcriptional upregulation of downstream genes.

A study showed that normal breast tissues have a median oxygen partial pressure of 65 mg Hg, with no participant having measurement below 10 mm Hg. In contrast, breast, as well as other cancers, had a median pO2 of 10 mm Hg[363]. Severe hypoxia was observed in many regions of the tumor, and 50% of locally advanced breast tumors showed a positive correlation between hypoxia and poor clinical outcomes[363]. Based on extensive literature review and loss-of-function assays, a study demonstrated a signature of 42 genes upregulated under hypoxic conditions by HIF-1α and HIF-2α. They also found that this signature was enriched in basal-like cell lines and basal tumors[364]. Hypoxic tumors upregulate key genes that are involved in cell survival and proliferation under such hostile conditions. The absence of oxygen switches cell metabolism to glycolysis, increasing glucose consumption and pyruvate, lactate, and H+/H3O+ generation[365,366]. Hypoxic cancers are highly aggressive, metastatic and correlate with poor prognosis[367,368]. Hypoxia also contributes to angiogenesis, intra-tumoral heterogeneity, genetic instability, stem cell renewal and evolution of therapy-resistant clones[369-373]. Hypoxic tumors are also generally resistant to traditional radiotherapy, phototherapy, chemotherapy[374-376] and even immunotherapy[377,378].

1.5.1 Hypoxia and immune resistance

There is a great deal of evidence for the immune-modulatory role of hypoxia in the TME[379-

[381](Fig 1.3). While tumor cells can continue to grow and thrive in the hypoxic micro-environment, it creates inhospitable conditions for immune cells and dampens the anti-tumor immune response resulting in immune suppression[381].

There are conflicting data regarding the impact of hypoxic conditions on T cells in the tumor. Several studies have suggested a less efficient activation by TCR derived signals and co-stimulation under hypoxic conditions[382-384]. Elevated glycolysis in the tumor mediated by HIF activity created metabolic competition between tumor cells and T cells, and a lack of nutrients resulted in T cell anergy or shifting of effector T cells to the Treg lineage[385-387]. Inhibition of glycolysis in T cells was also associated with a chronic expression of inhibitory receptor PD-1, which was further involved in hypo-responsiveness and exhaustion in T cells[388]. CTLA-4 was also upregulated on $CD8^+$T cells in hypoxia[389]. Interestingly, one study showed that T cells that survive in hypoxic niches exhibited enhanced cytolytic activity[390]. Yet another study showed that hypoxia could shorten effector function but enhance the generation of memory T cells, which plays a role in long-term immune responses[391]. Apart from our study on the impact of hypoxia on γδTc, another study recently demonstrated that hypoxia reduces γδTc Ca^{2+} efflux and degranulation in the presence of oral cancer targets. They also showed that under hypoxia, PD-L1 high γδTc induced apoptosis in PD-1 high $CD8^+$ T cells, when in co-culture[392].

Apart from T cells, hypoxia can also impact DC antigen uptake and downregulate differentiation and activation markers, including CD40, CD80, and MHC class II[393,394]. Under hypoxia, NK cells also undergo significant metabolic reprogramming that leads to impairment of their function and cytolytic activity[395]. Hypoxic niches are infiltrated by many immunosuppressive cells, such as MDSCs, TAMs and Tregs. Hypoxia in tumors has also been shown to aid switching of TAMs to the more aggressive phenotype capable of mediating resistance[396]. Further, TAM

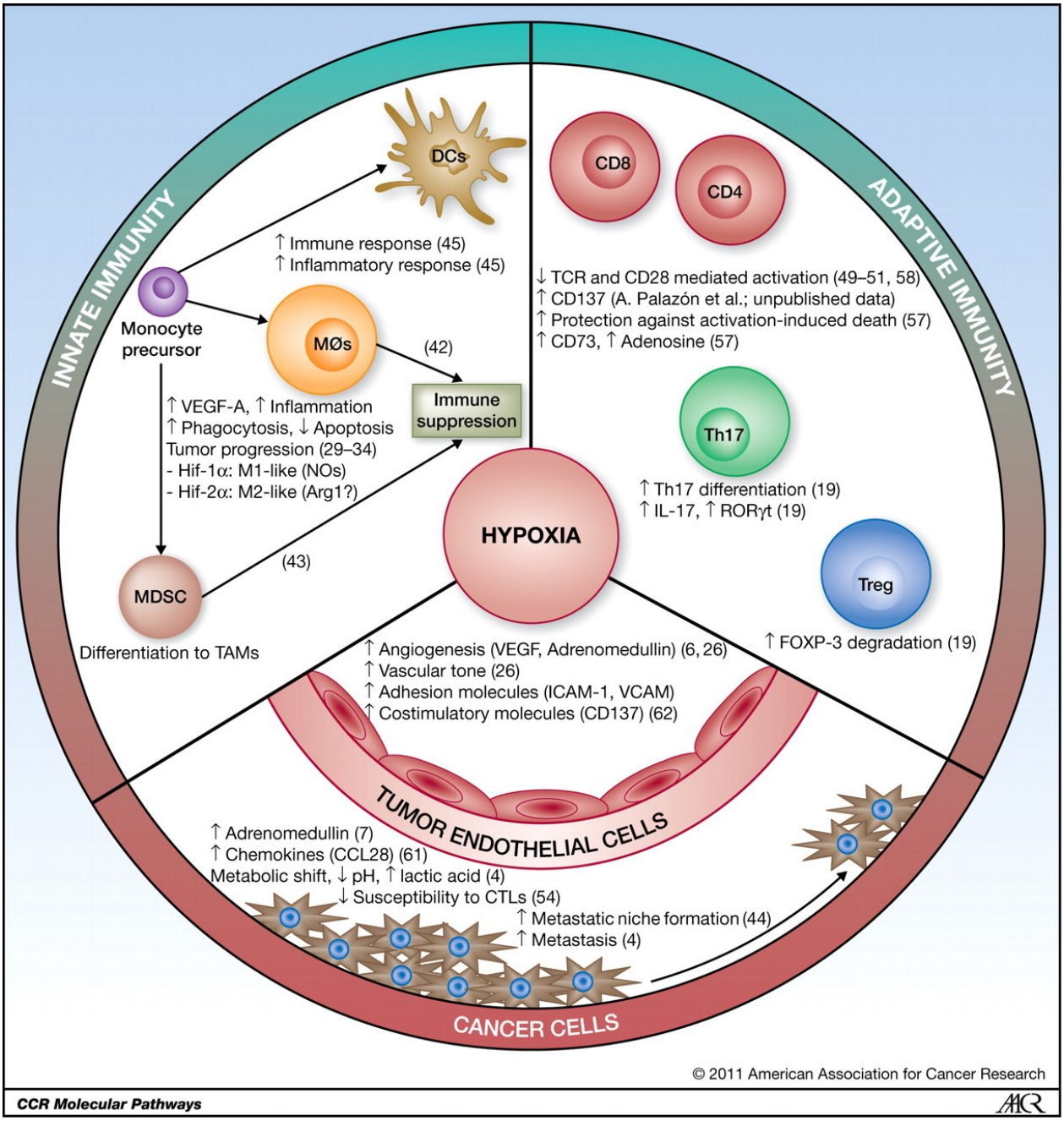

Figure 1.3 Impact of hypoxia on immune and other stromal cells in tumor microenvironment. Adapted with permission from AACR (Palazon *et al*., 2012).

infiltration into hypoxic/necrotic tumor niches positively correlated with worse prognostic outcomes[397]. Tumor infiltrating MDSCs induce T cell anergy as well as promote Treg proliferation[398,399].

Hypoxia can also affect immune cells by the upregulation of several immunosuppressive molecules, such as VEGF and IL-10[400,401]. Several reports illustrate that hypoxia can mediate the downregulation of MHC-I in tumor cells[402-404]. Additionally, hypoxic tumors express high levels of soluble MICs which are mediated by Nitric Oxide, which down-regulate NKG2D, enabling their immune escape[404]. As discussed earlier, NKG2D is essential for tumor recognition by γδTc; therefore, it is highly probable that hypoxia renders cancer cells resistant to γδTc killing. Another mechanism of immune evasion aided by hypoxia is the upregulation of PD-L1. PD-L1 is now a recognized target gene of HIF-1α and HIF-2α[302,405]. Hypoxic tumors also show high ROS levels due to anaerobic metabolism. ROS are detrimental to T cell viability and function[406]. ATP released by cells is metabolized more rapidly under hypoxic conditions leading to an excess of soluble adenosine, which in turn binds to adenosine receptors on the T cell surface to augment intracellular cAMP, a second messenger molecule known to repress T-cell functions[407]. It was recently found that HIF-1α favors the differentiation of Th17 T cells and increases IL-17, which promotes an immune-suppressive microenvironment[408]. Hence, targeting the hypoxic TME is crucial to reinvigorate immune cells. As we continue to deepen our understanding of the different factors involved in immune evasion of γδTc, novel approaches may be designed for a more effective next-generation γδTc immunotherapy.

1.6 Research objective

Our main goal is to exploit the power of γδTc immunotherapy to target highly resistant breast cancer cells. Breast cancer immunotherapy is plagued by two major challenges: (i) harsh

immune-suppressive environmental conditions exacerbated by factors such as hypoxia; and (ii) tumor plasticity, which is aided by the presence of BCSC, giving rise to therapy-resistant clones and promoting cancer relapse.

Several studies have demonstrated the immune evasive nature of CSC in general. They exploit numerous mechanisms to escape being recognized and targeted by numerous immunotherapeutic strategies. Additionally, previous studies have established that hypoxia promotes BCSC generation, and can modulate the tumor immune system. Thus, we hypothesize that BCSC are resistant to γδTc targeting and that hypoxia promotes breast cancer cell resistance to γδTc cytotoxicity. To address these questions, our specific aims are to determine:

I. **The impact of anti-γδ TCR antibodies on γδTc viability.** Mechanistic experiments such as cytotoxicity blocking assays play a crucial role in our understanding of the γδTc immune response. Reduction in γδTc cytotoxicity on blocking certain receptors and ligands help us determine their role in γδTc targeting. However, we found that blocking antibodies to γδ TCR can cause apoptosis in γδTc. This inadvertently leads us to misconstrue the reduction in cytotoxicity as an actual result of receptor blocking. To this end, we characterized the NKG2D antibody and different antibodies for γδ TCR that are commonly used and to determined their impact on γδTc viability and function. This gives us a more accurate picture and help us tease out the impact of real receptor blocking from the impact of γδTc apoptosis. This is crucial as we use blocking assays in the upcoming work and this study helped us to hone skills that we require for the rest of the project, and also helped us to recognize the strengths and limitations of this particular assay.

II. **The impact of hypoxia on γδTc efficacy against breast cancer cells**. We investigated the

impact of hypoxia on both the effector γδTc and the breast cancer cell targets, and highlighted the interplay between them. We determined how hypoxia may affect γδTc cytotoxicity against breast cancer cells, and at the same time, how it may impact the sensitivity of breast cancer cells to γδTc targeting. Additionally, as hypoxia diminished breast cancer targeting, we studied the various immune evasion mechanisms promoted by hypoxia.

III. **The efficacy of γδTc against BCSC and in the event of reduced cytotoxicity, investigation of immune evasion mechanisms employed by BCSC.** In addition, we determined strategies to overcome these resistance mechanisms.

Through these findings, we intend to overcome the challenges posed by tumor plasticity and hypoxia, facilitating a more effective next-generation γδTc immunotherapy**.**

Chapter 2 Apoptosis Induced via Gamma Delta T Cell Antigen Receptor "Blocking" Antibodies: A Cautionary Tale

Apoptosis Induced via Gamma Delta T Cell Antigen Receptor "Blocking" Antibodies: A Cautionary Tale

Short title: Gamma delta T cell antigen receptor blocking antibodies cause apoptosis

Indrani Dutta, Lynne-Marie Postovit and Gabrielle M. Siegers
Department of Oncology, University of Alberta, Edmonton, AB, Canada

Address correspondence to:

Gabrielle M. Siegers
Research Scientist
Department of Oncology
University of Alberta
5-142W Katz Group Centre
Edmonton, AB
CANADA T6G 2E1
Phone: 780-248-5714
Fax: 519-492-8160
email: siegers@ualberta.ca

Keywords
gamma delta T cells, blocking antibodies, cytotoxicity, mechanism, apoptosis

Abbreviations

αβTc, alpha beta T cells
AICD, activation-induced cell death
AnnV, Annexin V
CalAM, Calcein AM
FB, FACS buffer
FBS, fetal bovine serum
FSC, forward scatter
IL-, interleukin
mAb, monoclonal antibodies
γδTc, gamma delta T cells
γδTCR, gamma delta T cell antigen receptor
PBMCs, peripheral blood mononuclear cells
SSC, side scatter
ZA, Zombie Aqua

Abstract

Mechanistic studies contribute greatly to our understanding of γδ T cell (γδTc) biology, aiding development of these cells as immunotherapeutic agents. The antibody blocking assay is an accepted method to determine the receptors involved in γδTc killing of tumor targets. Effectors and/or targets are pre-incubated with microgram quantities of monoclonal antibodies (mAb), often described by commercial sources to be useful for blocking assays. We and others have used such assays extensively in the past, correlating decreases in cytotoxicity against specific targets with involvement of the blocked receptor(s). However, we wondered whether other mechanisms might be at play beyond cytotoxicity inhibition. Indeed, administration of certain "blocking" mAb to the γδ T cell antigen receptor (γδTCR) induced γδTc death. Upon further investigation, we discovered that γδTc underwent apoptosis triggered by incubation with mAb to the γδTCR. This effect was specific, as no apoptosis was observed when αβ T cells (αβTc) were incubated with these mAb. Apoptosis was further potentiated by the presence of interleukin (IL)-2, often included in cytotoxicity assays; however, exogenous interleukin-2 (IL-2) did not contribute significantly to γδTc cytotoxicity against breast cancer cell lines. Here, we have investigated the usefulness of four mAb for use in blocking assays by assessing blocking properties in conjunction with their propensity to induce apoptosis in cultured primary human γδTc. We found that the 5A6.E9 clone was usually a better alternative to the commonly used B1 (or B1.1) and 11F2 clones; however, some variability in susceptibility to apoptosis induction was observed among donor cultures. Thus, viability assessment of primary effector cells treated with mAb alone should be undertaken in parallel with cytotoxicity assays employing blocking antibodies, in order to account for cytotoxicity reduction caused by effector cell death. Previous findings should be reassessed in this light.

2.1 Introduction

γδ T cells (γδTc) are potent tumor cell killers, thought to identify their targets *via* cell surface receptors such as the γδTc antigen receptor (γδTCR) and Natural Killer receptors, like NKG2D[115]. γδTc are particularly attractive for cancer immunotherapy, as they recognize antigens directly on transformed cells and kill quickly (with no need for priming or clonal expansion); among other advantageous features, expertly reviewed in[2], γδTc do not cause graft-versus-host disease[112]. In preclinical studies, we and others have shown that γδTc kill many types of hematological and solid malignancies[112,409]. Furthermore, *in vivo* expansion of γδTc has yielded promising results in Phase I clinical trials treating metastatic prostate cancer[410], renal cell carcinoma[411], advanced breast cancer[111], low grade non-Hodgkin lymphoma and multiple myeloma[184] reviewed together with adoptive γδTc immunotherapy trials in[203]. We aim to learn more about γδTc in the context of breast cancer, in order to further development of γδTc immunotherapy for this disease.

Determining the mechanism(s) of action employed by γδTc against tumor cells is crucial for their further development as immunotherapy for cancer. The antibody blocking assay is an accepted method to determine the receptors involved in γδTc cytotoxicity against tumor targets[147,148,155,188,209,210,412-420]. Effectors and/or targets are pre-incubated with microgram quantities of "blocking" mAb and then co-incubated for the cytotoxicity assay, whereby decreased cytotoxicity against targets is attributed to involvement of the blocked receptor(s). A wide range of pan anti-γδTCR antibody clones have been used in these assays, including 11F2[413,417], B1[209], B1.1[148,155,412,418,420], δTCS1[414,419] and Immu510[155,412], as well as a mAb specific to the Vγ9 TCR[147,415,416]. Please note that clones B1 and B1.1 anti-γδTCR mAb clones are considered to be one and the same, simply sold by different companies (Biolegend's Product Data Sheet for B1,

Application Notes). Unfortunately, tracing the origins of commercially sold antibodies whose generation has not been documented in the literature is challenging, if not impossible.

While *bona fide* blocking of the γδTCR may indeed hinder γδTc cytotoxicity, other mechanisms, such as effector cell death, may contribute to decreases in cytotoxicity, thus leading to false interpretation of assay results. Indeed, an early study using γδTc clones showed that apoptosis can be induced by TCR/CD3 signaling in as little as 4h incubation with soluble or immobilized 7A5 (recognising an epitope on the Vγ9 TCR chain) or BMA030 (anti-CD3) and that this process was interleukin-(IL-)2 dependent[421]. To our knowledge, no further studies have been undertaken to characterize other anti-γδ TCR mAb in this way. We decided to test four pan anti-γδTCR mAb clones, three of which have been used previously in such blocking assays: B1[209], B1.1[148,155,412,418,420] and 11F2[413,417] plus 5A6.E9 that, to our knowledge, has only been reported once in the context of γδTCR blocking in the literature[419]. We set out to determine the best clone and conditions to use to further our understanding of mechanisms of γδTc cytotoxicity against tumor targets, through the correct interpretation of assay results.

2.2 Materials and Methods

2.2.1 Ethics statement

This study was carried out in accordance with the recommendations of the Research Ethics Guidelines, Health Research Ethics Board of Alberta – Cancer Committee with written informed consent from all subjects. All subjects gave written informed consent in accordance with the Declaration of Helsinki. The protocol was approved by the Health Research Ethics Board of Alberta – Cancer Committee.

2.2.2 Primary γδ T cells

Primary human γδTc and αβTc cultures were established and maintained as described.[412] Briefly, peripheral blood mononuclear cells (PBMCs) were isolated from healthy donor blood using density gradient separation (Lymphoprep, Stem Cell Technologies, Vancouver, BC) and cultured at 1 x 10^6 cells/ml in RPMI complete medium containing 1μg/ml Concanavalin A (Sigma-Aldrich, Oakville ON), 10% Fetal Bovine Serum (FBS), 1x MEM NEAA, 10 mM HEPES, 1 mM Sodium Pyruvate (all Invitrogen, Burlington, ON) plus10 ng/ml recombinant human IL-2 and IL-4 (Miltenyi Biotec, Auburn CA). Every 3-4 days, cells were counted and densities adjusted to 1 x 10^6 cells/ml by addition of fresh medium and cytokines. Cells were maintained in a humidified atmosphere at 37°C with 5% CO_2. After 1 week, αβ T cells were depleted after labeling with anti-TCRαβ PE antibodies (BioLegend, San Diego, CA, USA) and anti-PE microbeads (Miltenyi Biotec), filtering through a 50 μm Cell Trics filter (Partec, Görlitz, Germany) and running through an LD depletion column (Miltenyi Biotec). The flow-through contained γδ T cells, which were further cultured in RPMI complete medium plus cytokines (as above) at 37°C with 5% CO_2. For some experiments, the positively selected αβ T cells were also recovered and maintained. For cytotoxicity experiments, γδTc cultures were used at the end of the culture period (day 19-21), as they were most differentiated and therefore most cytotoxic at this time. Blocking assays were also typically done at this time, to mimic conditions used for cytotoxicity assays. Some experiments were done at earlier time points (days 14-16) and susceptibility to mAb-induced cell death did not appear to be significantly different, although this was not tested directly. Donor cultures are identified as follows: donor number – culture number; thus, 3-2 = the second culture derived from donor 3.

2.2.3 Breast cancer cell lines

Breast cancer cell lines MCF-7, T47D and MDA-MB-231 were obtained from the American Type Culture Collection (ATCC, Manassas, VA, USA) and maintained as per ATCC guidelines.

2.2.4 Calcein AM labeling of target cells

Target cells were labeled with 5μM Calcein AM (CalAM) as per manufacturer's instructions (Invitrogen/Thermo Fisher Scientific, Waltham, MA, USA). Cells were diluted to a density of 30,000 cells/100 μl medium for use in cytotoxicity assays.

2.2.5 "Blocking" Antibodies

The following anti-human anti-γδTCR mAb clones were used: B1 (BioLegend, San Diego, CA, USA), B1.1[422] (eBioscience, San Diego, CA, USA), 5A6.E9[423] (Thermo Fisher Scientific, Waltham, MA, USA) and 11F2[424] (Becton Dickinson, Mississauga, ON, Canada); mouse IgG (Sigma-Aldrich, Oakville, ON, Canada) was used as a control. The anti-NKG2D antibody was purchased from BioLegend (Clone 1D11). For immobilization, mAb were diluted at 1μg/ml in PBS, then plated at 100 μl/well and incubated overnight at 4°C. Prior to blocking assays, the plates were washed twice with PBS.

2.2.6 Blocking/Cytotoxicity Assay

γδTc cells were re-suspended at 6 x 10^6 cells/ml in complete medium (RPMI 1640 with 10% fetal bovine serum, heat-inactivated, 1 x MEM NEAA, 10 mM HEPES, 1 mM sodium pyruvate, 50 U/ml Penicillin-Streptomycin and 2 mM L-Glutamine – all from Invitrogen) plus 20 ng/ml recombinant human IL-2 (Miltenyi Biotec, Auburn, CA, USA) where indicated. For Fc blocking experiments, 5 μl Human TruStain FcX (BioLegend, San Diego, CA, USA) were added per 600,000 cells in 100 μl and incubated for 10 min at room temperature prior to the addition of

mAb. 6 µg mAb were added to 600 µl cell suspension/test in Eppendorf tubes, then 100 µl/well plated in a 96 well round-bottomed plate. After incubation at 37°C for 30 minutes, 100 µl complete medium only (blocking assay only), or CalAM-labeled targets were added (cytotoxicity assay). After further incubation at 37°C for 4 h, two wells/condition of re-suspended cells were pooled and stained for flow cytometry (blocking assay only). Experimental controls were untreated and IgG-treated cells. For cytotoxicity assays, plates were centrifuged and supernatants transferred to fresh 96-well plates (Falcon, U bottom, low evaporation) for CalAM fluorescence detection on a fluorimeter (FLUOstar Omega, BMG labtech). Controls were CalAM-labeled target cells incubated alone (spon = spontaneous release) and 0.05% Triton-X 100 (Thermo Fisher Scientific)-treated cells (max = maximum release). Percent lysis was calculated: [(test-spon)/(max-spon)] x 100%.

2.2.7 Flow cytometry

2.2.7.1 γδ T cell subset identification

Cultured γδTc were stained first with 5ng/µl Zombie Aqua fixable viability dye (BioLegend) and then with anti-TCR Vδ1 FITC (Thermo Fisher Scientific, clone TS8.2, 1:10), anti-TCR Vδ2 PerCP (Biolegend, clone B6, 1:50), and anti-TCRγδ PE (Biolegend, clone B1, 1:25). After staining and washing, cells were fixed in FACS buffer plus 2% paraformaldehyde, stored at 4° C and analyzed by flow cytometry within one week. Subset and purity data for all cultures are shown in Table S1.

2.2.7.2 Detection of apoptosis

Cultured γδTc were first stained with 5ng/µl Zombie Aqua fixable viability dye (BioLegend) for 15-20 minutes, washed with 1x Annexin V (AnnV) binding buffer (BioLegend)

and then stained on ice for 15 min in the dark with AnnV FITC (BioLegend, 1:20). Cells were washed and re-suspended in 200uL AnnV binding buffer plus 2% **paraformaldehyde** and stored at 4° C until analyzed. Flow cytometry was performed on a FACS Canto II (Becton Dickinson, Mississauga, ON), calibrated with Cytometer Set-up and Tracking (CS&T) beads (Becton-Dickinson). Gating in forward and side-scatter was done only to exclude debris; quadrant gates were set using single-stain controls. Analysis was performed using FlowJo© software (Tree Star, Ashland, OR, USA, Version 10.0.8).

2.2.8 Stimulation Experiments

γδTc were incubated for 4 h at 37° C, 5% CO_2 in serum-free and cytokine-free medium; they were then stimulated with 1μg mAb for 1 min at 37° C. Anti-CD3 (UCHT1, BioLegend) stimulated cells were a positive control. Lysates were run on 12% SDS PAGE and Western blotting performed using a 1:400 dilution of the PathScan® Multiplex Western Cocktail I (Cell Signaling Technology, Danvers, MA, USA) to detect phosphorylated signaling proteins.

2.2.9 Statistics

Paired 1-tailed Student's t-tests were performed (Fig. 2E-G only) using Microsoft Excel version 15.3 (Microsoft, Redmond, WA, USA). ANOVA analysis followed by Bonferroni's pairwise multiple comparison posthoc tests were performed using Prism 7.0 for Mac OSX, GraphPad Software, San Diego, CA, USA). Differences were considered significant when $P < 0.05$; degrees of significance are indicated by letters or asterisks as defined in the figure legends.

2.3 Results

2.3.1 An alternate explanation for reduced cytotoxicity upon treatment with "blocking" antibody.

Incubation of γδTc with anti-human pan γδTCR mAb clones B1, 5A6.E9 and 11F2 reduces the cytotoxicity of human γδTc against T47D breast cancer cells by 1.6 to 2.8-fold /14-25% compared to IgG controls (Fig. 2.1A). Yet if all three mAb perform an equivalent blocking function, we would expect the same decrease in lysis to occur in all cases. On the contrary, there was less reduction in average cytotoxicity with 5A6.E9 (12%) compared to 11F2 (22%) and B1 (25%) clones. One-way ANOVA followed by Bonferroni's multiple comparisons test revealed significant differences in cytotoxicity for B1- and 11F2-blocked γδTc ($p = 0.0023$ and $p = 0.0051$ respectively), whereas the decrease in cytotoxicity with 5A6.E9 mAb was not significant ($p = 0.1065$) compared to IgG. This lead us to further investigate whether other mechanisms may be at play. Untreated controls were included in parallel to IgG and mAb treatments in most experiments, to verify similarity to IgG controls. However, statistical analyses reported herein focus on mAb versus IgG treatments; for simplicity, statistical analyses of mAb versus untreated control samples are not shown.

When we incubated γδTc alone with anti-γδTCR (B1), anti-NKG2D or IgG control antibodies for 4.5 h, in the absence of targets, uptake of Zombie Aqua (ZA) viability dye indicated increased cell death in B1- but not in anti-NKG2D-treated cells (Fig 2.1B, gating controls in Fig 2.S1A). Thus, the decrease in cytotoxicity observed after γδTCR "blocking" appears to be at least

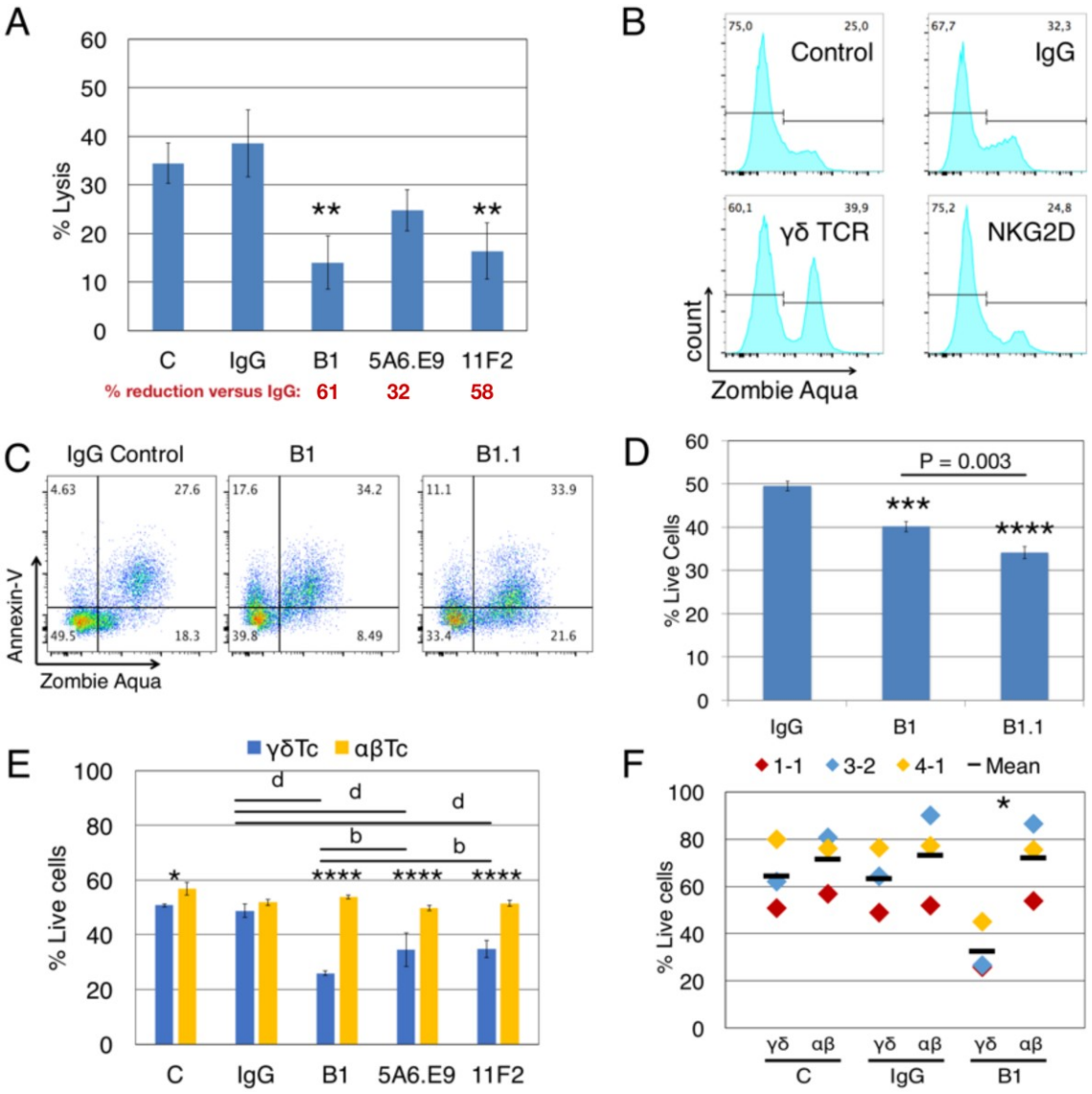

Figure 2.1 Anti-γδ TCR antibodies reduce lysis of breast cancer cells concomitant with γδT cell death. (**A)** Donor 1 day 21 primary human γδ T cells were pre-incubated for 30 min with (1µg/well) or without antibodies (C=control), then incubated with calcein AM-labeled T47D targets in triplicate at a 20:1 effector:target (E:T) ratio for 4 h. A significant reduction in %lysis was observed in the presence of anti-γδ TCR antibodies. Percent reduction compared to IgG (red font) was calculated: 100 - (% lysis or live cells treated with antibody/IgG*100). (**B)** Representative example showing that treatment of 600,000 Donor 2 day 14 γδ T cells for 4.5 h with 1 µg antibody alone induces cell death as evidence by zombie aqua viability dye uptake. (**C)** Representative example indicates induction of apoptosis in Donor 3 day 21 γδ T cells *via* antibody treatment as in **B**. (**D)** Summary of results from experiment shown in **C**. (**E)** Treatment of Donor 1 αβ T cells with anti-TCRγδ antibodies does not cause cell death. (**F)** Compiled results for 3 independent experiments focusing on B1 versus IgG. Error bars indicate standard deviation (n=3); Significant differences compared to IgG controls (A, D) or between αβ and γδ T cells (E, F) were determined by one way (A, D) or two way (E, F) ANOVA followed by Bonferroni's multiple comparison test (*p<0.05, ** p<0.01, *** p<0.001,**** p<0.0001; b, p<0.01, d, p<0.0001)

partially due to the untimely death of a significant proportion of effector γδTc. Importantly, this did not occur when anti-NKG2D was used, suggesting that prior interpretations implicating NKG2D in cytotoxicity were not compromised by the induction of effector cell death described here. To further define this cell death, we extended our experiments to include Annexin V (AnnV) staining for the detection of apoptotic cells via flow cytometry[425]. We categorized cell death into early apoptotic (AnnV+/ ZA-), late apoptotic (AnnV+/ ZA+) and necrotic (AnnV-/ ZA+) fractions. Treatment of γδTc with B1 and B1.1 anti-γδTCR blocking mAb resulted in increased apoptotic cell death compared to IgG controls, in both early (17.6% and 11.1% versus 4.6%) and late apoptotic compartments (34.2% and 33.9% versus 27.6%) in a representative example (Fig. 1C, gating controls in Fig. 2.S1B); combined results for technical replicates from this experiment are also shown (n=3, Fig. 2.1D). One-way ANOVA followed by Bonferroni pairwise multiple comparison posthoc analysis revealed significant reductions in cell viability after incubation with B1 ($P = 0.0003$) and B1.1 ($P < 0.0001$) mAb compared to IgG. Surprisingly, a significant γδTc viability difference was also found comparing B1 and B1.1 ($P = 0.0003$), considered to be the same mAb, simply sold by different companies. The Biolegend product data sheet for B1 states "Clone B1 is also known as clone B1.1"; however, the nomenclature would suggest that B1.1 is a subclone of B1. Unfortunately, we were unable to learn anything about the generation of these clones, which is not reported in the literature. Since the effect (viability loss) was always similar in experiments carried out with both antibody clones (data not shown), yet B1.1 had a more significantly negative effect on γδTc, we used B1 for all experiments moving forward.

Induction of cell death *via* anti-γδTCR incubation was specific to γδTc, since the viability of αβTc expanded in parallel from the same donor was not compromised by incubation with B1, 5A6.E9 or 11F2 (Fig. 2.1E). αβTc viability remained unchanged, while once again, the strongly significant reduction in γδTc viability after treatment with B1, 5A6.E9 and 11F2 compared to IgG,

was confirmed ($p < 0.0001$). Notably, there was also a significant difference in viability between B1 and 5A6.E9 ($p=0.0034$) as well as between B1 and 11F2 ($P=0.0040$), demonstrating that the detrimental effect of B1 is greater than that of the other two clones. While there was a significant difference in γδTc versus αβTc viability in the control samples, which is understandable, as these are two different cultures (albeit derived from the same donor), there was no difference in αβTc viability among antibody treatments or controls. Three independent experiments with three different donor cultures testing B1 compared to IgG and control are shown and the significant drop in γδTc viability after incubation with B1 was confirmed (Fig. 2.1F, $p = 0.02$).

To determine whether stimulation with anti-γδTCR mAb clones differentially activates γδTc, we stimulated effector γδTc for 1 minute with anti-γδTCR mAb and used anti-CD3 stimulation with the UCHT1 clone as a positive control for activation. While clones B1 and B1.1 did not cause phosphorylation of signaling proteins AKT, ERK1/2 or S6 above that of the unstimulated control, clones 11F2 and 5A6.E9 elicited a phosphorylation pattern similar to that obtained with anti-CD3 stimulation (UCHT1) suggesting active signaling (Fig. 2.S2). Rab11 served as an internal loading control. Clones B1 and B1.1 behaved as blocking antibodies should, by not inducing activation; however, a lack of survival signaling through phosphoAKT cannot account for the cell death observed in B1-treated γδTc, since the untreated control cells in our blocking experiments did not die to the same extent, although their activation patterns are quite similar (Fig. 2.S2, compare lanes 1-3).

2.3.2 IL-2 enhances apoptotic cell death induced by anti-γδTCR antibody treatment.

We tested whether exogenous IL-2 impacts the viability of γδTc in the presence of B1, 5A6.E9 or 11F2 mAb in a 4.5 h assay. Representative dot plots show that incubation with mAb

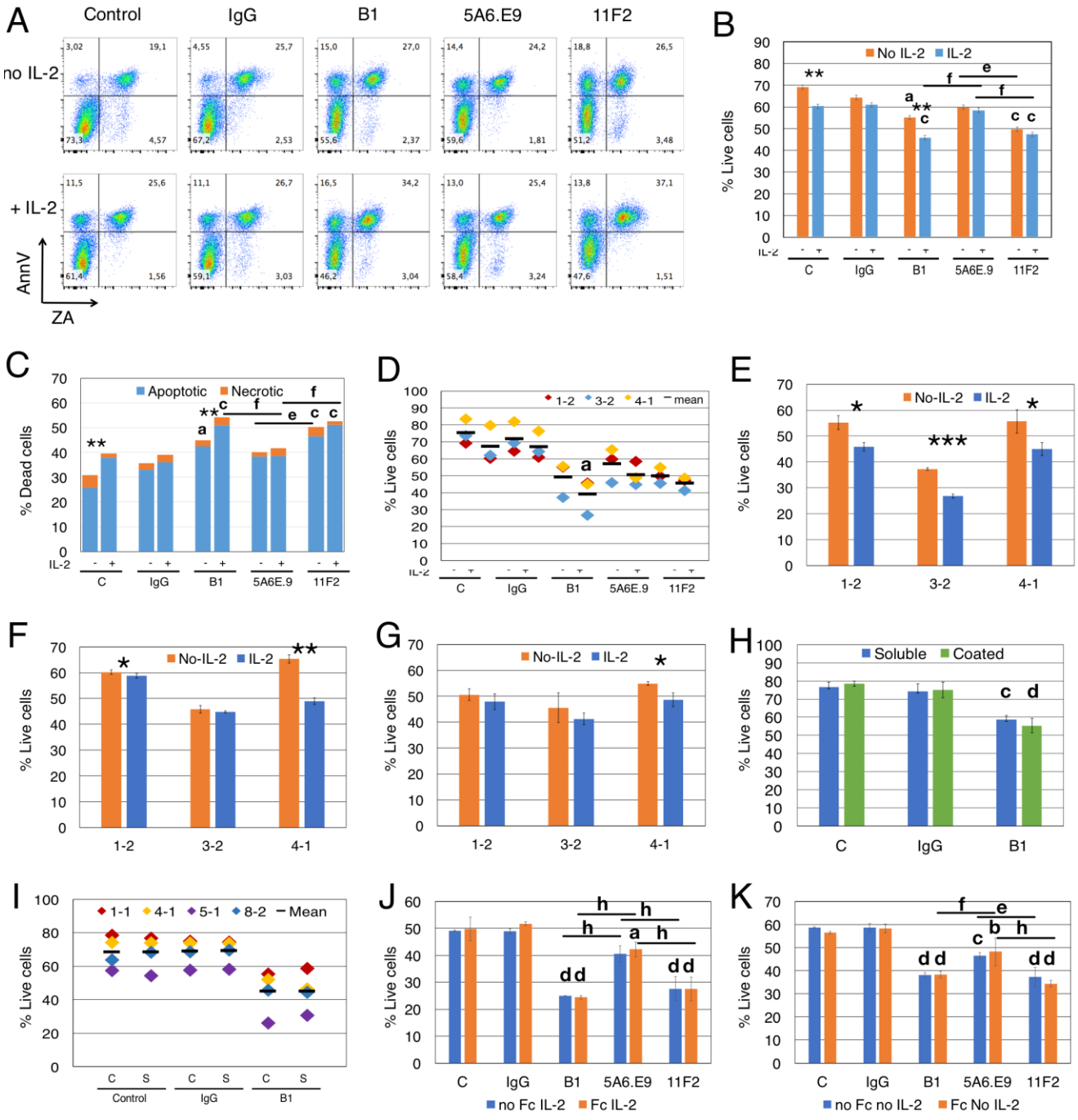

Figure 2.2. Anti-γδTCR antibodies induce apoptosis, and effects are exacerbated by IL-2. (A) Addition of IL-2 to blocking assays increases apoptotic cell death of γδ T cells (Donor 1, culture =1-2). Apoptotic cells are annexinV(AnnV) positive; early apoptotic cells are in the top left quadrant. Positive staining for Zombie Aqua (ZA) indicates dead cells. (**B**) For the experiment shown in **A**, % live cells are plotted for γδ T cells treated with antibodies for 4.5 h in the presence or absence of IL-2. Error bars are standard deviation for technical replicates. This experiment is representative of three biological replicates. (**C**) Most cell death induced by antibody treatment is apoptotic cell death (blue) and is enhanced in the presence of Il-2; orange indicates necrotic cell

death. The graph depicts results from the experiment shown in **A** and **B**. (**D**) Compiled results of experiment shown in panel (B) from three different donor cultures (1-2,3-2 and 4-1). **(E)** Individual experiments in which γδ T cells were incubated with B1, **(F)** 5A6.E9 or **(G)** 11F2. In **E**, **F** and **G**, Student's t-tests reveal a significant difference in cell viability in the presence or absence of IL-2; (*$p<0.05$, ** $p<0.01$, *** $p<0.001$, **** $p<0.0001$). (**H)** No differences in cell death were induced by soluble or immobilized (coated) B1 antibody treatment; however, significant cell death is observed comparing soluble B-1 to IgG- treated cells. This is a representative example of three independent experiments; for this experiment, cells were from culture 1-1 on day 16. **(I)** Compiled results of experiment shown in F with four different donor cultures (1-1, 4-1, 5-1 and 8-2). **(J)** A representative example of two independent experiments in which γδ T cells were incubated with or without Fc blocking reagent for 10 min at room temperature prior to the addition of antibodies in the presence of IL-2. Shown here is the experiment with donor culture 8-2. **(K)** The experiment in J carried out in the absence of IL-2. Statistical analyses for all but E,F and G were as follows: two way ANOVA followed by Bonferroni's multiple comparisons tests were performed to identify significant differences between antibody-treated and IgG-treated cells (a, $p<0.0.5$; b, $p<0.01$; c, $p<0.001$; d, $p< 0.0001$) or among antibody treatments (line indicates groups compared; e, $p<0.05$; f, $p<0.01$; g, $p<0.001$; h, $p< 0.0001$) as well as to determine significant viability differences in the presence or absence of IL-2 (* $p<0.05$, *** $p<0.001$)

resulted in an increase in both early apoptotic (AnnV+/ZA-) and late apoptotic (AnnV+/ZA+) γδTc, even in the absence of exogenous IL-2 (Fig.2.2A, gating shown in Fig. 2.S1C). Two-way ANOVA followed by Bonferroni's multiple comparison posthoc statistical analysis revealed significant loss of γδTc viability due to IL-2 only in control ($p < 0.0074$) and B1-treated groups ($p = 0.0042$, Fig. 2.2B). In contrast, no IL-2-induced differences in viability were observed in cell populations treated with IgG, 5A6.E9 or 11F2 mAb; however, both B1 and 11F2 mAb decreased γδTc viability significantly compared to IgG controls. Notably, 5A6.E9 treatment did not elicit significant loss of cell viability compared to IgG in this experiment. In the presence of IL-2, 5A6.E9 treated cells were more viable than those incubated with B1 ($p = 0.0016$) or 11F2 ($p = 0.0067$); the decrease in γδTc viability after incubation with 11F2 compared to 5A6.E9 in the absence of IL-2 was also deemed significant ($p = 0.0163$). Importantly, the difference in average γδTc viability between IgG- and B1-treated cells could account for a large proportion (if not all) of the decrease in cytotoxicity associated with the use of this mAb in blocking experiments. The cell death associated with mAb incubation was mostly apoptotic cell death (Fig 2.2C), with significant increases in IL-2-dependent cell death observed in control and B1-treated γδTc. Statistical analysis performed on cell death data shown in Fig. 2C revealed the same results as in the reciprocal live cell data in Fig. 2.2B.

We compiled the results for three independent experiments and statistical analysis thereof confirmed significant loss of cell viability ($p = 0.0308$) in B1- but not in 11F2- or 5A6.E9-treated γδTc compared to IgG in the presence of IL-2 (Fig 2.2D). To further demonstrate this effect, we show the impact of IL-2 on B1-treated cells from all three experiments (Fig. 2.2E); a synergy was observed between B1 and IL-2 that resulted in significant loss of cell viability compared to B1 treatment in the absence of IL-2. This loss was evident in all three cultures, but was most pronounced in the experiment performed with Donor culture 3-2 ($p = 0.0006$). Looking more

closely at 5A6.E9 treatments of these three cultures (Fig. 2.2F) revealed a small but significant difference with IL-2 in culture 1-2 (60.3 ± 1.0 versus 58.8 ± 0.8% live cells, without or with IL-2, respectively, $p = 0.039$), and sensitivity of 4-1 to IL-2 combined with this clone ($p = 0.0048$). Culture 4-1 viability was also decreased significantly with combined 11F2 and IL-2 treatment (Fig. 2.2G, $p = 0.029$). The full experiment done with culture 4-1 is shown in Fig. S3B. No significant difference in γδTc viability was observed among the three mAb-treated groups in the presence of IL-2 (Fig. 2.S3B, $p > 0.9999$). In the absence of IL-2, 5A6.E9 elicited the least degree of γδTc cell death, and was significantly better than both B1 ($p = 0.0026$) and 11F2 ($p = 0011$), which were equally detrimental (Fig. 2.S3B). Donor culture 4-1 was 78.8% $V\delta2^+$ (Fig. 2.S3A, Table 2.S1), whereas 1-2 with 14.9% and 3-2 with 50.8% $V\delta2^+$ (Table S1) exhibited little to no difference in viability upon incubation with 5A6.E9 or 11F2, with or without IL-2 (Figs. 2.2F, G).

Western blot analysis of cleaved Caspase 3 in total cell lysates did not reveal clear differences among IL-2-treated and untreated cells or mAb treatments over 4.5h; however, this is a less sensitive method than flow cytometry, thus it was not surprising that we were unable to detect ~10% differences (data not shown).

We found no differences in γδTc viability when comparing the use of soluble and immobilized mAb, all in the absence of IL-2; however, B1 treatment resulted in a significant loss of viability compared to IgG-treated γδTc in both cases in the representative example shown (soluble, $p < 0.0005$; coated, $p < 0.0001$; Fig. 2H). When we included 5A6.E9 and 11F2 in this experiment, again no differences in viability were observed using soluble or immobilized mAb, but significant viability losses compared to IgG were noted (Fig. 2.S4). When we compiled results for control, IgG and B1 treatments from four independent experiments, no significant differences were identified (Fig. 2.2I). This is likely due to inter-donor variation, suggesting that variability in

cell viability among donors is greater than that observed after treatment with soluble or immobilized mAb.

We tested whether the Fc receptor might be involved in apoptosis induced by mAb treatment, but found that there were no differences in viabilities of γδTc that were or were not pre-treated with an Fc blocking reagent prior to mAb incubation Figs. 2J, K). This was true whether IL-2 was present (Fig. 2.2J) or not (Fig. 2.2K). Significant decreases in viability were noted for mAb treated cells (Figs. 2.2J, K), confirming previous results (Figs.2. 2A-I).

To understand the kinetics of apoptosis, we performed a time course experiment that revealed a highly significant decrease in live cells after 3.5 h of stimulation with B1 that extended to 4.5 h ($p < 0.0001$, Fig.2.S5A); of note, there was a significant difference in viability, compared to IgG-treated cells, at the 30-min time point ($p = 0.043$), but this was no longer evident at 1.5 and 2.5 h post mAb treatment. A graph showing the percentage of dead cells over time is also shown (Fig. 2.S5B). Since cytotoxicity experiments are usually conducted over a minimum of 4 h, this loss of effector viability should be taken into account.

2.3.3 IL-2 is not required for assessment of γδTc cytotoxicity against breast tumor targets.

Since the presence of IL-2 during blocking mAb treatment caused unwanted γδTc death, we investigated whether IL-2 is necessary for assessment of γδTc cytotoxicity against breast tumor targets. In the representative example shown, IL-2 did not significantly enhance γδTc cytotoxicity against T47D at any effector:target ratio tested (Fig. 2.3A). This was also true for the individual and compiled results of four independent experiments testing γδTc cytotoxicity against T47D (Fig. 2.3B). We further confirmed these results in cytotoxicity assays against MCF-7 (Fig. 2.3C and D) and MDA-MB-231 (Fig. 2.3E and F) targets. In each case at all ratios tested, there was no

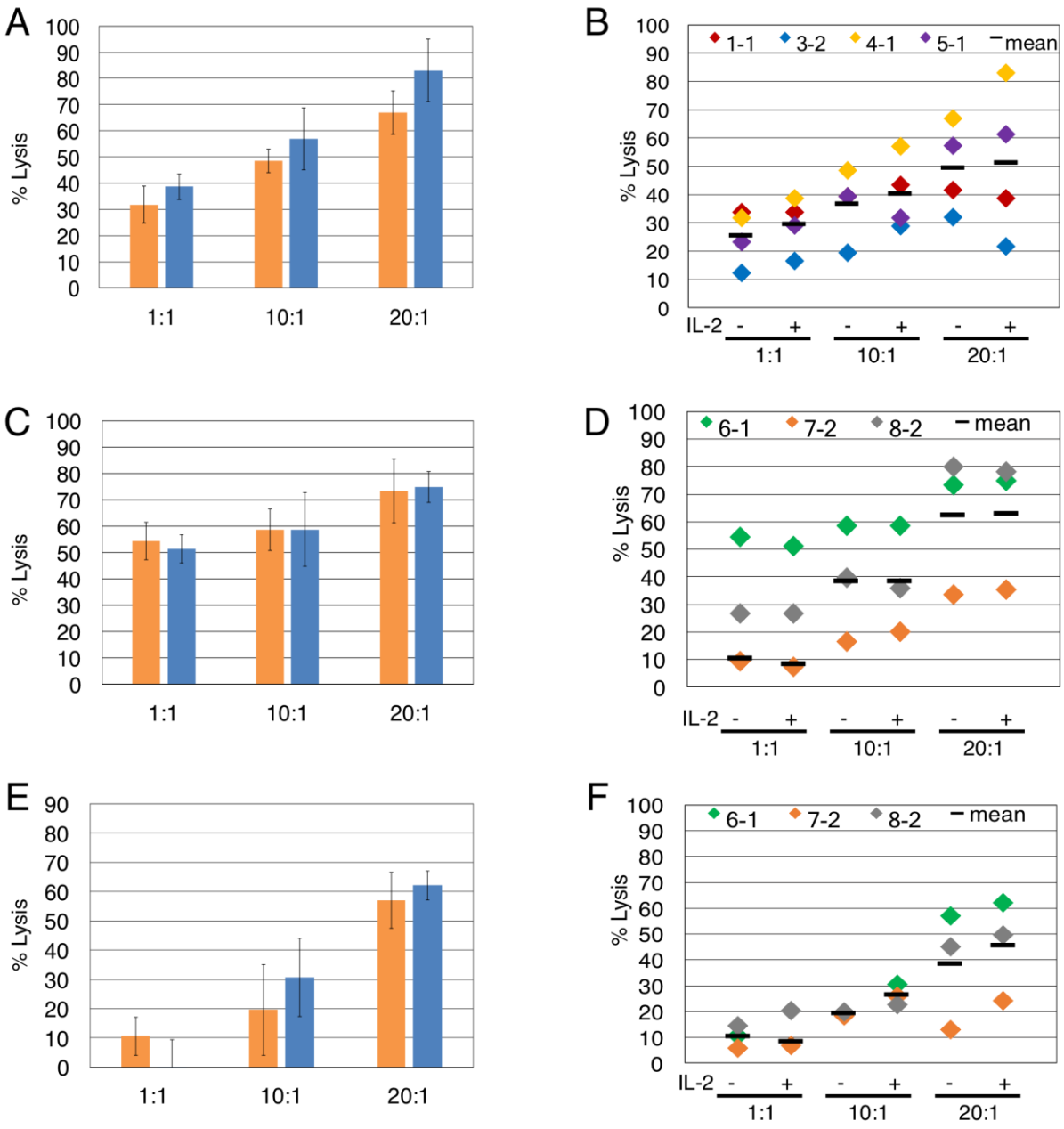

Figure 2.3. The presence of Il-2 does not significantly impact γδ T cell cytotoxicity against breast cancer cell lines. Comparison of γδ T cell cytotoxicity, at the indicated effector:target ratios, in the absence (orange) or presence (blue) of IL-2, against **(A)** T47D (Donor 4, culture 1, day 21 γδ T cells), representative of four independent experiments. **(B)** Compiled results of four independent cytotoxicity experiments using T47D cells as targets. **(C)** MCF-7 (Donor 6 day 19 γδ T cells), representative of three independent experiments. **(D)** Compiled results of three independent cytotoxicity experiments using MCF-7 cells as targets. **(E)** MDA-MB- 231breast cancer cell targets (Donor 6 day 19 γδ T cells). **(F)** Compiled results of three independent cytotoxicity experiments using MDA-MB- 231 cells as targets. Two way ANOVA followed by Bonferroni's multiple comparisons analysis were performed for all experiments; no significant differences were revealed.

significant difference in cytotoxicity of γδTc against breast tumor targets in the presence or absence of IL-2 (Fig.2.3).

2.3.4 A decrease in lysis of targets can be partially explained by effector cell death upon stimulation with anti-γδTCR antibodies and thus should be controlled for in γδTCR blocking experiments.

Taking all of our previous results into account, we designed parallel blocking-only and blocking plus cytotoxicity assays, in the absence of IL-2, in order to assess the involvement of γδTCR in killing T47D breast tumor targets, while considering anti-γδTCR mAb-induced effector cell death. Lysis of T47D targets was reduced dramatically upon treatment of γδTc with anti-γδTCR mAb; however, incubation with 5A6.E9 did not reduce lysis to quite the same extent, as significant differences in cytotoxicity observed after treatment with B1 ($p = 0.0072$) and 11F2 ($p = 0.0128$) versus 5A6.E9 were evident (Fig. 2.4A). In line with these data, 5A6.E9 also induced significantly less cell death in these donor γδTc compared to B1, as did 11F2 (Fig. 2.4B, both $p < 0.0001$ versus B1). Looking at the percentage of reduction in lysis or live cells compared to IgG, it is evident that at least half of the decrease in percent lysis attributed to γδTCR blocking by B1 is due to γδTc death, as opposed to blocking interactions between effectors and targets. In this experiment, 5A6.E9 and 11F2 appear to be the better clones for blocking, as γδTc viability was only reduced by 14% and 23%, respectively, compared to IgG, while they still caused 63% and 87% reductions in lysis of T47D (Fig. 2.4A, B). A compilation of data from three independent experiments confirmed a decrease in percent lysis of T47D upon treatment with all three anti-γδTCR mAb clones; however, there was considerable variability in observed cytotoxicity of these different donor cultures against T47D breast cancer targets, rendering differences among treatment groups insignificant (Fig. 2.4C). In contrast, significant reductions in γδTc viability remained

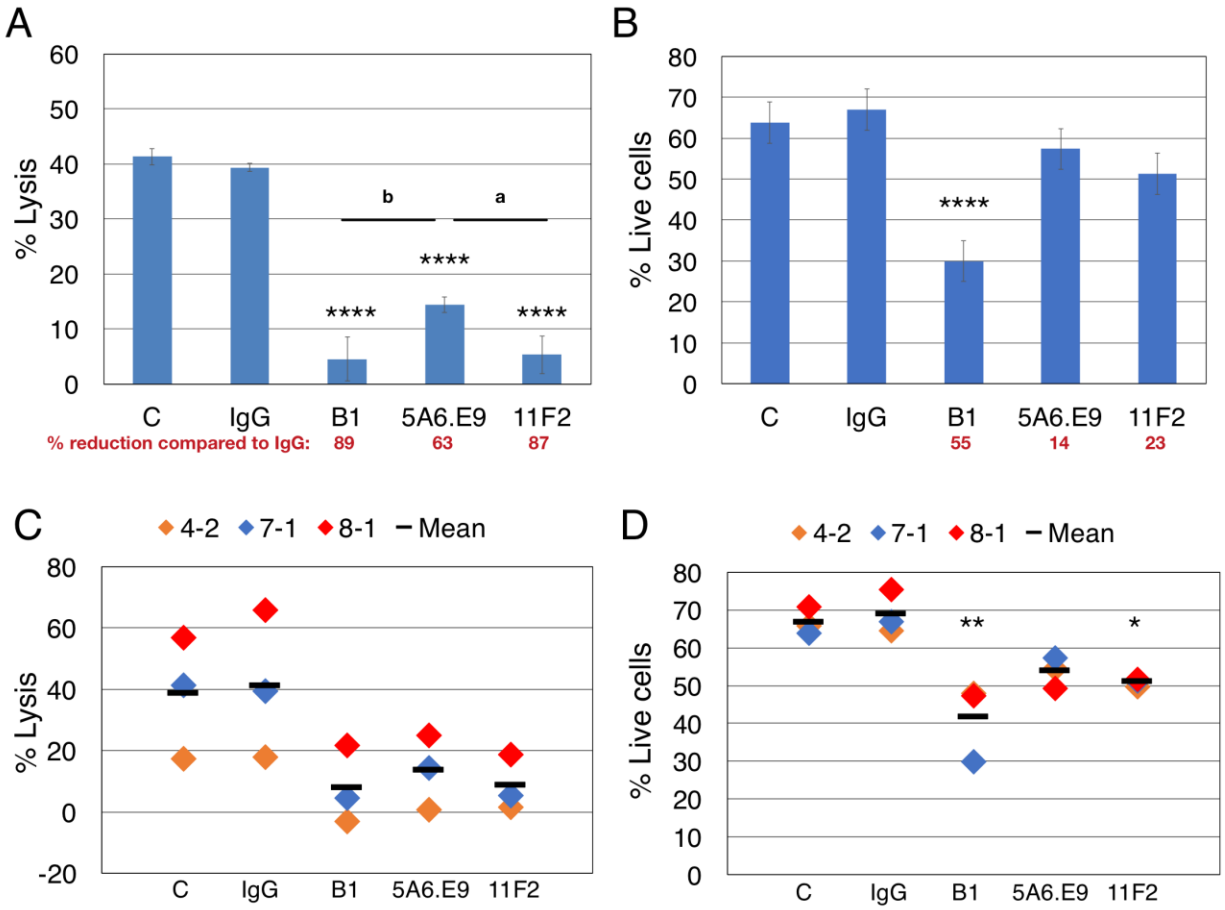

Figure 2.4. Effector blocking alone and blocking cytotoxicity assays should be performed in parallel to account for apoptosis induced by anti-γδTCR antibodies. (A) Donor 7 day 19 primary human γδ T cells were pre-incubated for 30 min with the indicated antibodies (1µg/well) and then incubated with calcien AM-labeled targets in triplicate at a 20:1 effector:target (E:T) ratio for 4 h. **(B)** 600,000 Donor 7 day 19 γδcT cells were stimulated with 1µg of the indicated antibodies for 4.5 h and labeled with zombie aqua viability dye and annexinV FITC; shown are the %live cells that excluded the uptake of dye and were negative for AnnexinV. (**C)** Complied blocking and cytotoxicity results of three independent experiments. (**D**) Compiled blocking and viability results of three independent experiments. **A** and **B** were done in parallel, as were experiments shown in **C** and **D**. A significant reduction in % lysis (**A, C**) or %live cells (**B**, **D**), was determined by one way ANOVA followed by Bonferroni's pairwise multiple comparison post hoc analysis (*p<0.05, ** p<0.01, *** p<0.001, **** p<0.0001 versus IgG; Among antibody treatments (as indicated): a, *p<0.05; b, p<0.01). Percent reduction compared to IgG (in red font) was calculated 100- (%lysis or live cells treated with antibody/IgG *100).

evident, despite interdonor variation, after treatment with B1 and 11F2, but not 5A6.E9 mAb (Fig. 2.4D). These data confirm results shown in Fig. 2.2A-D.

2.4 Discussion

A reduction of γδTc cytotoxicity against tumor targets following incubation with pan γδTCR blocking mAb has been attributed to γδTCR involvement in killing[148,209,412-415,417,419,420], yet we have discovered that certain anti-γδTCR antibodies cause γδTc apoptosis. This mechanism may be Fas-dependent, suggested by the uncoupling of TCR signaling and apoptosis revealed by anti-CD3 stimulation of mature conventional T cells in wild type (B6) versus Fas-deficient (B6.lpr) mice (Fas-deficient T cells did not undergo apoptosis)[426].

Gan and colleagues also described Fas-dependent apoptosis of Daudi-activated but not naïve human γδTc stimulated with 5A6.E9 in the context of magnetic cell separation[427]. While Fas was present throughout, surface expression of FasL on re-stimulated cells was most pronounced at 8 h post-stimulation, suggesting that an incubation time of 4 h for a cytotoxicity assay is appropriate to avoid even more pronounced effector cell death[427]. Our kinetics experiment with B1-treated γδTc showed that appreciable cell death was first detectable between 3.5 and 4.5 h (Fig. S5), supporting even shorter incubation times. In line with most of our results with 5A6.E9 (Fig. 2A-D, F), the presence or absence of IL-2 in culture after stimulation did not alter the rate or extent of γδTc cell death[427].

We typically include exogenous IL-2 in our cytotoxicity assays (Fig. 1), since IL-2 is thought to enhance the cytotoxic potential of γδTc. While not inducing cytotoxicity on its own, IL-2 increased Vδ2 γδTc lysis of Daudi Burkitt's lymphoma and TU167 squamous carcinoma cell lines in a dose-dependent manner in the presence of tumor cells or phosphoantigen[428]. Janssen and colleagues determined that the apoptotic effect of TCR stimulation was IL-2 dependent[421]; such

synergy was also evident in γδTc treated with the B1 anti-γδTCR clone in the presence of IL-2 (Fig. 2). In published reports of *in vitro* γδTc cytotoxicity against breast cancer cell lines, it is unclear whether IL-2 was included in the assays[188,197]. Our data suggest that exogenous IL-2 is unnecessary for the assessment of γδTc cytotoxicity against breast cancer cell lines (Fig. 3) and indeed its propensity to drive activated T cells into apoptosis[429] further warrants its exclusion from such assays.

Our experiments have revealed that the 5A6.E9 clone is a better mAb to "block" the γδTCR than B1, as it typically induced the least amount of apoptosis and appeared not to synergize with IL-2 to enhance this unwanted effect; however, this behaviour was somewhat donor- and likely γδTc subset-dependent (Fig. 2A-D, F), further discussed below).

We admittedly did not screen every available anti-γδTCR antibody in our assays, but rather sought to document this unwanted effect in order to encourage investigators to consider this issue when performing their own blocking experiments. It is possible that primary γδTc generated using other protocols may be more or less sensitive to apoptosis induction via B1 or 11F2. Thus, it will be important for researchers to test blocking mAb on γδTc cultured using their own protocols. For example, Guo and Lopez' apoptosis-resistant γδTc[430] may be less susceptible to B1-induced apoptosis than γδTc cultured in our lab[412]. In that study, it is unclear which anti-γδTCR clone was used for blocking[430]; however, the best way to assess γδTc susceptibility to apoptosis upon anti-γδTCR treatment would have been to perform blocking assays on γδTc alone and assess viability in parallel with cytotoxicity assays, as we have done here (Fig. 4).

We did not test V-segment-specific mAb in our study; however, Janssen and colleagues have shown that Vγ9-specific mAb 7A5 induced apoptosis in γδTc clones, potentiated by addition of IL-2[421]. The extent of apoptosis was the same with soluble or immobilized mAb, as we also observed with B1 (Figs. 2H, I). It could be informative to determine whether other V-segment-

specific mAb induce γδTc apoptosis; if researchers propose to employ these mAb in blocking experiments, then it would indeed be important to test for this effect in advance. If apoptosis induction is evident, these mAb may be employed for specific *in vivo* elimination of these cells. Furthermore, if we could map the epitopes recognized by pan-γδTCR and V-segment-specific mAb that induce apoptosis in γδTc, perhaps small molecules could be designed to induce apoptotic signaling pathways and thereby deplete specific γδTc subsets implicated in various pathologies *in vivo*.

Controversy over the effectiveness of *in vivo* depletion strategies was addressed by Koenecke and colleagues, who determined that injection of anti-γδTCR mAb into mice did not delete γδTc as expected, but rather caused receptor internalization, rendering the cells "invisible"[431]. Kinetics experiments revealed, however, that ~10-20% of γδTc were indeed lost as of 14 days; the authors attributed this to activation-induced γδTc death[431], which is what we observed here on a much shorter time scale *in vitro*. While GL3 and UC7-13D5 mAb recognize at least partially overlapping epitopes, the higher affinity of GL3 led to greater TCR internalization[431], confirming that even mAb recognizing similar structures have differential effects and should therefore be tested and chosen wisely.

In our hands, in separate experiments, B1 mAb stimulation typically resulted in an average γδTc viability loss of ~10-15% (Figs. 1D, 2B-G). This was in line with cytotoxicity differences observed comparing blocking with B1 to 5A6.E9 (38.6% – 24.8% = 13.8%), suggesting that roughly half of the dramatic "blocking" effect observed upon B1 incubation can be attributed to unintended induction of apoptosis in γδTc. While in assays done in parallel these numbers were higher (Fig. 4), the estimate of a ~50% reduction attributable to B1-induced cell death still held true. Importantly, our results with 5A6.E9 suggest that the γδTCR is indeed involved in γδTc killing of breast cancer targets.

While we did not directly address the susceptibility of individual γδTc subsets to apoptosis induction via anti-γδTCR antibodies, we might assume that the Vδ2 subset was most strongly affected, due to this subset's documented sensitivity to activation induced cell death[432-434]. Donor culture 4-1 was mainly Vδ2 (78.8%, Fig. S3A, Table S1) and susceptible to enhanced apoptosis through IL-2 in combination with each of the three tested anti-TCRγδ mAb (Figs. 2E-G and S3B). Note that Student's t-tests were employed to assess significant differences in IL-2-treated versus -untreated cells in Figs. 2E-G, but that ANOVA was used for the full experiment in Fig. S3B, explaining differences in statistical outcomes for 11F2-treated samples (compare 2G and S3B). Cultures comprising lower percentages of Vδ2 cells (1-2 and 3-2, Table S1) exhibited little to no difference in viability upon incubation with 5A6.E9 or 11F2, with or without IL-2 (Figs. 2F, G). These data suggest that Vδ2 are more sensitive to apoptosis induced by anti-TCRγδ mAb in the presence of IL-2. Since most studies focus on the Vδ2 subset, it is crucial that researchers take this unintended effect into account.

Previous blocking assays reported in the literature have potentially unwittingly overstated γδTCR involvement in lysis of target cells by assuming that decreased target death is due to blocking of the TCR, not realizing that a proportion of effector γδTc may have undergone apoptosis. If, for example, anti-TCRVδ1 mAb clones induce γδTc apoptosis, then the TCR may not be involved in Vδ1 γδTc killing of MEC1 leukemia cells since B1 and anti-Vδ1 both appeared to "block" MEC1 lysis to a similar extent.[209] In our own previous work, Immu510 and B1.1 clones decreased percent lysis of PC-3M prostate cancer cells to the same extent, suggesting that Immu510 may be as detrimental to γδTc viability as B1.1[412]. In that experiment, using a Vδ2-predominant culture (77.4% Vδ2, 14.2% Vδ1), neither anti-Vδ1(TS8.2) nor anti-Vδ2 (B6) clones significantly reduced cytotoxicity against PC-3M, suggesting that the TCR was not involved[412]. In another experiment with a Vδ1 predominant γδTc culture (55.1% Vδ1, 11.7% Vδ2), derived from a

different donor, anti-Vδ1 did decrease lysis significantly, yet this may have been due to loss of γδTc as opposed to bona fide Vδ1 TCR blocking[412], although Vδ1 may be less susceptible to apoptosis induction than Vδ2, as discussed above. In contrast, a lack of decrease in tumor cell death after mAb treatment suggests that the γδTc employed were not susceptible to mAb-induced apoptosis. For example, Vδ1 γδTc expressing natural cytotoxicity receptors were not susceptible to apoptosis induced by B1.1 or Immu510, as no drop in MOLT4 lysis was observed[155]. Likewise, blocking with B1.1 and Immu510 had no influence on Vδ2 γδTc cytotoxicity against Jurkat or Molt4[418]. Thus, the TCR was not implicated in cytotoxicity and no false misinterpretation resulted[155,418]. Yet γδTCR involvement in killing of ULBP4-overexpressing murine thymoma EL4[148] as well as hMSH2-expressing HeLa cells[420] may have been overstated, if the γδTc employed in these studies were as susceptible to B1.1-mediated apoptosis as ours were.

In conclusion, we strongly suggest that researchers employing the mAb blocking assay using anti-γδTCR mAb perform γδTc alone controls in parallel, to quantify the extent of effector cell death occurring as a result of mAb treatment. This cell death can then be taken into account and subtracted from the difference observed in cytotoxicity upon application of this mAb, which should give a more accurate value for the extent to which true receptor blocking impairs cytotoxicity. IL-2 may be excluded from cytotoxicity assays to minimize the deadly synergy observed upon B1 stimulation, keeping in mind that this may reduce overall cytotoxicity and thus perhaps should be tested for each target cell line in advance. Previous work using B1 or B1.1 for blocking, ours included, should be reevaluated in this light. Perhaps the γδTCR is not as involved in target killing as we thought.

2.5 Conflict of Interest Statement

The authors declare no conflicts of interest.

2.6 Author Contributions

All authors contributed to research design. I.D. and G.M.S. conducted experiments and performed data analysis. G.M.S. wrote the manuscript.

2.7 Funding

This project has been funded by a Cancer Research Society Operating Grant (LMP and GMS), Alberta Cancer Foundation Antoine Noujain and University of Alberta Doctoral Recruitment Scholarships (ID) and an Alberta Innovates Health Solutions Translational Health Chair (LMP).

2.8 Acknowledgements

We would like to thank Dr. Dalam Ly for inspiring us to pursue this line of research by suggesting that the B1 mAb may cause γδTc cell death. We also thank Dr. Rebecca O'Brien for her insights into *in vivo* depletion of γδTc. This work has been supported by the Sawin-Baldwin Chair in Ovarian Cancer, Dr. Anthony Noujaim Legacy Oncology Chair and Alberta Innovates Health Solutions Translational Health Chair to L.M.P. We thank Dr. Aja Rieger (Flow Cytometry Core, Faculty of Medicine and Dentistry, University of Alberta) for her support. We also thank Dr. Ing Swie Goping for providing us with antibodies to cleaved Caspase 3.

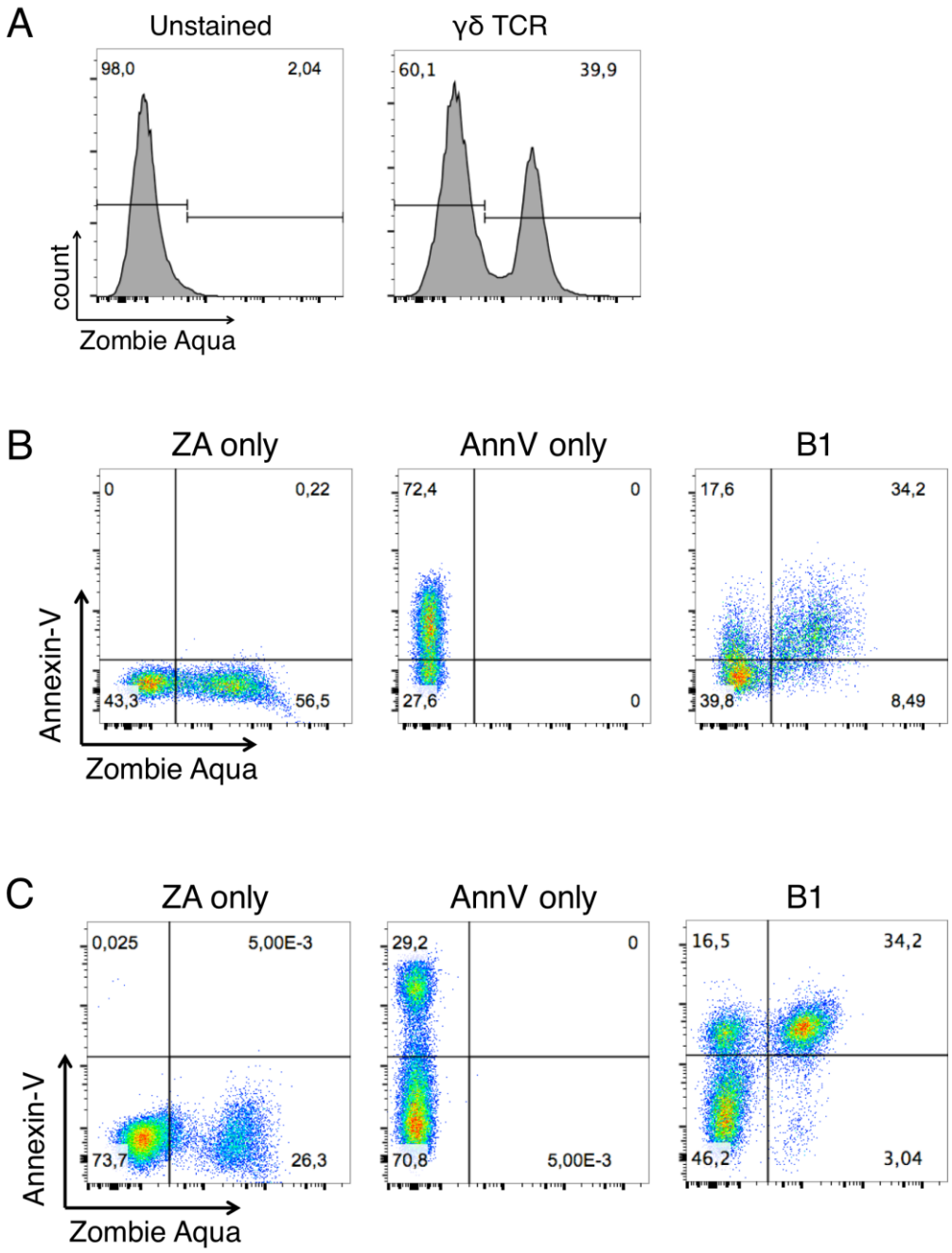

Figure S2.1 Gating controls for flow cytometry experiments. (A) Donor 2 day 14 γδ T cells were untreated and unstained (left) or incubated with 1µg anti-γδTCR antibody for 4.5 h and stained with zombie aqua viability dye (gating for Fig. 2.1B). **(B)** Donor 3 day 21 γδ T cells were treated with 1µg anti-γδTCR antibody for 4.5 h and stained with zombie aqua and annexinV FITC. Single stained controls for zombie aqua (left, ZA only) and annexinV (middle, AnnV only) were used to set gates for the experiment shown in Fig 2.1C. **(C)** Gating for Fig. 2.2A 'no IL-2" sample shown here.

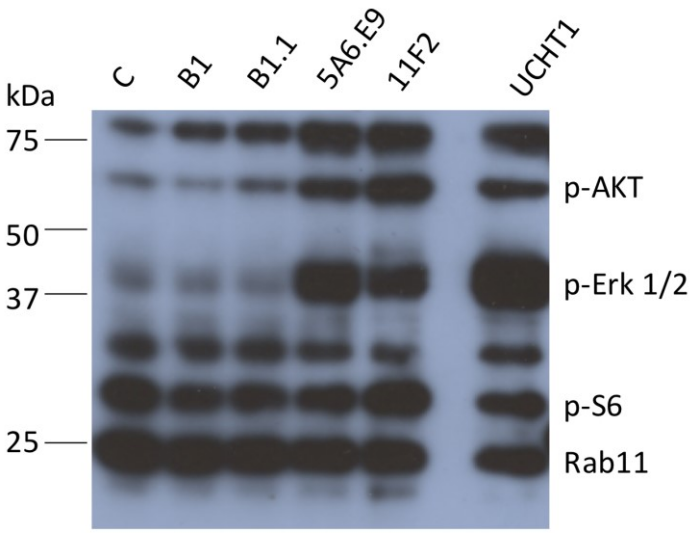

Figure S2.2. 5A6.E9 and 11F2 anti-γδTCR antibody clones induce γδ T cell activation. Day 20 donor γδ T cells were stimulated with 5μg of the indicated antibodies for 1 min. Lysates were run on 12% SDS-PAGE gels, transferred to PVDF membranes and probed with the PathScan Multiplex Western Cocktail I (Cell signaling Technology) to detect the indicated signaling proteins. Shown here is a representative example from three independent experiments.

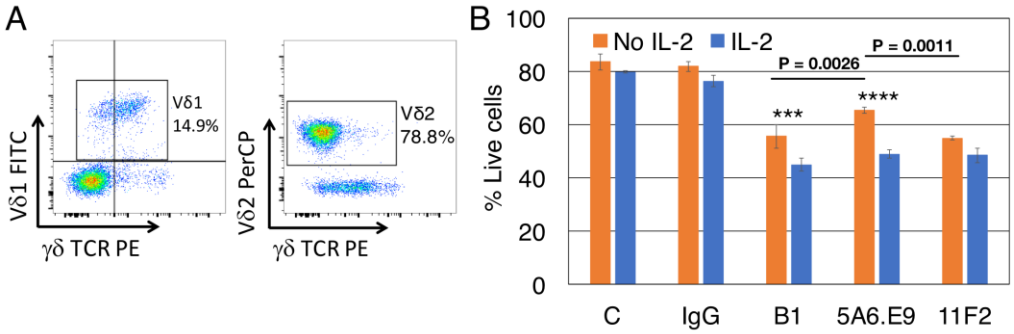

Figure S2.3 γδ T cell culture with Vδ2 predominance is sensitive to apoptosis induced by all three anti-TCRγδ antibody clones tested. A. Day 19 donor culture 4-1 was stained with anti-TCR Vδ1 FITC and Vδ2 PerCP, and anti-γδ PE, then analyzed by flow cytometry. Plots of Vδ1 FITC and Vδ2 PerCP versus anti-γδ PE are shown. **B.** Day 19 donor culture 4-1 cells were incubated without (C=control) or with the indicated antibodies in the presence or absence of IL-2 for 4.5 h, stained with zombie aqua and annexinV FITC then acquired by flow cytometry. % Live cells were ZA- and annexinV- negative. Two way ANOVA followed by Bonferroni's multiple comparisons analysis were performed and identified highly significant differences between all antibody-treated and IgG-treated cells with and without IL-2 (not indicated, $p<0.0001$). Significant differences in γδ T cell viability for each antibody treatment with or without IL-2 are indicated (*** $p<0.001$, **** $p<0.0001$). p values are shown for comparison of 5A6.E9 with B1 and 11F2 in the absence of IL-2. No significant differences were observed among antibody treatments in the presence of IL-2.

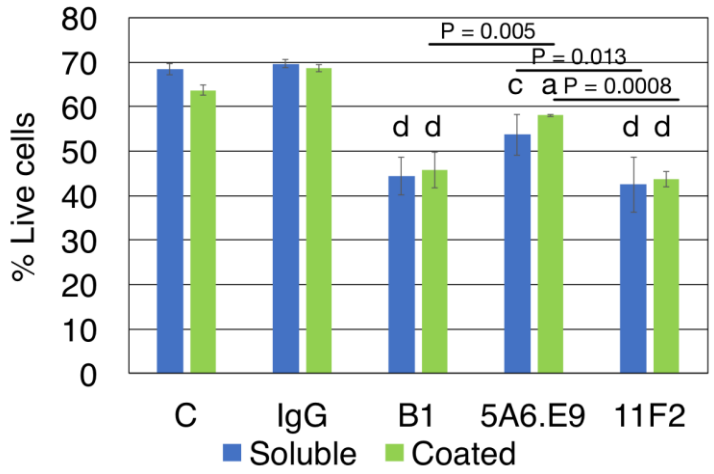

Figure S2.4. There is no difference in viability of cells treated with soluble versus immobilized anti-TCRγδ antibody clones. No difference in viability of Donor 8 culture 2 day 18 cells were induced by soluble versus immobilized (coated) B1, 5A6.E9 or 11F2 antibody treatments; however, significant decreases in viability were observed comparing antibody-treated to IgG-treated cells. Two way ANOVA followed by Bonferroni's multiple comparisons analysis were performed to identify significant differences between antibody-treated and IgG-treated cells (a, $p<0.0.5$; b, $p<0.01$; c, $p<0.001$; d, $p< 0.0001$) or among antibody treatments (line indicated groups compared and p values are given)

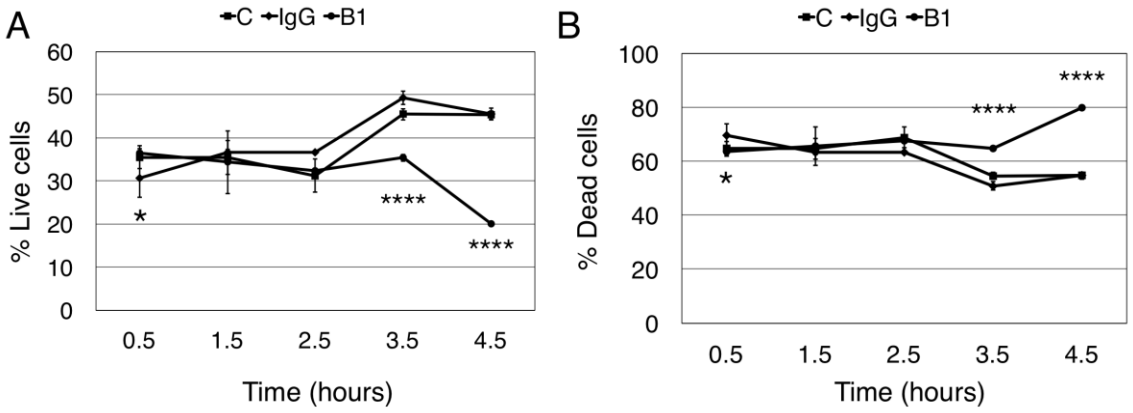

Figure S2.5. Kinetics of apoptosis induction by B1 antibody. (A) 600,000 donor 8 day 17 γδ T cells were untreated (C) or incubated with 1µg IgG control or B1 anti-γδTCR antibody, as indicated, for 30 minutes in 100 µl medium, then additional 100 µl medium was added (t=0 h). Cells were further incubated for 1-4 h and stained with Zombie Aqua and AnnexinV FITC. Live cells were ZA- and AnnexinV- negative. **B.** For the experiment described in A, the sum of early apoptotic, late apopototic and necrotic cells make up the dead cell fractions shown here. Two way ANOVA followed by Bonferroni's multiple comparisons analysis were performed to identify significant differences between B-treated and IgG-treated cells at the indicated time point. (*$p<0.05$, **** $p<0.0001$).

S2.1. γδ T cell subset percentages and purities for donor cultures. Donor cultures were stained with zombie aqua and then with antibodies recognizing pan γδ TCR, Vδ1 TCR and Vδ2 TCR on the indicated day. Purity is the sum of % Vδ1, % Vδ2 and %γδ TCR+ Vδ1- Vδ2-. The figures in which results were obtained using these cultures are listed.

ID	Day	% Vδ1	% Vδ2	% γδTCR+Vδ1-Vδ2-	% Purity	Figure(s)
1-1	21	49.1	32.2	8.7	90.0	1A,E,F; 2H,I; 3B
1-2	20	70.0	14.9	11.5	96.4	2A-G; S1C
2-1	14	38.1	51.6	5.5	95.2	1B; S1A
3-1	21	23.2	58.3	3.5	85.0	1C,D; S1B
3-2	19	28.7	50.8	6.7	86.2	1F; 2D-G; 3B
4-1	19	14.9	78.8	4.2	97.9	1F; 2D-G,I; 3A,B; S3A,B
4-2	18	14.8	67.8	2.4	85.0	4C,D
5-1	22	40.3	49.0	6.2	95.5	2I; 3B
6-1	19	43.4	42.1	11.1	96.6	3C-F
7-1	19	39.1	16.1	11.0	66.2	4A-D
7-2	19	2.1	89.1	1.1	92.2	3D,F
8-1	19	27.1	49.0	5.5	81.6	4C,D
8-2	19	77.9	6.2	12.0	96.1	2I-K; 3D,F; S4; S5A,B
9-1	21	11.1	77.1	3.8	92.0	S2

Chapter 3- Functional Plasticity of γδ T Cells and Breast Tumor Targets in Hypoxia

Functional Plasticity of γδ T Cells and Breast Tumor Targets in Hypoxia

Short title: Gamma delta T cell plasticity in hypoxia

Gabrielle M. Siegers[1,2], Indrani Dutta[1], Raymond Lai[1] and Lynne-Marie Postovit[1,2]
[1]Department of Oncology, University of Alberta, Edmonton, AB, Canada
[2]Department of Anatomy and Cell Biology, Robarts Research Institute, Western University, London, ON, Canada

Address correspondence to:

Gabrielle M. Siegers
Research Scientist
Department of Oncology
University of Alberta
5-142W Katz Group Centre
Edmonton, AB
CANADA T6G 2E1
Phone: 780-248-5714
Fax: 519-492-8160
email: siegers@ualberta.ca

Keywords

gamma delta T cells, plasticity, hypoxia, breast cancer, tumor evasion, MICA

Abbreviations

bp, band pass
CAIX, carbonic anhydrase IX
CalAM, Calcein AM
CD40L, CD40 ligand (or CD154)
E:T, effector:target ratio
ER, estrogen receptor
FBS, fetal bovine serum
FMO, fluorescence minus one
γδTc, gamma delta T cells
HIF1α, hypoxia inducible factor 1 alpha
HRP, horseradish peroxidase
IL, interleukin
lp, long pass
MICA, MHC class I polypeptide-related sequence A
MIP1α, macrophage inflammatory protein 1α (or CCL3 = chemokine (C-C motif) ligand 3)
MFI, median fluorescence intensity
NKG2D, natural killer group 2, member D
O_2, oxygen
PBMCs, peripheral blood mononuclear cells,
PBS, phosphate buffered saline
PIC, protease and phosphatase inhibitor cocktail
PR, progesterone receptor
RANTES, regulated on activation, normal T cell expressed and secreted (or CCL5)
TBST, tris-buffered saline plus 0.05% Tween-20
TCR, T cell antigen receptor
TIL, tumor infiltrating lymphocytes
TME, tumor microenvironment
TNFα, tumor necrosis factor alpha
ZA, Zombie Aqua fixable viability dye

Abstract

Interactions between immune and tumor cells in the tumor microenvironment (TME) often impact patient outcome, yet remain poorly understood. In addition, the effects of biophysical features such as hypoxia [low oxygen (O_2)] on cells within the TME may lead to tumor evasion. Gamma delta T cells (γδTc) naturally kill transformed cells and are therefore under development as immunotherapy for various cancers. Clinical trials have proven the safety of γδTc immunotherapy and increased circulating γδTc levels correlate with improved patient outcome. Yet, the function of γδTc tumor infiltrating lymphocytes (TIL) in human breast cancer remains controversial. Breast tumors can be highly hypoxic, thus therapy must be effective under low O_2 conditions. We have found increased infiltration of γδTc in areas of hypoxia in a small cohort of breast tumors; considering their inherent plasticity, it is important to understand how hypoxia influences γδTc function. *In vitro*, the cell density of expanded primary healthy-donor blood-derived human γδTc decreased in response to hypoxia (2% O_2) compared to normoxia (20% O_2). However, the secretion of MIP1α/MIP1β, RANTES and CD40L by γδTc were increased after 40 h in hypoxia compared to normoxia concomitant with the stabilization of Hypoxia Inducible Factor 1-alpha (HIF1α) protein. Mechanistically, we determined that NKG2D on γδTc and the NKG2D ligand MICA/B on MCF-7 and T47D breast cancer cell lines are important for γδTc cytotoxicity, but that MIP1α, RANTES and CD40L do not play a direct role in cytotoxicity. Hypoxia appeared to enhance the cytotoxicity of γδTc such that exposure for 48 h increased cytotoxicity of γδTc against breast cancer cells that were maintained in normoxia; conversely, breast cancer lines incubated in hypoxia for 48 h prior to the assay were largely resistant to γδTc cytotoxicity. MICA/B surface expression on both MCF-7 and T47D remained unchanged upon exposure to hypoxia; however, ELISAs revealed increased MICA shedding by MCF-7 under hypoxia, potentially

explaining resistance to γδTc cytotoxicity. Despite enhanced γδTc cytotoxicity upon pre-incubation in hypoxia, these cells were unable to overcome hypoxia-induced resistance of MCF-7. Thus, such resistance mechanisms employed by breast cancer targets must be overcome to develop more effective γδTc immunotherapies.

3.1 Introduction

Low O_2 levels (hypoxia) characterize the microenvironment of many solid tumors, occurring as a consequence of structurally disorganized blood vessels and tumor growth that exceeds the rate of vascularization. Hypoxia is common within breast cancers, which have a median O_2 concentration of 1.4%, as compared to ~9.3% for normal breast tissue[435]. In response to hypoxia, cells express genes that are essential for their survival. In tumor cells, this O_2-regulated gene expression leads to more aggressive phenotypes, including those that increase the ability of cells to resist therapy, recruit a vasculature, and metastasize[436-438]. Accordingly, there is a growing body of evidence correlating tumor hypoxia with poor clinical outcome for patients with a variety of cancers[439-441]. O_2 availability has also been shown to regulate immune editing, allowing cancer cells to evade the immune system *via* a variety of mechanisms[442]. For example, hypoxia upregulates HIF1α-dependent ADAM10 expression resulting in MHC class I polypeptide-related sequence A (MICA) shedding from the surface and decreased lysis of tumor cells[443]. While many studies have focussed on myeloid derived suppressor cells or conventional CD8+ T cells[442], so far none have considered the impact of tumor hypoxia on gamma delta T cells (γδTc).

While γδTc kill cancer cell lines, derived from both hematological and solid tumors alike (reviewed in[112]), it is unclear whether they are still active cancer killers when confronted with the harsh and immunosuppressive tumor microenvironment (TME)[112,131,444,445]. We have focussed on breast cancer, since there have been conflicting reports in the literature with respect to γδTc

function in this disease. While *in vitro* studies clearly show that γδTc are able to kill breast cancer cell lines MDA-MB231, MCF-7 and T47D[188,189,446], it is unclear as to whether γδTc retain their cytotoxic properties once exposed to the breast tumor TME[131].

Here we set out to determine how γδTc behave under low oxygen (O_2), a TME factor likely encountered by γδTc in many malignancies. Carbonic anhydrase IX (CAIX) is a transmembrane protein that catalyzes the reversible hydration of carbon dioxide. It is expressed in response to hypoxia and is thus used as a surrogate marker for hypoxia[447]. High CAIX expression indicates poor prognosis in many cancers, including breast cancer[448-450]. Breast cancer cell lines express MICA, a ligand for the natural killer group 2, member D (NKG2D) receptor expressed by γδTc and implicated in γδTc cytotoxicity[127,146,160,161,451]. Thus, we have further explored the integral role for NKG2D/MICA in γδTc cytotoxicity against breast cancer cell lines under hypoxia and normoxia.

Since γδTc are being developed for cancer immunotherapy[409,452-456], and have shown both safety and even some efficacy - despite advanced disease stage – in a Phase I trial for breast cancer[111], it is imperative that we learn how the TME impacts the function of γδTc infiltrating breast and other solid tumors.

3.2 Materials and Methods

3.2.1 Ethics statement

This study was carried out in accordance with the recommendations of the Research Ethics Guidelines, Health Research Ethics Board of Alberta – Cancer Committee with written informed consent from all subjects. All subjects gave written informed consent in accordance with the Declaration of Helsinki. The protocol was approved by the Health Research Ethics Board of Alberta – Cancer Committee.

3.2.2 Patients and Tissues

We assessed 17 surgically resected breast tumors from cancer patients diagnosed at the Cross Cancer Institute, Edmonton, AB from 1997 to 1998. Patient and tumor characteristics are listed in Table 3.1.

3.2.3 Immunohistochemistry

Anti-human T cell antigen receptor (TCR)δ staining was performed as reported[457]. Briefly, 4.5 µm serial sections from formalin-fixed paraffin-embedded tumors were melted on a slide warmer at 60ºC for a minimum of 10 min followed by de-paraffinization using a fresh Xylenes (Thermo Fisher Scientific, Burlington, ON, Canada) bath. Sections were then hydrated with a series of graded ethanol (100%, 95%, 70%, 60%) followed by brief incubation in water, then tris-buffered saline plus 0.05% Tween-20 (TBST). Antigen retrieval was performed at 100ºC for 20 min in target retrieval solution pH 9 (DAKO North America, Carpinteria, CA, USA). After cooling to room temperature, tissues were circled with an ImmEdge pen (Vector Laboratories, Burlingame, CA, USA) and blocked with Peroxidase Block (DAKO) for 5 min. Slides were washed in TBST for 5 min then blocked with Protein Block Serum Free (DAKO) for 10 min. Protein block was gently removed and replaced with 1:150 dilution of mouse monoclonal anti-human TCRδ antibody (clone H-41, Santa Cruz Biotechnology, Dallas, TX, USA) or 1:50 dilution of rabbit monoclonal anti-human CAIX (clone EPR4151(2), abcam, Cambridge, MA, USA) or corresponding isotype control

Table 3.1. Characteristics of breast cancer cohort

n = 17	*n* (%)	Median (range)
Age at diagnosis		51 (40 – 69)
Histology		
Invasive ductal carcinoma	14 (82)	
Invasive non-ductal tubular	1 (6)	
Invasive non-ductal mucinous	1 (6)	
Non-invasive	1 (6)	
Tumor size (cm)		
<2	11(65)	1.4 (0.2– 5.5)
2-5	4 (24)	
>5	1 (6)	
Not specified	1 (6)	
Tumor grade		
1/3	4 (24)	
2/3	5 (29)	
3/3	8 (47)	
Nodal Status		
Positive	9 (53)	
Negative	8 (47)	
ER		
Positive	12 (71)	
Negative	3 (18)	
Not available	2 (12)	
PR		
Positive	10 (59)	
Negative	5 (29)	
Not available	2 (12)	

control of staining. Sections were incubated in a humidified chamber for 30 min at 25ºC. Slides were then rinsed and washed five times in TBST for 5 min. Slides were then incubated with 100 µl secondary antibody, labeled polymer – horseradish peroxidase (HRP) anti-mouse or – HRP anti-rabbit (DAKO), for 60 min at room temperature in the humidified chamber. Washing was done as before, and then slides were treated with 75-100 µl 3,3'-diaminobenzidine chromogen solution (DAKO) for 8-10 min before the reaction was stopped by rinsing in water. Haematoxylin (DAKO) counterstaining was performed, slides were rinsed in water and then dehydrated using a series of graded ethanol (60%, 70%, 95%,100%). Slides were then cleared with Xylenes, dried and coverslips mounted with VectaMount permanent mounting medium (Vector Laboratories).

3.2.4 Assessment of CAIX expression and γδTc infiltration

Light microscopy and semi-quantitative scoring for CAIX was performed by a single pathologist; scores were 0, no staining; 1, weak and/or very focal staining; 2+, strong but focal staining; and 3, strong and extensive staining. Serial sections stained for TCRγδ and CAIX were scanned. Areas of CAIX-positivity and negativity were defined, and images from slides superimposed to enable counting of γδTc in CAIX-positive and –negative areas. Five consecutive areas within each region were quantified for the frequency of γδTc infiltration.

3.2.5 Primary γδ T cells

We established and maintained primary human γδTc cultures as described[412]. Briefly, healthy donor blood was diluted with phosphate buffered saline (PBS) and peripheral blood mononuclear cells (PBMCs) isolated using density gradient separation (Lymphoprep, Stem Cell Technologies, Vancouver, BC). PBMCs were cultured in a humidified atmosphere at 37°C with

5% CO_2 at 1 x 10^6 cells/ml in RPMI complete medium containing 1μg/ml Concanavalin A (Sigma-Aldrich, Oakville ON), 10% Fetal Bovine Serum (FBS), 1x MEM NEAA, 10 mM HEPES, 1 mM Sodium Pyruvate (all Invitrogen, Burlington, ON), and 10 ng/ml recombinant human interleukin (IL)-2 and IL-4 (Miltenyi Biotec, Auburn CA). Cells were counted and viability assessed via Trypan Blue Exclusion Assay (Invitrogen/Thermo Fisher Scientific, Waltham, MA, USA); fresh medium and cytokines added to adjust density to 1 x 10^6 cells/ml every 3-4 days. After 1 week, αβ T cells were labeled with anti-TCRαβ PE antibodies (BioLegend, San Diego, CA, USA) and anti-PE microbeads (Miltenyi Biotec), and depleted after filtering (50 μm Cell Trics filter, Partec, Görlitz, Germany) and passing over an LD depletion column (Miltenyi Biotec). Gamma delta T cells, which did not bind to the column, were further cultured in complete medium plus cytokines (as above). For cytotoxicity and blocking experiments, γδTc cultures were used on days 19-21, as they were most cytotoxic then. Some hypoxia experiments were done at earlier time points. Donor cultures are identified as follows: donor number culture letter – culture day; thus, 7B-13 = the second culture derived from donor 7 on day 13. Culture purities and subset compositions are shown in Table S1.

3.2.6 Breast cancer cell lines

Human breast carcinoma cell lines, MCF-7 and T47D, were obtained from the American Type Culture Collection (ATCC, Manassas, VA, USA) and maintained as per ATCC guidelines. For surface marker staining of breast cancer cell lines, cells were harvested by washing with PBS followed by dissociation in Accutase (Sigma-Aldrich) for 20 min at 37°C.

3.2.7 Hypoxia Experiments

To examine the effects of hypoxia, cells were cultured in O_2 concentrations as indicated for 40-48 h using an X3 Xvivo Closed Incubation System (BioSpherix). After incubation under normoxic or hypoxic conditions, cell culture supernatants were collected, chilled on ice and then frozen at -80°C until further analysis; harvested cells were used in cytotoxicity assays or stained for flow cytometric analysis. In some cases, cells were cold harvested, pellets frozen on dry ice and stored at -80°C until lysis for Western blotting.

3.2.8 Flow Cytometry

3.2.8.1 Antibodies

For surface marker staining of γδTc, the following anti-human antibodies from BioLegend, unless otherwise indicated, were employed: TCRγδ PE (clone B1, 1:25); TCR Vδ1 FITC (Miltenyi, clone REA173, 1:10); TCR Vδ2 PerCP (clone B6, 1:25); NKG2D APC (BD Biosciences, Mississauga ON, 1:25); CD56 FITC (clone MEM-188, 1:5); CD69 AF700 (clone FN50, 1:4); CD94 FITC (clone DX22, 1:5); CD95 APC (clone DX2, 1:100); HLA ABC PE (clone W6/32, 1:10); FasL PE (clone NOK-1, 1:5); and CD40L APC (clone 24-31, 1:5). Anti-human MICA/B PE (Biolegend, clone 6D4, 0.1 μg) was used to stain breast cancer cell lines.

3.2.8.2 Surface marker staining

γδTc and breast cancer cell lines were adjusted to 10 x 10^6 cells/ 1 ml, stained with 1 μl/10^6 cells Zombie Aqua fixable viability dye in PBS (ZA, BioLegend) for 15-30 min at room temperature in the dark. γδTc were stained directly with fluorochrome-conjugated antibodies diluted in FACS buffer [PBS containing 1% FBS and 2 mM EDTA (Invitrogen)] as indicated above. Breast cancer cell lines at 10 x 10^6 cells/ml were blocked in FACS buffer containing 50

µl/ml Trustain FcX (Biolegend) and incubated on ice for 30 minutes prior to antibody incubation. After blocking, cells were centrifuged and supernatants removed, leaving 10 µl FACS buffer plus block/10^6 cells. Antibodies and FACS buffer were added to 20 µl, and cells incubated on ice 15-20 min followed by washing. All cells were fixed in FACS buffer containing 2% paraformaldehyde (Sigma-Aldrich), stored at 4°C and acquired within one week.

3.2.8.3 Flow cytometer specifications

Cells were analyzed using a FACS CANTO II (Becton Dickinson, Mississauga ON) equipped with: an air-cooled 405-nm solid state diode, 30mW fiber power output violet laser, with 450/50 and 510/50 band pass (BP) (502 long pass (LP) detector); a 488-nm solid state, 20-mW blue laser with 530/30 Bp (502 LP), 585/42 BP (556 LP), 670 LP (655 LP) and 780/60 BP (735 LP) filters; and a 633-nm HeNe, 17-mW red laser with 660/20 BP and 780/60 BO (735 LP) filters. Calibration was performed with CS&T beads (Becton Dickenson, Mississauga ON). Live singlets were gated based on forward and side-scatter properties. Fluorescence minus one (FMO) controls were used to set gates. Analysis was performed using FlowJo© software (Tree Star, Ashland, OR, USA, Version 10.0.8r1).

3.2.9 Cytokine Arrays

The Proteome Profiler Human Cytokine Array Kit, Panel A (R&D Systems, Minneapolis, MN, USA) was used to detect proteins secreted by γδTc cultured under normoxic or hypoxic conditions. Undiluted culture supernatants were used in these assays, which were carried out according to the manufacturer's instructions. Analysis of resulting films was done as follows: Pixel intensities were measured using FIJI software (ImageJ Version 2.0.0-rc-15/1.49m) using a consistent circular region of interest; measured values from duplicate spots were subtracted from

255. The average intensity from the two negative spots was subtracted from all values to obtain net values. The intensities of the six reference spots (positive controls) were averaged and a multiplier was defined for each array (normalized to the array with the lowest pixel intensity). Values were adjusted accordingly and then values for the duplicates were averaged. Finally, ratios were calculated for each cytokine, normalized to normoxia.

3.2.10 ELISAs

1-2 ml aliquots of culture supernatants stored at -80 ºC were thawed on ice. Halt™ Protease and Phosphatase Inhibitor Cocktail (PIC, Thermo Fisher Scientific) was added to samples prior to use in ELISAs or further storage at 4 ºC. The following ELISA kits were used: ELISA MAX Deluxe RANTES/CCL5 (BioLegend), Human MIP-1a and Human CD40L Quantikine ELISA kits (R&D Systems) and Human MICA ELISA Kit (abcam). For RANTES and CD40L ELISAs, culture supernatant samples were diluted up to 16-fold to obtain readings within range (1:2, 1:4, 1:8, 1:16). For MIP1α ELISAs, samples were diluted up to 1:20. For MICA ELISAs, culture supernatants stored at -80ºC were thawed overnight in at 4 ºC, then 4 ml applied to Amicon Ultra-4 10K spin columns (Merck-Millipore, Carrigtwohill, Ireland) that were subsequently centrifuged at 3000g for 2 h at 12ºC. Concentrated media was then transferred into 1.5 ml Eppendorf tubes and diluted to 200µl and 20 µl of a 1:10 dilution of PIC were added. For the ELISA, 100µl per well were assayed in duplicate. All ELISAs were done according to the manufacturer's instructions. Absorbance at 450 and 550 nm was measured using a FLUOstar Omega plate reader (BMG Labtech, Offenburg, Germany) with Omega Software version 5.11. The difference linear regression fit of the standard curve was used for concentration calculations. ELISA data were normalized to γδTc cell numbers and culture volumes.

3.2.11 Immunoblotting

Cell lysates were prepared by mixing γδTc with M-PER Mammalian Protein Extraction Reagent (Thermo Fisher Scientific) containing PIC at 10 µl lysis buffer per million γδTc followed by incubation at room temperature for 10 min. Lysates were then centrifuged at 13,000 rpm for 15 min 4 ºC, after which supernatants were transferred to fresh tubes and 5x reducing sample buffer (0.0625 M Tris/HCl pH6.8, 2% SDS, 20% glycerol, 0.05% β-mercaptoethanol, 0.025% (w/v) Bromophenol Blue) added. Samples were boiled 5 min, cooled and briefly centrifuged in a benchtop centrifuge prior to running on 10% or 12% SDS-PAGE gels. Proteins were transferred onto Immobilon-FL PVDF membranes (Millipore) using the Trans-Blot Turbo Transfer System (Bio-Rad, Mississauga ON). The high molecular weight (MW) program was used when transferring proteins for HIF1α detection. Otherwise, the mixed MW program was used. Membranes were blocked 40 min in 3% milk in TBST, followed by overnight incubation in primary antibody baths at 4ºC. After washing, membranes were incubated with the corresponding species-specific HRP-labeled secondary antibody for 1 h, followed by further washing and then detection using Clarity™ Western ECL Substrate (Bio-Rad). Primary antibodies were diluted in PBS containing 2% bovine serum albumin and 0.05% sodium azide at the following dilutions: 1:500 mouse anti-human HIF-1α (clone MOP1, BD Biosciences); 1:2000 goat anti-human CCL3/MIP1α (R&D Systems); 1:1000 mouse anti-human/primate CCL5/RANTES (Clone #21418, R&D Systems); 1:500 mouse anti-human CD40 Ligand/TNFSF5 (Clone #40804, R&D Systems); 1:2000 rabbit anti-human β-Actin (Cell Signaling Technologies, Danvers, MA, USA). Secondary antibodies were diluted in blocking buffer as follows: 1:10,000 goat anti-mouse IgG HRP (BioRad); 1:20,000 goat anti-rabbit IgG HRP (BioRad); 1:1000 donkey anti-goat IgG HRP (R&D Systems).

3.2.12 Quantification of bands on Western Blots

Band intensities for CD40L, MIP1α and RANTES were measured using FIJI software (ImageJ Version 2.0.0-rc-15/1.49m) on converted grayscale images using consistent rectangular regions of interest. Measured values for bands and background (region of same size beneath each band) were subtracted from 255, then background was subtracted from bands to obtain net values for protein bands of interest and loading control bands (actin). The ratios of protein bands to loading control bands were then calculated. In the case of CD40L and RANTES, these values were multiplied by 10 to obtain values between 0.1 and 10. For calculation of induction, hypoxia values were divided by normoxia values, and average values for each protein were plotted. Calculations were done in Microsoft Excel version 15.3 (Microsoft, Redmond, WA, USA).

3.2.13 Cytotoxicity Assays

3.2.13.1 Target Cell labeling with Calcein AM

As per the manufacturer's instructions, target cells were labeled with 5μM Calcein AM (CalAM, Invitrogen/Thermo Fisher Scientific). Cells were diluted to 30,000 cells/100 μl medium for cytotoxicity assays.

3.2.13.2 Blocking Antibodies

The following anti-human antibodies were used: LEAF purified anti-NKG2D (BioLegend, Clone 1D11), anti-human CCL3/MIP1α (R&D Systems); anti-human/primate CCL5/RANTES (Clone #21418, R&D Systems) and anti-human CD40 Ligand/TNFSF5 (Clone #40804, R&D Systems). Mouse IgG (Sigma-Aldrich) was used as a control.

3.2.13.3 Blocking/Cytotoxicity Assay

For blocking and cytotoxicity assays, 6 x 10^6 cells/ml γδTc cells were re-suspended in complete medium: RPMI 1640 plus 10% heat-inactivated fetal bovine serum; 10 mM HEPES; 1 x MEM NEAA; 1 mM sodium pyruvate; 50 U/ml Penicillin-Streptomycin and 2 mM L-Glutamine, all purchased from Invitrogen) Blocking antibodies were added at 6 μg mAb per 600 μl cell suspension/test in Eppendorf tubes, then plated at 100 μl/well in a 96 well round-bottomed plate and incubated at 37°C for 30 minutes. Thereafter, 100 μl CalAM-labeled targets were added. For cytotoxicity assays, the effector:target (E:T) ratio is indicated; blocking assays were done at 20:1. Co-cultures were incubated at 37°C for 4 h, after which plates were centrifuged and supernatants transferred to black clear-bottom 96-well (flat) plates (Costar, VWR International, Edmonton, AB). CalAM fluorescence was then detected on a FLUOstar Omega, BMG labtech fluorimeter. Controls were untreated and IgG-treated cells (for blocking assays), CalAM-labeled target cells incubated alone (spontaneous release) as well as 0.05% Triton-X 100 (Thermo Fisher Scientific)-treated cells (maximum release). The calculation for percent lysis is: [(test-spontaneous release)/(maximum-spontaneous release)] x 100%.

3.2.14 Statistics

The following tests were used to determine significance: paired 1-tailed Student's t-tests [Fig. 2A-F only, Microsoft Excel version 15.3 (Microsoft, Redmond, WA, USA)]; paired 2-tailed Student's t-tests [Fig. 2G-U, Prism 7.0 for Mac OSX (GraphPad Software, San Diego, CA, USA)]; one-way ANOVA analysis (Fig. 4, Prism); and Shapiro-Wilk normality tests followed by two-way ANOVA (Fig. 1E, 3, 5, 6, Prism). Sidak's pairwise multiple comparison posthoc tests were

performed alongside ANOVA analyses. The threshold for significance was set at $P < 0.05$; asterisks indicate degrees of significance as defined in the figure legends.

3.3 Results

3.3.1 γδTc can be found in hypoxic regions in breast cancer cases

In order to determine whether γδTc are present in areas of hypoxia in breast tumors, we performed immunohistochemistry to detect the hypoxia marker CAIX and γδTc using single stains of serial sections from a panel of 17 breast tumors (Table 3.1). Examples from one case (case 14) are shown (Fig. 3.1A-D), including images of a CAIX-positive region (Fig. 3.1A), an area with no appreciable CAIX positivity (Fig. 3.1B), and increased magnification of γδTc found in the same region depicted in Fig. 3.1A (Fig. 3.1C) and Fig. 3.1B (Fig. 3.1D). Of these 17 cases, 47% (8/17) stained positively for CAIX. In CAIX-negative cases, there was little γδTc infiltration; however, when γδTc were quantified in CAIX-positive versus CAIX-negative areas of breast tumors, γδTc frequency was greater in hypoxic regions, significantly so in three cases in particular (Fig. 3.1E, cases 13, 14 and 17, $P < 0.0001$). Images for cases 13 and 17 are in Fig. S1. In our cohort, 71% (12/17) of tumors were estrogen receptor positive (ER+); most ER+ cases were CAIX-negative (Fig. 1E, ER status indicated below case numbers).

3.3.2 Exposure to hypoxia reduces γδTc density

Given the co-localization of γδTc and CAIX in breast tumors, we measured the effects of hypoxia on γδTc viability and density *in vitro*. We cultured γδTc for 12 to 19 days, then subjected them to 48 h in hypoxic (2% O_2) or normoxic (20% O_2) conditions. We found that exposure to hypoxia had variable effects on γδTc viability (Fig. 3.2A, $P = 0.08$), and significantly decreased cell density (Fig. 3.2B, $P = 5.7 \times 10^{-4}$). Immunophenotyping was performed using flow cytometric

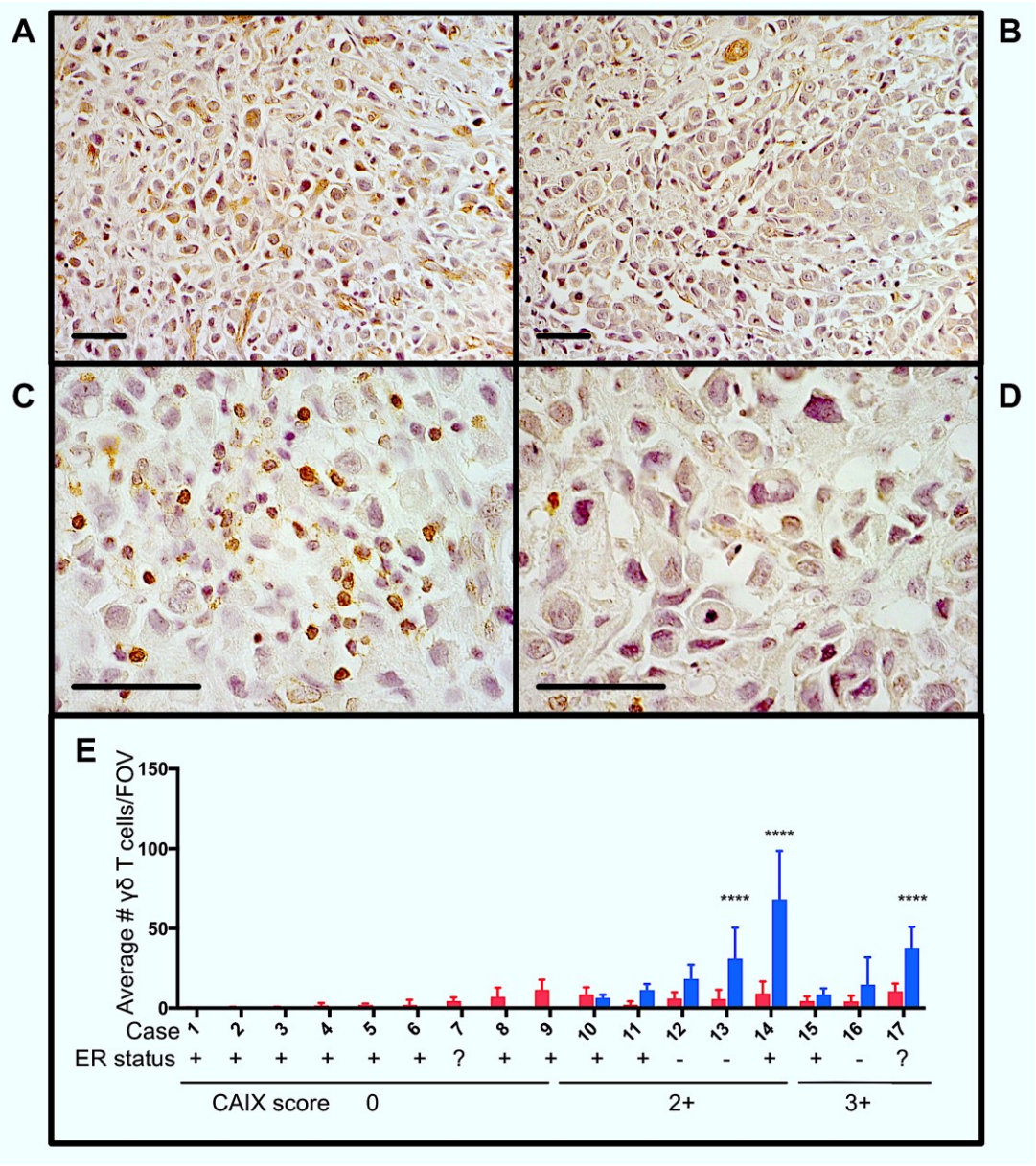

Figure 3.1. γδ T cells are present in areas of hypoxia in ER+ breast tumors. Serial sections from ER+ breast tumors were stained for carbonic anhydrase IX (CAIX) and TCRδ. **(A)** Example of CAIX-positive staining at 400x magnification from case 14; **(B)** CAIX-negative field of view (FOV) from the same slide as in **(A)**; **(C)** γδ T cells in the same area as (A) at 1000x magnification; and **(D)** γδ T cells in the same area as **(B)** at 1000x magnification. Scale bars are 50 µm. Brown indicates positive staining; (**E)** Parallel staining for γδ T cells and CAIX suggests that γδ T cell infiltration increases in hypoxic regions. CAIX scoring is indicated below the case numbers: 0 = no staining, 1 = weak and/or very focal staining; 2+ = strong but focal staining; and 3 = strong and extensive staining. Quantification and statistical analysis of γδ T cell frequency in CAIX-positive versus –negative regions (blue and red bars, respectively) reveal significantly increased γδ T cell infiltration in hypoxic regions (two-way ANOVA, **** $P < 0.0001$).

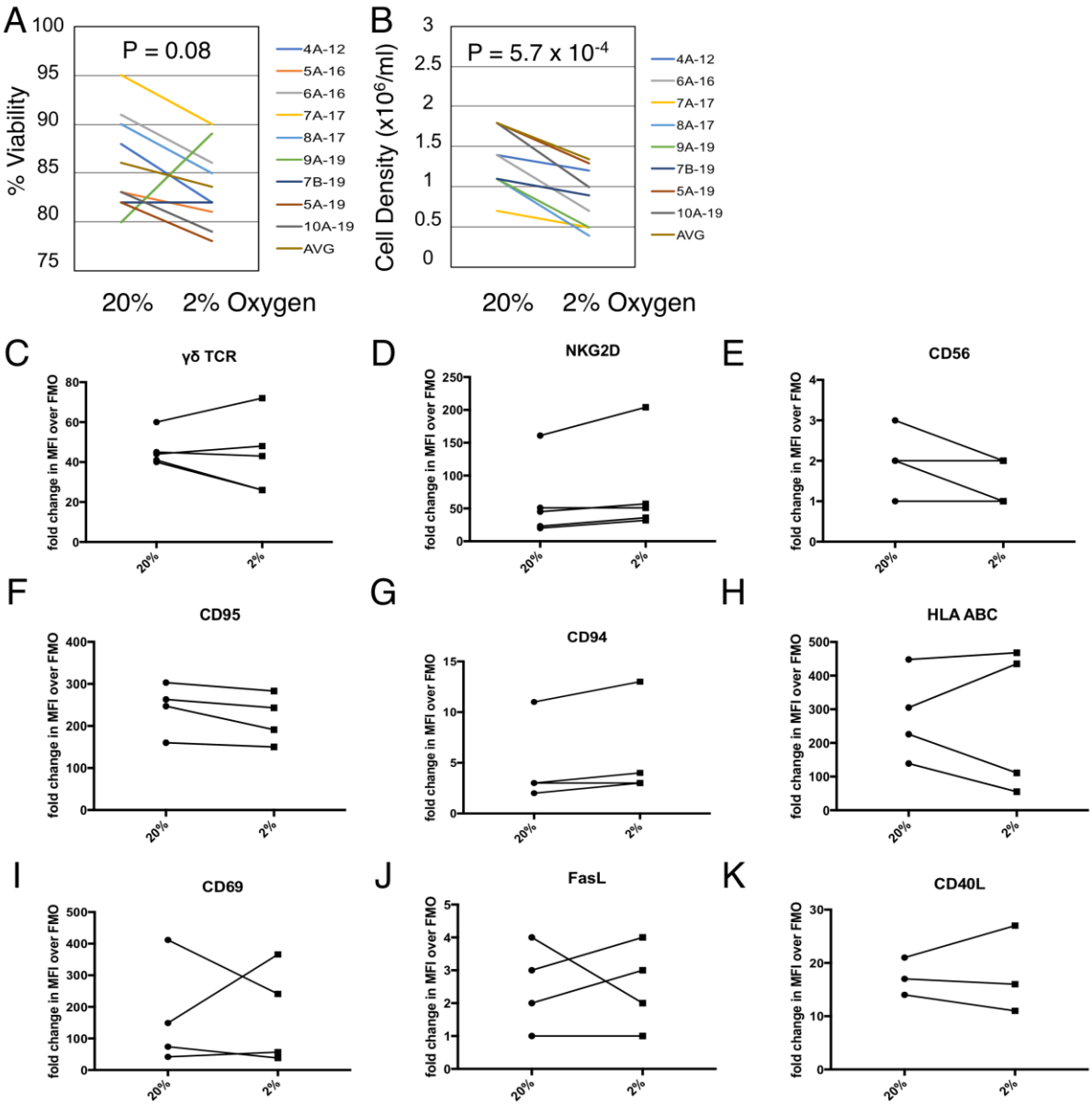

Figure 3.2 γδ T cell viability and proliferation under hypoxia/normoxia differ, but overall surface marker expression is not significantly impacted by oxygen levels. (A) Viability of γδ T cells cultured under 20% versus 2% O_2 for 48 h beginning on culture days 12-19, for 8 cultures from 7 different donors, assessed *via* Trypan Blue exclusion. Donor numbers are given with A and B indicating different cultures from the same donor; numbers after the hyphen are the culture days on which the experiment was begun; **(B)** Cell density assessment from experiment shown in **(A)**; (**C-K)** The indicated surface markers were assessed by flow cytometric analysis (**C, D**, n = 5; **E-J**, n = 4; **K**, n = 3 different donor cultures).

analyses of activation markers including γδTCR, NKG2D, CD56, CD69, CD95, CD40L, and HLA ABC as well as the inhibitory markers FasL and CD94. γδTc were stained with live/dead Zombie Aqua fixable viability dye (ZA) prior to surface marker staining. Median fluorescence intensity values (MFIs) of hypoxia and normoxia samples were divided by the MFI of fluorescence minus one (FMO) controls to obtain fold-change values. Surface markers on γδTc cultures subjected to 48 h 20% or 2% O_2 were not significantly different (Fig. 3.2C-K).

3.3.3 MIP1α, RANTES and CD40L are secreted by γδTc in hypoxia.

Culture supernatants from three different donor γδTc cultures subject to 40 h of normoxia or hypoxia were analyzed by cytokine array. While IL-8 appears elevated in the cumulative results graph depicted here (Fig. 3.3A), this cytokine was only greatly increased under hypoxia in one of three experiments (Fig. S3.2B, $p < 0.0001$), was moderately increased in one experiment (Fig. S3.2A, $p < 0.05$) and not significantly elevated in the third experiment (Fig. S3.2C). Due to significant variation among donor cultures, cumulative results reveal significantly increased secretion of only CD40 ligand (CD40L or CD154) under hypoxia compared to normoxia (Fig. 3.3A, $p = 0.0472$). However, in all three individual cytokine arrays, significantly increased secretion of macrophage inflammatory protein 1α [MIP1α or CCL3 = chemokine (C-C motif) ligand 3], regulated on activation, normal T cell expressed and secreted (RANTES or CCL5) and CD40L under hypoxia compared to normoxia was observed (Fig. S3.2A-C). Note that equal cell numbers were plated, and relative values at 2% and 1% O2 were normalized to normoxia without taking harvested cell numbers into account. Considering the decrease in γδTc densities observed under hypoxia, this suggests an even greater effect would be observed if comparing the output of equal cell numbers.

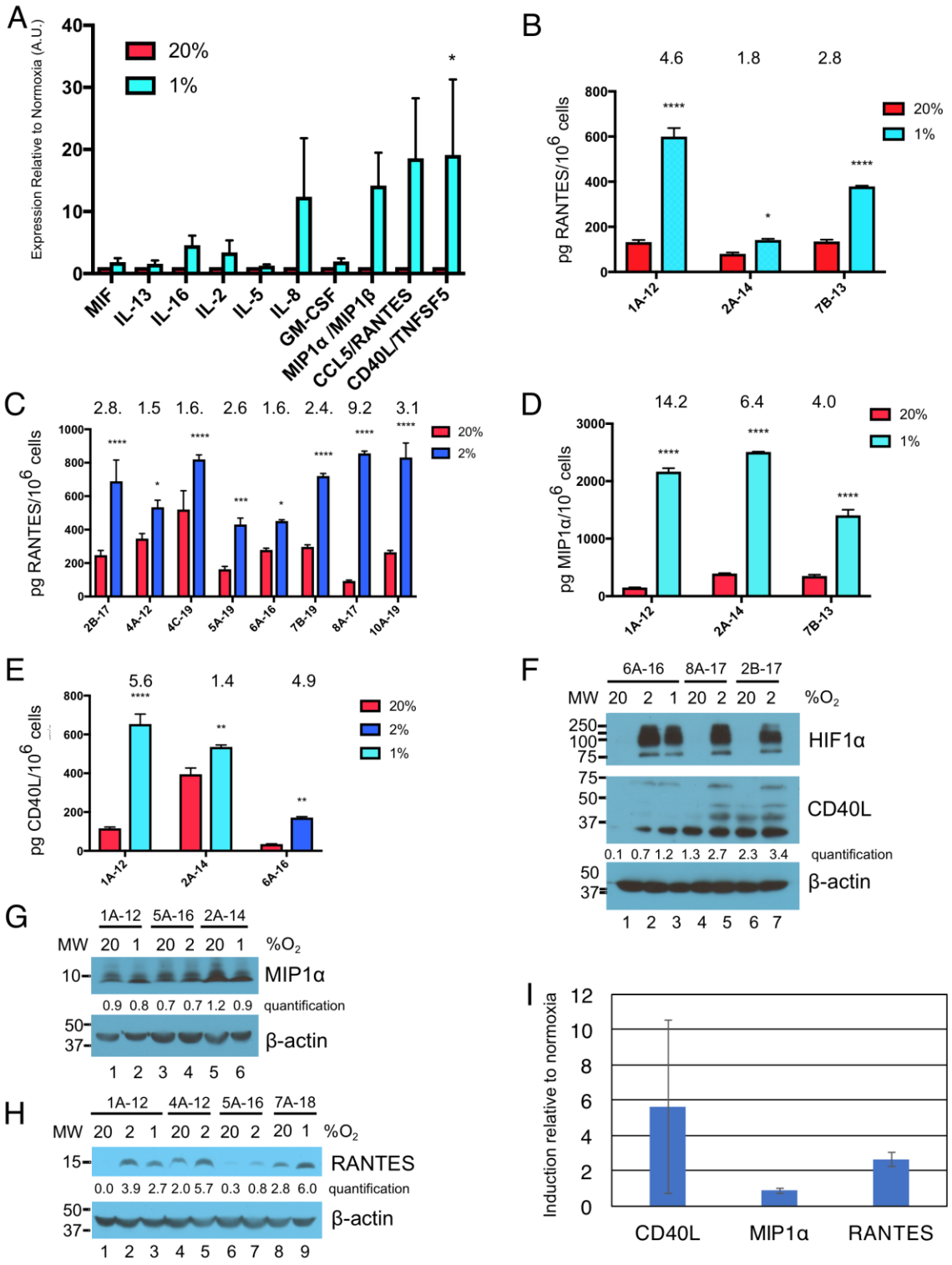

Figure 3.3. Hypoxia induces secretion of MIP1α, CCL5/RANTES and CD40L/TNFSF5 by γδ T cells. **(A)** Culture supernatants from γδ T cells subjected to 40 h at 20% or 1% O_2 were analysed by cytokine array. Cumulative results of three independent experiments for a panel of cytokines that were differentially secreted by γδ T cells under hypoxia compared to normoxia is shown. Error

bars are standard error of the mean; **(B)** ELISA validation of RANTES cytokine results shown in **(A)** for three independent experiments carried out at 20% and 1% O_2 for 40 h; **(C)** RANTES ELISA for eight hypoxia experiments carried out for 48 h at 20% and 2% O_2; **(D)** MIP1α ELISA for the same experiments shown in **(B)**; **(E)** CD40L ELISA for culture 6A-16 subject to 48 h 20% or 2% O_2, and two of the experiments shown in (B) and **(D)**. Statistical analyses for **(A-E)**: two-way ANOVA, * $P < 0.05$, ** $P < 0.01$, *** $P < 0.001$, **** $P < 0.0001$; **(F-H)** Western blot analysis of lysates from γδ T cell cultures subject to 20%, 2% and/or 1% O_2 for 48 h as indicated. γδ T cell culture identification is given above the blots and molecular weight (MW) markers are shown on the left; corresponding β-actin loading controls are shown in the bottom panels; relative band intensities were quantified and are indicated in arbitrary units; **(F)** Three examples shown for detection of HIF1α (n = 6, 5 different donors) and CD40L (n= 8, 7 γδTc cultures from 6 donors); **(G)** MIP1α (n = 7, 6 γδTc cultures from 5 donors); **(H)** RANTES (n = 7); and **(I)** Induction of proteins in **(F)** – **(H)** was determined by dividing protein band intensities from hypoxic samples by their corresponding normoxia control, and averaging these values. Error bars are standard deviation.

ELISA validation for expression of RANTES, MIP1α and CD40L was performed with culture supernatants from three different γδTc cultures (Fig. 3.3B-E, hypoxia = 1% or 2% O2 as indicated). For RANTES expression, an additional eight experiments were assayed, for secretion over 48 h at 20% or 2% O2 (Fig.3. 3C). In this case, and in contrast to the cytokine array data, ELISA values were normalized to cell numbers. Significantly increased secretion of these cytokines by γδTc was observed when cells were cultured in hypoxia compared to normoxia (asterisks indicate significance). A wide range of average secreted RANTES levels was observed, ranging from 93 –521 pg/million γδTc in normoxia to 431 – 856 pg/million γδTc under hypoxia; the average ratio hypoxia:normoxia is indicated above the bars (Fig. 3.3B-E). Likewise, secreted MIP1α and CD40L levels were quantified for three independent experiments using ELISA (Fig. 3.3D, E). MIP1α levels ranged from 152 – 394 pg/million γδTc in normoxia to 1406 – 2509 pg/million γδTc under hypoxia, with fold changes from 4.0 to 14.2 (Fig. 3.3D). Similarly, CD40L secretion by γδTc increased significantly when cultured in low O_2, with 2% O_2 in one experiment yielding an average of 171 pg CD40L/million γδTc in hypoxia, a 4.9-fold increase over just 35 pg CD40L/million γδTc in normoxia (Fig. 3.3E). Two experiments conducted with 1% O_2 yielded a wide range of CD40L secretion by γδTc in both conditions (Fig. 3.3E, 120 – 395 and 536 – 653 pg CD40L/million γδTc in normoxia and hypoxia, respectively).

Western blotting was done to verify induction of hypoxia inducible factor 1α (HIF1α) in γδTc under hypoxia, and also to investigate whether intracellular levels of CD40L, MIP1α and RANTES reflected those of secreted proteins (Fig. 3.3F-G). HIF1α was clearly induced in γδTc at 2% and 1% O_2 in all cases; three examples from six independent experiments with five donor cultures are shown (Fig. 3.3F, top panel, compare lane 1 versus 2 and 3, 4 versus 5, 6 versus 7). CD40L appears visibly increased in hypoxia samples for γδTc culture 6A-16 (Fig. 3.3F, middle panel, compare lane 1 versus 2 and 3), and quantification suggests this is also the case for the other

two donor cultures shown (lane 4 versus 5, and lane 6 versus 7). Note that several forms of CD40L are evident here, which were included in the quantification of bands. Of eight experiments with seven γδTc cultures from six donors, intracellular CD40L was clearly visibly increased in three (38%). HIF1α and CD40L blots originated from the same gel, which was transferred and then cut at 75 kDa; thus, the β-actin loading control serves for both (Fig. 3.3F lower panel). MIP1α levels were not consistently higher in γδTc subject to hypoxia versus normoxia (Fig. 3.3G, representative of seven experiments with six γδTc cultures from five donors), as demonstrated by very similar quantification values within each experiment. In contrast, RANTES was typically induced by hypoxia, with higher protein levels evident in cellular lysates from γδTc cultured in 1% or 2% O_2 compared to normoxia (Fig. 3.3H, compare lane 1 versus 2 and 3, 4 versus 5, 8 versus 9; n = seven independent experiments, seven donors, induction clear in six, unclear in one). Longer exposure of this blot also revealed RANTES induction in lane 7 versus 6 (Fig. S3.1). The average induction of CD40L, MIP1α and RANTES in γδTc under hypoxia relative to normoxia was calculated using Western blot band intensity values, and confirmed elevated levels of intracellular CD40L and RANTES, but not MIP1α, under hypoxia (Fig. 3.3I).

3.3.4 NKG2D expressed on γδTc and MICA/B on breast cancer targets are critical for γδTc killing.

MCF-7 and T47D are estrogen receptor positive luminal A breast carcinoma cell lines[458]. Both of these cell lines express MICA/B on the surface as identified by flow cytometric analysis (Fig. 3.4A, B). Blocking NKG2D on γδTc significantly decreased lysis of MCF-7 (Fig. 3.4C, one-way ANOVA vs IgG control, $p < 0.0001$, representative of four independent experiments, n = 4) and T47D (Fig. 4.4D, $p = 0.0002$, n = 5). Likewise, blocking the NKG2D ligand MICA/B on targets prevented MCF-7 and T47D cell lysis (Figs. 3.4C and 3.4D, both $p < 0.0001$, n = 2 and 3,

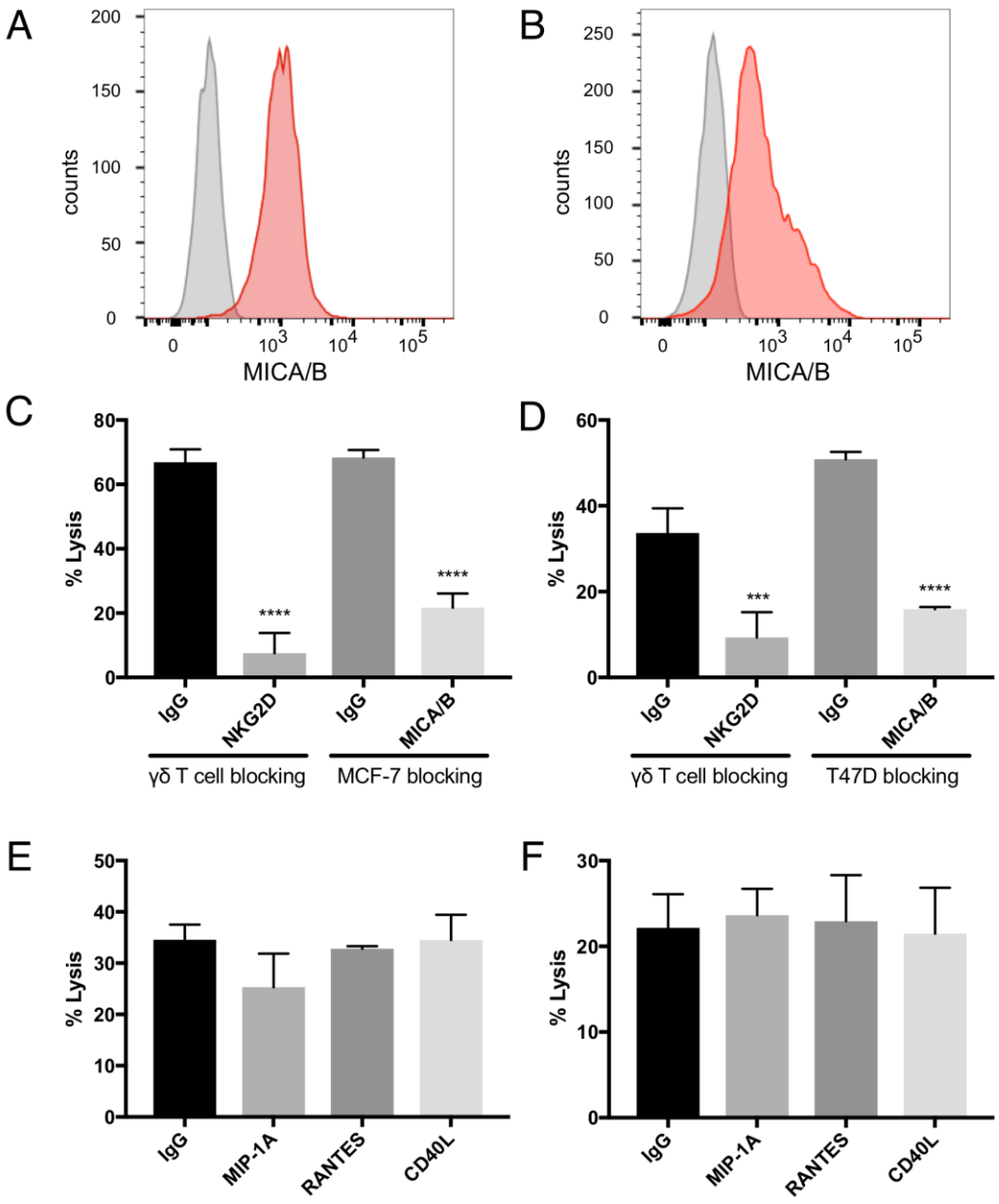

Figure 3.4. NKG2D on γδ T cells and MICA/B on breast cancer cell lines mediate γδ T cell cytotoxicity. Flow cytometric analysis of **(A)** MCF-7 (n = 4) and **(B)** T47D (n = 2) confirms that both cell lines express MICA/B; **(C)** Cytotoxicity assays in which NKG2D on γδ T cells or MICA/B on MCF-7 cells are blocked with antibodies confirm γδTc recognition of breast cancer targets via this receptor/ligand interaction, (n = 3 = representative of 3 independent experiments with 3 different donor cultures); **(D)** Blocking assays as in (C) using T47D targets, (n = 3); **(E)** Blocking MIP1α, CCL5/RANTES and CD40L/TNFSF5 does not decrease lysis of MCF-7 (n = 3 independent experiments with 2 different donor cultures) or **(F)** T47D (n = 2). Statistical analyses for (C-F): one-way ANOVA, *** $P < 0.001$, **** $P < 0.0001$.

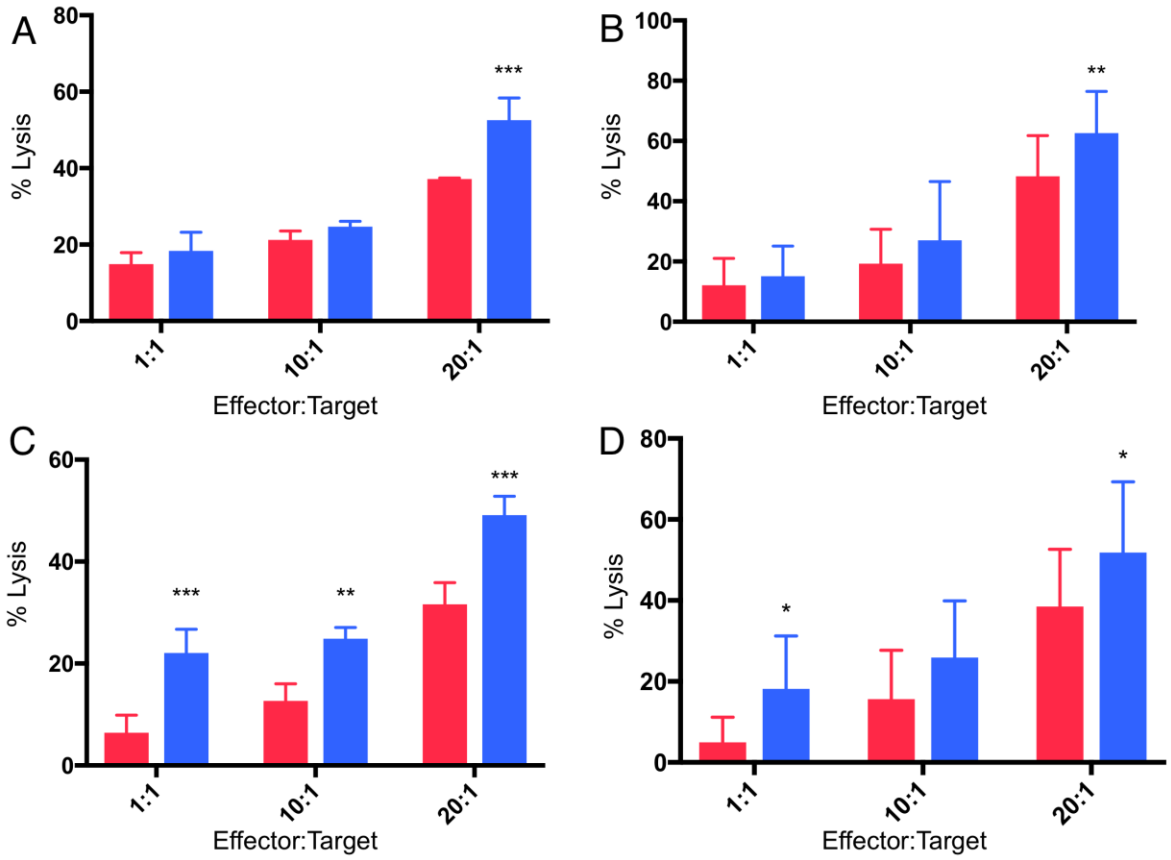

Figure 3.5. Enhanced cytotoxicity of γδ T cells cultured in hypoxia. Cytotoxicity assays comparing γδTc cultured in 20% (red bars) or 2% O_2 (blue bars) 48 h prior to co-culture with breast cancer target lines cultured at 20% O_2. **(A)** A representative example of γδTc targeting MCF-7 cells; **(B)** Compiled results from six independent experiments with γδTc cultures from five different donors targeting MCF-7; **(C)** A representative example with T47D targets; **(D)** Compiled results from five independent experiments with γδTc cultures from four different donors targeting T47D. Two-way ANOVA, * $P < 0.05$, ** $P < 0.01$, *** $P < 0.001$.

respectively). In contrast, no decrease in cell lysis of either line was observed when γδTc were pre-incubated with antibodies against MIP-1α, RANTES or CD40L (Figs. 3.4E and 3.4F, n = 3 and 2, respectively). Since antibodies were not washed away prior to co-incubation with targets, blocking should have been effective against both membrane-bound and soluble proteins. Thus, it appears that MIP-1α, RANTES and CD40L are not directly involved in γδTc cytotoxicity against MCF-7 or T47D.

3.3.5 γδTc cytotoxicity against MCF-7 and T47D targets is enhanced in hypoxia.

Cytotoxicity experiments were performed in which γδTc effectors and breast cancer cell lines were pre-incubated for 48 h under normoxia or hypoxia (2% O_2) and then co-cultured at 1:1, 10:1 and 20:1 E:T ratios in parallel under normoxia or hypoxia, as per target pre-incubation conditions, for 4 h. Pre-incubation in hypoxia enhanced γδTc cytotoxicity against MCF-7 targets cultured in normoxia (Fig. 3.5A, B). In a representative example, significantly increased MCF-7 cell lysis was observed at 20:1 (Fig. 3.5A, $p = 0.0005$); when data from all six experiments performed with day 21 γδTc from five different donors (six different cultures) were compiled and subject to statistical analysis, this result was confirmed (Fig. 3.5B, $p = 0.007$). Likewise, γδTc cultured in hypoxia were better able to kill T47D cultured in normoxia (Fig. 3.5 C, D). In an example representative of five experiments with day 21 γδTc from four different donors, target cell lysis was significantly increased at all E:T ratios tested (Fig. 3.5C, $P < 0.01$); analysis of compiled results from all five experiments revealed significantly increased lysis of targets by hypoxia-treated γδTc at 1:1 and 20:1 E:T (Fig. 3.5D, $P < 0.05$).

3.3.6 Breast cancer targets in hypoxia are resistant to γδTc killing due to MICA shedding.

As outlined above, cytotoxicity experiments were performed in which breast cancer cell lines were pre-incubated for 48h under normoxia or hypoxia (2% O_2) and then co-cultured with γδTc at 1:1, 10:1 and 20:1 E:T in parallel under normoxia or hypoxia for 4 h. In most cases (4/6, 67%), pre-incubation in hypoxia induced MCF-7 resistance to γδTc cytotoxicity (Fig. 3.6A-C). In a representative example from an experiment performed with γδTc culture 4B-21, significantly decreased MCF-7 cell lysis was observed at 10:1 (Fig. 3.6A, $p = 0.0054$) and 20:1 (Fig. 3.6A, $p = 0.0119$). In contrast, in two experiments with two different γδTc cultures from the same donor, no resistance was observed; one example is shown in which MCF-7 cultured under hypoxia appeared to be more susceptible to γδTc killing (Fig. 3.6B, $p < 0.0001$ at 1:1 and 10:1). When data from five experiments performed with day 21 γδTc from five different donors were compiled and subject to statistical analysis, the overall effect of hypoxia inducing MCF-7 resistance was confirmed (Fig. 3.6C, $p = 0.0011$). Likewise, T47D cultured in hypoxia were more resistant to γδTc killing at 20:1 than those cultured in normoxia (Fig. 3.6D, $p = 0.0043$), although the 1:1 result is opposite ($p = 0076$); these compiled results were from four experiments conducted with four different γδTc donor cultures. Flow cytometric analysis of MICA/B surface expression on breast cancer lines subjected to 48 h normoxia or hypoxia revealed no significant change in MFI; representative examples are shown for MCF-7 (Fig. 3.6E, n=4) and T47D (Fig. 3.6F, n=2). Of note, Accutase was used for dissociation of these adherent cell lines, out of concern for potential trypsin sensitivity of surface MICA/B that might have confounded our results. Supernatants from MCF-7 and T47D subject to 48 h 20% or 2% O_2 were subject to MICA ELISA (Fig. 3.6G). MICA could not be detected in supernatants directly, thus samples were concentrated and MICA ELISA was repeated. MICA in

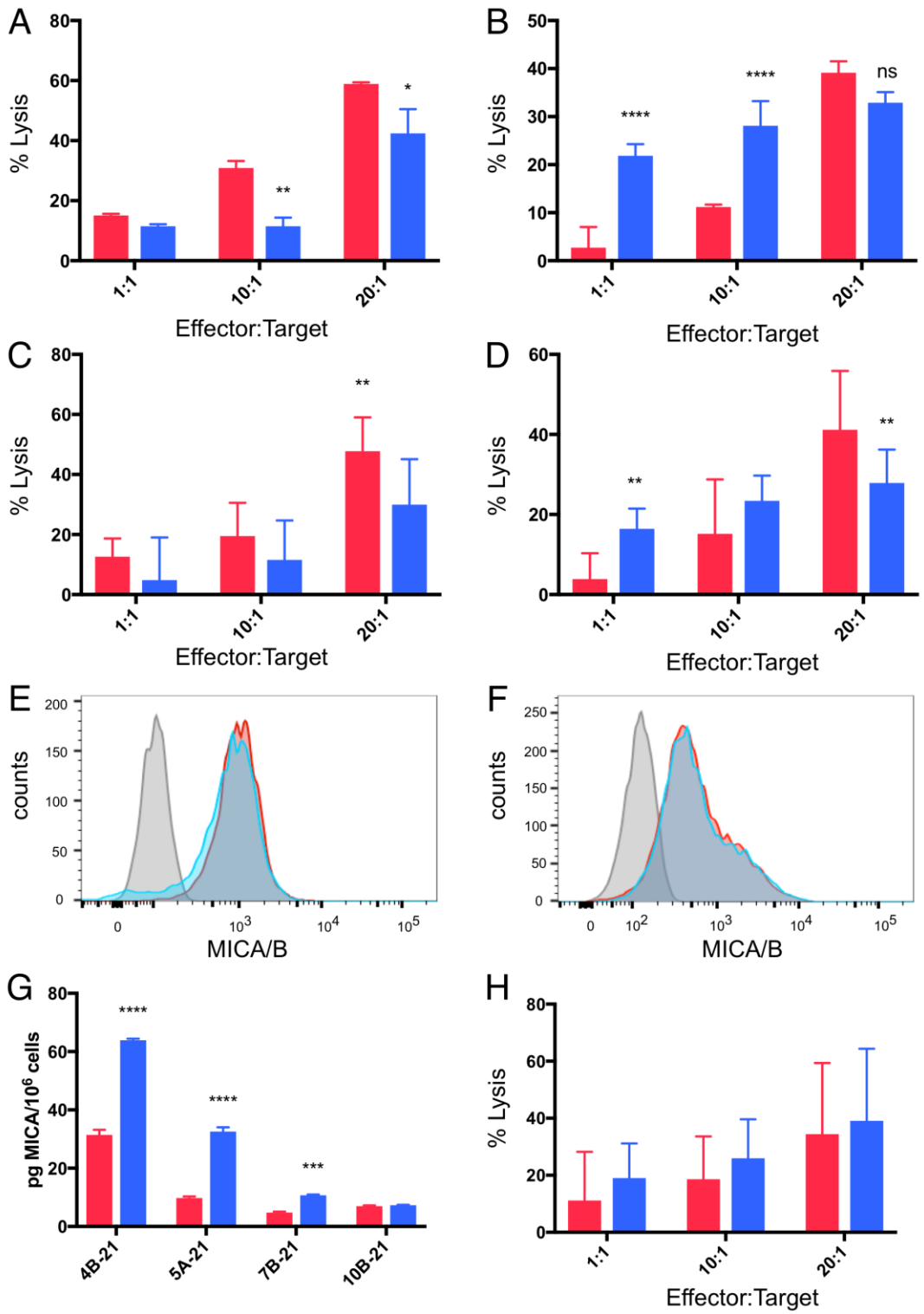

Figure 3.6. Breast cancer cell lines pre-incubated in hypoxia are resistant to γδ T cell killing. Cytotoxicity assays comparing the ability of γδTc cultured under normoxia to target breast cancer target lines cultured at 20% O_2 (red bars) or 2% O_2 (blue bars) for 48 h prior to co-culture under hypoxia; **(A)** A representative example in which MCF-7 cells were resistant to γδTc killing (4B-

21); **(B)** An example in which MCF-7 cells cultured under 2% O_2 were susceptible to γδTc killing (10B-21); **(C)** Compiled results from five independent experiments with γδTc cultures from five different donors targeting MCF-7; **(D)** Compiled results from four experiments with four different donor-dervied γδTc cultures targeting T47D; **(E)** Surface expression of MICA/B on T47D remains unchanged under hypoxia versus normoxia; **(F)** Surface expression of MICA/B on MCF-7 is not differentially impacted by hypoxia versus normoxia; **(G)** MICA ELISA on concentrated supernatants of MCF-7 from experiments in **(A)**; **(H)** Compiled results from five independent experiments with γδTc cultures from five different donors cultured at 20% O_2 or 2% O_2 targeting MCF-7 cultured under hypoxia for 48 h prior to co-culture under hypoxia. Two-way ANOVA, * $P < 0.05$, ** $P < 0.01$, *** $P < 0.001$, **** $P < 0.0001$.

T47D remained below the detection limit; however, after normalization to cell numbers, a significant increase in secreted MICA by MCF-7 cells under hypoxia was observed in 3/4 experiments (Fig. 3.6G, *** $p = 0.0005$, **** $p < 0.0001$). These results match those observed in cytotoxicity experiments, with ELISA from MCF-7 targets used in cytotoxicity assays with 4B-21 showing increased MICA secretion under hypoxia that fits with the observed resistance to γδTc cytotoxicity in Fig. 3.6A. Likewise, no difference in MICA secretion was observed in MCF-7 targets under 20% or 2% O_2 subject to cytotoxicity assays with γδTc culture 10B-21, which also showed no MCF-7 resistance to γδTc killing in Fig. 3.6B. Thus, resistance to γδTc killing appears to be correlated with MICA secretion by breast cancer targets. Despite enhanced cytotoxicity of γδTc cultured under 2% compared to 20% O_2 against targets cultured under normoxia (Fig. 3.5), they are unable to overcome resistance exhibited by MCF-7 under 2% O_2, as revealed by analysis of five compiled experiments comparing γδTc cultured under 20% or 2% O_2 against MCF-7 cells cultured in hypoxia (Fig. 2.6H).

3.4 Discussion

γδTc are being developed as immunotherapeutic agents for a variety of cancer indications and clinical trials (Phase I/II) thus far have shown excellent safety profiles[203]. Yet, they are known to embody remarkable functional plasticity, dependent on the environment in which they find themselves[115,127,459,460]. Thus, it is important to explore the function of γδTc infiltrating solid tumors, some of which may be hypoxic. In our small cohort of 17 breast cancer cases, 47% of tumors contained areas of CAIX positivity indicating hypoxia (Fig. 1). The CAIX-negative cases were 89% ER+ (Fig. 1E, cases 1-9, case 7 was of unknown ER status); of ER+ cases, 76% were CAIX negative. This confirms reports showing up to 80% CAIX negativity in studies assessing ER+ breast tumors; in these cases, CAIX negativity correlated with low histological grade[461].

While our cohort was admittedly small, the very low levels of γδTc infiltrates in CAIX-negative tumors, correlated with low histological grade, confirm results showing that levels of γδTc infiltration correlate positively with higher histological grades[462]. Unfortunately, our cohort size was too limited to determine whether γδTc infiltration correlated with patient outcome. We did, however, find γδTc in areas of hypoxia in some tumors. While we did not have the power in our study, or *in vivo* functional data, to claim that γδTc are preferentially attracted to hypoxic regions, our results at least provide an indication that γδTc can be found in hypoxic areas of tumors, and that studying their function under low O_2 is worthwhile. As CAIX is associated more so with triple negative breast cancers (TNBC)[448,463], future studies of γδTc and hypoxia should focus on a larger cohort of TNBC patients. Indeed, the groundwork for such studies has been laid by Hidalgo and colleagues, who recently reported on the pattern of distribution of γδTc in TNBC[199].

It was unsurprising that γδTc cell density decreased under hypoxia (Fig. 2), as terminally differentiated γδTc stop proliferating to become cytotoxic[464], and hypoxia enhanced γδTc cytotoxicity (Fig. 5). Delayed cell-cycle progression was also noted in a study on PBMC in hypoxia[465]. To our knowledge, the only study of γδTc in the context of hypoxia showed that circulating γδTc in patients with obstructive sleep apnea had elevated intracellular tumor necrosis factor alpha (TNFα) and IL-8 levels, increased TNFα and L-selectin-mediated adhesion properties, and enhanced cytotoxicity against endothelial cells compared to those isolated from healthy donors[466]. While that study compared freshly isolated blood-derived γδTc from patients and healthy donors, we used healthy donor derived *in vitro* expanded γδTc for our experiments, which potentially accounts for different results. TNFα secretion was not impacted by hypoxia in our study, as no differential effects were detected by cytokine array (data not shown). While we did observe strongly elevated hypoxia-induced IL-8 in the supernatant of one of three γδTc cultures subject to cytokine array analysis (Fig. S2), this was not the case for the other two cultures.

More significant were cytokine array data pointing to increased secretion of RANTES, MIP1α and CD40L by γδTc under low O_2 compared to normoxia that were confirmed by subsequent ELISAs (Fig. S2A-C and Fig. 3B-E). Intracellular protein levels induced by hypoxia matched ELISA results only in the case of RANTES (Fig. 3H); the same could not be said for CD40L and MIP1α, where hypoxia treatment did not appear to increase intracellular levels (Figs. 3F, G), and surface expression of CD40L was variable (Fig. 2K). Since blocking these proteins appeared to have no impact on γδTc cytotoxicity against breast cancer target lines (Fig. 4 E,F), they must have an indirect function related to enhanced cytotoxicity of γδTc under hypoxia.

Human memory Vγ2Vδ2 cells were reported to store cytoplasmic RANTES that was secreted rapidly in response to TCR signaling, but little MIP1α protein was found in these cells[467]. RANTES is a chemokine employed to recruit antigen presenting cells, such as dendritic cells[468,469], and thus speaks to the anti-tumor function of γδTc in hypoxia, though breast tumors may use this to their own advantage to promote malignancy[470]. RANTES and MIP1α expression were also reported to aid Vδ1 cell suppression of HIV replication[471]. CD40 ligation is thought to enhance the immunogenicity of tumors[472], thus γδTc may secrete CD40L in order to better "see" tumor targets. CD40L may also inhibit growth of CD40-expressing tumors directly[472-475]. Further investigation will be required to determine the functions served by these cytokines with respect to γδTc targeting solid tumors.

A study of the Vγ9Vδ2 γδTc subset in the context of breast cancer suggested that surface levels of MICA/B on breast cancer target cell lines were associated with γδTc cytotoxicity against these lines; however, direct blocking assays were not carried out[189]. Both MCF-7 and T47D cells expressed surface MICA/B, in contrast to an earlier report suggesting a lack of MICA/B expression on MCF-7[192]. If trypsin was used to dissociate MCF-7 in that study, it might explain their inability to detect MICA/B; to avoid this issue, we used Accutase to dissociate our adherent cell lines, as

detachment of cells is gentler and protects most surface epitopes. We have confirmed the involvement of NKG2D on γδTc and MICA/B on MCF-7 and T47D in cytotoxicity of γδTc against breast tumor targets (Fig. 4), although differences in the ability of γδTc to kill targets pre-incubated in hypoxia or normoxia do not appear to be related to surface levels of MICA (Fig. 6).

One mechanism of hypoxia-mediated tumor evasion is MICA shedding[400]. MICA downregulation related to shedding under hypoxia, as well as downregulated expression of NKG2D on PBMCs incubated with culture supernatants of prostate cancer cells exposed to hypoxia - abrogated upon incubation with MICA blocking antibodies - has been reported[404]. MICA shedding is not a universal evasion mechanism employed by all cancer cells, however, as glioblastoma cell lines did not shed MICA, although this study was only carried out under normoxia[416]. While we assume that soluble MICA may bind NKG2D and block or downregulate this receptor to prevent γδTc recognition of breast cancer targets, a recent report suggests that, in mice, soluble NKG2D might activate NK cells and aid in tumor eradication, but this anti-tumor effect has yet to be shown in humans or with γδTc[476]. In contrast, soluble MIC was shown to decrease γδTc cytotoxicity in pancreatic cancer[217] and has been implicated in evasion of human ovarian cancer cells from γδTc recognition[451]. Thus, we were surprised that surface expression of MICA/B on MCF-7 and T47D breast cancer lines appeared unaffected by 48 h under hypoxia (Fig. 6). However, MICA secretion did not correlate with MICA surface levels, as soluble MICA increased in the supernatants of MCF-7 cells cultured under hypoxia, while surface MICA levels remained unchanged (Fig. 6). Thus, it appears that we would need to neutralize soluble MICA to improve γδTc cytotoxicity, since target surface expression did not appear to be affected by hypoxia. That said, we did not directly assess MICA expression during co-culture with γδTc, and it is possible that MICA was downregulated in the presence of γδTc, although the correlation between resistance to γδTc killing and soluble MICA levels in culture supernatants under hypoxia speaks

against this (Fig. 6). One way to overcome MICA shedding may be to increase nitric oxide signaling[404], although its impact on γδTc would have to be assessed.

Although the γδTc TIL signature was deemed the most positive prognosticator across a range of cancers, including breast cancer[178], some reports suggest that γδTc may take on a regulatory phenotype within the breast TME[192,462,477,478]. In one study, γδTc TIL isolated from a breast tumor were expanded in high levels of IL-2 for several weeks prior to immunosuppression assays and proved to inhibit dendritic cell maturation and CD8+ T cell cytotoxicity[192]; however, given the known functional plasticity of γδTc, such assays conducted on *ex vivo* expanded cells removed from the TME cannot inform the function of γδTc *in situ*. A positive correlation was observed between γδTc infiltration and breast cancer stage, leading the authors to suggest that γδTc may contribute to disease pathology; however, causality was not established[462]. Although our cohort size was much smaller, we too observed a positive correlation between CAIX expression, indicating hypoxia – typically an indicator of cancer progression – and γδTc infiltration (Fig. 1). This could just as easily indicate the greater need for γδTc attempting to eradicate disease. Our hypoxia experiments reveal enhanced cytotoxicity of γδTc exposed to 48 h of low O_2, suggesting that γδTc are indeed able to kill in this environment (Fig. 5). Soluble MICA appears to inhibit γδTc cytotoxicity against breast tumor targets in hypoxia and, despite their increased killing capacity under low O_2, γδTc are unable to overcome resistance exhibited by MCF-7 under 2% O_2 (Fig. 6), a condition under which γδTc must operate within at least some parts of a tumor. Further studies will be required to definitively identify γδTc function in breast tumors *in situ*.

3.5 Conflict of Interest Statement

The authors declare no conflicts of interest.

3.6 Author Contributions

GMS and LMP contributed to research design. GMS and ID conducted experiments; data analysis was carried out by GMS, ID and RL. GMS wrote the manuscript; all authors provided feedback and approved the final version.

3.7 Funding

This work has been funded by the London Regional Cancer Program, London, ON (Translational Breast Cancer Postdoctoral award to GMS), the Cancer Research Society (CRSOG2013 to LMP and GMS) and the Canadian Breast Cancer Foundation (LMP). Support was also provided by the Sawin-Baldwin Chair in Ovarian Cancer, Dr. Anthony Noujaim Legacy Oncology Chair, and Alberta Innovates Health Solutions Translational Health Chair to LMP. ID has been supported by the Queen Elizabeth II Graduate Scholarship, the University of Alberta Doctoral Recruitment Scholarship and the Alberta Cancer Foundation Antoine Noujaim Scholarship.

3.8 Acknowledgements

Flow Cytometry was performed at the University of Alberta, Faculty of Medicine and Dentistry Flow Cytometry Facility, which received financial support from the Faculty of Medicine and Dentistry and the Canadian Foundation for Innovation (CFI) awards to contributing investigators. We thank Nidhi Gupta for assistance in obtaining the breast tumor tissues, and Achim Jungbluth for sharing his protocol for detection of γδTc by immunohistochemistry prior to its publication.

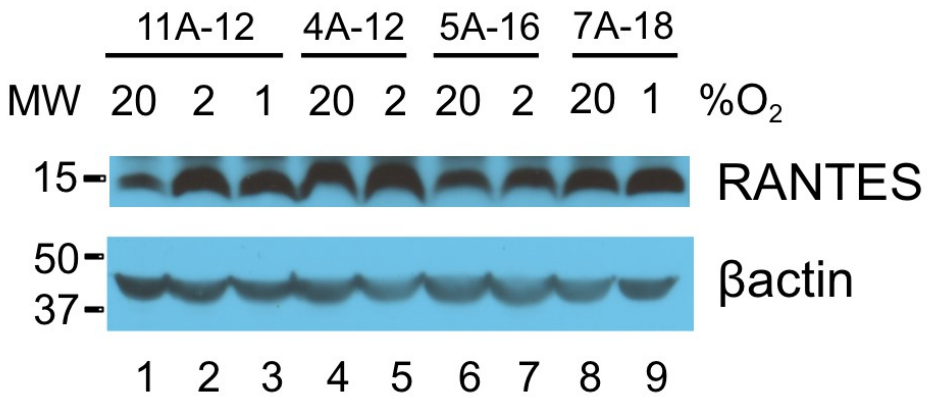

Figure S3.1 Intracellular RANTES is induced in γδ T cells under hypoxia. Western blot analysis of lysates from γδ T cell cultures subjected to 20%, 2% and/or 1% oxygen as indicated. γδ T cell culture identification is given above the blots and molecular weight (MW) markers are shown on the left. This is a longer exposure of the RANTES blot shown in Fig. 3.3H, with the same β-actin loading controls.

Table S3.1 Edmonton donor γδ T cell culture subset percentages and purities. Cells were harvested on the indicated day, stained with zombie aqua fixable viability dye followed by antibodies recognizing pan γδ TCR, Vδ1 TCR and Vδ2 TCR and acquired by flow cytometry. The sum of %Vδ1, %Vδ2 and %γδTCR+Vδ1-Vδ2- is the purity. Figures in which results from these cultures appear are listed.

ID	Day	% Vδ1	% Vδ2	% γδTCR+Vδ1-Vδ2-	% Purity	Figure(s)
1A	21	23.2	69.3	5.5	98.0	3A,B,D,E,G,H
2A	17	11.6	74.8	1.8	88.2	3B,D,E,G
2B	19	5.4	91.0	0.9	97.3	3C,F
4A	12	47.0	22.4	11.0	80.4	2C-F; 3C,H
4B	21	36.3	42.1	6.0	84.4	5B,D; 6C,D,G,H
4C	21	20.1	58.0	5.1	83.2	3C; 4E,F
5A	21	11.4	78.8	4.2	94.4	2C-F; 3C,G,H; 4C,D; 5B,D; 6C,D,G,H
6A	21	12.1	79.3	3.4	94.8	2C-F; 3C,E,F
7A	21	1.1	86.7	3.6	91.4	2C-F; 3H
7B	19	2.3	88.9	2.7	93.9	2C,D; 3B-D; 5B,D; 6C,G,H
8A	21	42.0	46.2	9.5	97.7	2C-F; 3C,F
9A	21	6.6	85.0	2.7	94.3	2C,D; 5B; 6C,H
10A	21	7.5	73.3	2.5	83.3	2C,D; 3C; 5A,B,D; 6C,D
10B	21	19.9	64.0	3.7	87.6	5B-D; 6B,D,G,H

Chapter 4: ADAM protease inhibition overcomes resistance of breast cancer stem-like cells to γδ T cell immunotherapy

ADAM protease inhibition overcomes resistance of breast cancer stem-like cells to γδ T cell immunotherapy

Indrani Dutta[1], Dylan Dieters-Castator[2], James W. Papatzimas[3], Anais Medina[1], Julia Schueler[4], Darren J. Derksen[3], Gilles Lajoie[5], Lynne-Marie Postovit[1] and Gabrielle M. Siegers[1*]

[1]Department of Experimental Oncology, University of Alberta, Edmonton, AB, Canada.
[2]Department of Anatomy and Cell Biology, Western University, London, ON, Canada.
[3]Department of Chemistry, University of Calgary, Calgary, AB, Canada.
[4]Charles River Discovery Research Services Germany, Freiburg, Germany.
[5]Department of Biochemistry, Western University, London, ON, Canada.

*To whom correspondence should be addressed: Gabrielle M. Siegers, 5-142G Katz Group Building, University of Alberta, Edmonton AB, Canada T6G 2E1. E-mail: siegers@ualberta.ca

Running Title: γδ T cell immunotherapy against breast cancer stem cells

Abstract

Gamma delta T cells (γδTc) have tremendous anti-tumoral activity, thus γδTc immunotherapy is currently under development for various malignancies. We targeted breast cancer stem-like cells (BCSC), a rare cell population responsible for patient mortality. BCSC were mostly susceptible to γδTc immunotherapy, yet some escaped. The BCSC secretome rendered γδTc hypo-responsive, and resistant BCSC expressed more PD-L1 and anti-apoptotic protein MCL-1 than non-stem-like cells (NSC). BCSC resistance was partially overcome by dMCL1-2, an MCL-1 degrader, or more fully by blocking PD-1 on γδTc. Increased MICA shedding was prevented by the ADAM inhibitor GW280264X, rendering BCSC as sensitive to γδTc cytotoxicity as NSC. Our data show promising potential for γδTc immunotherapy against BCSC while unraveling immune evasion mechanisms exploited by BCSC, which likely also enable their resistance to cytotoxic T and NK cells. Overcoming this resistance, as we have done here, will improve cancer immunotherapy, leading to better cancer patient outcomes.

Keywords: gamma delta T cells, breast cancer stem cells, immune evasion, MICA, PD-1

4.1. Introduction

Breast cancer is the most frequently diagnosed neoplasia and the leading cause of cancer-related mortality in women worldwide[479]. This mortality rate is attributed to drug resistance, recurrence and metastatic spread due to breast cancer stem-like cells (BCSC), a subpopulation of cells driving tumor initiation and progression. The $CD44^{+}/CD24^{-/low}$ phenotype enriches for BCSC in cell lines and tumor samples, correlates with distant metastases[480] and predicts poor prognosis in triple-negative breast cancer (TNBC)[481]. Hence, BCSC have emerged as a crucial therapeutic target.

Immunotherapy has revolutionized cancer treatment. While most immunotherapies have focused on harnessing the potential of alpha beta T cells (αβTc), γδTc also have potent anti-tumoral activity[112]. Gamma delta T cells offer several notable advantages over αβTc: Clinical trials have established their safety, γδTc do not cause graft-versus-host disease, they are not impacted by peptide-MHC antigen loss, and they respond faster to stress signals[115].

Target recognition is mediated by the γδ T-cell antigen receptor (TCR) and/or Natural Killer receptors such as NKG2D that recognizes NKG2D ligands (NKG2DL) upregulated on transformed cells[482]. Upon recognition, γδTc lyse tumors *via* perforin, granzymes, Fas Ligand (FasL) and TNF-related apoptosis-inducing ligand (TRAIL)[112]. Activated γδTc also secrete high levels of pro-inflammatory cytokines such as interferon-γ (IFN-γ) that stimulate and regulate the function of other immune cells[112].

Breast cancer cells are targeted by γδTc [165,166,187,189,200,446,483]. In a clinical trial treating advanced-stage refractory breast cancer, three of ten patients survived past 12 months and showed durable maintenance of robust γδTc numbers[111].

Here, we used primary human γδTc derived and expanded from the blood of healthy donors[207] to

determine whether γδTc can target BCSC. While γδTc could kill BCSC, some were resistant. This resistance was orchestrated by several immune evasion mechanisms, which we specifically targeted to restore sensitivity to γδTc immunotherapy.

4.2. Materials and Methods

4.2.1 Ethics Statement

This study was conducted in compliance with the recommendations of the Research Ethics Guidelines, Health Research Ethics Board of Alberta—Cancer Committee with written informed consent from all participants according to the Declaration of Helsinki. The Animal Use Subcommittee at the University of Alberta approved the *in vivo* experiment protocol used in this study (AUP00001288).

4.2.2 Primary Human γδ T Cells

Primary human γδTc cultures were established and maintained as described [207]. Briefly, peripheral blood mononuclear cells were extracted from blood drawn from healthy donors using density gradient separation (Lymphoprep, Stem Cell Technologies, Vancouver, BC, Canada) and cultured at 1×10^6 cells/ml in RPMI complete medium containing 1μg/ml Concanavalin A (Sigma-Aldrich, Oakville, ON, Canada), 10% fetal bovine serum (FBS), 1× MEM NEAA, 10mM HEPES, 1 mM sodium pyruvate (all Invitrogen, Burlington, ON, Canada) plus 10ng/ml recombinant human IL-2 and IL-4 (Miltenyi Biotec, Auburn, CA, USA). Cells were maintained in a humidified incubator at 37°C with 5% CO_2. Cells were counted every two to three days and densities were adjusted back to 1×10^6 cells/ml by adding fresh medium and cytokines. After seven days, αβTc were depleted by labeling with anti-TCRαβ PE antibodies (BioLegend, San Diego, CA, USA) followed by anti-PE microbeads (Miltenyi Biotec), filtering through a 50μm Cell Trics filter

(Partec, Görlitz, Germany) and passing through an LD depletion column on a MidiMACS magnet (both from Miltenyi Biotec). The flow-through contained γδTc, which were collected and further cultured in RPMI complete medium plus cytokines (as above) at 37°C with 5% CO_2. Subset percentages and purities of different donor-derived γδTc cultures are listed in Table S1. As γδTc were most differentiated and therefore most cytotoxic by the end of the culture period (days 19-21), most experiments including cytotoxicity assays were done on those days. Exceptions were proliferation and inhibitory receptor assays, which were begun earlier in the culturing period.

4.2.3 Breast Cancer Cell Lines

Inflammatory TNBC SUM149 cells were obtained from ATCC and cultured in Ham's F-12 medium with 5% heat-inactivated FBS, 10mM HEPES, 1µg/mL hydrocortisone and 5µg/mL insulin. SUM149 cells were last tested for mycoplasma in house using the ATCC PCR-based mycoplasma detection kit in May 2019. The patient derived xenograft cell line PDX401, obtained *via* collaboration with Oncotest (Charles River Discovery, Freiburg, Germany), was derived from a well-differentiated basal-like TNBC tumor. PDX401 cells were cultured in RPMI-1640 containing 10% FBS and 1% Gentamycin. Luminal A breast cancer cell lines, MCF-7 and T47D, were obtained from ATCC and cultured in RPMI with 10% FBS. All breast cancer cells were authenticated at the Sick Kids Research Institute, Toronto, ON, Canada in June 2018. Cells were used for up to 8 passages after thawing.

4.3.4 Mice

8-11-week-old NOD.Cg-Prkdc^{SCID}Il2rg^{tm1Wjl}/SzJ (NSG) mice were injected intravenously with SUM149 cells alone or SUM149 cells previously treated with γδTc. 500,000 cells were suspended in 100µl PBS plus 0.2% BSA and injected into the tail vein, however, some mice only

received 90µl cell suspension, as indicated. 18 weeks later, the mice were sacrificed and their lungs stained with India Ink to identify macro metastasis[484]. The lungs were then stored in Fekete's solution. The metastases appear white on the black stained lungs.

4.3.5 Image Analysis

Lung images were taken with an iPhone 11, which has a 12 mega-pixel wide-angle camera, with the lungs submerged in Fekete's solution. The images were opened with ImageJ (Wayne Rasband National Institute of Health, USA, version 1.52q), converted to 8-bits and inverted. Regions of Interest (ROI) were traced around the "white metastases" (that appear black when inverted) and around total lung, and the areas of these regions were noted. Percent metastases were calculated as 100 x (area of white metastasis/area of total lung).

4.3.6 Calcein AM (CalAM) Cytotoxicity/Blocking Assays

Cytotoxicity and blocking assays were done as described[446]. Target cells were labeled with 5µM CalAM in PBS (Invitrogen/Thermo Fisher Scientific, Waltham, MA, USA). Target cells were diluted to a density of 30,000 cells/100µl medium (RPMI 1640 plus 10% heat-inactivated FBS; 10mM HEPES; 1× MEM NEAA; 1 mM sodium pyruvate; 50U/ml penicillin–streptomycin; and 2mM l-glutamine, all from Invitrogen) and γδTc were re-suspended to 600,000 cells/100µl in medium. An aliquot of the diluted γδTc was further diluted down to 300,000 cells/100µl in medium and 30,000 cells/100µl to obtain effector:target ratios of 20:1, 10:1 and 1:1, respectively. 100µl CalAM-labeled targets were added to 100µl γδTc in 96-well round-bottom plates in triplicate followed by incubation at 37°C for 4 h. For blocking experiments (including PD-1 blocking), 4µg of blocking antibody were added to 400µl cell suspension of γδTc or targets (as indicated) for each test in Eppendorf tubes, then 100µl were plated per well in a 96-well round-bottom plate in

triplicate. For blocking assays, untreated and IgG-treated cells were used as experimental controls. After incubation with blocking antibody at 37°C for 30 min, CalAM-labeled targets were added to γδTc followed by incubation at 37°C for 4h. Plates were then centrifuged and supernatants transferred to fresh 96-well plates (Corning 96-well, black cell culture-treated flat-bottom microplate with clear bottom, Fisher Scientific) for CalAM fluorescence detection on a fluorimeter (FLUOstar Omega, BMG labtech). Controls were CalAM-labeled target cells incubated alone (spon = spontaneous release) or with 0.05% Triton-X 100 (Thermo Fisher Scientific, max = maximum release). Percent lysis was calculated: [(test − spon)/(max − spon)] × 100%.

For degrading MCL-1 during cytotoxicity assays, 500nM dMCL1-2 or DMSO was added directly to the co-incubation. The MCL-1 degrader, dMCL1-2, was synthesized by the Dersken lab, University of Calgary[268]. For ADAM inhibition experiments, 3μM ADAM inhibitor (GW280264X, Aobious Inc., Massachusetts, USA) or DMSO was added to the co-incubation.

4.3.7 Mammosphere Assays

Target cells were trypsinized, passed through a 50μm cell strainer (CellTrics) and seeded into ultra-low adherent plates (Corning, NY, USA) in MammoCult media (StemCell Technologies, Vancouver, BC, Canada) as per manufacturer's instructions. Mammospheres formed after 7 days were collected by centrifugation at 1000 rpm. For serial passaging, mammospheres were dissociated into single cells and seeded again into ultra-low adherent plates (Corning).

4.3.8 Flow Cytometry

4.3.8.1 Surface Marker Staining

Gamma delta T cells and/or breast cancer cell lines were stained as described in [165]. Briefly, γδTc and/or breast cancer cell lines were stained with Zombie Aqua (ZA, BioLegend) or Zombie

Near Infrared (ZNIR, BioLegend) fixable viability dye as per the manufacturer's instructions, washed and then fluorochrome-conjugated antibodies diluted in FACS buffer [PBS containing 1% FBS and 2mM EDTA (Invitrogen)] were used to stain γδTc. Breast cancer cell lines were blocked at 10×10^6 cells/ml in FACS buffer containing 50µl/ml Trustain FcX (BioLegend) on ice for 30 min prior to antibody incubation. After blocking, cells were centrifuged and supernatants were removed, leaving 10µl FACS buffer plus block/10^6 cells. Antibodies and FACS buffer were added to 20µl, and cells were then incubated on ice for 10–15 min followed by washing. All cells were fixed in FACS buffer containing 2% paraformaldehyde (Sigma-Aldrich), stored at 4°C and acquired within one week. For flow sorting, cells were stained as described above in sorting buffer (dPBS with 2% FBS, 1mM EDTA, 10mM HEPES and 5% penicillin/streptamycin). Live cells were gated according to their forward scatter and side scatter profiles. The detailed list of antibodies and dilutions used can be found in Supplementary Table S4.

4.3.8.2 CD107 Assays

CD107 assays were performed as previously published[137]. Briefly, 1 x 10^5 γδTc with 5µL anti-CD107 AF647 antibody (Biolegend) were plated alone or mixed with 5 x 10^5 target cells in 200µl complete media in a 96-well round-bottom plate in triplicate. To the positive control wells, phorbol-12-myristate-13 acetate (PMA)/ionomycin (0.15nM/0.3µg/mL final concentrations) was added. Cells were incubated for 1h at 37°C and then 6µg/ml monensin (Golgi-stop, BD) was added. Cells were further incubated for another 2h at 37°C, after which cells were covered and put on ice. Further staining was performed as described in surface marker staining above.

4.3.8.3 Detection of Intracellular IFN-γ

Conditioned media (CM)-treated γδTc were incubated with 5μg anti-CD3 antibody (UCHT1, BioLegend) per million cells followed by addition of 6μg/ml of monensin (Golgi-Stop, BD) after an hour. After another 5h, cells were washed, fixed, permeabilized and stained with anti-IFN-γ antibody according to the manufacturer's instructions (Cytoperm/Cytofix™ solution kit, BD Biosciences). PMA/ionomycin-stimulated cells were used as a positive control.

4.3.8.4 Detection of Apoptosis

Apoptosis analyses were performed as previously published[446]. Cultured γδTc or cancer cells were stained with 5ng/μl ZA fixable viability dye (BioLegend) for 15–20 min after which they were washed with 1× Annexin V (AnnV) binding buffer (BioLegend), and stained with AnnV FITC (BioLegend, 1:20) on ice for 15 min in the dark. Cells were then washed and re-suspended in 200μl AnnV binding buffer plus 2% paraformaldehyde and stored at 4°C until analyzed, within one week.

4.3.8.5 CellTrace Violet Proliferation Assay

Gamma delta T cells were incubated with the indicated CM for 24h, washed, labeled with 1μM CellTrace Violet™ (Thermo Fisher Scientific) as per the manufacturer's instructions, and cultured in fresh media for six additional days. Cells were then washed and fixed in FACS buffer containing 2% paraformaldehyde prior to flow acquisition. Proliferation modeling was performed using FlowJo™ software, version 10.5.3.

4.3.8.6 Flow Cytometers

Antibody-stained cells were analyzed using a FACS CANTO II (Becton Dickinson, Mississauga, ON, Canada). For calibration, CS&T beads (Becton Dickenson, Mississauga, ON,

Canada) were used. Forward and side-scatter properties were used to gate on singlets. Fluorescence minus one (FMO) controls were used to set gates. Cell sorting was done using a FACSAria III cell sorter (Becton Dickinson, Mississauga, ON, Canada). Analysis of acquired data was performed using FlowJo© software (Tree Star, Ashland, OR, USA, Version 10.0.8r1) unless otherwise indicated.

4.3.8.7 Flow Cytometer Specifications

The FACS CANTO II (Becton Dickinson, Mississauga, ON, Canada) has an air-cooled 405-nm solid state diode, 30 mW fiber power output violet laser, with 450/50 and 510/50 band pass (BP) [502 long pass (LP) detector]; a 488-nm solid state, 20-mW blue laser with 530/30 BP (502 LP), 585/42 BP (556 LP), 670 LP (655 LP), and 780/60 BP (735 LP) filters; and a 633-nm HeNe, 17-mW red laser with 660/20 BP and 780/60 BO (735 LP) filters.

The FACSAria III cell sorter (Becton Dickinson, Mississauga, ON, Canada) has fiber-launched fixed-wavelength air cooled lasers: 488 nm blue laser with 530/30nm, 695/40 nm filters; 561nm yellow/green laser with 582/21 nm, 610/20 nm, 670/14 nm,710/50 nm, 780/60 nm filters; 633 nm red laser with 660/20 nm, 730/45 nm, 780/60 nm filters; and 405 nm violet or 375 nm near UV laser with 450/40 nm, 510/50 nm, 610/20 nm, 660/20 nm, 710/50 nm and 780/60 nm filters.

4.3.9 ELISA

Culture supernatants (1-2 ml) were stored at −80°C. Upon thawing, Halt™ Protease and Phosphatase Inhibitor Cocktail (PIC, Thermo Fisher Scientific) was added to samples prior to use in ELISAs or further storage at 4°C. The following ELISA kits were used: human MICA DuoSet ELISA (R&D systems) and ELISA MAX™ Deluxe Set Human IFN-γ (Biolegend). For MICA ELISAs, supernatants were concentrated using Amicon Ultra-4 10 K spin columns (Merck-

Millipore, Carrigtwohill, Ireland). The columns were centrifuged at 3,000 g for 2h at 12°C. The final volume of concentrated media was adjusted to 200µl, and 100µl per well were plated in duplicate. All ELISAs were done according to the manufacturer's instructions. Absorbance was measured at both 450 and 550 nm using a FLUOstar Omega plate reader (BMG Labtech, Offenburg, Germany) with Omega Software version 5.11. For calculating concentrations, the difference linear regression fit of the standard curve was used. ELISA data were normalized to cell numbers.

4.3.10 Immunoblotting

Cell lysates were prepared by treating γδTc or breast cancer cell lines with M-PER Mammalian Protein Extraction Reagent (Thermo Fisher Scientific) containing PIC at 10µl lysis buffer per million γδTc or 50µl per million tumor cells followed by incubation at room temperature for 10 min. Lysates were then centrifuged at 13,000 rpm for 20 min at 4°C, after which supernatants were transferred to fresh tubes. Then 5× reducing sample buffer [0.0625 M Tris/HCl pH6.8, 2% SDS, 20% glycerol, 0.05% β-mercaptoethanol, 0.025% (w/v) Bromophenol Blue] was added. Samples were boiled 5 min, cooled, and briefly centrifuged in a benchtop centrifuge prior to running on 10% or 12% SDS-PAGE gels. Proteins were transferred onto Immobilon-FL PVDF membranes (Millipore) using the Trans-Blot Turbo Transfer System (Bio-Rad, Mississauga, ON, Canada). The "high MW" program was used for ADAM 10 and ADAM 17 detection; "mixed MW" program was used for all other proteins. Membranes were blocked for 40 min in 3% milk in TBST, followed by overnight incubation in primary antibody baths at 4°C. The next day, after washing, membranes were incubated with the corresponding species-specific HRP-labeled secondary antibody for 1h, followed by further washing and then detection using Clarity™ Western ECL Substrate (Bio-Rad). Antibodies used are listed in Supplementary Table S4.

4.3.11 Mass Spectrometry

4.3.11.1 Sample preparation

Samples were prepared as described in [485]. Briefly, to prepare CM for LC-MS, concentrated CM were lyophilized and re-suspended in 8M urea, 50mM ammonium bicarbonate (ABC), 10mM dithiothreitol (DTT) and 2% sodium dodecyl sulfate. CM proteins were quantified using a Pierce™ 660nm Protein Assay with Ionic Detergent Compatibility Reagent (Thermo Scientific™). 10-50 µg were reduced in 10mM DTT for 30 minutes and alkylated in 100mM iodoacetamide for 30 minutes at room temperature in the dark. Proteins were immediately precipitated in methanol/chloroform. Briefly, samples were topped up to 150µL with 50mM ABC, mixed with 600µL ice cold methanol and 150µL of ice cold chloroform, and vortexed thoroughly. An additional 450µL 4°C distilled water were added followed by vortexing and centrifugation at 14,000 xg for 5 min. The upper aqueous/methanol phase was carefully removed to avoid disturbing the precipitated protein interphase. A second 450µL of cold methanol were added to each sample before the tube was inverted several times and centrifuged at 14,000 xg for 5 min. The remaining methanol/chloroform was discarded and the precipitated protein pellet was left to air dry in a fume hood. On-pellet in-solution protein digestion was performed. Briefly, precipitated protein pellets were reconstituted in 100µL 50mM ABC (pH 8) and sonicated (~3 x 0.5s pulses) with a probe sonicator (Fisher Scientific, Waltham, MA) to the break up the pellet. LysC (Wako Chemicals, USA) and mass spec grade trypsin/LysC mix (Promega, Madison, WI, USA) were added to protein samples at 1:100 and 1:50 ratios, respectively. Protein digestion was carried out at 37°C on a ThermoMixer C (Eppendorf) at 400 rpm overnight (~18h). The next day an additional volume of trypsin/LysC mix (1:100 ratio) was added to each sample and mixed at 1400 rpm. After 3-4h,

digests were acidified to pH 3-4 with 10µL 10% formic acid (FA) and centrifuged at 14,000xg to pellet insoluble material prior to LC-MS/MS.

4.3.11.2 LC-MS/MS

Digests were analyzed on Q Exactive Plus mass spectrometer (Thermo Scientific) connected to a Waters ACQUITY M-Class UPLC. Solvent A consisted of water/0.1% FA and solvent B consisted of acetonitrile/0.1% FA. Peptides (~1µg estimated using a Pierce™ bicinchoninic acid assay) were initially loaded onto an ACQUITY UPLC M-Class Symmetry C18 Trap Column (5µm, 180µm x 20mm) and trapped for 6 min at a flow rate of 5µl/min at 99% A/1% B. Peptides were separated on an ACQUITY UPLC M-Class Peptide BEH C18 Column (130Å, 1.7µm, 75µm X 250mm) operating at a flow rate of 300nL/min at 35°C using a non-linear gradient consisting of 1-7% B over 1 minute, 7-23% B over 179 minutes and 23-35% B over 60 minutes, followed by washing and re-equilibration. The MS acquisition instrument settings are same as used in [485]

4.3.11.3 Data analysis

MS files were searched in MaxQuant against the Human Uniprot database (reviewed entries plus isoforms) [486]. Missed cleavages were set to 3 and cysteine carbamidomethylation was set as a fixed modification. Oxidation (M), N-terminal acetylation (protein), and deamidation (NQ) were set as variable amino acid modifications (max. number of modifications per peptide = 5). LFQ min. ratio count was set to 1 and all other settings were left as default settings. Protein and peptide FDR was left at 0.01 (1%) and the decoy database was set to revert. The ‘match between runs’ feature was utilized to maximize proteome coverage and label-free quantification. Search results were loaded into Perseus or R, and proteins labeled as ‘only identified by site’, ‘matched to reverse’ or

'potential contaminant' were removed similar to previously reported in [485]. Protein identifications with label-free quantification (LFQ) values in ≥2 biological replicates were retained for downstream analysis, and missing values were imputed using a width of 0.3 and down shift of 1.8. Gene ontology cellular component (GOCC) annotations were performed using Metascape (version 3.0). Gene set enrichment analysis (GSEA) were performed in GSEA v3.0 (Broad Institute) with a minimum gene set size of 10 and permutation type set to gene_set. Molecular Signature Database (MSigDB) v6.2 collections used were: canonical pathways, hallmark, KEGG gene sets, and C2 curated sets. Heatmaps were produced using the Bioconductor package complexHeatmap.

4.3.12 Statistics

All statistical tests were performed, as indicated in the figure legends, using Prism 7.0 for Mac OSX (GraphPad Software, San Diego, CA, USA). Sample sizes were chosen empirically to ensure sufficient statistical power and were in line with field standards for the techniques used in this study. The Shapiro-Wilk test was done to determine normality for all data. In cases where normality was not achieved, non-parametric tests were employed. Depending on the experimental design, the following methods were used to determine significance: Student's t-test, Wilcoxon test, one-way analysis of variance (ANOVA), or two-way ANOVA. ANOVA tests were followed by Tukey's, Bonferroni's, or Sidak's post hoc test for multiple comparisons between groups as indicated. All data tested for differences were considered significant when $p<0.05$. Levels of significance are denoted by asterisks or letters as defined in the figure legends. All statistical analyses and p-values are listed in Supplementary Table S2 for experiments shown in main figures and Table S3 for supplementary figures.

4.3. Results

4.3.1 Breast cancer stem-like cells are more resistant to γδ T cell targeting than non-stem-like cells

We used three cell line models and two different techniques to isolate BCSC. A panel of human breast cancer cell lines exhibited a range of $CD44^+CD24^-$ BCSC from 0.5 to 88.6% (Fig. S4.1A-G). We used SUM149 TNBC cells as targets, since SUM149 comprise ~10% BCSC on average (Fig. S4.1A). We sorted SUM149 into $CD44^+CD24^-$ BCSC and $CD44^+CD24^+$ NSC using fluorescence activated cell sorting (FACS). After sorting and culturing BCSC and NSC (Fig. S4.1H,I), the $CD44^+CD24^-$ population reverted back to the original culture heterogeneity after 24h (Fig. S4.1I,J). Hence, we used sorted cells directly in experiments. Serial dilution and sphere formation assays with sorted populations confirmed that SUM149 $CD44^+CD24^-$ cells have much higher sphere forming ability than $CD44^+CD24^-$ cells. Sphere formation is a functional indicator of BCSC (Fig. S4.1K). Mammospheres (3D) derived from the patient-derived xenograft (PDX) cell line PDX401 were also enriched for $CD44^+CD24^-$ cells compared to adherent monolayer cultures (2D) (Fig. S4.1L). Thus, we used mammosphere assays to enrich for BCSC from PDX401 cells. We derived primary γδTc cell cultures from twenty different healthy donors for our study. Culture subset compositions and purities are listed in Table S1. In cytotoxicity assays, SUM149 BCSC were 10 to 30% less susceptible to γδTc killing than NSC (Fig. 4.1A, BCSC versus NSC p=0.0054). Figure 1a shows the cumulative results from three independent experiments conducted with different donor-derived cultures (n=3) shown in Fig. S4.1M. Here and elsewhere biological

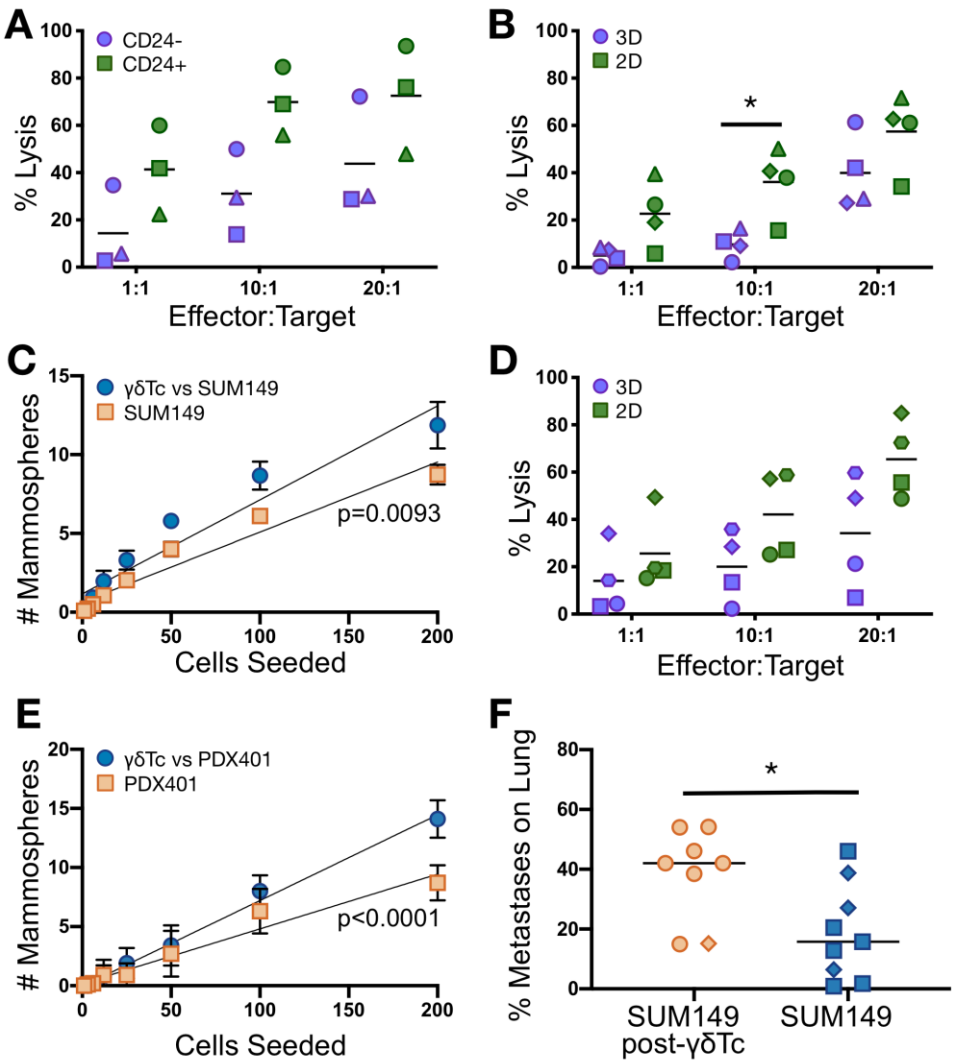

Figure 4.1. Breast cancer stem-like cells are resistant to γδ T cell targeting. (A) SUM149 cells were sorted and used in cytotoxicity assays (cumulative, n=3). **(B)** Second generation mammospheres (3D) and adherent (2D) SUM149 were dissociated, filtered into single cell suspensions and used as targets in Calcein AM cytotoxicity assays (cumulative, n=4). **(C)** SUM149 cells were co-cultured with γδTc at 1:1 for 24h, γδTc were removed, and mammosphere forming potential of targets determined over two generations (cumulative, n=3). **(D)** The patient derived xenograft cell line PDX 401 was used as a target in cytotoxicity assays as in **A** (n=4). **(E)** PDX401 were co-cultured with γδTc and mammospheres quantified as in **C**; a representative example is shown. **(F)** Quantification of lung metastasis in mice injected with SUM149 alone (n=9) or SUM149 treated with γδTc (n=8). Mice injected with 90µl cell suspension are denoted with diamond shape, the rest who received 100µl are all denoted by circles or squares. Data are presented as means in **A**, **B** and **D**, mean ± SEM in **C** and **E**, and medians in **F**. Statistical tests employed were: (**A**, **B**, **D**) two-way ANOVA followed by Sidak's post hoc test for multiple comparisons between groups; (**C**, **E**) simple linear regression; (**F**) unpaired two-tailed t-test, *p<0.05.

replicates conducted with different donor cultures are indicated by different symbols in graphs. Statistical analyses and p-values are listed in Tables S2 and S3. This decreased susceptibility also held true for SUM149-derived 3D versus 2D target cells [Fig. 4.1B, p=0.0261 at 10:1 effector:target (E:T) ratio, n=4, Fig. S4.1N]. We co-cultured breast cancer cells with γδTc at 1:1 for 24h and assessed mammosphere forming capacity over two generations. Surviving resistant cells exhibited significantly higher mammosphere forming ability compared to untreated cells, indicating BCSC enrichment (Fig. 4.1C, p=0.0093, n=3, Fig. S4.1O). 3D PDX401 cells were also more resistant to γδTc cytotoxicity than 2D cells (Fig. 1D, n=4, Fig. S4.1P), and 24h 1:1 co-cultures of γδTc with PDX401 yielded more mammospheres compared to targets cultured alone (Fig. 1E, p<0.0001, Fig. S4.1Q, representative mammosphere image in Fig. S1R). Untreated SUM149 or those treated with γδTc 1:1 for 24h were then injected intravenously into NSG mice, and lung metastases assessed 18 weeks later (Fig. S14.S,T). SUM149 that had been treated with γδTc generated significantly more metastatic lesions compared to untreated SUM149 cells (42% versus 15.7%), indicating a larger stem-like cell population (Fig. 4.1F, p=0.0110).

4.3.2 Gamma delta T cell degranulation and IFN-γ secretion are impaired in the presence of breast cancer stem-like cells

In flow cytometric CD107a assays, γδTc incubated with BCSC degranulated significantly less compared to those incubated with NSC (SUM149 Fig. 4.2A, p=0.0361; PDX401 Fig. 4.2B; biological replicates in Fig. S4.2A-G). Conditioned medium (CM) from co-cultures of γδTc with SUM149 or PDX401 BCSC compared to NSC contained significantly less IFN-γ (Fig. 4.2C, p<0.0001 γδTc+$CD24^-$ versus γδTc+$CD24^+$, S4.2H,I; Fig. 4.2D, p=0.0010 γδTc+3D versus γδTc+2D, S4.2J,K). Cumulative analyses confirmed our SUM149 results (Fig.4.2E, n=3, ratio

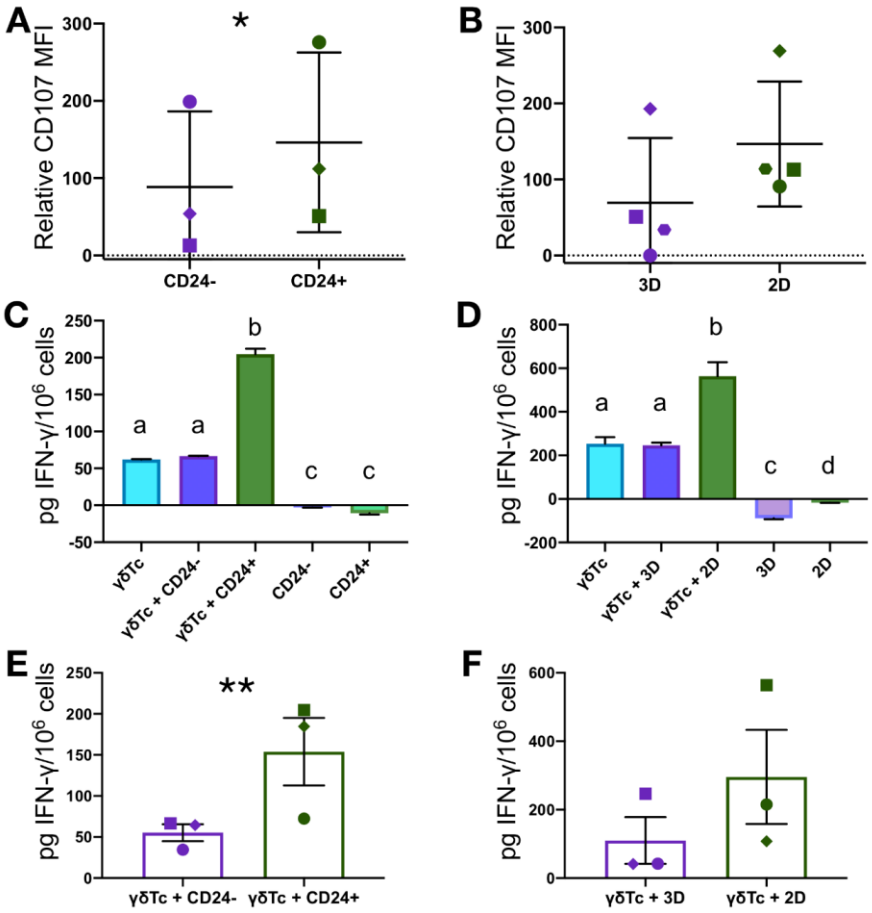

Figure 4.2. Gamma delta T cell degranulation and IFN-γ secretion are impaired in the presence of breast cancer stem-like cells. (A) Cumulative results of flow cytometric analysis of CD107a expression (degranulation) on γδTc cultures derived from different donors co-incubated with SUM149 (n=3). MFIs of CD107a were normalized over "no target" controls. **(B)** As in **A** but with PDX401 cells (n=4). **(C)** IFN-γ ELISA was performed on conditioned media (CM) from γδTc co-incubated with $CD24^-$ or $CD24^+$ SUM149 or **(D)** 3D or 2D PDX401 for 24h. **(E)** Cumulative results for IFN-γ secretion by γδTc incubated with $CD24^-$ or $CD24^+$ SUM149 including the experiment in **C** (n=3). **(F)** 3D or 2D PDX401 targets including the experiment in **D** are shown (n=3). Data are presented as mean ± SD in **A**-**D**, and mean ± SEM in **E** and **F**. Statistical tests employed were: (**A**) two-tailed paired t-test, (**B**, **F**) Wilcoxon two-tailed test, (**C**, **D**) one-way ANOVA followed by Tukey's post hoc test for multiple comparisons between groups, and (**E**) one-tailed ratio paired t-test. *$p<0.05$, **$p<0.01$; a-b, $p<0.0001$ in **C** and a-b, $p=0.0010$ in **D**.

paired one-tailed t- test, p=0.0071) and showed a similar trend in experiments in which γδTc had been co-cultured with 3D or 2D PDX401 cells (Fig. 4.2F, one-tailed Wilcoxon test, p=0.1250).

4. 3.3 Breast cancer stem-like cells secrete factors that inhibit γδ T cell function

To investigate the impact of secreted factors produced by BCSC on γδTc, we incubated CellTrace Violet (CTV)-labeled γδTc with SUM149 or PDX401 BCSC or NSC CM for 24h, replaced CM with fresh media, and assessed proliferation by flow cytometry six days later. Gamma delta T cells incubated with NSC CM proliferated more than those incubated with BCSC CM (Fig. 4.3A,B). Proliferation modeling indicated a greater proportion of γδTc cells in earlier proliferation divisions in BCSC CM compared to NSC CM (Fig. S4.3A-I, n=3, compare peaks 0 and 1 in Fig. S4.3B and S3C, respectively, depicted graphically in Fig. S4.3D). Viabilities of γδTc incubated with BCSC compared to NSC CM for 24-72 h were similar (Fig. S3K-M).

We incubated γδTc for 24h in different CM, replaced CM with complete medium, and measured inhibitory receptors on γδTc seven days later. PD-1 expression was similar, but CTLA-4, LAG-3 and TIM-3 expression on γδTc treated with SUM149 BCSC was markedly increased (Fig. S4.3N). These differences did not always achieve significance, likely due to inherent donor variability (Fig. 4.3C, D, S4.3N-S). CTLA-4 trended higher on γδTc treated with $CD24^-$ versus $CD24^+$ CM (Fig. 4.3E, S4.3N-P), and was significantly higher on 3D compared to 2D CM-treated γδTc (Fig. 4.3F, p=0.0371, S3Q-S). The same was true for LAG-3 (Fig. 4.3G, p=0.0797; 3H, p=0.0282, S3N-S). Cytotoxicity of γδTc incubated in $CD24^-$ CM was reduced by half compared to $CD24^+$ CM-treated γδTc against SUM149 targets (Fig. 4.3I, n=3, p=0.0043 at 20:1, S3T). PDX 2D CM-treated γδTc were ~1.5 times more cytotoxic than PDX 3D-CM treated γδTc at 20:1 (Fig. 4.3J,

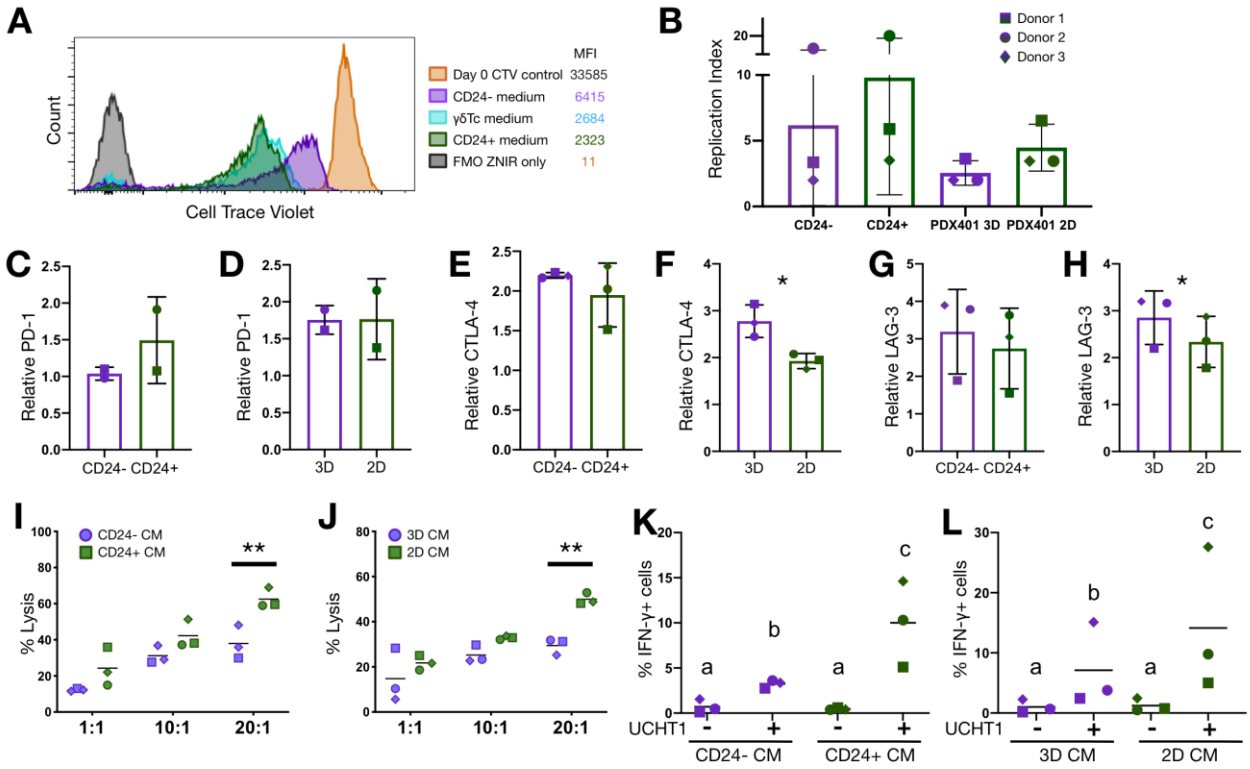

Figure 4.3. **Breast cancer stem-like cells secrete factors that inhibit gamma delta T cell function.** **(A)** To assess proliferation, γδTc were labeled with CellTrace Violet (CTV) and incubated with SUM149 $CD24^+$ and $CD24^-$ conditioned medium (CM) for 24h, washed, then further cultured in fresh medium. Six days later, the CTV signal was measured using flow cytometry. **(B)** Graph of cumulative replication indices of γδTc treated with SUM149 or PDX401 CM including experiment in Fig 3**A** (n=3). **(C-H)** Cumulative results for MFI normalized to corresponding FMOs for the indicated co-inhibitory receptors on γδTc incubated with SUM149 $CD24^+$ and $CD24^-$ CM or PDX401 2D and 3D CM (n=2 **C** and **D**, n=3 for **E-H**; see symbols unique to biological replicates). **(I)** After incubation with SUM149 $CD24^+$ or $CD24^-$ CM or **(J)** PDX401 2D or 3D CM, γδTc were used to target the unsorted population of SUM149 and PDX401, respectively, in Calcein AM cytotoxicity assays at the indicated effector: target (E:T) ratios (n=3). **(K)** Cumulative results for % IFN-γ producing γδTc are depicted for γδTc incubated with SUM149 $CD24^+$ and $CD24^-$ CM (n=3) and **(L)** PDX401 2D and 3D CM (n=3). Data are presented as mean ± SD in **B-H**, and mean values are represented by lines in **I**, **J**, **K** and **L**. Statistical tests employed were: (**B**) one-way ANOVA followed by Sidak's post hoc test for multiple comparisons between groups; (**E-H**) one-tailed paired t-test, (**I**, **J**) two-way ANOVA followed by Sidak's post hoc test, (**K**) one-tailed paired ratio t-test, a-b p=0.0482, b-c p=0.0255, a-c p=0.0107, and (**L**) one-tailed paired ratio t-test, a-b p=0.0094, b-c p=0.0085, a-c p=0.0079. *p<0.05, **p<0.01.

n=3, p=0.0022, S3U). Significantly reduced intracellular IFN-γ was observed in anti-CD3-stimulated-γδTc treated overnight with BCSC CM compared to NSC CM (SUM149, Fig. 4.3K, n=3, b versus c: p=0.0255; PDX401, Fig. 4.3L, b versus c: p=0.0085, S3V-X, S3Y-AA).

4.3.4 The PD-1/PD-L1 pathway contributes to resistance of breast cancer stem-like cells to γδ T cell killing

We co-stained SUM149 with antibodies against CD24 and CD44 together with PD-L1 alone or PD-L1 and PD-L2 simultaneously and acquired samples by flow cytometry (gating controls in Fig. S4.4A,B). PD-L1 expression was unexpectedly slightly higher on SUM149 NSC compared to BCSC (Fig. 4.4A, S4.4C), and PD-L1 positively correlated with CD24 (Fig. 4.4B). Conversely, PDX401 3D expressed significantly higher PD-L1 than 2D cells (Fig. 4.4C, p=0.0288; S4.4D-F), and PD-L2, trended higher in PDX401 3D versus 2D cells (Fig. 4D, S4.4G-H). After treatment with γδTc overnight, PD-L1 expression was significantly elevated on SUM149 resistant to γδTc killing ended higher in PDX401 3D versus 2D cells (Fig. 4.4D, S4G-H). After treatment with γδTc overnight, compared to SUM149 that had not been incubated with γδTc (Fig. 4.4E, F, n=3, p=0.0310, S4.4I-J). This was similar with PDX401 (Fig. 4.4G, S4.4K-L); however, the difference was not significant when biological replicates were combined for analysis (Fig. 4.4H, n=3, p=0.0939). PD-L2 also trended higher in γδTc-resistant targets (Fig.4.4I-J, S4.4M-S). Anti-PD1 treatment significantly increased γδTc lysis of SUM149 $CD24^-$ cells but not to the level of $CD24^+$ SUM149 lysis (Fig. 4.4K, n=3, p=0.0222, S4.4T-V, all $p<0.05$). Anti-PD-1 treatment also increased $CD24^+$ cell lysis (Fig. S4.4V, p=0.0045). Cumulative results trended toward increased PDX401 3D lysis (Fig.4. 4L). Two of three biological replicates showed significantly increased

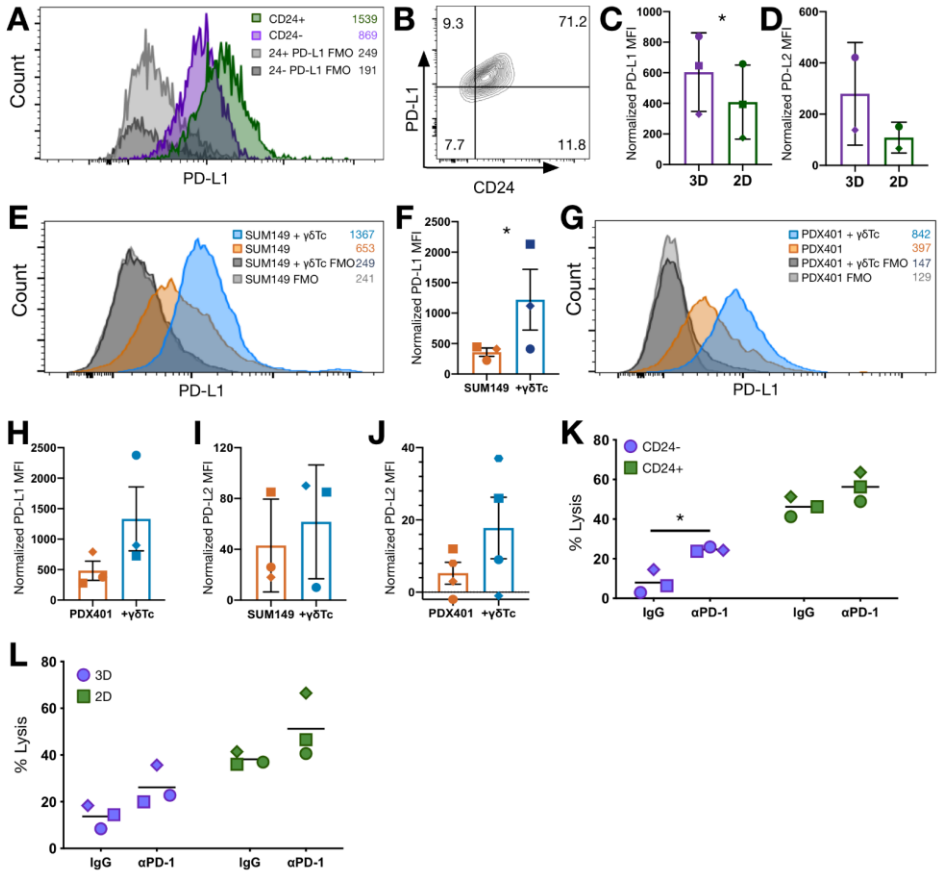

.

Figure 4.4. Figure 4.4. Inhibitory ligands are expressed on breast cancer stem-like cells resistant to γδ T cell killing. (A) PD-L1 expression was detected by flow cytometry on $CD24^-$ and $CD24^+$ SUM149 and **(B)** CD24 versus PD-L1 is plotted. **(C)** MFI (normalized to FMO) of PD-L1 (n=3) and **(D)** PD-L2 (n=2) on 2D and 3D PDX401 cells were measured. **(E)** Target cells were co-incubated with γδTc at a 1:1 ratio overnight and surface expression of PD-L1 was detected. **(F)** Cumulative results of PD-L1 MFI normalized to FMO including the experiment in E are shown (n=3). **(G)** Experiment done as in E but with PDX401 3D and 2D cells. **(H)** Cumulative results of three biological replicates including G. **(I)** PD-L2 was compared between co-incubated targets and targets alone on SUM149 (n= 3) and **(J)** PDX401 cells (n=4). **(K)** γδTc were incubated with anti-PD-1 blocking antibody and then co-incubated with SUM149 $CD24^-$ or $CD24^+$ cells or **(L)** PDX401 3D or 2D cells at E: T 20:1 for 4h. Cumulative results are shown (n=3). Data are presented as mean ± SD in C, D, K and L, and as mean ± SEM in F and H-J. Mean values are represented by lines in K and L. Statistical tests employed were: **(C, F, H-J)** one-tailed paired ratio t-test, and (K, L) two-way ANOVA followed by Tukey's post hoc test. *$p<0.05$

3D lysis with anti-PD-1 treatment (Fig. S4.4W, Fig. S4.4X, p=0.0141; S4.4Y, p=0.0267), and in one case, 2D lysis was also significantly enhanced (Fig. S4.4Y, p=0.0033).

4.3.5 The anti-apoptotic protein MCL-1 is upregulated in breast cancer stem-like cells

Blocking FasL or TRAIL on γδTc reduced cytotoxicity against SUM149, and cytotoxicity was significantly reduced on blocking NKG2D (Fig. S4.5A, p=0.0472, NKG2D versus IgG). Note that we did not block the γδ TCR in these experiments, since use of pan anti-γδ TCR antibodies induces apoptosis in γδTc, confounding interpretation of results[446]. Blocking MICA/B or CD54 also significantly reduced lysis (Fig. S4.5B, p=0.0286 and 0.0240, respectively). This was also evident when PDX401 were used as targets (Fig. S4.5C, NKG2D p=0.0117, FasL 0.0042, S4.5C). Using sorted targets, we found similar significant reductions in cytotoxicity against $CD24^-$ SUM149 when sTRAIL, MICA/B or CD54 were blocked (Fig. 4.5A; p=0.0216, 0.0006, <0.0001, respectively); however, blocking NKG2D or FasL did not reduce cytotoxicity against $CD24^-$ targets (Fig. 4.5A, S4.5D-G). In contrast, blocking any of these receptors significantly reduced SUM149 $CD24^+$ target lysis (Fig. 4.5B, all p<0.001 versus Ig, S5D-G). Cumulative results for log2 fold change in cytotoxicity on blocking FasL versus IgG control approached significance (Fig. 4.5C, n=4, p=0.0591). Cytotoxicity of γδTc against 3D PDX401 remained unchanged despite blocking (Fig. S4.5H-K). However, blocking any of the above-mentioned factors significantly reduced γδTc cytotoxicity against PDX401 2D cells (Fig. S4.5H, all p<0.001, S4.5I-K). In particular, decreases in γδTc cytotoxicity upon blocking FasL were significantly different between 2D and 3D PDX401 (Fig. 4.5D, n=3, p<0.0037).

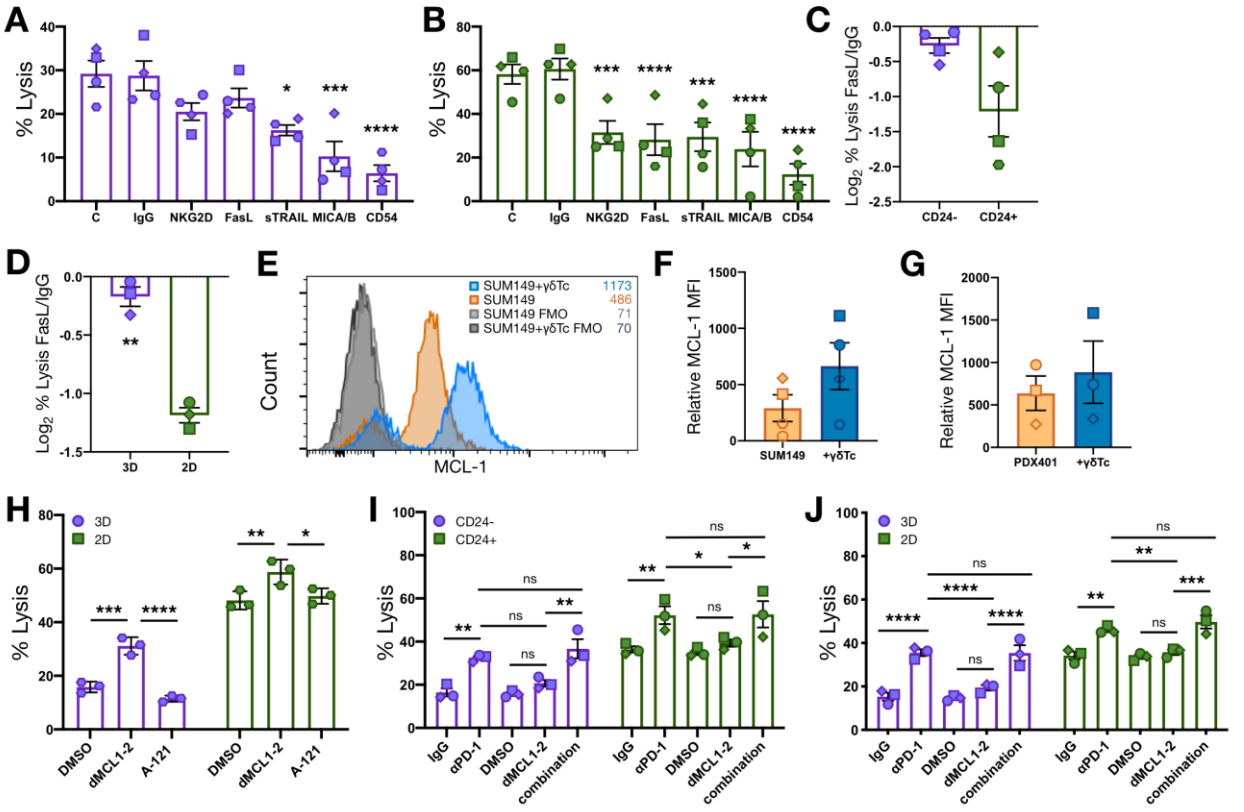

Figure 4.5. The Fas-FasL pathway is dysfunctional in breast cancer stem-like cells. (A) SUM149 were sorted into $CD24^+$ and **(B)** $CD24^-$ fractions, incubated with the indicated antibodies for 30 min and then co-incubated with γδTc at E:T 20:1 for 4h. Cumulative results are shown (n=4). **(C)** The log2 fold decrease in target cell lysis upon FasL blocking compared to IgG control was calculated for the experiment shown in **A** and **B** (n=4). **(D)** Similarly, PDX401 3D and 2D cells were incubated with antibodies followed by γδTc and the log2 fold decrease in target lysis upon FasL blocking compared to IgG control was calculated (n=3). **(E)** SUM149 cells were subjected to a γδTc cytotoxicity assay at 1:1 (E: T) overnight. Target cells were then stained for intracellular MCL-1 protein and acquired *via* flow cytometry. **(F)** Cumulative results for SUM149 are shown including the experiment in **E** (n=3). **(G)** Cumulative results for similar experiments done with PDX401 3D and 2D cells (n=3). **(H)** Sorted SUM149 $CD24^-$ and $CD24^+$ cells were co-incubated with γδTc at E:T 20:1 in a 4h Calcein AM cytotoxicity assay (n=4). Where indicated 500nM dMCL1-2 or A-1210477 (A-121) were added to the co-incubation, with the same volume of DMSO as a vehicle control. **(I)** Cumulative results of cytotoxicity assays done with dMCL1-2 or anti-PD-1 antibody against SUM149 (n=3) or **(J)** PDX401 cells (n=3). Data are presented as mean ± SEM in all graphs except **H**, which shows mean ± SD. Statistical tests employed were: (**A**, **B**) RM one-way ANOVA followed by Bonferroni's post hoc test, (**C**, **D**, **F**, **G**) one-tailed paired t-test, (**H**) two-way ANOVA followed by Sidak's post hoc test, (**I-J**) two-way ANOVA followed by Tukey's post hoc test. *p<0.05, **p<0.01, ***p<0.001, ****p<0.0001.

Given that the Fas-FasL pathway, which induces apoptosis in target cells, was dysregulated in BCSC of both cell lines, we explored surface expression of Fas(CD95). Fas levels on BCSC versus NSC were similar, as were expression of TRAIL R1 and TRAIL R2 (Fig. S4.5L, M). Since CSC upregulate anti-apoptotic proteins to resist apoptosis induction[487], we quantified anti-apoptotic proteins *via* western blotting. MCL-1 was upregulated in $CD24^-$ cells, and Bcl-XL was increased in two of three replicates (Fig. S4.5N, left panels). Surface MCL-1 expression was higher in SUM149 and PDX401 cells resistant to γδTc killing compared to targets alone (Fig. 4.5E; 5F, n=4, p=0.09; 4.5G, n=3; S4.5O,P). PDX401 3D also expressed more MCL-1, Bcl-XL and survivin than 2D cells (Fig. S4.5N, right panels). We then employed the failed inhibitor A-1210477 (A-121) as a negative control and its derivative - the novel MCL-1 protein degrader, dMCL1-2 - [268] to target MCL-1, confirming degradation in both cell lines *via* western blotting (Fig. S4.5Q).

Addition of dMCL1-2 in a cytotoxicity assay with γδTc derived from one particular donor showed significantly increased PDX401 2D and 3D cell lysis compared to vehicle control (Fig. 4.5H, p=0.0073 and p=0.0003, respectively). Significant increases in cytotoxicity against $CD24^-$ SUM149 in the presence of dMCL1-2 were confirmed with two other γδTc cultures derived from this donor (Fig. S4.5R, p=0.0254, and S4.5S, p=0.0239). However, dMCL1-2 had no effect in assays with γδTc derived from five other donors (Fig. S4.5T-X). In cytotoxicity assays combining anti-PD1 antibody and dMCL1-2, we saw no synergistic effect in experiments using BCSC and NSC SUM149 (Fig. 4.5I, n=3; S4.5V-X left panels) or PDX401 targets (Fig. 4.5J, n=3; S5V-X right panels). We confirmed that γδTc viability was not affected by dMCL1-2 (Fig. S4.5Y).

4.3.6 Breast cancer stem-like cells display lower expression of MICA/B on their surface

Multiple experiments revealed that MICA/B, ULBP-3 and ULBP-4 expression was

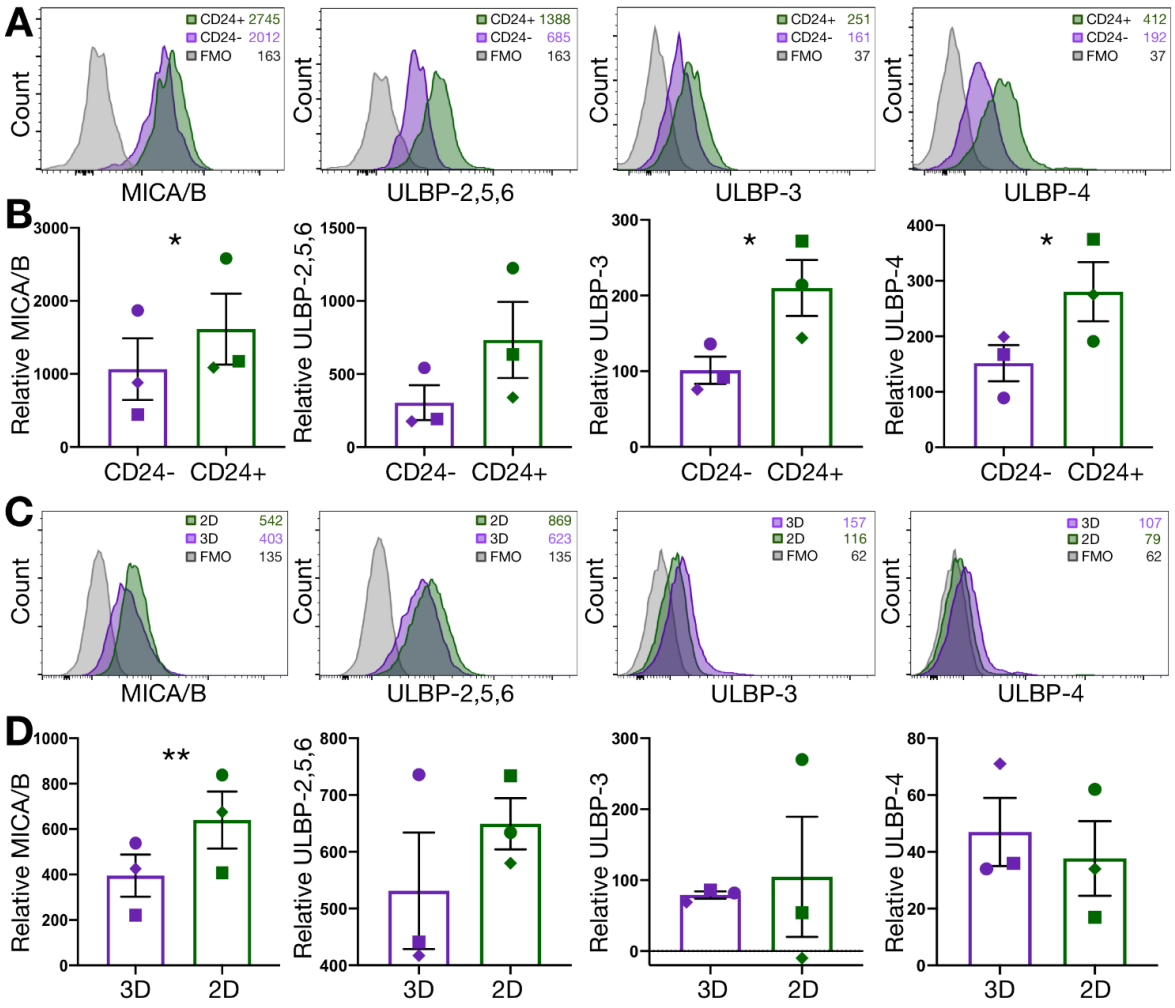

Figure 4.6. Breast cancer stem-like cells have lower surface expression of MICA/B. (A) NKG2DL expression was determined on SUM149 $CD24^-$ and $CD24^+$ cells by flow cytometry and **(B)** cumulative results for normalized values including those from the experiment in **A** are shown (n=3). **(C)** NKG2DL on 2D and 3D PDX401 cells and **(D)** cumulative data comprising normalized values including those from the experiment in **C** are shown (n=3). Data in graphs are presented as mean ± SEM. For statistics shown in **B** and **D**, one-tailed paired t-tests were employed. *p<0.05, **p<0.01.

significantly lower on CD24- compared to CD24+ SUM149 cells (Fig. 4.6A; 4.6B, n=3, p=0.0428, 0.0467, and p=0.0430 respectively; S4.6A-E), while ULBP-2,5,6 was down-regulated on SUM149 CD24 (Fig. 4.6A; 4.6B, p=0.0518; S4.6B-E). MICA/B surface expression was also significantly lower on PDX 3D versus 2D cells (Fig.4.6C,D left panels, p=0.0088; S4.6F,G), but NKG2DL expression was otherwise variable (Fig. 4.6C and D, S4.6F,G).

4.3.7 Breast cancer stem-like cells shed higher levels of MICA conferring resistance to γδ T cell killing that can be overcome with ADAM inhibition

One mechanism regulating NKG2DL on the surface of cancer cells is shedding, which occurs by proteolytic cleavage[172]. Strikingly, proteomic analysis of CM from BCSC and NSC revealed MICA as a top upregulated protein secreted by both SUM149 and PDX401 BCSC (Fig. 4.7A-B). This was confirmed by ELISAs (Fig. 4.7C, D, n=4, p=0.0033 and p=0.0038; S4.7E,F). "A disintegrin and metalloproteinase" (ADAM)10 and 17, involved in tumor-associated proteolytic release of soluble MICA[172], were also upregulated in BCSC CM (Fig. 4.7B, S4.7C-D). Using GW280264X (ADAMi), an inhibitor of both ADAM10 and ADAM17, significantly increased surface MICA/B on both SUM149 (Fig. 4.7E top panel, 4.7F, n=3, p=0.0008; S7G) and PDX401 cells (Fig. 4.7E bottom panel, 4.7G, n=3, p=0.0011; S4.7H). MICA shedding, evidenced by soluble MICA levels in supernatants, was also significantly abrogated upon addition of ADAMi (Fig.4.7H, n=3, p=0.0332, S4.7I; 4.7I, n=3, p=0.0058, S4.7J). In cytotoxicity assays, ADAMi significantly enhanced γδTc cytotoxicity against both BCSC and NSC SUM149 (Fig. 4.7J, $CD24^-$ DMSO versus ADAMi p<0.0001; $CD24^+$ DMSO versus ADAMi, p=0.0007; S4.7K-M) and PDX401 targets (Fig. 4.7K, 3D DMSO versus ADAMi, p<0.0001; 2D DMSO versus ADAMi, p<0.0001; S4.7N-P). Notably, combining ADAMi with γδTc brought BCSC lysis levels to those of untreated NSC

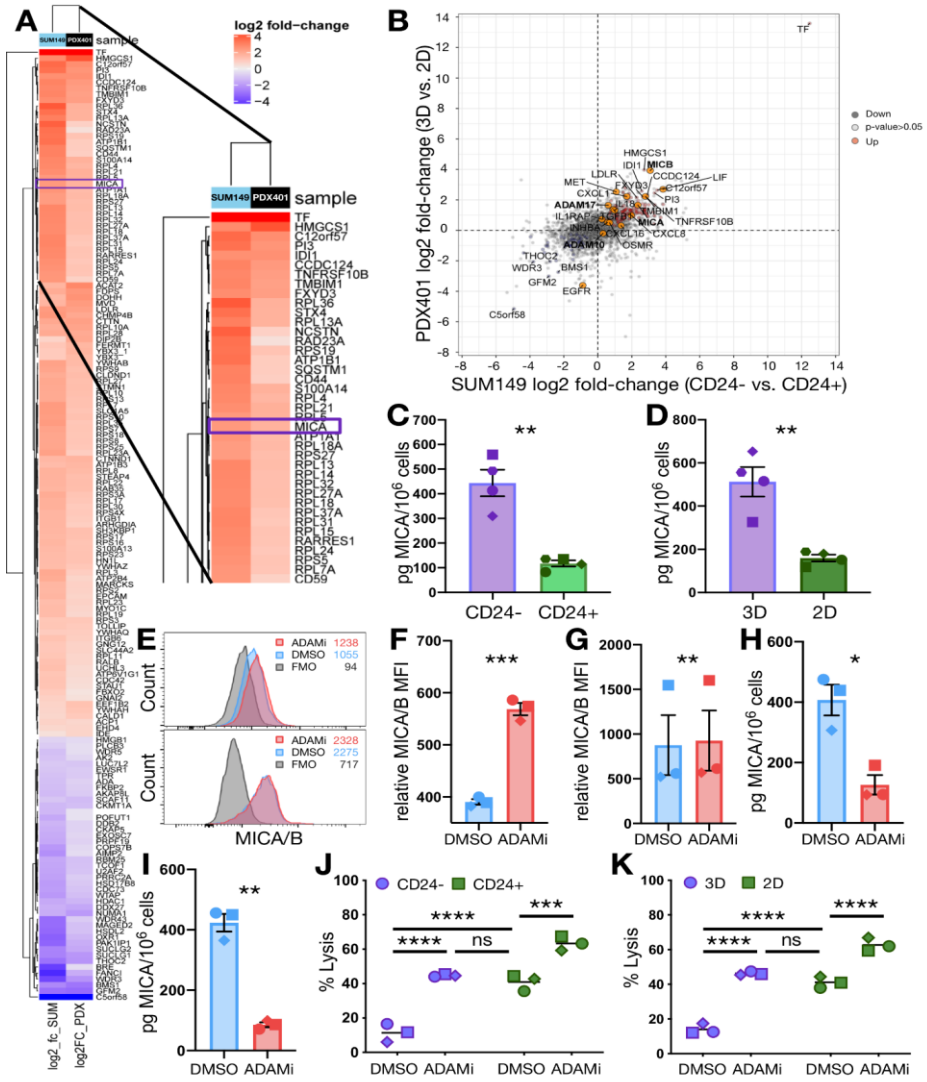

Figure 4.7. Breast cancer stem-like cells shed MICA rendering them resistant to γδ T cell killing, which can be reversed by inhibiting ADAM proteases. (A) Secretome analysis of SUM149 and PDX401 BCSC was performed with mass spectrometry. The log2 fold changes of the most differentially secreted proteins are depicted as a heat map. A magnified version of the top 39 proteins, with MICA boxed in purple is provided. **(B)** Scatter plot depiction of secretome analysis shown in A. **(C)** ELISA quantification of MICA shed by sorted CD24- versus CD24+ SUM149 cells (n=4) and **(D)** 2D and 3D PDX401 (n=4). **(E)** Targets were treated with the ADAM protease inhibitor GW280264X (ADAMi) for 4h and MICA/B surface expression was determined via flow cytometry. Representative overlays of SUM149 (top) and PDX401 cells (bottom) and **(F)** cumulative results for MICA MFI (normalized to FMO controls) on SUM149 (n=3) and **(G)** PDX401 are shown (n=3). **(H)** Soluble MICA secreted by SUM149 in the presence of ADAMi or vehicle control was measured by ELISA (n=3) and **(I)** the same was done with supernatants from PDX401 cells treated in the same way (n=3). **(J)** SUM149 CD24- and CD24+ cells (n=3) or **(K)** PDX401 3D and 2D cells (n=3) were incubated with ADAMi and then co-incubated with γδTc at E:T 20:1 for 4h. Data are presented as mean ± SEM in C, D and F-I. Mean values are represented by lines in J and K. Statistical tests employed were: (C, D, F-I) one-tailed paired t-test, and (J and K) two-way ANOVA followed by Tukey's post hoc test. *p<0.05, **p<0.01, ***p<0.001, ****p<0.0001.

(Fig. 4.7J, $CD24^-$ ADAMi versus $CD24^+$ DMSO, p=0.6781; S4.7K-M; 4.7K 3D ADAMi versus 2D DMSO, p=0.2139, S4.7N-P), overcoming BCSC resistance to γδTc cytotoxicity.

We performed most of these experiments with MCF-7 cells and obtained similar results (Fig. S4.8).

4.4 Discussion

Early phase clinical trials with γδTc have thus far focused on treatment-refractory advanced stage cancer patients, and have unsurprisingly shown variable efficacy[218]. Given these findings, discussion has arisen over activation-induced anergic or unresponsive γδTc cells[488] as well as the need to improve therapies by mitigating immune evasion. We addressed this issue by interrogating mechanisms by which BCSC may overcome γδTc-mediated killing. In doing so, we determined that BCSCs employ numerous mechanisms, including MICA shedding, to evade killing, and that the efficacy of γδTc-based therapies may be improved through the pharmacological inhibition of such processes. Indeed, we found that inhibiting ADAM proteases can restore γδTc-mediated cytotoxicity in BCSC, concomitant with reduced MICA shedding. While other studies have investigated CSC targeting by γδTc in colon and ovarian cancers, and neuroblastoma [237-239], this is, to our knowledge, the first study to compare γδTc cytotoxicity against CSC and NSC in parallel. In this study, we used polyclonal primary human γδTc, containing both Vδ1 and Vδ2 cells (Table S1). This follows studies in the extant literature which suggest that both subsets should be considered for development of γδTc-based immunotherapies[210]. Indeed, in a recent study, pre-treatment of BCSC with Zoledronate followed by primary autologous Vδ2 γδTc and $CD8^+$ T cells combined was more effective than either cell type alone[489]. However, some pre-clinical studies suggest that Vδ1 may be superior to Vδ2 cells in terms of both cytotoxicity and durability[137,209].

For example, Vδ1 cells are more resistant to activation-induced cell death (AICD)[409], which has posed significant problems in clinical trials due to chronic stimulation of Vδ2 cells[488]. Furthermore, an elegant study recently identified Vδ1 cells in both healthy human breast tissue and tumors that were equally functionally competent and lysed breast cancer cells *via* NKG2D engagement; importantly, Vδ1 cells were also more abundant in tissues from remission compared to relapsed cases[200].

While γδTc could kill BCSC, BCSC employed multiple strategies to evade γδTc attack, resulting in reduced susceptibility of BCSC compared to NSC (Figs. 4.1,4.4,4.5,4.7). *In vivo,* mice injected with SUM149 cells previously treated with γδTc exhibited significantly more metastatic lesions compared to mice injected with untreated SUM149 (Fig. 4.1F) suggesting BCSC enrichment during co-incubation with γδTc, as observed *in vitro* (Fig. 4.1C,E). Activated γδTc degranulate to release perforins and granzymes, and they produce IFN-γ[112]. These functions were inhibited in the presence of BCSC from three different cell lines (Fig. 4.2A-F, S4.8B). In addition, BCSC CM rendered γδTc dysfunctional by chronically increasing co-inhibitory receptor expression while reducing proliferation and cytotoxicity (Fig. 4.3). This is similar to results reported in a study using CSC CM from colorectal cancer patients [490].

Programmed cell death-ligand 1 (PD-L1) is often expressed by tumor cells, enabling binding to PD-1 on immune cells and thereby attenuating their responses. PD-L1 is associated with poor prognosis in solid tumors, including breast cancer[491]. Since checkpoint inhibition has become a widely used and effective tool in the clinic, we tested differential expression of PD-L1. PD-L1 expression was higher on 3D compared to 2D PDX401 cells (Fig. 4.4C), and also on target cells resistant to γδTc cytotoxicity (Fig. 4.4E-H). Hence, ligands on BCSC, and resistant target cells in general, may engage PD-1 on γδTc to suppress γδTc activity. However, PD-1 is a T cell activation

marker that is transiently upregulated, while chronic expression indicates dysfunction[320]. PD-1 on γδTc was not differentially expressed upon exposure to BCSC CM (Fig. 4.3C,D, S4.3N), yet blocking the PD-1/PD-L1 pathway was able to partly surmount BCSC resistance to γδTc cytotoxicity (Fig. 4.4K,L). Our results concur with studies showing enhanced γδTc cytotoxicity against lymphoma, multiple myeloma, leukemia, and neuroblastoma upon blocking the PD-1/PD-L1 pathway[354,355,357,492].

Blocking assays demonstrated that Fas/FasL signaling, an important pathway γδTc exploit to trigger apoptosis in targets, is dysfunctional in BCSC (Fig. 4.5A,C,D, S5H). In line with this, the anti-apoptotic protein MCL-1 was overexpressed in BCSC compared to NSC (Fig. S4.5N), and in cells resistant to γδTc targeting (Fig. 4.5E-G, S4.5P). MCL-1 overexpression renders cancer cells resistant to several drugs[493] and is associated with poor outcome in breast cancer[264]. We verified that A-1210477 lead to MCL-1 accumulation and the novel dMCL1-2 degrader reduced MCL-1 levels (Fig. S4.5Q)[268]. However, the success of dMCL1-2 in sensitizing BCSC to γδTc (Fig. 4.5H-J, S4.5R-X) appeared to be donor dependent: all of our successful experiments were done with different γδTc cultures derived from the same donor (Figs. 4.5H, S4.5R,S). Interestingly, this donor's cells were used in the only experiment in which MCL-1 expression was not upregulated after γδTc treatment (Fig. S4.5O, top panel). If this was also the case in cytotoxicity assays, and MCL-1 was not upregulated in response to this donor's γδTc, it could explain why dMCL1-2 worked so well in those particular experiments. We would likely need to use more dMCL1-2 to overcome MCL-1 upregulated in the presence of other donor-derived γδTc. This also raises the intriguing question as to why γδTc from this particular donor did not incite MCL-1 upregulation while those from other donors did. Apart from various intrinsic factors, MCL-1 expression can be modulated by extrinsic factors like IL-6 and IFN-α[494], which were perhaps

secreted differentially by this specific donor's γδTc and played a role in regulating MCL-1 in targets.

Several soluble factors released by tumor or stromal cells exert suppressive effects on immune cells[241]. Mass spectrometry analysis indicating global differences in protein expression between BCSC and NSC secretomes identified potential "hits" that could translate into therapeutic targets (Tables S4.5,S4.6). TGF-β1 was upregulated in both SUM149 and PDX401 BCSC, and its impact on γδTc is unclear. TGF-β1 reportedly enhances cytotoxic activity of Vδ2 cells[483], while TGF-β1 and IL-15 polarize Vδ2 cells to FOXP3+ regulatory γδTc, suppressing proliferation of activated PBMC, including αβTc[358]. Another study suggested Vδ2 cells, in the presence of TGF-β1, IL-6 and IL-1 β, can be polarized into γδT17 cells[495], which are associated with the immune-suppressive TME, further aiding development of cancer[131]. Using gain- and loss-of-function models, we recently found that the TGF-β family member NODAL inversely correlated with MICA/B expression on breast cancer cells, impacting γδTc targeting[165]. Compared to NSC, BCSC consistently displayed lower expression of cell surface MICA/B (Fig. 4.6A-D, 4.S6), likely rendering BCSC invisible to γδTc, similar to what we previously observed [165]. Leukemia stem cells (LSC) do not express cell surface NKG2DL, rendering them resistant to NK cell cytotoxicity, and leading the authors of the study to suggest that the lack of NKG2DL could be considered an LSC marker[163]. Furthermore, NKG2DL$^-$ cells express higher PARP1 enzyme levels, and PARP inhibition upregulates surface NKG2DL on LSC, sensitizing them to NK cell targeting[163]. In the future, PARP inhibitors could also be tested on BCSC in the context of γδTc or NK cell therapies. Soluble MICA shed from the cell surface can downregulate NKG2D on T and NK cells[167], and elevated levels of circulating soluble MICA have been associated with poor clinical prognosis and metastasis in multiple cancer types, including breast cancer[496]. Proteomic analysis followed by

ELISA verification demonstrated significantly enhanced MICA shedding by BCSC compared to NSC (Fig. 4.7C-D).

Increased expression of ADAM10 and ADAM17 in BCSC CM was also evident (Fig. 4.7B, S4.7C,D). ADAMs are proteases that release ectodomains of trans-membranous proteins, such as cytokines, growth factors, and cell adhesion molecules, including MICA[169]. ADAMs are associated with cancer progression, inflammation, tissue damage and repair. While preclinical studies with ADAM inhibitors have shown encouraging results, clinical trials have not yet been successful[289]. GW280264X has not yet been tested in clinical trials. However, GW280264X blocked MICA shedding, which lead to significantly enhanced γδTc cytotoxicity against BCSC. In fact, lysis of BCSC reached the level of NSC lysis in the absence of the inhibitor, suggesting that MICA shedding is the main mechanism underlying BCSC resistance to γδTc cytotoxicity (Fig. 4.7J,K). Since using GW280264X in combination with γδTc also increased cytotoxicity against NSC, this approach could be considered to generally enhance γδTc targeting of cancer types using MICA shedding as an immune evasion mechanism. This mechanism was also employed under hypoxia, a biophysical property of the TME associated with poor patient outcome, in which we observed increased MICA shedding correlated with reduced cytotoxicity of γδTc against breast cancer cell lines[166].

Since the GW280264X ADAM inhibitor overcame BCSC resistance to γδTc targeting, and also enhanced the cytotoxicity of γδTc against NSC, such inhibitors should be further developed for therapeutic applications. Our study provides a strong rationale for additional pre-clinical and clinical validation of ADAM inhibitors in combination with γδTc immunotherapy to improve patient outcomes.

4.5 Acknowledgements

Flow cytometry was performed at the University of Alberta in the Faculty of Medicine and Dentistry Flow Cytometry Facility, who received financial support from the Faculty of Medicine and Dentistry and the Canadian Foundation for Innovation awards to contributing investigators. Special thanks to Aja Rieger and Sabina Baghirova for cell sorting. This work has been supported by the Alberta Innovates Health Solutions Translational Health Chair to L-MP. ID has received the Queen Elizabeth II Graduate Scholarship, the University of Alberta Doctoral Recruitment Scholarship and the Alberta Cancer Foundation Antoine Noujaim Scholarship.

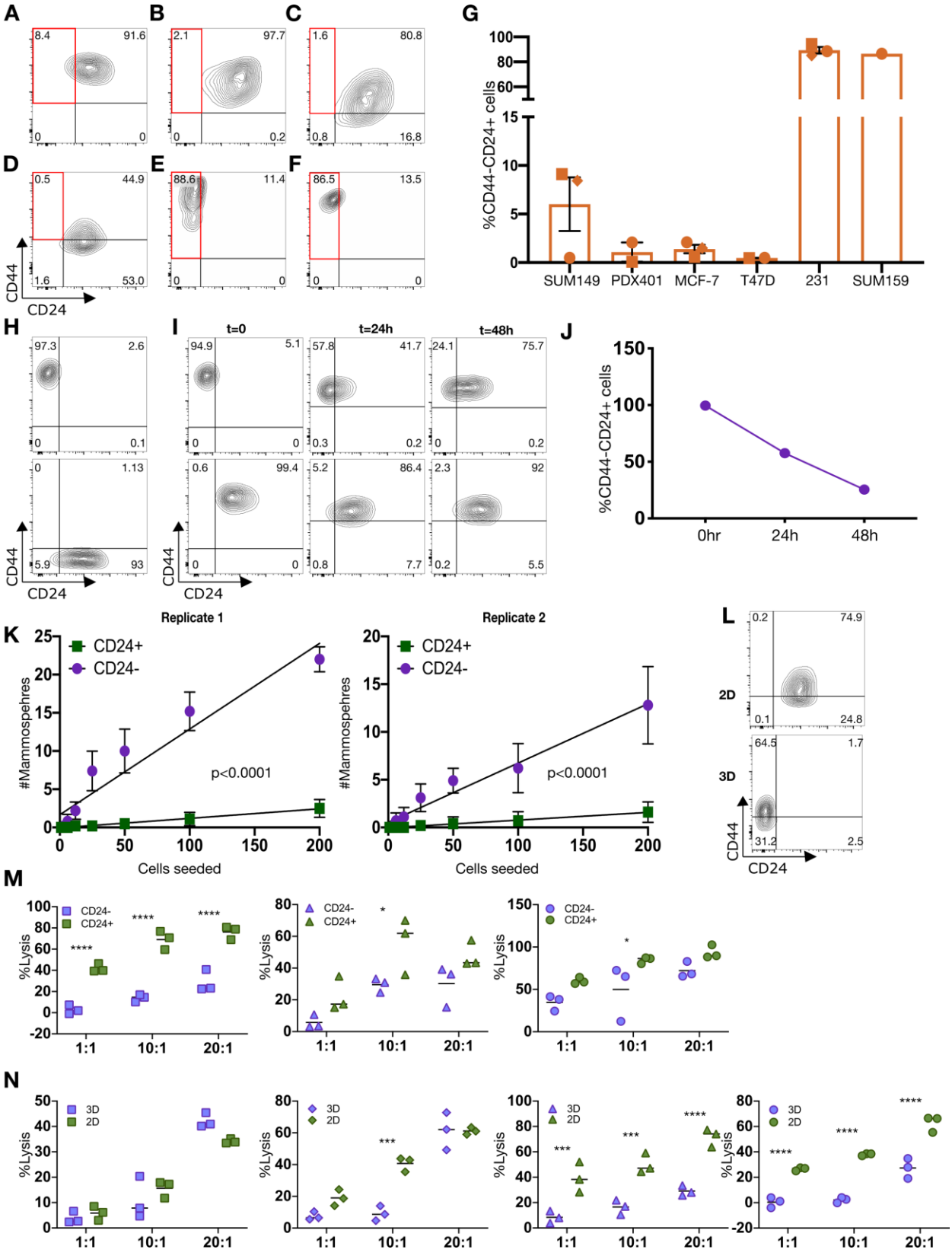
A
B
C
D
E
F
CD44
CD24
G
%CD44-CD24+ cells
SUM149
PDX401
MCF-7
T47D
231
SUM159
H
I
t=0
t=24h
t=48h
J
%CD44-CD24+ cells
0hr
24h
48h
K
Replicate 1
Replicate 2
CD24+
CD24-
#Mammospehres
p<0.0001
Cells seeded
L
2D
3D
M
%Lysis
CD24-
CD24+
1:1
10:1
20:1
N
3D
2D

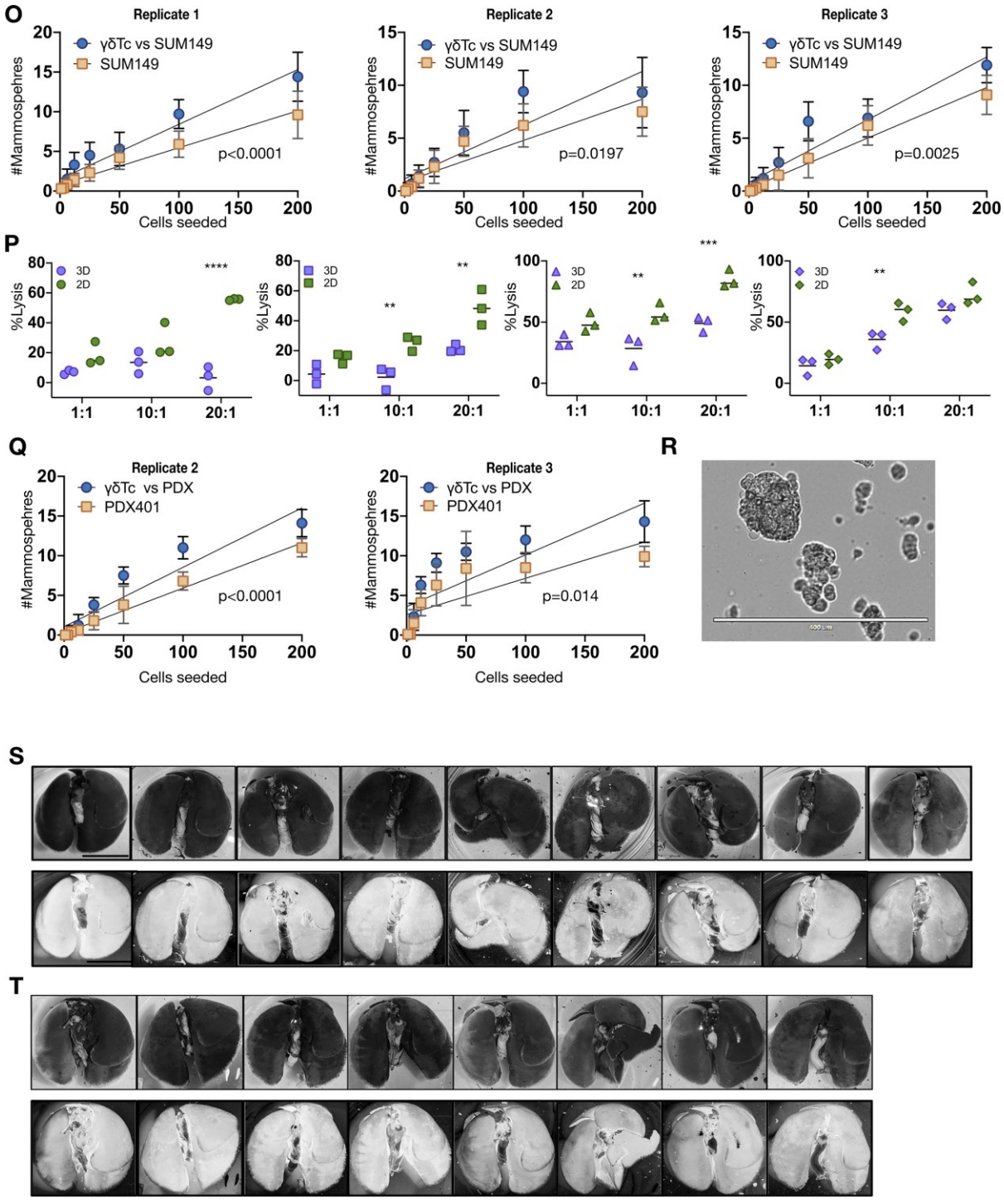

Figure S4.1. Breast cancer stem-like cells in CD44+CD24- SUM149 and PDX401 3D mammospheres are further enriched upon co-incubation with γδ T cells. Representative examples from a panel of breast cancer cell lines **(A)** SUM149 (n=3), **(B)** PDX401 (n=2), **(C)** MCF-7 (n=3), **(D)** T47D (n=2), **(E)** MDA-MB-231 (n=3), and **(F)** SUM159 (n=1) that were stained for surface expression of CD44 and CD24 followed by flow cytometric acquisition,

which is graphically represented in **(G)**. **(H)** Quadrant gates were set for analyses in A-F using fluorescence minus one (FMO) controls as shown in this representative example for **(I)** SUM149 cells sorted into $CD44^{+}CD24^{-}$ (top left panel) and $CD44^{+}CD24^{+}$ (bottom left panel) fractions; sorted populations were maintained in culture and stained with CD24 and CD44 after the indicated times to determine the kinetics of differentiation, depicted graphically in **(J)**. **(K)** Sorted SUM149 cells were seeded as indicated and cultured for seven days under low-serum and low attachment conditions. The spheres that formed were counted (n=2). **(L)** Second-generation PDX401 adherent cells (2D) and mammospheres (3D) were dissociated, then CD44 and CD24 expression were determined by flow cytometry (n=1). **(M)** SUM149 cells were sorted and used in Calcein AM cytotoxicity assays with γδTc derived from three different donors. **(N)** Second generation mammospheres (3D) and adherent (2D) SUM149 were dissociated, filtered into single cell suspensions and used as targets in cytotoxicity assays with γδTc from four different donors. **(O)** SUM149 alone or SUM149 treated with γδTc, from which γδTc were removed, were seeded and the number of spheres formed were counted. In each experiment, ten technical replicates were counted. Three biological replicates of this experiment, in which γδTc were derived from different donors, are shown. **(P)** Experiment done as in **(N)** but with PDX401 3D and 2D cells, and with γδTc derived from four different donors. The symbols used here match the donor symbols from the cumulative figure. **(Q)** Experiments done as in O but with PDX401 target cells. **(R)** Image of second generation PDX401 mammospheres. **(S)** SUM149 cells alone or those previously treated with γδTc **(T)** were injected into the tail veins of NSG mice and, 18 weeks later, mice were sacrificed and lungs stained with India ink. White spots in the black stained lungs indicate macroscopic metastases; scale = 1 cm. Corresponding inverted images of the lungs are below each set of original lung images. are Data are presented as mean ± SEM in G; mean ± SD in K, O and Q; and mean in M, N and P. Statistical tests employed were: (K, O, Q) Simple linear regression, p values are indicated in figure; (M, N, P) Two-way ANOVA followed by Sidak's post hoc test for multiple comparisons between groups. *$p<0.05$, **$p<0.01$, ***$p<0.001$, ****$p<0.0001$.

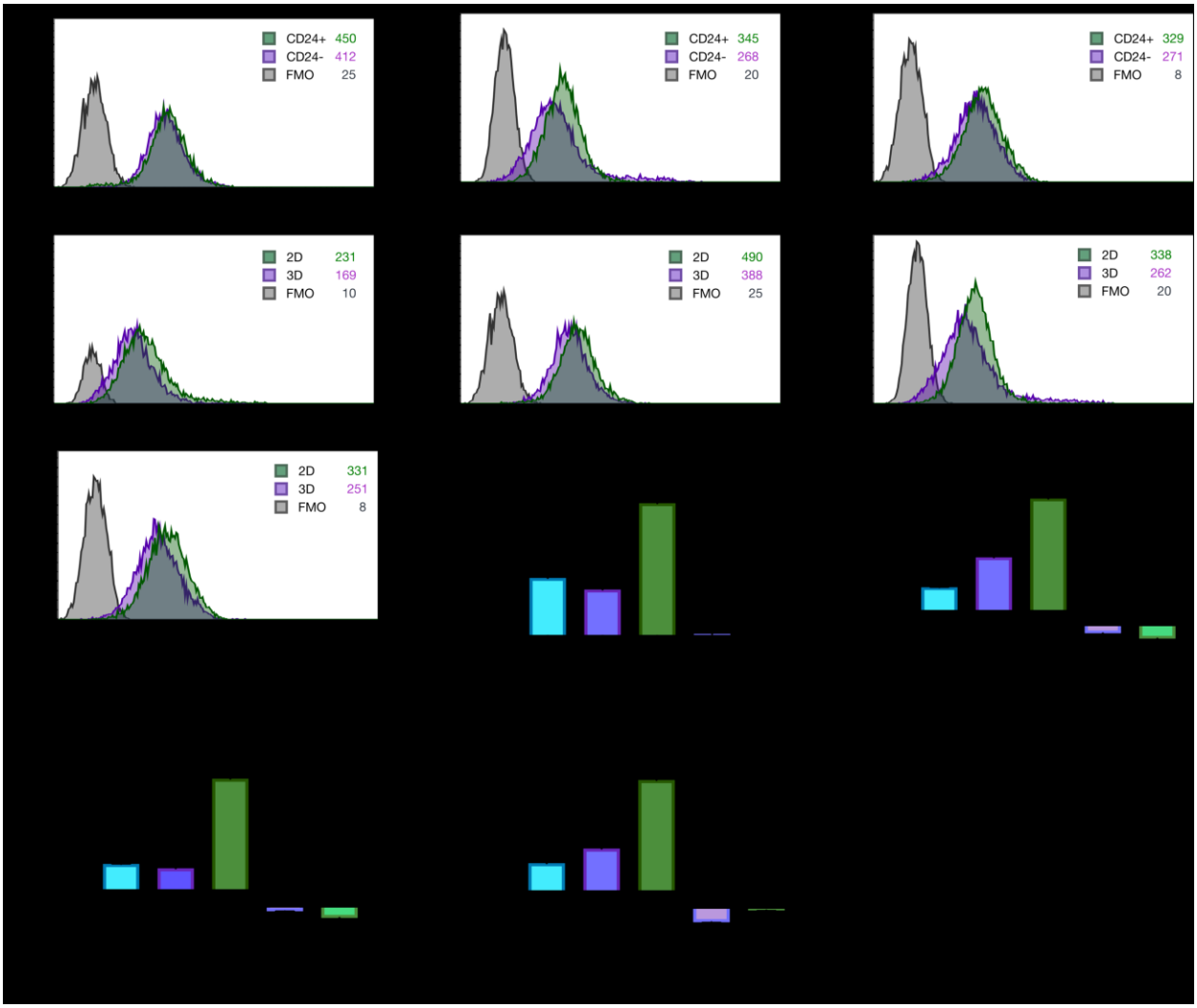

Figure S4.2.Gamma delta T cell degranulation and IFN-γ secretion are impaired in the presence of breast cancer stem-like cells. (A) Overlay of of CD107a expression (degranulation) is shown for γδTc incubated with SUM149 $CD24^-$ and incubated with $CD24^+$ cells is shown for γδTc derived from donor 1, **(B)** donor 2 and **(C)** donor 3. **(D)** Experiments done as in **A-C** but with PDX401 3D (BCSC) or 2D (NSC) cells and γδTc from donor 1 **(E)** donor 2, **(F)** donor 3 and **(G)** donor 4. **(H)** INF-γ ELISA was performed on conditioned media (CM) from $CD24^+$ or $CD24^-$ SUM149 co-incubated with γδTc derived from donor 2 and **(I)** donor 3 for 24h. **(J)** INF-γ ELISA on conditioned media (CM) from 2D or 3D PDX401 co-incubated with γδTc derived from donor 2 and **(K)** donor 3 for 24h. Donor numbers were reset for each set of experiments. Data are presented as mean ± SD. Statistical tests employed were: **(G-J)** One-way ANOVA followed by Tukey's post hoc test for multiple comparisons. In **H**, a-b, $p<0.01$; in **I** and **J**, b-c, $p<0.0001$; in **K**, b-c, $p=0.0038$.

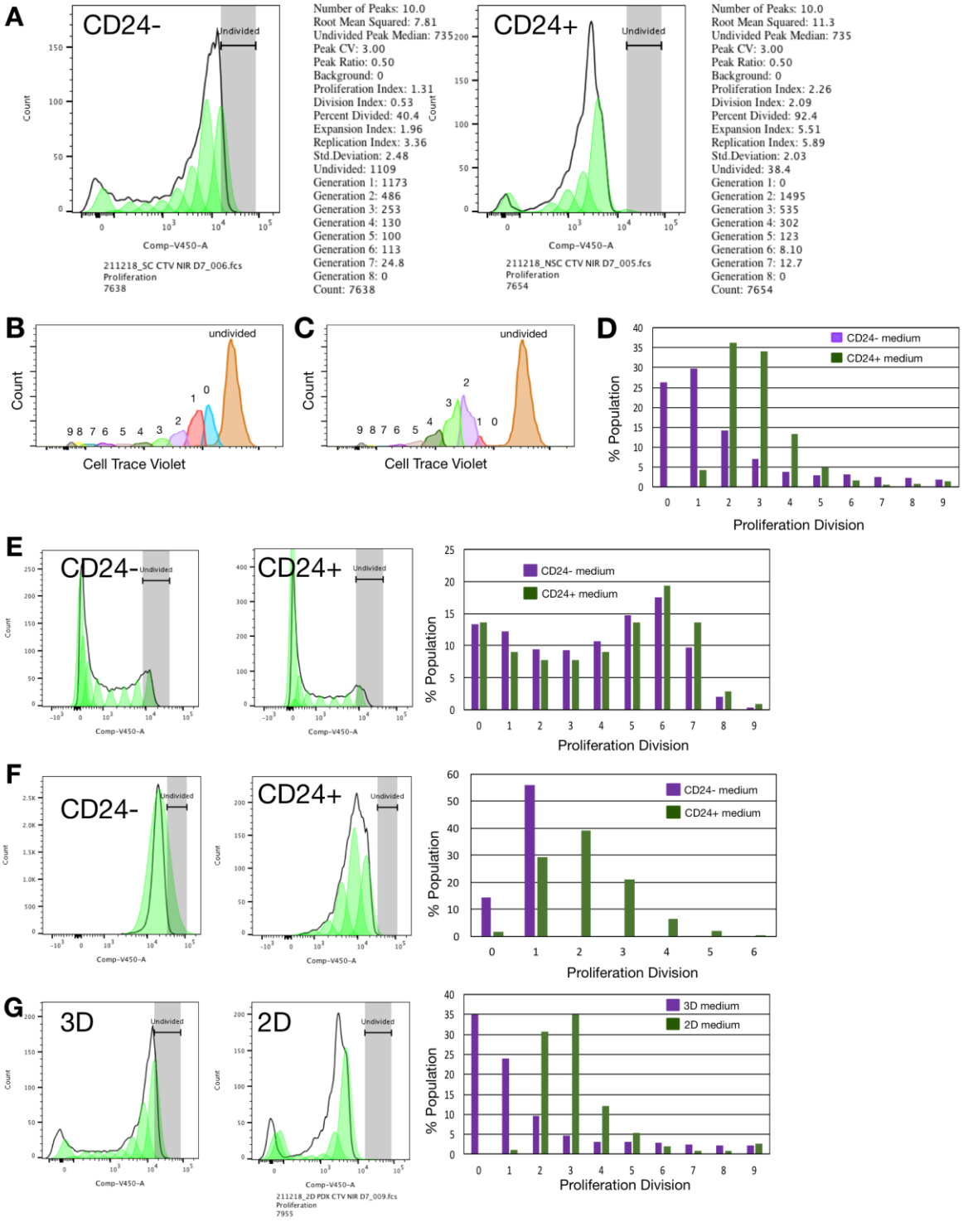
A
CD24-
Undivided
Count
Comp-V450-A
211218_SC CTV NIR D7_006.fcs
Proliferation
7638
Number of Peaks: 10.0
Root Mean Squared: 7.81
Undivided Peak Median: 735
Peak CV: 3.00
Peak Ratio: 0.50
Background: 0
Proliferation Index: 1.31
Division Index: 0.53
Percent Divided: 40.4
Expansion Index: 1.96
Replication Index: 3.36
Std.Deviation: 2.48
Undivided: 1109
Generation 1: 1173
Generation 2: 486
Generation 3: 253
Generation 4: 130
Generation 5: 100
Generation 6: 113
Generation 7: 24.8
Generation 8: 0
Count: 7638
CD24+
Undivided
Count
Comp-V450-A
211218_NSC CTV NIR D7_005.fcs
Proliferation
7654
Number of Peaks: 10.0
Root Mean Squared: 11.3
Undivided Peak Median: 735
Peak CV: 3.00
Peak Ratio: 0.50
Background: 0
Proliferation Index: 2.26
Division Index: 2.09
Percent Divided: 92.4
Expansion Index: 5.51
Replication Index: 5.89
Std.Deviation: 2.03
Undivided: 38.4
Generation 1: 0
Generation 2: 1495
Generation 3: 535
Generation 4: 302
Generation 5: 123
Generation 6: 8.10
Generation 7: 12.7
Generation 8: 0
Count: 7654
B
undivided
Count
Cell Trace Violet
C
undivided
Count
Cell Trace Violet
D
CD24- medium
CD24+ medium
% Population
Proliferation Division
E
CD24-
Undivided
CD24+
Undivided
CD24- medium
CD24+ medium
% Population
Proliferation Division
F
CD24-
Undivided
CD24+
Undivided
CD24- medium
CD24+ medium
% Population
Proliferation Division
G
3D
Undivided
2D
Undivided
211218_2D PDX CTV NIR D7_009.fcs
Proliferation
7955
3D medium
2D medium
% Population
Proliferation Division

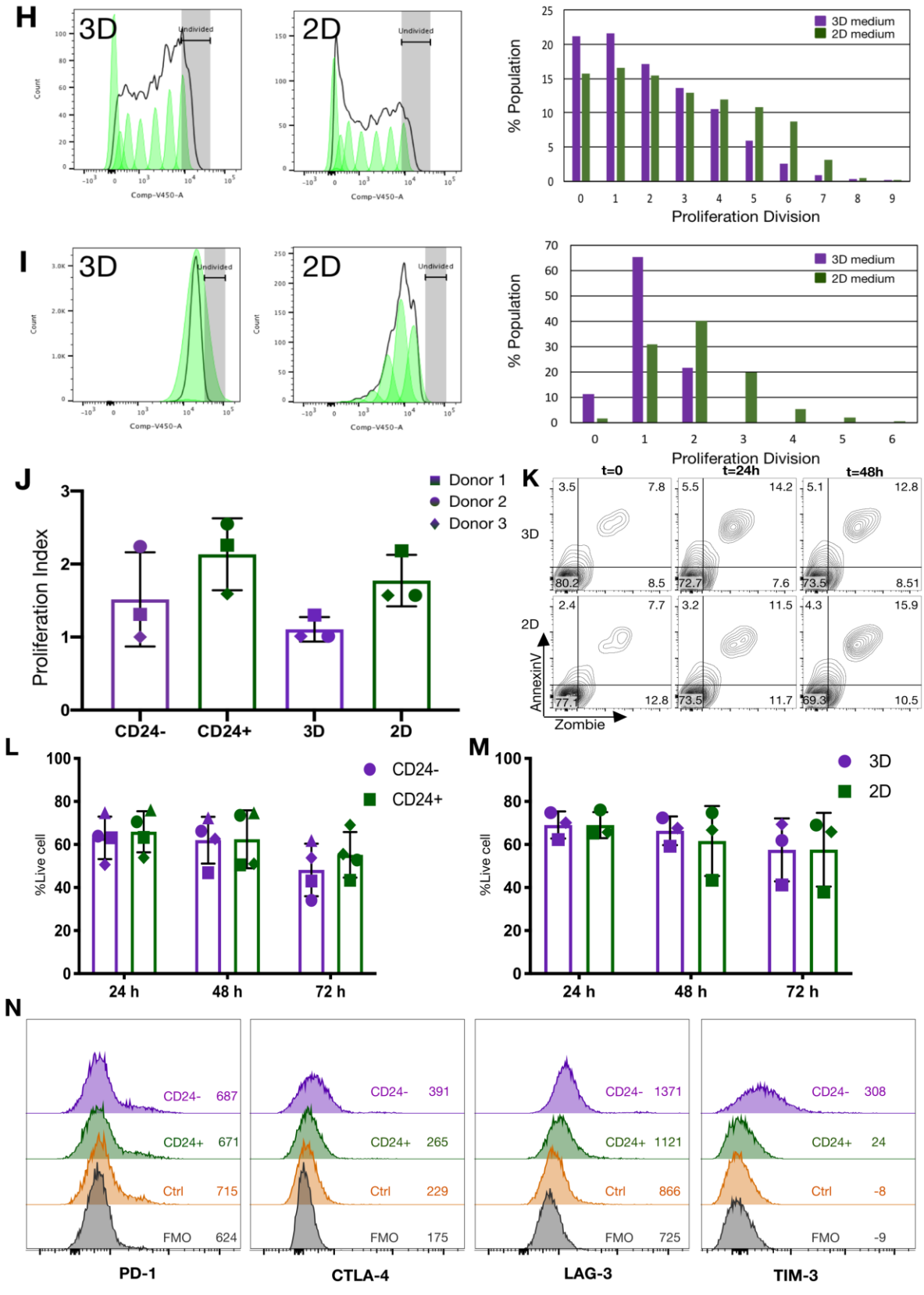
H
3D
2D
Undivided
Count
Comp-V450-A
% Population
Proliferation Division
3D medium
2D medium
I
J
Donor 1
Donor 2
Donor 3
Proliferation Index
CD24-
CD24+
3D
2D
K
t=0
t=24h
t=48h
AnnexinV
Zombie
L
M
%Live cell
24 h
48 h
72 h
N
CD24- 687
CD24+ 671
Ctrl 715
FMO 624
CD24- 391
CD24+ 265
Ctrl 229
FMO 175
CD24- 1371
CD24+ 1121
Ctrl 866
FMO 725
CD24- 308
CD24+ 24
Ctrl -8
FMO -9
PD-1
CTLA-4
LAG-3
TIM-3

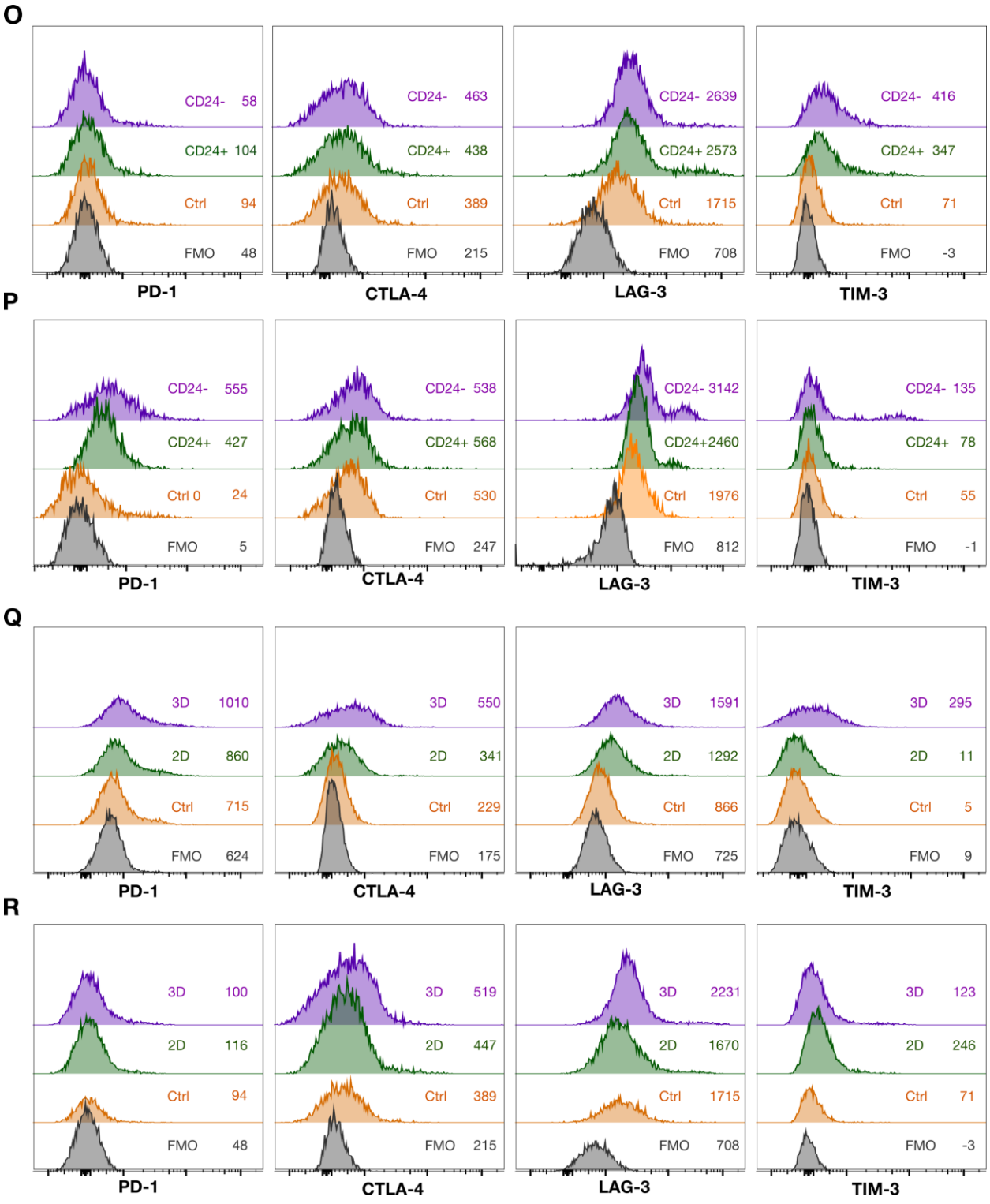
O
CD24- 58
CD24+ 104
Ctrl 94
FMO 48
PD-1
CD24- 463
CD24+ 438
Ctrl 389
FMO 215
CTLA-4
CD24- 2639
CD24+ 2573
Ctrl 1715
FMO 708
LAG-3
CD24- 416
CD24+ 347
Ctrl 71
FMO -3
TIM-3
P
CD24- 555
CD24+ 427
Ctrl 0 24
FMO 5
PD-1
CD24- 538
CD24+ 568
Ctrl 530
FMO 247
CTLA-4
CD24- 3142
CD24+2460
Ctrl 1976
FMO 812
LAG-3
CD24- 135
CD24+ 78
Ctrl 55
FMO -1
TIM-3
Q
3D 1010
2D 860
Ctrl 715
FMO 624
PD-1
3D 550
2D 341
Ctrl 229
FMO 175
CTLA-4
3D 1591
2D 1292
Ctrl 866
FMO 725
LAG-3
3D 295
2D 11
Ctrl 5
FMO 9
TIM-3
R
3D 100
2D 116
Ctrl 94
FMO 48
PD-1
3D 519
2D 447
Ctrl 389
FMO 215
CTLA-4
3D 2231
2D 1670
Ctrl 1715
FMO 708
LAG-3
3D 123
2D 246
Ctrl 71
FMO -3
TIM-3

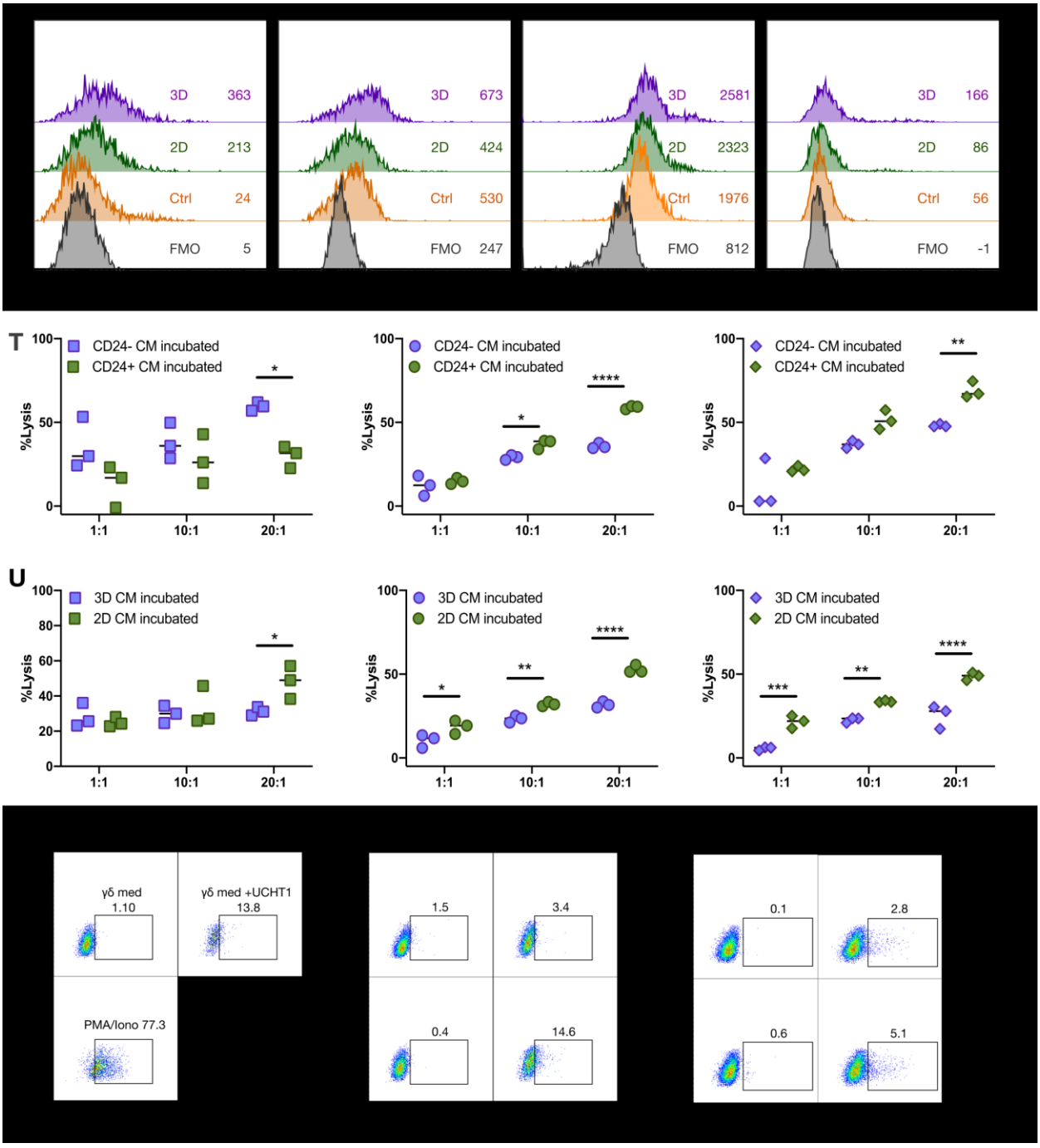
3D 363
2D 213
Ctrl 24
FMO 5
3D 673
2D 424
Ctrl 530
FMO 247
3D 2581
2D 2323
Ctrl 1976
FMO 812
3D 166
2D 86
Ctrl 56
FMO -1
T
CD24- CM incubated
CD24+ CM incubated
%Lysis
1:1
10:1
20:1
U
3D CM incubated
2D CM incubated
γδ med
1.10
γδ med +UCHT1
13.8
PMA/Iono 77.3
1.5
3.4
0.4
14.6
0.1
2.8
0.6
5.1

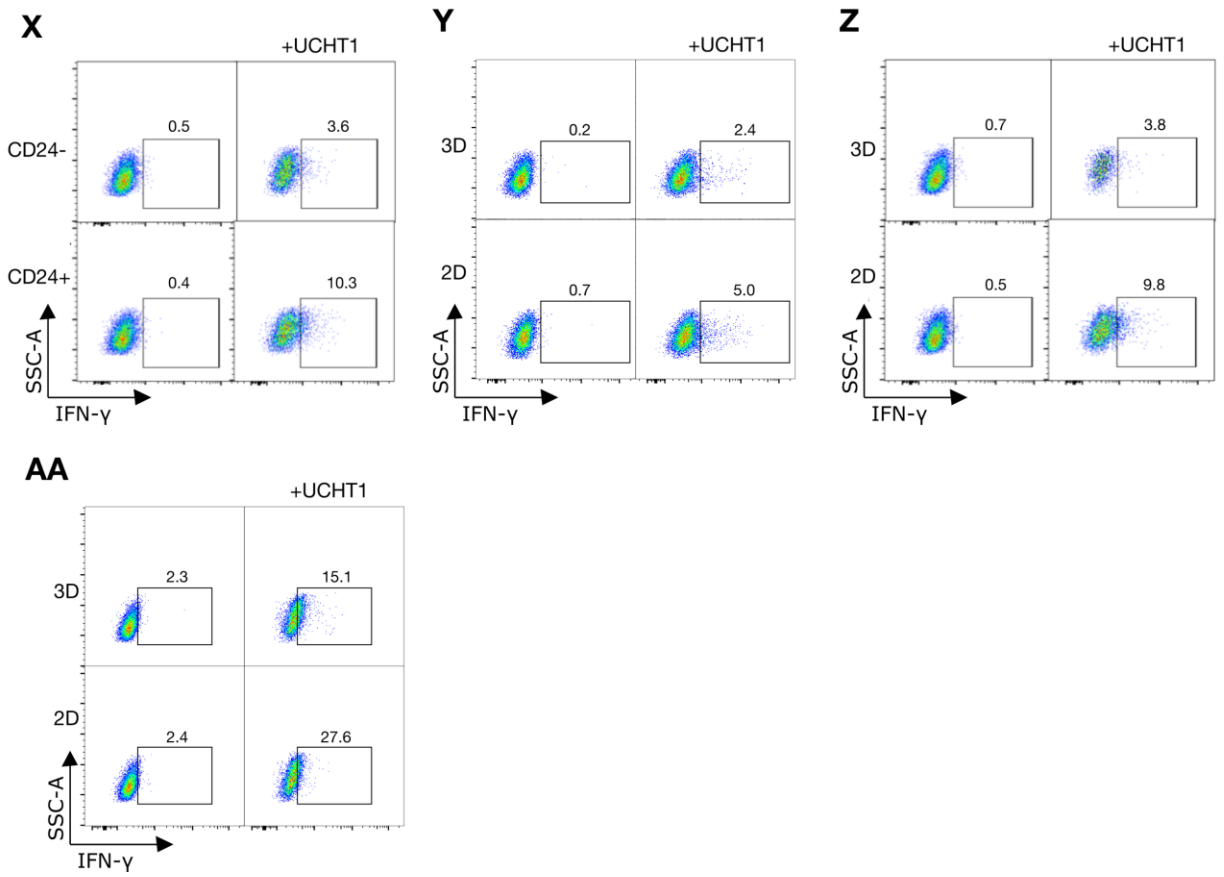

Figure S4.3. Breast cancer stem-like cells secrete factors that inhibit gamma delta T cell function but do not impact their viability. (A) γδTc from Donor 1 were labeled with Cell Trace Violet (CTV) and incubated with SUM149 SC ($CD24^-$) or NSC ($CD24^+$) conditioned medium (CM) for 24h, washed and their proliferation measured six days later using flow cytometry. Shown are data generated upon analysis using the FlowJo 10.5.3 Proliferation Modeling Tool. **(B)** Histogram for γδTc that had been incubated in $CD24^-$ CM showing the proliferation peaks from the $CD24^-$ panel in **A**; numbered peaks correspond to divisions of the populations within the cultures that proliferated to different extents. **(C)** As in **B** for γδTc that had been incubated in $CD24^+$ CM. **(D)** Graphical representation of replication divisions undergone by γδTc in the proliferation experiment shown in Fig 3**A** and S3**B** and **C**. **(E)** Output from the FlowJo 10.5.3 Proliferation Modeling Tool for γδTc derived from donor 2 and **(F)** donor 3. **(G)** Experiments done as in A-C but with PDX401 3D and 2D media treatment of γδTc from donor 1, **(H)** donor 2 and **(I)** donor 3. **(J)** Graph of cumulative proliferation index values from the three donor cultures treated with SUM149 or PDX401 CM. **(K)** γδTc were incubated with PDX 2D and 3D CM for 24 h, washed and viability was accessed using Zombie Aqua and AnnexinV staining after indicated duration. **(L)** Cumulative results for percent live γδTc incubated with SUM149 $CD24^-$ and $CD24^+$ CM (n=4) or **(M)** PDX401 3D and 2D CM (n=3). **(N)** γδTc were incubated with SUM149 $CD24^+$ or $CD24^-$ CM for 24h; histograms for expression of the indicated co-inhibitory receptors on γδTc seven days after incubation with CM are depicted with median fluorescence intensities for donor 1. **(O)** Same experiment done as in **N** with CM of γδTc from donor 2 and **(P)** donor 3. **(Q)** Experiments done as in **N-P** but with PDX401 3D and 2D media treating γδTc from donor 1, **(R)** donor 2 and **(S)** donor 3. **(T)** After incubation with SUM149 $CD24^-$ and $CD24^+$ CM, γδTc were used to target unsorted

SUM149 in Calcein AM cytotoxicity assays at the indicated effector: target (E:T) ratios. Results from biological replicates using γδTc from three different donors are shown. **(U)** Cytotoxicity assays done as in **T** but with PDX401 3D and 2D media-treated γδTc from three different donors targeting PDX401 cells. **(V)** γδTc incubated with SUM149 $CD24^-$ and $CD24^+$ CM were treated with anti-CD3 antibody (UCHT1) for 6h and IFN-γ expression was determined *via* intracellular flow cytometry. Unstimulated cells were used to set gates and γδTc treated with PMA/Ionomycin were used as a positive control. Control gates and percentage of IFN-γ-producing γδTc is depicted for γδTc derived from donor 1, **(W)** donor 2 and **(X)** donor 3. **(Y)** Similarly, results from PDX401 3D and 2D CM-treated γδTc derived from donor 1, **(Z)** donor 2 and **(AA)** donor 3 are shown. Donor numbers were reset for each set of experiments. Ctrl = γδTc incubated with regular γδTc media instead of CM. Data are presented as mean ± SD in **J**, **L-M**, and median in **T-U**. Statistical tests employed were: (**J**) One-way ANOVA followed by Sidak's post hoc test for multiple comparisons between groups. (**L-M, T-U**) One-way ANOVA followed by Sidak's post hoc test for multiple comparisons between group. No significance was achieved for **J, L-M**. *P<0.05, **P<0.01, ***P<0.001, ****P<0.0001.

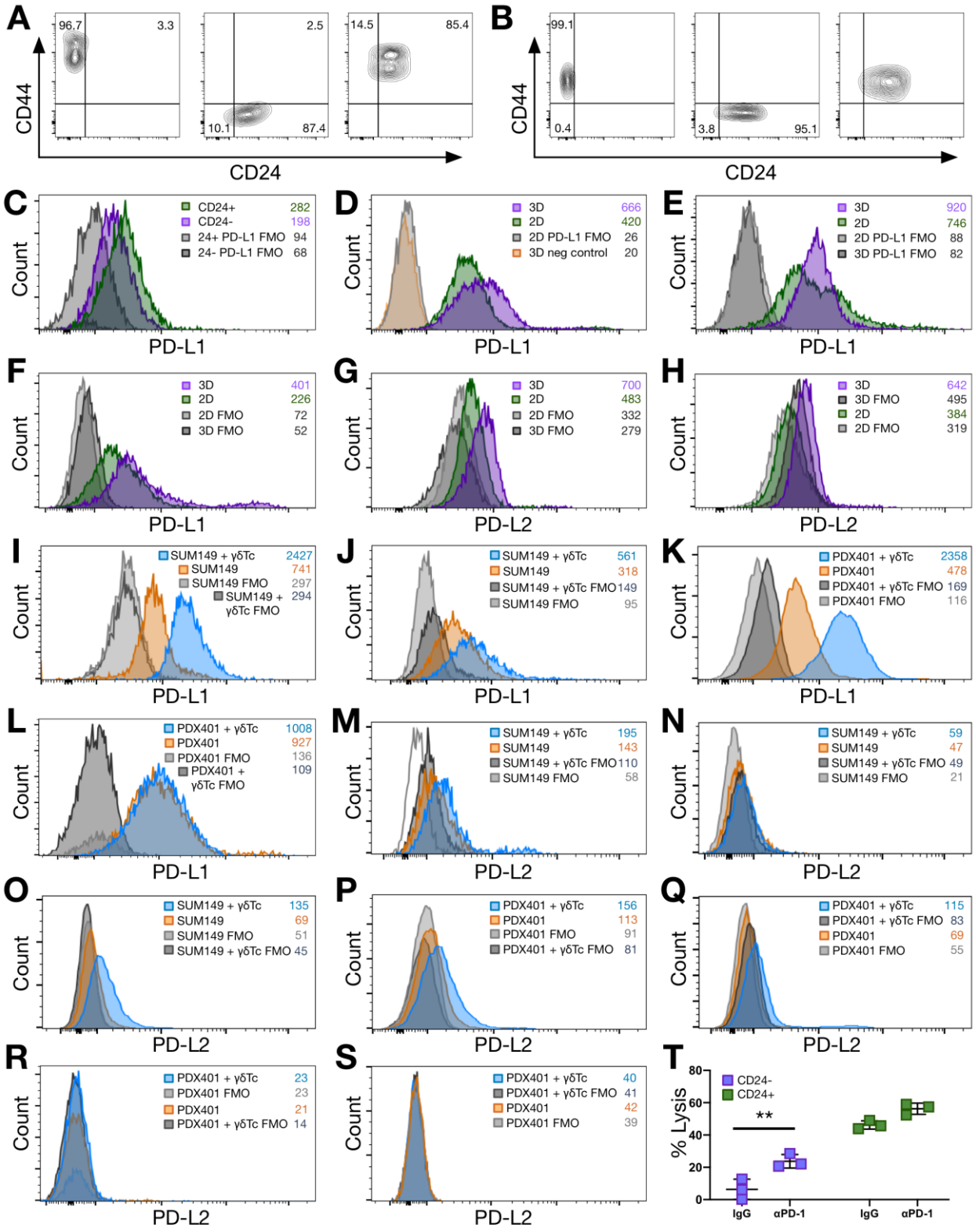
A
96.7
3.3
10.1
87.4
2.5
14.5
85.4
CD44
CD24
B
99.1
0.4
3.8
95.1
CD44
CD24
C
CD24+ 282
CD24- 198
24+ PD-L1 FMO 94
24- PD-L1 FMO 68
Count
PD-L1
D
3D 666
2D 420
2D PD-L1 FMO 26
3D neg control 20
Count
PD-L1
E
3D 920
2D 746
2D PD-L1 FMO 88
3D PD-L1 FMO 82
Count
PD-L1
F
3D 401
2D 226
2D FMO 72
3D FMO 52
Count
PD-L1
G
3D 700
2D 483
2D FMO 332
3D FMO 279
Count
PD-L2
H
3D 642
3D FMO 495
2D 384
2D FMO 319
Count
PD-L2
I
SUM149 + γδTc 2427
SUM149 741
SUM149 FMO 297
SUM149 + γδTc FMO 294
Count
PD-L1
J
SUM149 + γδTc 561
SUM149 318
SUM149 + γδTc FMO 149
SUM149 FMO 95
Count
PD-L1
K
PDX401 + γδTc 2358
PDX401 478
PDX401 + γδTc FMO 169
PDX401 FMO 116
Count
PD-L1
L
PDX401 + γδTc 1008
PDX401 927
PDX401 FMO 136
PDX401 + γδTc FMO 109
Count
PD-L1
M
SUM149 + γδTc 195
SUM149 143
SUM149 + γδTc FMO 110
SUM149 FMO 58
Count
PD-L2
N
SUM149 + γδTc 59
SUM149 47
SUM149 + γδTc FMO 49
SUM149 FMO 21
Count
PD-L2
O
SUM149 + γδTc 135
SUM149 69
SUM149 FMO 51
SUM149 + γδTc FMO 45
Count
PD-L2
P
PDX401 + γδTc 156
PDX401 113
PDX401 FMO 91
PDX401 + γδTc FMO 81
Count
PD-L2
Q
PDX401 + γδTc 115
PDX401 + γδTc FMO 83
PDX401 69
PDX401 FMO 55
Count
PD-L2
R
PDX401 + γδTc 23
PDX401 FMO 23
PDX401 21
PDX401 + γδTc FMO 14
Count
PD-L2
S
PDX401 + γδTc 40
PDX401 + γδTc FMO 41
PDX401 42
PDX401 FMO 39
Count
PD-L2
T
CD24-
CD24+
**
% Lysis
0
20
40
60
80
IgG
αPD-1
IgG
αPD-1

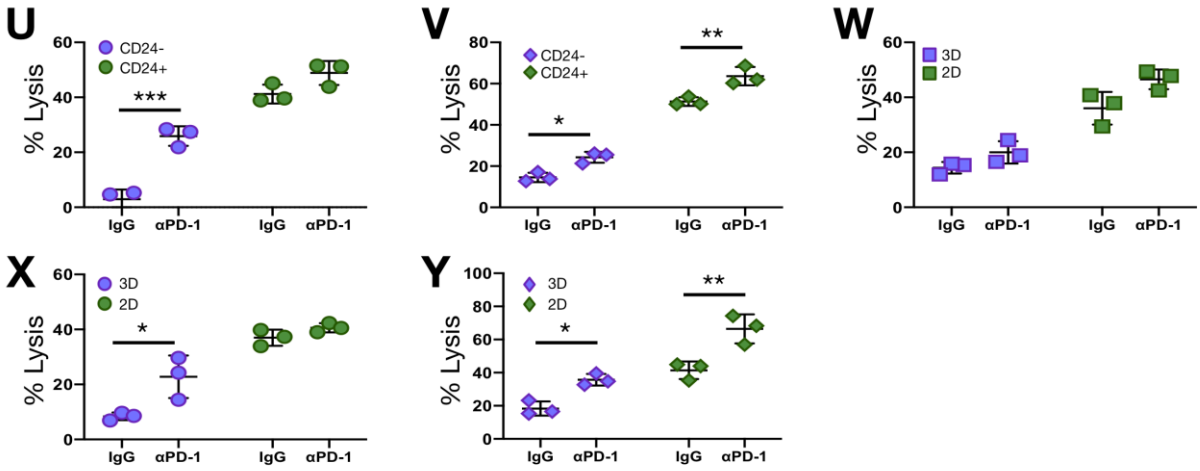

Figure S4.4. Inhibitory ligands are expressed on breast cancer stem-like cells resistant to gamma delta T cell killing. PD-L1 expression on SUM149 $CD24^-$ and $CD24^+$ cells were detected by flow cytometry **(A)** Florescence minus one (FMO) controls are shown for replicate 1 and **(B)** replicate 2. **(C)** Histogram overlays of PD-L1 expression on SUM149 replicate 2. **(D)** Histogram overlays for PD-L1 expression on PDX 401 3D and 2D cells, replicate 1, **(E)** replicate 2 and **(F)** replicate 3 is shown. **(G)** Histogram overlays for PD-L2 expression on PDX 401 3D and 3D cells, replicate 1 and **(H)** replicate 2. Target cells were co-incubated with γδTc at a 1:1 ratio overnight and surface expression of PD-L1 was determined using flow cytometry. **(I)** Histogram overlays PD-L1 expression are shown for replicate 2, and **(J)** replicate 3. **(K)** Experiments done as in **I-J** but with PDX401 cells, replicate 2 and **(L)** replicate 3. **(M)** PD-L2 was also compared between co-incubated targets and targets alone on SUM149 replicate 1, **(N)** replicate 2, **(O)** replicate 3, and **(P)** PDX401 cells replicate 1, **(Q)** replicate 2, **(R)** replicate 3 and **(S)** replicate 4. γδTc were incubated with blocking antibody for PD-1 and then co-incubated with **(T)** SUM149 $CD24^-$, $CD24^+$ cells replicate 1, **(U)** replicate 2 and **(V)** replicate 3, or **(W)** PDX401 2D, PDX 3D cells replicate 1, **(X)** replicate 2 and **(Y)** replicate 3; at E: T 20:1 for 4 h. Donor numbers were reset for each set of experiments. Data are presented as mean ± SD in **T-Y**. Statistical tests employed were: **(T-Y)** One-way ANOVA followed by Tukey's post hoc test. *P<0.05, **P<0.01, ***P<0.001.

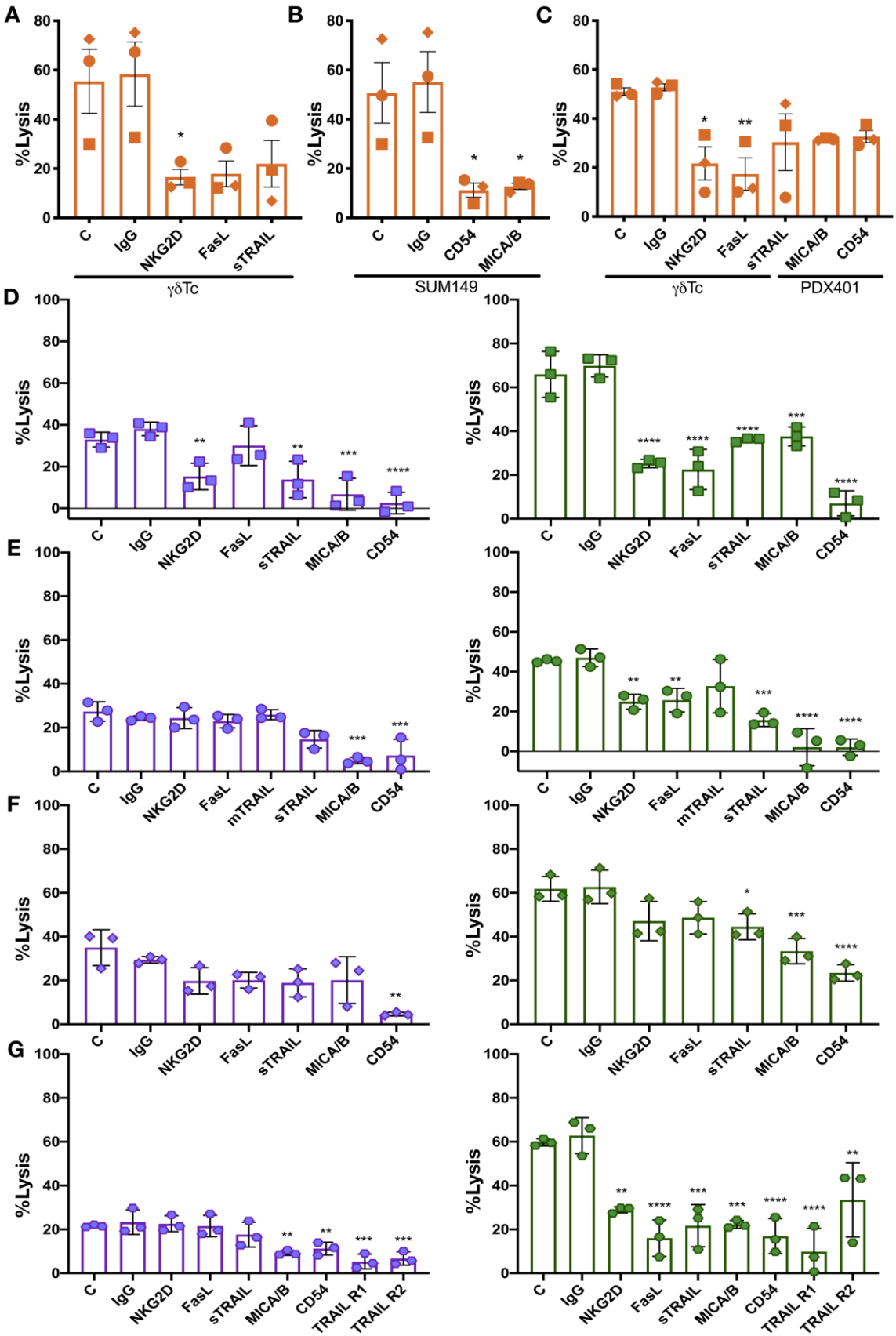
A
B
C
%Lysis
C
IgG
NKG2D
FasL
sTRAIL
CD54
MICA/B
γδTc
SUM149
PDX401
D
E
F
G
mTRAIL
TRAIL R1
TRAIL R2

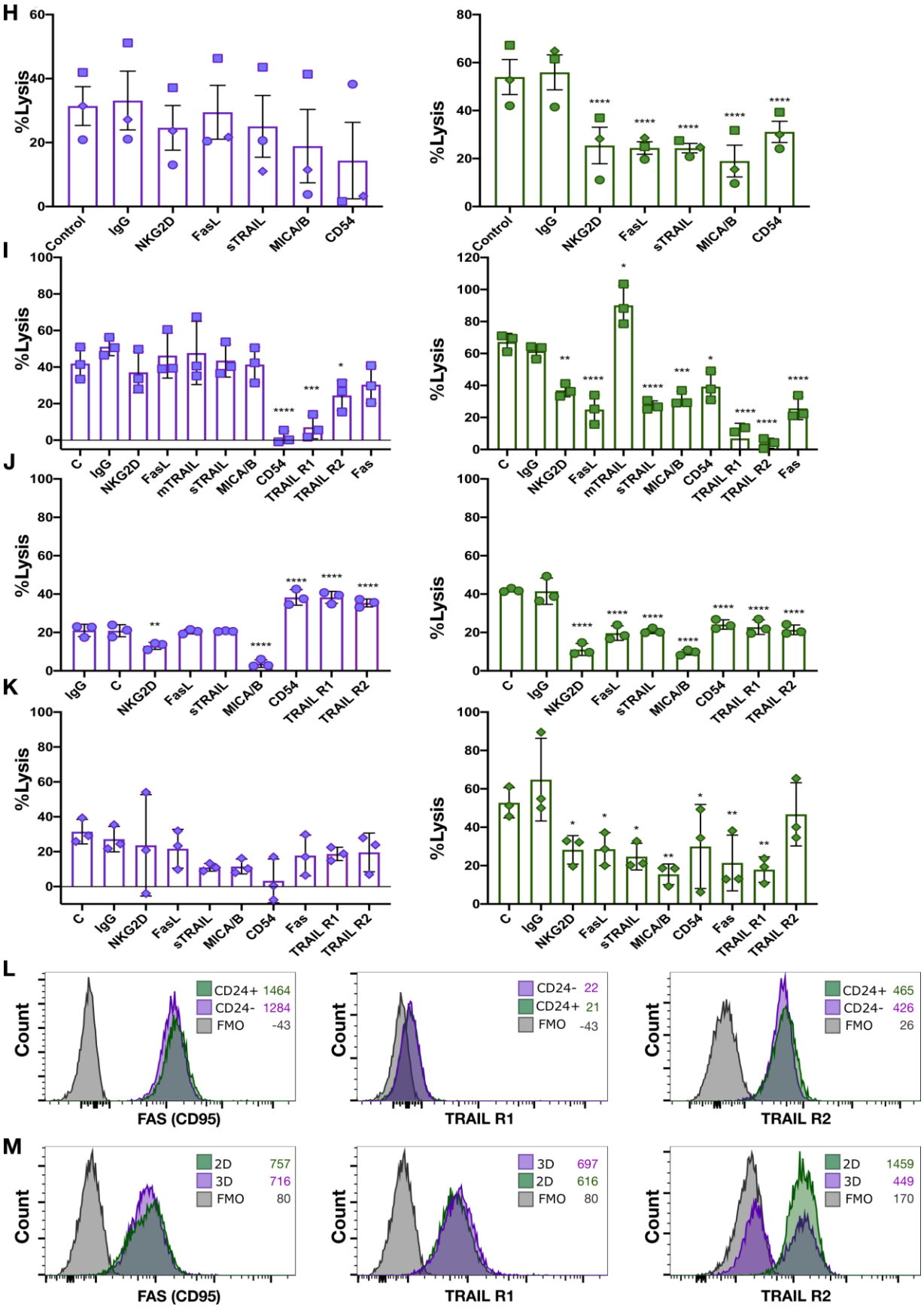
H
%Lysis
Control
IgG
NKG2D
FasL
sTRAIL
MICA/B
CD54
I
C
mTRAIL
TRAIL R1
TRAIL R2
Fas
J
K
L
Count
CD24+ 1464
CD24- 1284
FMO -43
FAS (CD95)
CD24- 22
CD24+ 21
FMO -43
TRAIL R1
CD24+ 465
CD24- 426
FMO 26
TRAIL R2
M
2D 757
3D 716
FMO 80
3D 697
2D 616
FMO 80
2D 1459
3D 449
FMO 170

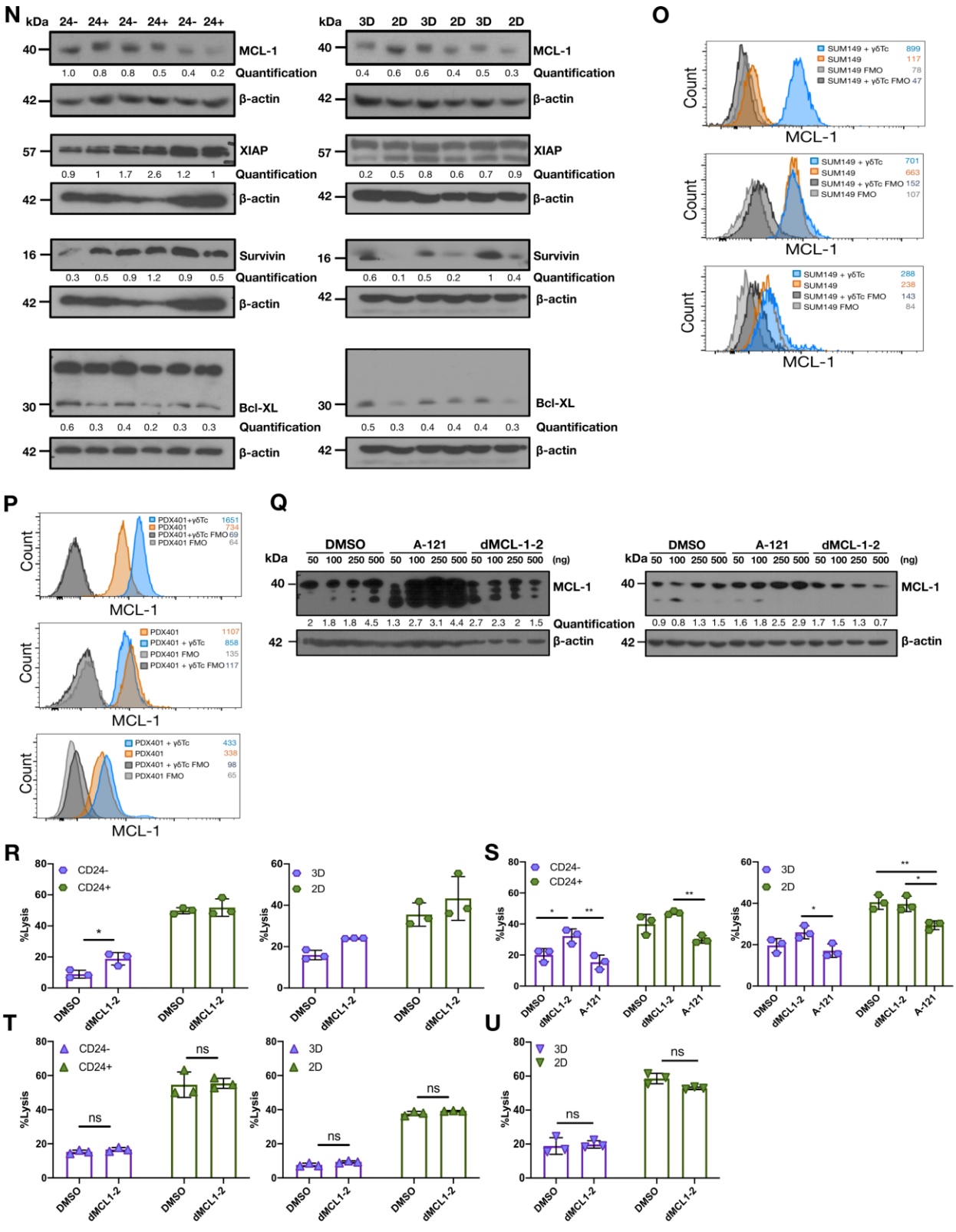
N
kDa 24- 24+ 24- 24+ 24- 24+
MCL-1
Quantification
β-actin
XIAP
Survivin
Bcl-XL
kDa 3D 2D 3D 2D 3D 2D
O
SUM149 + γδTc
SUM149
SUM149 FMO
SUM149 + γδTc FMO
Count
MCL-1
P
PDX401+γδTc
PDX401
PDX401+γδTc FMO
PDX401 FMO
PDX401 + γδTc
Q
DMSO
A-121
dMCL-1-2
(ng)
R
CD24-
CD24+
3D
2D
%Lysis
S
T
U
ns

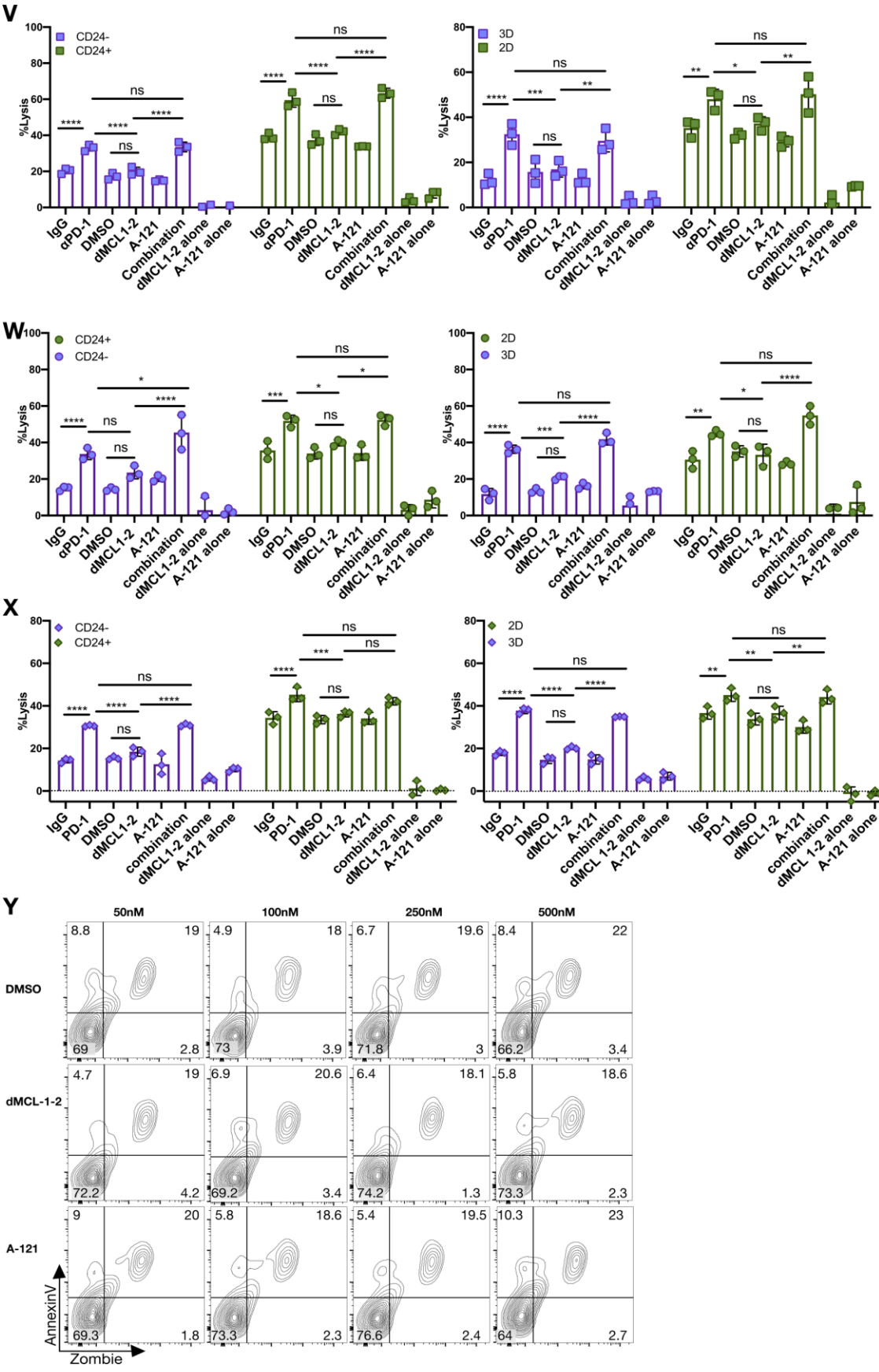
V
CD24-
CD24+
%Lysis
IgG
αPD-1
DMSO
dMCL1-2
A-121
Combination
dMCL1-2 alone
A-121 alone
3D
2D
W
CD24+
CD24-
2D
3D
X
PD-1
Y
50nM
100nM
250nM
500nM
DMSO
dMCL-1-2
A-121
AnnexinV
Zombie

Figure S4.5. Fas-FasL pathway dysfunctional in breast cancer stem-like cells. (A) γδTc or **(B)** SUM149 cells were incubated with the indicated antibodies for 30 mins and then co-incubated at E:T 20:1 for 4h in a Calcein AM release assay to assess cytotoxicity **(C)** Blocking and cytotoxicity assay as in A and B, but with γδTc and PDX401 target cells. **(D)** SUM149 were sorted into $CD24^-$ (left panel) and $CD24^+$ (right panel) fractions, incubated with the indicated antibodies and then co-incubated with γδTc at E: T 20:1 for 4h from donor 1, **(E)** donor 2, **(F)** donor 3 and **(G)** donor 4. **(H)** Similarly, PDX401 3D and 2D cells were incubated with antibodies followed by γδTc; cumulative results are shown (n=3) for experiments performed with γδTc from **(I)** donor 1, **(J)** donor 2 and **(K)** donor 3. **(L)** Histogram overlays of indicated receptors on SUM149 $CD24^-$ and $CD24^+$ cells and **(M)** PDX 3D and 2D cells are shown. **(N)** Expression of indicated anti-apoptotic proteins was determined using western blot analysis of lysates from three sets of sorted SUM149 $CD24^-$ and $CD24^+$ cells (left panel) and PDX401 3D and 2D cells (right panel). Molecular weight markers are shown on the left in kDa; β-actin loading controls and quantifications are shown below corresponding panels. For SUM149 cells, XIAP and Survivin were probed on the same blot and for PDX401 cells, Survivin and Bcl-XL were probed on the same blot. **(O)** SUM149 cells were subject to a γδTc cytotoxicity assay at 1:1 (E: T) ratio overnight. Target cells were then stained for intracellular MCL-1 protein that was detected *via* flow cytometry. Histogram overlays of experiments done with γδTc from donor 2 (top), donor 3 (middle) and donor 4 (bottom) are shown. **(P)** Experiment done as in N with PDX401 cells and γδTc from three different donors. **(Q)** SUM149 (left) and PDX401 (right) that were treated with the MCL-1 degrader dMCL1-2 and failed inhibitor A-1210477 (A-121) are depicted. Molecular weight markers are shown on the left in kDa; β-actin loading controls and quantifications are shown below corresponding panels. **(R)** Sorted SUM149 $CD24^+$ and $CD24^-$ cells (left) were co-incubated with γδTc derived from donor 1 at E: T 20:1 in a 4 h Calcein AM cytotoxicity assay; indicated treatments were added to the co-incubation. The same experiment was performed in parallel with PDX401 3D and 2D cells (right). Experiments done with γδTc derived from **(S)** donor 2, **(T)** donor 3, **(U)** donor 4, **(V)** donor 5, **(W)** donor 6 and **(X)** donor 7 are shown. **(Y)** γδTc were incubated with the indicated concentration of DMSO, dMCL1-2 and A-121 for 4h and viability was accessed using Zombie Aqua and AnnexinV staining. Donor numbers were reset for each set of experiments. mTRAIL stands for membrane bound TRAIL and sTRAIL stands for soluble TRAIL. Data are presented as mean ± SEM in **A-C** and mean ± SD in **D-K** and **R-X**. Statistical tests employed were: (**A-K**, **R-U**) One-way ANOVA followed by Sidak's post hoc test, (**V-X**) Two-way ANOVA followed by Tukey's post hoc test. *P<0.05, **P<0.01, ***P<0.001, ****P<0.0001.

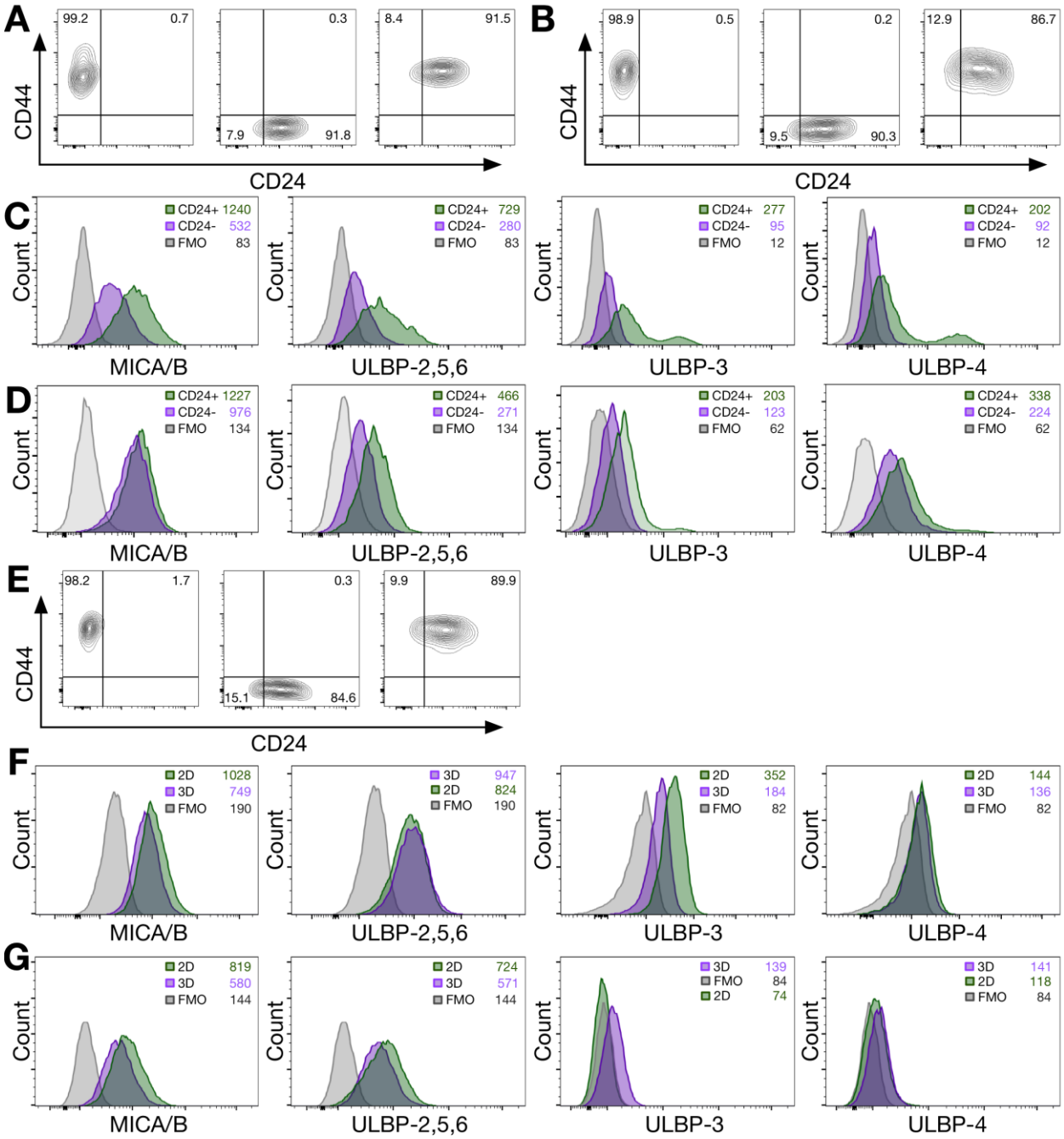

Figure S4.6. MICA/B is downregulated on the surface of breast cancer stem-like cells. (A) NKG2D ligand expression was determined on SUM149 $CD24^-$ and $CD24^+$ cells by flow cytometry. Florescence minus one (FMO) controls used to set gates for CD44 and CD24 for replicate 1 and **(B)** replicate 2. **(C)** Histogram overlays of NKG2D ligand expression on SUM149 $CD24^-$ and $CD24^+$ cells for replicate 2 and **(D)** replicate 3. **(E)** FMO controls are also shown for replicate 3. **(F)** Histogram overlays of NKG2D ligand expression on PDX401 3D and 2D cells for replicate 2 and **(G)** replicate 3.

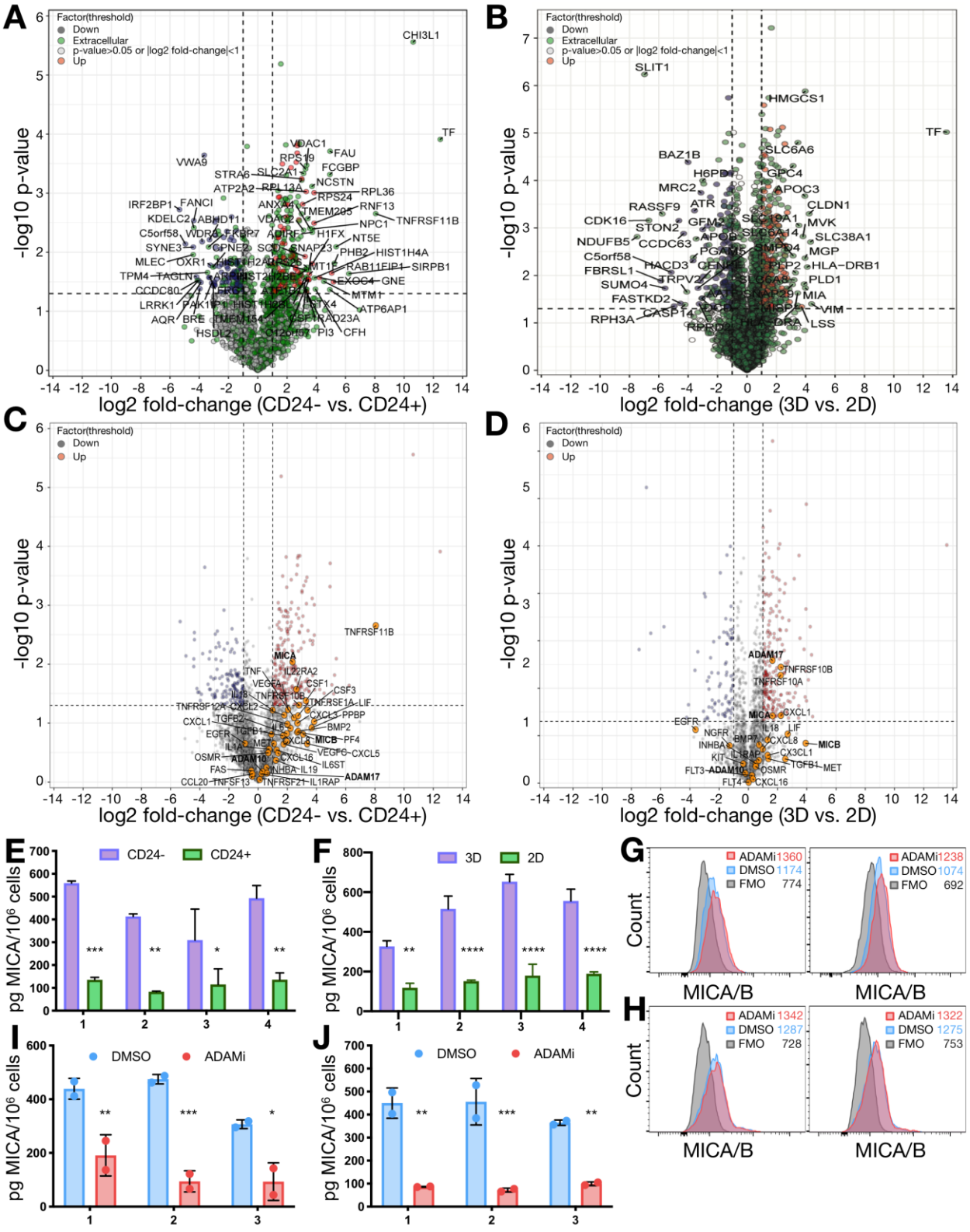
A
B
C
D
E
F
G
H
I
J
Factor(threshold)
Down
Extracellular
p-value>0.05 or |log2 fold-change|<1
Up
-log10 p-value
log2 fold-change (CD24- vs. CD24+)
log2 fold-change (3D vs. 2D)
CD24-
CD24+
3D
2D
pg MICA/10^6 cells
DMSO
ADAMi
Count
MICA/B
ADAMi1360
DMSO1174
FMO 774
ADAMi1238
DMSO1074
FMO 692
ADAMi 1342
DMSO 1287
FMO 728
ADAMi 1322
DMSO 1275
FMO 753

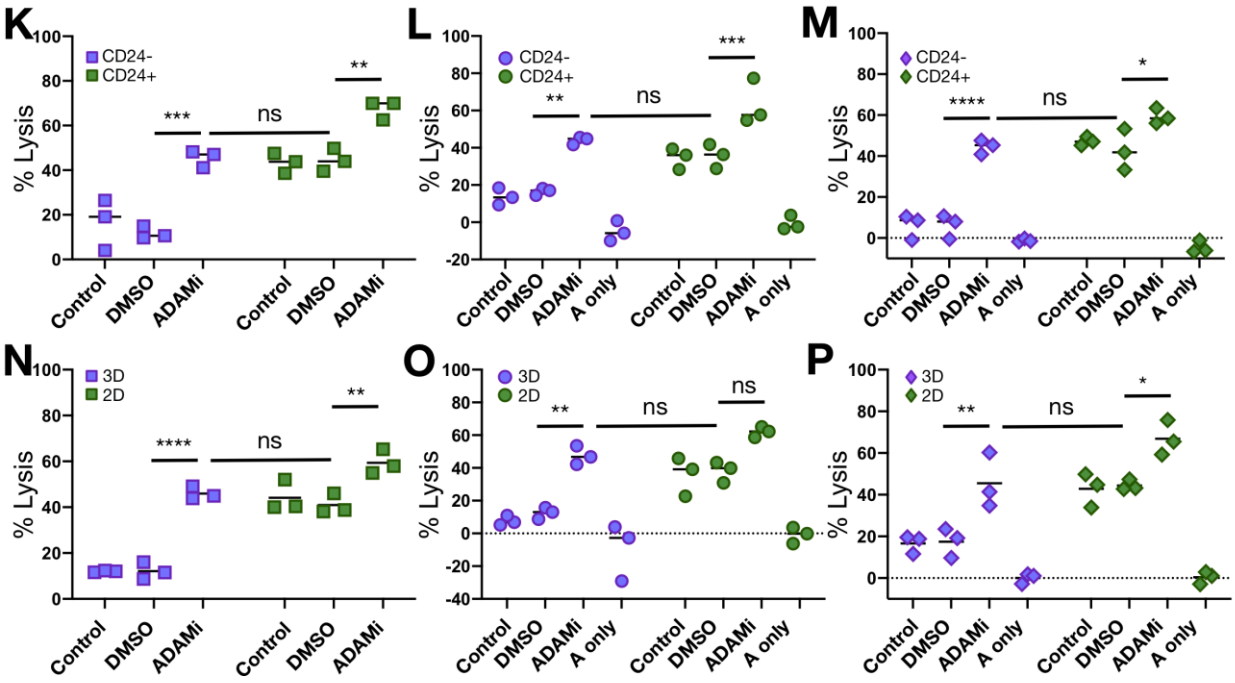

Figure S4.7. The ADAM inhibitor GW280264X prevents MICA shedding and enhances γδ T cell cytotoxicity against breast cancer stem-like cells. Mass spectrometry analysis of SUM149 $CD24^-$ and $CD24^+$ cells and PDX401 3D and 2D conditioned media was done and **(A)** Volcano plot shows analytes that showed most significant differential expression between SUM149 $CD24^-$ and $CD24^+$ and **(B)** PDX401 3D and 2D. **(C)** KEGG analysis of cytokine/cytokine receptor interaction for SUM149 sorted cells and **(D)** PDX401 3D and 2D cells. MICA shedding by **(E)** SUM149 sorted cells and **(F)** 2D and 3D PDX401 was determined by ELISA. Replicate number is indicated on x-axis. **(G)** Target were treated with ADAM proteases inhibitor GW280264X for 4 h and MICA/B surface expression was determined *via* flow cytometry for SUM149 replicate 2 (left) and replicate 3 (right) and **(H)** PDX401 replicate 2 (left) and (right) **(I)** Soluble MICA after treatment was determined using ELISA for SUM149 and **(J)** PDX401 cells, replicate numbers are indicated on x-axis. (K) SUM149 $CD24^-$, $CD24^+$ cells were incubated with ADAM inhibitor, GW280264X and then co-incubated with γδTc at E: T 20:1 for 4 h. Results from experiments done with γδTc from donor 1, **(L)** 2 and **(M). (N)** Experiments done as in K-M but with PDX401 2D, 3D cells donor 1, **(O)** donor 2 and **(P)** donor 3. "A only" stands for target cells treated with ADAM inhibitor only. Donor numbers were reset for each set of experiments. Data are presented as mean ± SD **(E,F,I,J)** and median **(K-P)**. Statistical tests employed were: **(E,F,I,J)** Two-way ANOVA followed by Bonferroni's post hoc test. (K-P) Two-way ANOVA followed by Tukey's post hoc test. *P<0.05, **P<0.01, ***P<0.001, ****P<0.0001.

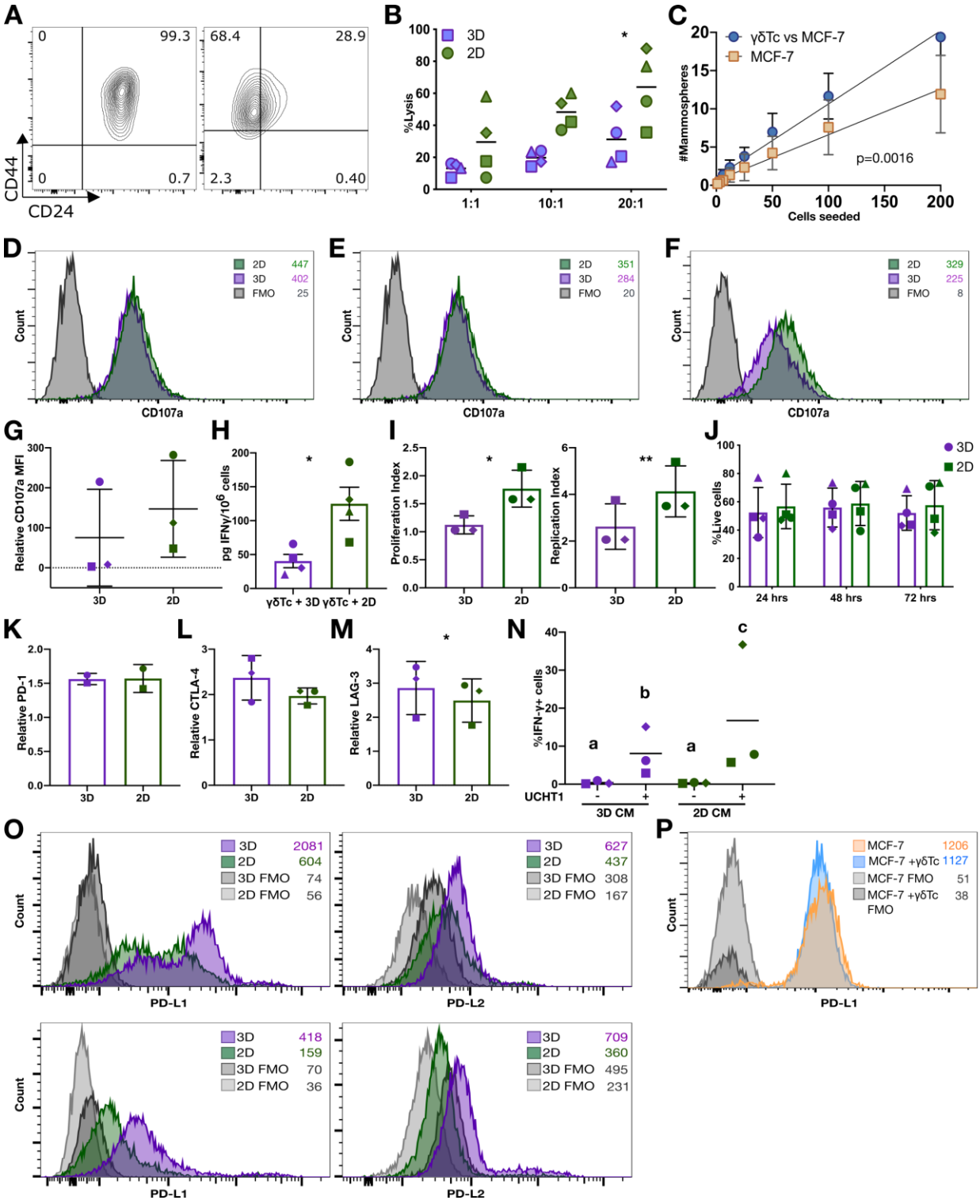
A
0
99.3
68.4
28.9
0
0.7
2.3
0.40
CD44
CD24
B
3D
2D
%Lysis
1:1
10:1
20:1
*
C
γδTc vs MCF-7
MCF-7
#Mammospheres
p=0.0016
Cells seeded
D
2D 447
3D 402
FMO 25
Count
CD107a
E
2D 351
3D 284
FMO 20
F
2D 329
3D 225
FMO 8
G
Relative CD107a MFI
H
pg IFNγ/10^6 cells
γδTc + 3D
γδTc + 2D
I
Proliferation Index
Replication Index
**
J
%Live cells
24 hrs
48 hrs
72 hrs
K
Relative PD-1
L
Relative CTLA-4
M
Relative LAG-3
N
%IFN-γ+ cells
a
b
c
UCHT1
3D CM
2D CM
O
3D 2081
2D 604
3D FMO 74
2D FMO 56
PD-L1
3D 627
2D 437
3D FMO 308
2D FMO 167
PD-L2
3D 418
2D 159
3D FMO 70
2D FMO 36
3D 709
2D 360
3D FMO 495
2D FMO 231
P
MCF-7 1206
MCF-7 +γδTc 1127
MCF-7 FMO 51
MCF-7 +γδTc FMO 38

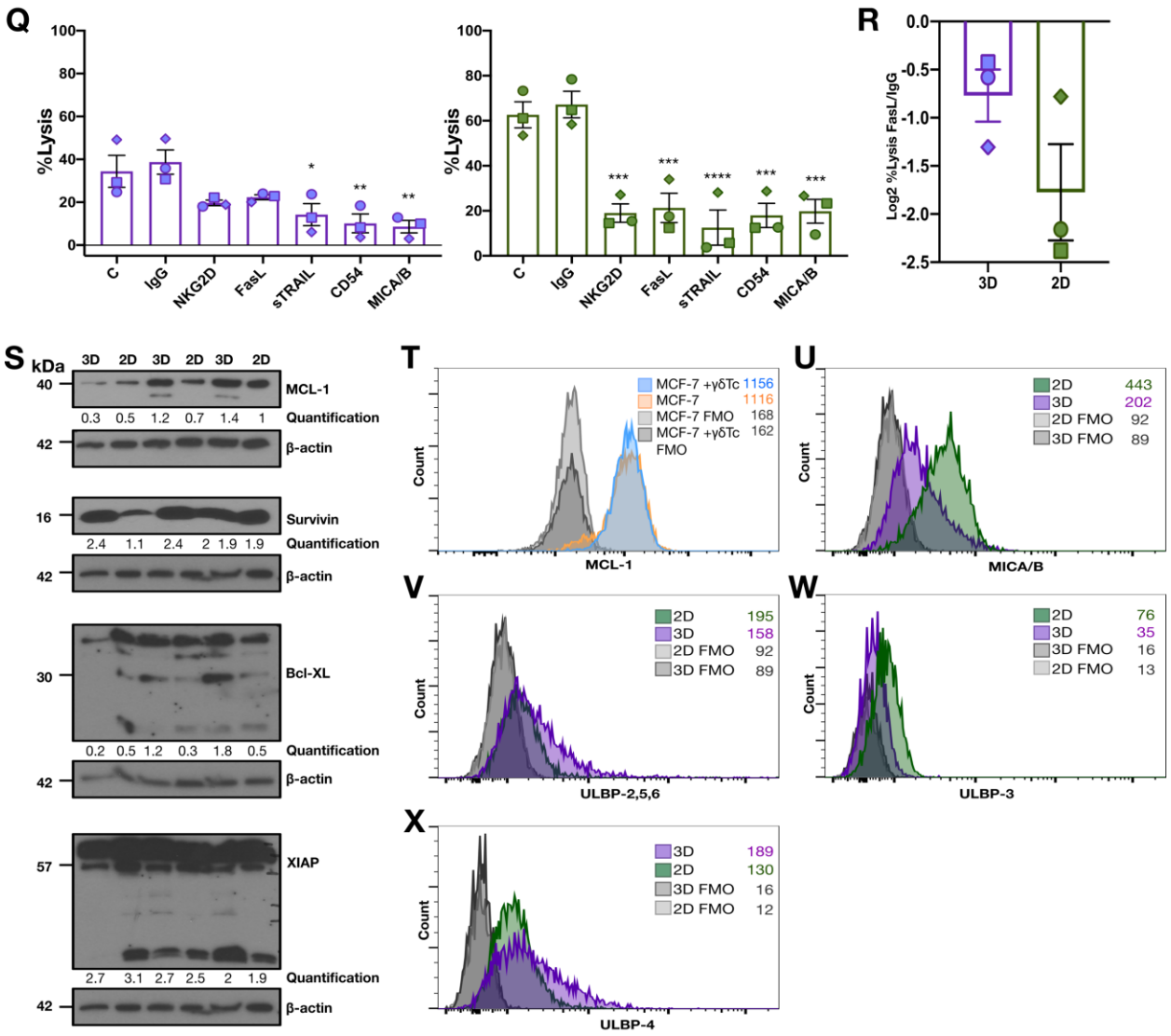

Figure S4.8. The MCF-7 stem-like cell population behaves very similar to SUM149 and PDX401 stem-like cells. **(A)** Second generation mammospheres (3D) and adherent (2D) MCF-7 cells were dissociated, then CD44 and CD24 expression were determined by flow cytometry (n=1). **(B)** Second generation mammospheres (3D) and adherent (2D) MCF-7 were dissociated, filtered into single cell suspensions and used as targets in Calcein AM cytotoxicity assays (n=4) **(C)** MCF-7 cells were co-cultured with γδTc at 1:1 overnight, γδTc were then removed, and mammosphere forming potential of targets determined over two generations (cumulative, n=3). **(D)** Overlay of CD107a expression (degranulation) for γδTc incubated with MCF-7 3D and 2D cells for γδTc derived from donor 1, **(E)** donor 2 and **(F)** donor 3. **(G)** Cumulative results (n=3) for MFI of CD107a. **(H)** IFN-γ ELISA was performed on conditioned media (CM) from γδTc co-incubated with 3D or 2D MCF-7 for 24h (n=4). **(I)** Using the FlowJo 10.5.3 Proliferation Modeling Tool, proliferation index values and replication index values were calculated for three donor cultures treated with MCF-7 3D and 2D CM; cumulative data are shown (n=3). **(J)** γδTc viability after incubation with MCF-7 3D or 2D conditioned medium (CM) was assessed using AnnexinV and Zombie Aqua at specified time points; cumulative results are shown (n=4). **(K)** γδTc were

incubated with MCF-7 3D and 2D cells for 24h; cumulative results for expression of co-inhibitory receptors PD-1 (n=2), **(L)** CTLA-4 (n=3), and **(M)** LAG-3 (n=4) on γδTc seven days later. **(N)** γδTc incubated with MCF-7 3D and 2D CM were treated with anti-CD3 antibody overnight and IFN-γ expression was determined *via* intracellular flow cytometry; cumulative results for % IFN-γ producing cells (n=3). **(O)** Histogram overlays showing PD-L1 expression (top left) and PD-L2 expression (top right) on second generation 3D and adherent 2D MCF-7 cells. The same experiment with a different biological replicate is shown in the bottom panels. **(P)** MCF-7 cells were treated with γδTc at 1:1 overnight, and surface expression of PD-L1 was compared between treated and untreated cells. **(Q)** 3D and 2D cells were incubated with the indicated antibodies and then co-incubated with γδTc at E:T 20:1 for 4h (n=3). Cumulative results for three experiments are depicted. **(R)** The decrease in target cell lysis upon FasL blocking (n=3) is indicated for the experiment. **(S)** Expression of anti-apoptotic proteins was determined using western blot analysis of lysates from three different sets of MCF-7 3D and 2D cells as indicated. Molecular weight (MW) markers are shown on the left; β-actin loading controls and quantification of band intensities normalized to β-actin controls are shown below corresponding panels. Survivin and XIAP were probed on the same blot **(T)** MCF-7 were subject to a γδTc cytotoxicity assay at 1:1 (E:T) ratio overnight. Post-cytotoxicity, target cells were stained for intracellular MCL-1 expression, detected *via* flow cytometry. (**U**) Histogram overlays of MICA/B (**V**) ULBP-2,5,6 **(W)** ULBP-3 and **(X)** ULBP-4 expression on MCF-7 3D and 2D cells is shown. Data are presented as: mean in B and N; mean ± SD in C, G, and I-M; mean ± SEM in H, Q, and R. Statistical tests employed were: (B, J); Two-way ANOVA followed Sidak's post hoc test for multiple comparisons between groups; (C) simple linear regression; (G, L) One-tailed Wilcoxon test; (H) Two-tailed ratio paired t-test; (I) Two-tailed paired t-test; (K, M, R) One-tailed paired t-test; (N) One-tailed ratio paired t-test, b-c, p= 0.0452; (Q) One-way ANOVA followed by Bonferroni's post hoc test. *p<0.05, **p<0.01, ***p<0.001, ****p<0.0001.

Chapter 5- Discussion and Future Directions

Breast cancer remains a significant cause of cancer-related mortality due to the metastatic spread of the tumor, as well as therapy resistance and relapse[1,2]. Research is focused on the mechanisms underlying cancer resistance and how to overcome them. We sought to target breast cancer using a unique population of the immune system, the γδTc. γδTc are a significant contributor to lymphoid anti-tumor surveillance. They are a promising alternative to αβTc for T cell immunotherapy[152,452-455]. In recent years, γδTc have emerged as a novel immunotherapeutic approach for different malignancies.

However, there is substantial scope to improve our understanding of the interplay between γδTc and tumors. It is crucial to tackle mechanisms that limit the protective γδTc responses. The two major factors contributing to breast cancer therapy resistance are hypoxia and CSC. Our study shed some light on the efficacy of γδTc therapy against these factors of therapy resistance.

In chapter two, we first characterized the impact of different γδ TCR antibodies on γδTc viability. This helped us determine the validity of the blocking cytotoxicity assays that employ these antibodies and are integral to determining the mechanism of γδTc action against target cells. In chapter three, we determined the impact of hypoxia on γδTc and lastly in chapter four we determined the efficacy of γδTc against BCSC.

5.1 γδTc blocking antibodies

Understanding the mechanism of action of γδTc and other immune cells has been essential for their development as immunotherapeutic agents. Blocking various receptors and ligands is a standard method to determine the mechanism γδTc use to kill tumor targets. If blocking a particular receptor or ligand with an antibody reduces the ability of γδTc to kill target cells, then we know that receptor or ligand is necessary for γδTc cytotoxicity. Using this method, there is extensive

evidence that the γδ TCR is crucial for γδTc cytotoxicity[147,188,207]. In our study, we discovered that monoclonal antibodies (mAb) for the γδ TCR caused γδTc apoptosis, and this is further exacerbated with the addition of IL-2, a staple addition in γδTc cytotoxicity assays. A study by Janssen *et al.,* observed something similar back in 1991[421]. They observed that treatment of γδTc with a TCR mAb and IL-2 makes them susceptible to apoptosis. Contrary to our study, they found that this effect was lost when IL-2 was removed. This discrepancy may be attributed to the differing techniques used for γδTc isolation and culturing in our research compared to the Janssen group. γδTc were cultured on irradiated feeder cells in their study, but not in our protocol. In our protocol, we first isolate PBMCs from blood on day 0, stimulate them with the T cell mitogen, concavalin A, and then culture them in the presence of IL-2 and IL-4. To deplete αβTc we use specific antibodies and magnetic beads. Since we do not stimulate the cells with N-bis, the γδTc generated by this protocol are polyclonal with varying subset compositions, the majority being Vδ1 and Vδ2. The protocol we use is clinically relevant, gives us significant fold-expansion of both the Vδ1 and Vδ2 subsets, and generates predominantly EM and EMRA cells that are highly cytotoxic. Additionally, the protocol we use also gives us expansion of αβTc that can be used as experimental controls[207]. Moreover, the γδ TCR antibody used by Janssen *et al*., was clone 7A5, which is also different from the clones that we characterized.

In the field of conventional αβTc, IL-2 is known to enhance *in vitro* T cell proliferation and differentiation, which is why it was originally named T-cell growth factor (TCGF)[497]. IL-2 also has the ability to re-invigorate the proliferation block of anergic αβTc *in vitro* and *in vivo*[498]. However, many studies have also highlighted some seemingly contradictory functions of this cytokine. IL-2 plays a key role in maintaining immune tolerance and preventing autoimmunity[499]. IL-2 can promote AICD of T cells and is thus implicated in the decline of a number of antigen-specific T

cells after the expansion phase of an immune response[500-502]. We also found increased γδTc apoptosis upon addition of IL-2 and the γδ TCR mAb. However, our study demonstrated that IL-2 did not impact the cytotoxicity of γδTc against breast cancer cells in the four-hour assay. Hence, we removed IL-2 from our assays.

In conclusion, our work revealed the misinterpretation of results obtained from γδ TCR blocking assays. A part of the "blocking" effect detected can be attributed to inadvertent induction of apoptosis in γδTc and hence we strongly advocate performing the appropriate control assays in parallel to quantify the extent of reduction in cytotoxicity as a result of antibody treatment. All the blocking antibodies used in our subsequent studies have been vetted and excluded if we witness apoptosis. We used blocking assays to determine the important role of NKG2D ahead and this study helped us ascertain that the anti-NKG2D antibody does not induce γδ T cell apoptosis; as such, these blocking results were correctly interpreted and gave us the basis for looking more closely at NKG2D ligands on breast tumor targets, including BCSC.

5.2 γδTc and hypoxia

The TME is a complicated system playing an essential role in tumor initiation and progression. Hypoxia is an integral regulator of the TME and a crucial driver of tumor plasticity[22,503], tumorigenicity[504], as well as an immune-suppressive micro-environment[442]. It remains unclear how γδTc are impacted by the harsh immunosuppressive TME[131,444,445], therefore in this study we investigated the impact of hypoxia on γδTc. Understanding the impact of hypoxia on γδTc activation and function is important to predict the efficiency of γδTc immune therapy and immune response. Indeed, in the case of adoptive T cell transfer, the T cells will have to function under the harsh hypoxic conditions of the tumor to be effective. In our small cohort of 17 TNBC

cases, we found that γδTc infiltrated to hypoxic pockets of the tumor, however, we could not achieve statistical significance due to the low number of cases. Moreover, we showed that ex-*vivo* expanded γδTc cultured under hypoxic conditions have increased cytotoxicity towards breast cancer cells and secreted activating factors such as MIP-1a, RANTES and CD40. On the other hand, hypoxic breast cancer cells resisted targeting by the γδTc. We observed a correlation between resistance to γδTc killing, and elevated MICA shedding, which was later observed in BCSC as well. As we have shown inhibition of MICA shedding sensitizes BCSC to γδTc, it would be appropriate to speculate that the same will be true for hypoxic cancer cells, but this needs to be tested.

Our results have been corroborated in a recent study with pancreatic cancer cells that showed increased MICA shedding, which was mediated by upregulation of protease ADAM10 in a HIF-1α dependent manner. Furthermore, knocking down HIF-1α led to reduced MICA shedding and increased sensitivity to NK cells[505]. An earlier study showed that ADAM10 is required for MICA shedding under hypoxia, and that ADAM10 is upregulated in a HIF-1α dependent manner in prostate and breast cancer. Additionally, they demonstrated that nitric oxide can inhibit this phenomenon by accumulating HIF-1α[443]. ADAM17 is yet another protease involved in MICA shedding and a recent study illustrated that hypoxia induces ADAM17 over-expression in a ribosomal S-6 kinase 1 and C/EBPβ dependent manner[506]. Our study showed that inhibition of ADAM10 and ADAM17 can restrain MICA shedding, and in turn improve sensitivity to γδTc. It would be interesting to see if ADAM 10 and ADAM17 are upregulated in breast cancer cells under hypoxia, and if this upregulation is mediated by HIF-1α.

Not many studies have looked at the impact of hypoxia on γδTc, but there have been a few studies examining the impact of hypoxia on CD8+ T cells. These studies have predominantly

revealed enhanced cytotoxicity of T cells under hypoxic conditions, which was recapitulated in our study[390,507-509]. One of the studies showed that CD8+ T cells under hypoxia had the same number of granules, but the granules had more granzyme B packed in them[509]. Granzyme B is a serine protease that is commonly found in the granules of effector immune cells such as CD8+ T cells, NK cells, as well as γδTc. Upon target recognition and activation, granules are released by the effector cells into the targets to induce apoptosis[510]. Therefore, it is possible that hypoxia has a similar effect on granzyme B production by γδTc as well. However, these studies used hypoxia treated T cells against normoxic target cells. In our study, we used four different combinations, we tested and compared the effectivity of hypoxic and normoxic γδTc against hypoxic and normoxic breast cancer cells, and also performed the cytotoxicity assays under hypoxia. It was when we treated the tumor cells and performed the cytotoxicity assays under hypoxia that we found the enhanced cytotoxicity of the γδTc is over-powered by the superior immune evasion capabilities of the target cells.

Since the publication of our paper, another group has determined the impact of hypoxia on γδTc in oral cancer[392]. They found that γδTc presented reduced cytotoxicity under hypoxia. This study is in contradiction to what we saw. The reason for this contradiction is not clear, but could be because of the differences in hypoxia chambers, different γδTc expansion protocol, or the cancer type[392]. However, they also compared the impact of hypoxia on target cells along with γδTc and in this case our results are in agreement, as they too found reduced susceptibility of hypoxic target cells to hypoxic γδTc compared to normoxic target cells and γδTc. Moreover, this study found that γδTc exhibited reduced degranulation and Ca^{2+} efflux and increased expression of PD-L1 in the presence of hypoxia[392]. We have not looked at these features in our γδTc, and it might be worth examining in future.

5.3 γδTc and breast cancer stem cells

As discussed earlier, BCSC are highly tumorigenic and one of the major contributors to therapy resistance and relapse, hence it is imperative for treatments to effectively target them. Recently there has been rising interest in targeting CSC, including BCSC, to develop efficient and successful therapy alternatives[511-513]. The focus of this study is to determine if γδTc can target BCSC. Our study revealed that γδTc can kill BCSC, however not as effectively as they can target NSC. BCSC employ multiple mechanisms to escape γδTc immune attack (Fig. 5.1). These mechanisms include: (i) the secretion of immune-suppressive factors to quell γδTc response, (ii) the upregulation of inhibitory ligand PD-L1 that can bind to inhibitory receptor PD-1 on γδTc and inhibit the γδTc response, (iii) the upregulation of anti-apoptotic protein MCL-1 that can counter the apoptosis induced by γδTc, (iv) the down-regulation of MICA/B on the cell surface to escape recognition by γδTc, and (v) enhanced shedding of MICA, which can bind NKG2D receptor on γδTc rendering them incapable of recognizing other NKG2D ligands on tumor cells.

Studies have shown that CSC have increased potential to form lung metastasis[514]. We performed an *in vivo* tail-vein lung metastasis assay to determine the tumor colonization capacity of the resistant cells, and used the India ink technique to quantify lung macro-metastasis[484]. Our results showed that the tumor cells that are resistant to γδTc treatment have increased potential for colonization in the lungs and suggested that γδTc treatment-resistant breast cancer cells have a higher population of stem-like cells. A more direct way of testing our hypothesis would be to inject BCSCs into mice followed by γδTc injection to determine if BCSC can be targeted by these cells.

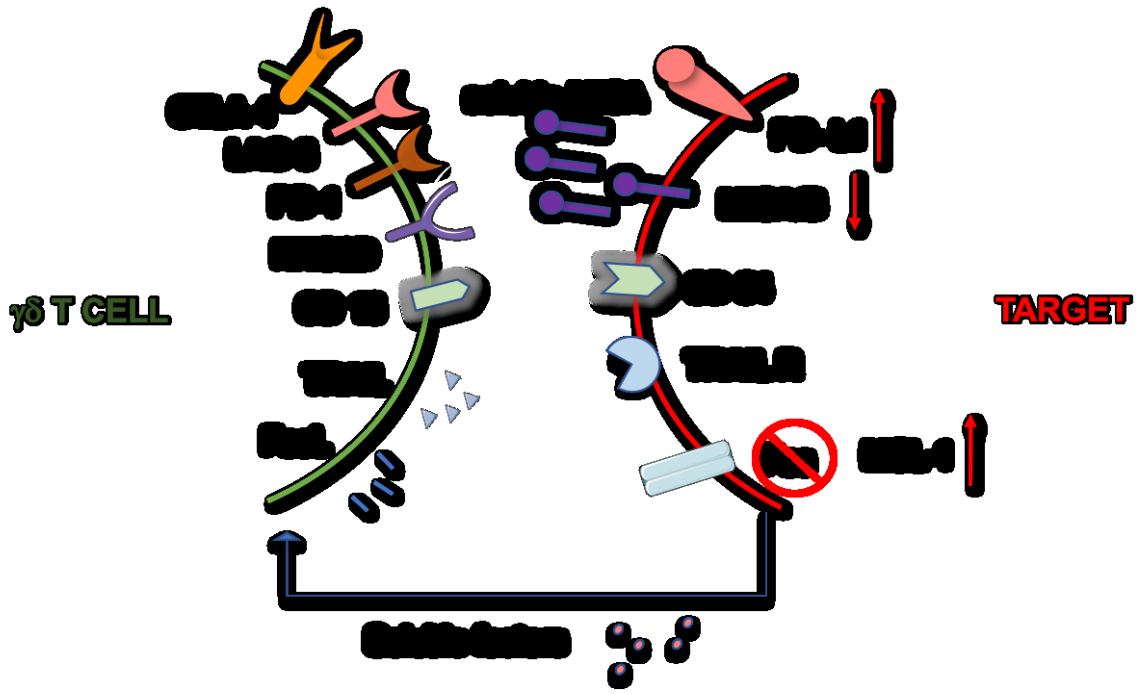

Figure 5.1. **A model of how breast cancer stem cells escape γδTc immune targeting.** Cancer stem cells employ various mechanisms to escape γδTc killing. This includes secretion of soluble factors that can render γδTc hypo-responsive, upregulation of anti-apoptotic protein MCL-1 that leads to inhibition of Fas/FasL apoptotic pathway, upregulation of inhibitory ligand PD-L1 to block γδTc activity, downregulation of surface MICA/B to escape recognition by γδTc and shedding of MICA to further inhibit NKG2D receptor on γδTc.

However, the big caveat here is that once BCSC are injected into mice, they differentiate and divide to form a tumor that is heterogeneous. This makes it impossible to tease out the effect of γδTc treatment on the BCSC specifically, and makes studying BCSC *in vivo* very challenging. Moreover, due to the evolutionary divergence of the TCRγ and TCRδ loci between rodents and primates, mouse and human γδTc subsets are different. In fact, the human Vδ2 subset is absent in mice. Thus, we cannot recapitulate immunotherapy with a blood-derived phospho-antigen-reactive expanded γδTc population in mice.

Furthermore, we discovered that BCSC secreted factors rendered γδTc hypo-responsive. Mass spectrometry analysis indicated global differences in the secretome between BCSC and NSC in both SUM149 cells as well as PDX401. Several cytokines and chemokines, including CXCL8 (IL-8), were more highly secreted by BCSC. While the impact of CXCL8 on γδTc is unknown, CXCL8 is known as a pro-inflammatory chemokine with many functions. In cancer, CXCL8 is highly expressed in the TME and predicts poor prognosis[515]. CXCL8 is known to promote neutrophil migration, and may promote cancer cell growth through increased angiogenesis and tumor cell proliferation[516]. In the future, it would be interesting to study the direct effects of CXCL8 on γδTc.

In SUM149 BCSC, VEGFA and VEGFC were significantly upregulated and are known to have immune-suppressive properties on γδTc[246]. Clinical trials of γδTc against various cancers have shown that high serum levels of VEGF pre-treatment correlate either with lack of clinical response or poor prognosis[221,517]. Hence, targeting these factors using antagonists may help sensitize the BCSC to γδTc targeting. This was beyond the scope of our current study, but can be considered moving forward. BCSC-secreted factors not only contribute to evasion of γδTc killing but can shape the TME and modulate tumor progression.

We also demonstrated that PD-L1 surface expression is upregulated in PDX BCSC. A study in 2011 using Daudi (B-cell lymphoma) cells, was the first to show *in vitro* that the PD-1/PD-L1 axis is important for the anti-tumor immune response by γδTc[354]. Castella *et al*., in 2015 showed that PD-1 expression can contribute to the inadequate expansion of Vγ9Vδ2 T in Multiple Myeloma (MM) patients. They found the Vδ2 cells had high PD-1 expression and were located in proximity to PD-L1+ MM cells and MDSCs. Additionally, PD-1 blocking antibody treatment resulted in a five-fold increase in the cytotoxic ability of the cells following zoledronate stimulation[355]. Another study showed that Pembrolizumab (anti-PD-1) treatment upregulated IFN-γ expression by γδTc, which might facilitate anti-leukemia effects (acute myeloid leukemia and chronic myeloid leukemia)[357]. PD-1$^+$ γδTc were also identified in B cell lymphoma[518] and neuroblastoma patients[492].

Contrary to the common perception, PD-1 expression can imply T cell activation as well. PD-1 is specifically expressed on activated T cells *in vivo*, and not on resting T cells. It is induced transiently on naïve T cells upon activation and declines once the antigen in cleared[519], but it can remain chronically upregulated in cases of chronic viral infection or cancer[520]. It is difficult to differentiate between activated and dysfunctional T cells as they have some overlapping features. There are several instances where PD-1 expression coincides with an activated T cell phenotype. PD-1 protein can be detected in normal murine thymus and splenic T cells at low levels, but is strongly induced on thymocytes and on T cells from the spleen and lymph nodes after stimulation with an anti-CD3 mAb *in vitro*[521]. A study in a melanoma mouse model revealed that the infiltrating tumor-specific CD8$^+$ T cells had significantly higher PD-1, LAG-3, CD69 (activation marker), and 4-1BB (costimulatory molecule) expression, and gained higher activation-related (but not exhaustion-related) accessible chromatin regions than the tumor-ignorant bystander CD8$^+$ T

cells[522]. In adoptive T cell therapy, cells expanded from PD-1$^+$ CD8$^+$ TILs, but not from PD-1$^-$ or bulk CD8$^+$ TILs, showed tumor-reactivity and therapeutic benefit *in vivo*[523].

However, chronic PD-1 expression is associated with ineffective co-stimulation and T cell dysfunction, specifically with cancer and chronic viral infection. There are abundant reports suggesting a positive correlation between PD-1 upregulation and T cell dysfunction in various cancers, including breast cancer[315,524,525]. This incoherence in the association of PD-1 expression with T-cell function (exhaustion or activation) may be due to the complex interplay between several driving forces and effectors in the PD-1 pathway. T cell dysfunction, particularly T cell exhaustion, evolved as a process to balance T cell activation with self-regulation in the presence of chronic or persistent antigen exposure, therefore it can be difficult to discern the distinction between the two phenotypes. Thus, it is important to evaluate the different aspects of the T cell aside from PD-1 expression, such as other activation markers, cytotoxicity, cytokine secretion, and many more, to establish its functional status.

Next we evaluated and compared the expression of anti-apoptotic proteins between BCSC and NSC. We find that BCSC have higher expression of anti-apoptotic protein MCL-1. We also found that treatment of breast cancer cells with γδTc lead to an upregulation of MCL-1 in most experiments, except for experiments done with γδTc from one particular donor. MCL-1 expression seemed to be differentially regulated in the targets in the presence of γδTc from this particular donor. There are several mechanisms involved in the regulation of MCL-1 expression. Apart from the previously mentioned IL-6 and IFN-α, a growing list of trophic factors such as IL-3, IL-5, GM-CSF, epidermal growth factor (EGF) and VEGF are also shown to induce MCL-1 transcription mediated by STAT transcription factor[526]. These factors may be differentially secreted by this particular donor resulting in contradictory results. Interestingly, using an MCL-1 degrader[268]

sensitized BCSC to cytotoxicity assays done with γδTc from only the above-mentioned donor, but not any other donor. This could be explained by the lower expression of MCL-1 by the target cells even upon treatment with γδTc from the donor. Hence, we may need to increase the concentration of MCL-1 degrader used to effectively sensitize the BCSC and resistant cells that typically show upregulation of MCL-1 upon treatment with γδTc from almost all other donors. The degrader we used is a hetero-bifunctional small molecule capable of selectively targeting MCL-1 using a methodology known as proteolysis targeting chimera (PROTAC). PROTACS are small molecules that tether target proteins to E3 ligases inducing ubiquitination and labelling proteins for proteasomal degradation[268]. The use of PROTAC technology for selective degradation of several target proteins has recently become more common, with some compounds beginning to enter clinical trials[527,528].

We next investigated NKG2D ligands. NKG2D ligand binding by γδTc is a crucial step in the anti-tumor effect of γδTc. Blocking assays using antibodies against NKG2D receptor as well as MICA/B established their involvement in γδTc cytotoxicity. However, we also demonstrated that BCSC have a lower surface expression of MICA/B and higher MICA shedding compared to NSC. Although there are no reports of BCSC or other CSC that shed more MICA, there is previous evidence that BCSC have a lower surface expression of MICA/B, which is recapitulated in our study, and this downregulation makes them less sensitive to NK cell killing[164]. As mentioned above, we also found increased MICA shedding by breast cancer cells under hypoxic conditions. There are various strategies to target NKG2D ligand expression and shedding. Moreover, there are reports of significant correlation between circulating soluble MICA and tumor stage, as well as metastasis in various malignancies[529]. Histone deacetylase inhibitors (HDACi) have been used to upregulate MICA/B surface expression[530-532]. HDAC inhibitor treatment induces glycogen

synthase kinase-3 (GSK-3) activity, which is essential for MICA/B expression[530]. Arsenic compounds (phenylarsine oxide) have been used to block MICA/B shedding by impairing ERp5 catalytic domain. ERp5 facilitates MICA and MICB shedding by reducing the disulphide bond of MIC that allows proteolytic enzyme access[533]. Antibodies targeting the MICA α3 domain, which is the site of proteolytic cleavage, can also prevent loss of cell surface MICA and MICB[534]. However, we used the most common strategy to inhibit MICA shedding, whereby we inhibited the activity of proteases responsible, being ADAM10 and ADAM17.

One of the major findings in our study was the effectiveness of ADAM inhibitors in combination with γδTc to target BCSC. We found using ADAM inhibitors in combination with γδTc was able to increase BCSC killing by three-fold. This combination was also successful in further increasing NSC killing as well by 1.5-fold. Hence this combination can increase overall sensitivity of breast cancer cells to γδTc targeting. There are several ADAM inhibitors currently undergoing clinical trials. Strategies to target ADAMs include small molecules, antibodies and ADAM pro-domain. The first generation of inhibitors were hydroxamate inhibitors that mediate inhibition by chelating the Zn^{2+} of the protease active site[535]. G1254023X inhibits both ADAM10 and ADAM17, and was the first inhibitor tested clinically. However, the compound showed inadequate selectivity as it could additionally target MMP2 and MMP9 and patients experienced hepatotoxicity, which lead to the discontinuation of clinical trials[536]. Following this, more advanced hydroxamate inhibitors, INCB3619 and INCB7839, showed improved selectivity and bioavailability and showed promising pre-clinical results. INCB7839 was tested *in vivo* in combination with lapatinib (HER2 inhibitor) in a breast cancer xenograft model, where they showed reduced tumor growth[537]. Subsequently, INCB7839 was tested in clinical trials against breast cancer in combination with trastuzumab (Herceptin), but was discontinued despite initial

promising results, most likely due to increased side effects such as deep vein thrombosis in a number of patients[538]. Hence, regulating the dosage and scheduling of the drug to ensure optimum results is crucial. Monoclonal antibodies such as 8C7 specific for ADAM10 and D1(A12), A9(B8) and MEDI3622 against ADAM17 have shown promising results *in vitro* and *in vivo,* and are now entering, or are in clinical trials[539,540]. The inhibitor we used is GW280264X, which is not in clinical trials, but has shown efficient blocking of the proteolytic activity of both ADAM 10 and ADAM17[541]. Moreover, the inhibitor has also displayed effective inhibition of MICA shedding[169,172]. Hence, we propose that using γδTc in combination with ADAM inhibitors can help overcome BCSC resistance and be an effective way to target them. Further pre-clinical and clinical investigation is warranted, especially in the presence of a complete host immune system and TME to determine the true efficacy of this combination.

Overall, our study highlighted various mechanisms that the breast cancer cells and BCSC can employ to escape γδTc therapy, but we also demonstrated techniques to overcome this resistance. Therapy resistance is the principal hurdle we need to overcome to develop successful immunotherapies. Our study provides valuable insights that inform not only γδTc immunotherapy, but also T and NK cell immunotherapy since γδTc share features with both of these cell types. γδTc and NK cells employ NKG2D receptors to recognize stressed or transformed ligands[130], therefore NKG2D ligand and MICA shedding would also impact NK cells. γδTc also share common effector functions, such as the release of TRAIL and FasL, as well as perforins and granzymes with CTL and NK cells[121]. Hence, anti-apoptotic proteins, like MCL-1, can disrupt the function of CD8+ T cells and NK cells. Moreover, dysfunctional CD8+ T cells also show chronic upregulation of PD-1 on their surface[297] similar to γδTc. Combination approaches such as γδTc along with ADAM inhibitors, offer a new strategy to combat immune-resistance and thus require further investigation.

5.4 Future Directions

Our study has revealed several new avenues to be explored further:

- **Examination of the factors differentially secreted by BCSC compared to NSC and their impact on γδTc cytotoxicity.** We have demonstrated that γδTc become hypo-responsive when incubated with BCSC CM. Factors such as TGF-β1/2, IL-18, and CXCL8 (IL-8) are secreted more by BCSC than NSC. Therefore, it will be interesting to use neutralizing antibodies against these factors while incubating γδTc in the conditioned media. Following the incubation, we can wash off the media and determine the effect on γδTc proliferation, co-inhibitory receptor expression, and IFN-γ production. Further, it will be interesting to determine γδTc cytotoxicity, specifically against BCSC. We predict that blocking these factors will reverse their impact on γδTc and enhance their cytotoxicity against BCSC.
- **Optimization of MCL-1 degrader dosage in combination with γδTc**. As mentioned earlier, in experiments using γδTc derived from one particular donor, the MCL-1 degrader effectively enhanced γδTc cytotoxicity against breast cancer cells. The breast cancer cells did not exhibit MCL-1 upregulation upon treatment with γδTc from this donor, and 500nM MCL-1 degrader successfully overcame BCSC resistance in this case. However, in cases where MCL-1 was upregulated, the degrader failed to make a difference. Therefore, it will be worthwhile to perform γδTc cytotoxicity assays with a higher dosage of MCL-1 degrader and determine if that can make a difference. Moreover, the MCL-1 degrader did not impact γδTc viability at our working concentration of 500nM, but we would need to assess viability at higher concentrations of MCL-1 degrader as well. We will have to be careful in

optimizing MCL-1 degrader dosage such that it improves γδTc cytotoxicity effectively but does not impact γδTc viability.

- **Investigation of PD-1/PD-L1 interaction under hypoxia**. Our study revealed that γδTc cultured under hypoxia have enhanced cytotoxicity compared to γδTc cultured under normoxia. This activation of γδTc under hypoxia suggests PD-1 expression albeit transiently. However, since hypoxic breast cancer cells were resistant to γδTc targeting, it will be interesting to see if PD-L1 is upregulated on the target cells under hypoxia. There is sufficient evidence suggesting that PD-L1 is upregulated by various cancer cells, including breast cancer cells, under hypoxia[542]. If PD-L1 is upregulated on hypoxic target cells and PD-1 is upregulated on γδTc under hypoxia, their interaction could render γδTc less effective. This would provide another explanation for breast cancer cell resistance against γδTc under hypoxia.
- **Characterization of ADAM10 and ADAM17 expression in breast cancer cells under hypoxia.** Based on previous literature and our work on BCSC, we predict that breast cancer cells will upregulate ADAM10 and ADAM17 under hypoxia. This upregulation might be responsible for the enhanced MICA shedding. We can also determine if using ADAM inhibitors can block MICA shedding by breast cancer cells and enhance breast cancer cell sensitivity to γδTc under hypoxia.
- **Validation of efficacy of γδTc in combination with ADAM inhibitor *in vivo***. In order to validate the efficacy of this combination against BCSC, the next logical step will be to perform the lung metastasis assays with the target cells that are treated with both γδTc and ADAM inhibitor. We expect to see a lower number of lung metastatic lesions formed by the target cells treated with the combination compared to target cells treated with γδTc alone

or untreated target cells. This will imply that we were able to eliminate BCSC with the combination successfully.

The above-mentioned approaches may give us a better idea of how to improve γδTc immunotherapy. Furthermore, it might be beneficial to test the successful approaches in combination to develop a more robust attack against the breast tumor ultimately resulting in improved patient outcomes.

6. References

1 Siegel, R. L., Miller, K. D. & Jemal, A. Cancer statistics, 2020. *CA Cancer J Clin* **70**, 7-30, doi:10.3322/caac.21590 (2020).

2 Harbeck, N. *et al.* Breast cancer. *Nat Rev Dis Primers* **5**, 66, doi:10.1038/s41572-019-0111-2 (2019).

3 Yersal, O. & Barutca, S. Biological subtypes of breast cancer: Prognostic and therapeutic implications. *World J Clin Oncol* **5**, 412-424, doi:10.5306/wjco.v5.i3.412 (2014).

4 Poloz, Y. D., R.J.O.;Stambolic,V. in *Breast Cancer* (ed Goldhirsch A. Veronesi U., Veronesi P., Gentilini O., Leonardi M. (eds)) (Springer, Cham, 2017).

5 Fong, P. C. *et al.* Inhibition of poly(ADP-ribose) polymerase in tumors from BRCA mutation carriers. *N Engl J Med* **361**, 123-134, doi:10.1056/NEJMoa0900212 (2009).

6 Stewart, R. L. *et al.* A Multigene Assay Determines Risk of Recurrence in Patients with Triple-Negative Breast Cancer. *Cancer Res* **79**, 3466-3478, doi:10.1158/0008-5472.CAN-18-3014 (2019).

7 Marusyk, A. & Polyak, K. Tumor heterogeneity: causes and consequences. *Biochim Biophys Acta* **1805**, 105-117, doi:10.1016/j.bbcan.2009.11.002 (2010).

8 De Angelis, M. L., Francescangeli, F. & Zeuner, A. Breast Cancer Stem Cells as Drivers of Tumor Chemoresistance, Dormancy and Relapse: New Challenges and Therapeutic Opportunities. *Cancers (Basel)* **11**, doi:10.3390/cancers11101569 (2019).

9 Pece, S. *et al.* Biological and molecular heterogeneity of breast cancers correlates with their cancer stem cell content. *Cell* **140**, 62-73, doi:10.1016/j.cell.2009.12.007 (2010).

10 Beck, B. & Blanpain, C. Unravelling cancer stem cell potential. *Nat Rev Cancer* **13**, 727-738, doi:10.1038/nrc3597 (2013).

11 Lapidot, T. *et al.* A cell initiating human acute myeloid leukaemia after transplantation into SCID mice. *Nature* **367**, 645-648, doi:10.1038/367645a0 (1994).

12 Merlo, L. M., Pepper, J. W., Reid, B. J. & Maley, C. C. Cancer as an evolutionary and ecological process. *Nat Rev Cancer* **6**, 924-935, doi:10.1038/nrc2013 (2006).

13 Greaves, M. & Maley, C. C. Clonal evolution in cancer. *Nature* **481**, 306-313, doi:10.1038/nature10762 (2012).

14 Reya, T., Morrison, S. J., Clarke, M. F. & Weissman, I. L. Stem cells, cancer, and cancer stem cells. *Nature* **414**, 105-111, doi:10.1038/35102167 (2001).

15 Wang, Y. *et al.* Clonal evolution in breast cancer revealed by single nucleus genome sequencing. *Nature* **512**, 155-160, doi:10.1038/nature13600 (2014).

16 Navin, N. *et al.* Tumour evolution inferred by single-cell sequencing. *Nature* **472**, 90-94, doi:10.1038/nature09807 (2011).

17 Bonnet, D. & Dick, J. E. Human acute myeloid leukemia is organized as a hierarchy that originates from a primitive hematopoietic cell. *Nat Med* **3**, 730-737, doi:10.1038/nm0797-730 (1997).

18 Al-Hajj, M., Wicha, M. S., Benito-Hernandez, A., Morrison, S. J. & Clarke, M. F. Prospective identification of tumorigenic breast cancer cells. *Proc Natl Acad Sci U S A* **100**, 3983-3988, doi:10.1073/pnas.0530291100 (2003).

19 Ginestier, C. *et al.* ALDH1 is a marker of normal and malignant human mammary stem cells and a predictor of poor clinical outcome. *Cell Stem Cell* **1**, 555-567, doi:10.1016/j.stem.2007.08.014 (2007).

20 Chaffer, C. L. *et al.* Normal and neoplastic nonstem cells can spontaneously convert to a stem-like state. *Proc Natl Acad Sci U S A* **108**, 7950-7955, doi:10.1073/pnas.1102454108 (2011).
21 Chaffer, C. L. *et al.* Poised chromatin at the ZEB1 promoter enables breast cancer cell plasticity and enhances tumorigenicity. *Cell* **154**, 61-74, doi:10.1016/j.cell.2013.06.005 (2013).
22 Schwab, L. P. *et al.* Hypoxia-inducible factor 1alpha promotes primary tumor growth and tumor-initiating cell activity in breast cancer. *Breast Cancer Res* **14**, R6, doi:10.1186/bcr3087 (2012).
23 Iliopoulos, D., Hirsch, H. A., Wang, G. & Struhl, K. Inducible formation of breast cancer stem cells and their dynamic equilibrium with non-stem cancer cells via IL6 secretion. *Proc Natl Acad Sci U S A* **108**, 1397-1402, doi:10.1073/pnas.1018898108 (2011).
24 O'Brien-Ball, C. & Biddle, A. Reprogramming to developmental plasticity in cancer stem cells. *Dev Biol* **430**, 266-274, doi:10.1016/j.ydbio.2017.07.025 (2017).
25 Dontu, G. *et al.* In vitro propagation and transcriptional profiling of human mammary stem/progenitor cells. *Genes Dev* **17**, 1253-1270, doi:10.1101/gad.1061803 (2003).
26 Ponta, H., Sherman, L. & Herrlich, P. A. CD44: from adhesion molecules to signalling regulators. *Nat Rev Mol Cell Biol* **4**, 33-45, doi:10.1038/nrm1004 (2003).
27 Shipitsin, M. *et al.* Molecular definition of breast tumor heterogeneity. *Cancer Cell* **11**, 259-273, doi:10.1016/j.ccr.2007.01.013 (2007).
28 Zhou, J. *et al.* Stem Cells and Cellular Origins of Breast Cancer: Updates in the Rationale, Controversies, and Therapeutic Implications. *Front Oncol* **9**, 820, doi:10.3389/fonc.2019.00820 (2019).
29 Pires, B. R., IS, D. E. A., Souza, L. D., Rodrigues, J. A. & Mencalha, A. L. Targeting Cellular Signaling Pathways in Breast Cancer Stem Cells and its Implication for Cancer Treatment. *Anticancer Res* **36**, 5681-5691, doi:10.21873/anticanres.11151 (2016).
30 Kusoglu, A. & Biray Avci, C. Cancer stem cells: A brief review of the current status. *Gene* **681**, 80-85, doi:10.1016/j.gene.2018.09.052 (2019).
31 Phillips, T. M., McBride, W. H. & Pajonk, F. The response of CD24(-/low)/CD44+ breast cancer-initiating cells to radiation. *J Natl Cancer Inst* **98**, 1777-1785, doi:10.1093/jnci/djj495 (2006).
32 Fillmore, C. M. & Kuperwasser, C. Human breast cancer cell lines contain stem-like cells that self-renew, give rise to phenotypically diverse progeny and survive chemotherapy. *Breast Cancer Res* **10**, R25, doi:10.1186/bcr1982 (2008).
33 Li, X. *et al.* Intrinsic resistance of tumorigenic breast cancer cells to chemotherapy. *J Natl Cancer Inst* **100**, 672-679, doi:10.1093/jnci/djn123 (2008).
34 Yu, F. *et al.* let-7 regulates self renewal and tumorigenicity of breast cancer cells. *Cell* **131**, 1109-1123, doi:10.1016/j.cell.2007.10.054 (2007).
35 Codony-Servat, J. & Rosell, R. Cancer stem cells and immunoresistance: clinical implications and solutions. *Transl Lung Cancer Res* **4**, 689-703, doi:10.3978/j.issn.2218-6751.2015.12.11 (2015).
36 Choi, Y. H. & Yu, A. M. ABC transporters in multidrug resistance and pharmacokinetics, and strategies for drug development. *Curr Pharm Des* **20**, 793-807, doi:CPD-EPUB-20130513-2 [pii] (2014).
37 Calcagno, A. M. & Ambudkar, S. V. Molecular mechanisms of drug resistance in single-step and multi-step drug-selected cancer cells. *Methods Mol Biol* **596**, 77-93, doi:10.1007/978-1-60761-416-6_5 (2010).

38 Wang, Q. E. DNA damage responses in cancer stem cells: Implications for cancer therapeutic strategies. *World J Biol Chem* **6**, 57-64, doi:10.4331/wjbc.v6.i3.57 (2015).
39 Krause, M., Dubrovska, A., Linge, A. & Baumann, M. Cancer stem cells: Radioresistance, prediction of radiotherapy outcome and specific targets for combined treatments. *Adv Drug Deliv Rev* **109**, 63-73, doi:10.1016/j.addr.2016.02.002 (2017).
40 Chen, W., Dong, J., Haiech, J., Kilhoffer, M. C. & Zeniou, M. Cancer Stem Cell Quiescence and Plasticity as Major Challenges in Cancer Therapy. *Stem Cells Int* **2016**, 1740936, doi:10.1155/2016/1740936 (2016).
41 Madjd, Z. *et al.* CD44+ cancer cells express higher levels of the anti-apoptotic protein Bcl-2 in breast tumours. *Cancer Immun* **9**, 4 (2009).
42 Chu, J. E. & Allan, A. L. The Role of Cancer Stem Cells in the Organ Tropism of Breast Cancer Metastasis: A Mechanistic Balance between the "Seed" and the "Soil"? *Int J Breast Cancer* **2012**, 209748, doi:10.1155/2012/209748 (2012).
43 Sampieri, K. & Fodde, R. Cancer stem cells and metastasis. *Semin Cancer Biol* **22**, 187-193 (2012).
44 Liao, W. T., Ye, Y. P., Deng, Y. J., Bian, X. W. & Ding, Y. Q. Metastatic cancer stem cells: from the concept to therapeutics. *Am J Stem Cells* **3**, 46-62 (2014).
45 Croker, A. K. *et al.* High aldehyde dehydrogenase and expression of cancer stem cell markers selects for breast cancer cells with enhanced malignant and metastatic ability. *J Cell Mol Med* **13**, 2236-2252, doi:10.1111/j.1582-4934.2008.00455.x (2009).
46 Mani, S. A. *et al.* The epithelial-mesenchymal transition generates cells with properties of stem cells. *Cell* **133**, 704-715, doi:10.1016/j.cell.2008.03.027 (2008).
47 Abraham, B. K. *et al.* Prevalence of CD44+/CD24-/low cells in breast cancer may not be associated with clinical outcome but may favor distant metastasis. *Clin Cancer Res* **11**, 1154-1159 (2005).
48 Balic, M. *et al.* Most early disseminated cancer cells detected in bone marrow of breast cancer patients have a putative breast cancer stem cell phenotype. *Clin Cancer Res* **12**, 5615-5621, doi:10.1158/1078-0432.CCR-06-0169 (2006).
49 Aktas, B. *et al.* Stem cell and epithelial-mesenchymal transition markers are frequently overexpressed in circulating tumor cells of metastatic breast cancer patients. *Breast Cancer Res* **11**, R46, doi:10.1186/bcr2333 (2009).
50 Theodoropoulos, P. A. *et al.* Circulating tumor cells with a putative stem cell phenotype in peripheral blood of patients with breast cancer. *Cancer Lett* **288**, 99-106, doi:10.1016/j.canlet.2009.06.027 (2010).
51 Eyler, C. E. & Rich, J. N. Survival of the fittest: cancer stem cells in therapeutic resistance and angiogenesis. *J Clin Oncol* **26**, 2839-2845, doi:10.1200/JCO.2007.15.1829 (2008).
52 Kruger, S. *et al.* Advances in cancer immunotherapy 2019 - latest trends. *J Exp Clin Cancer Res* **38**, 268, doi:10.1186/s13046-019-1266-0 (2019).
53 Ehrlich, P. Über den jetzigen Stand der Chemotherapie. *Berichte der deutschen chemischen Gesellschaft* **42**, 17-47, doi:10.1002/cber.19090420105 (1909).
54 Thomas, L. Discussion of cellular and humoral aspects of hypersensitive states. *In: Lawrence HS* (1959).
55 Foley, E. J. Antigenic properties of methylcholanthrene-induced tumors in mice of the strain of origin. *Cancer Res* **13**, 835-837 (1953).
56 Burnet, F. M. The concept of immunological surveillance. *Prog Exp Tumor Res* **13**, 1-27, doi:10.1159/000386035 (1970).

57 Shankaran, V. *et al.* IFNgamma and lymphocytes prevent primary tumour development and shape tumour immunogenicity. *Nature* **410**, 1107-1111, doi:10.1038/35074122 (2001).
58 Dunn, G. P., Bruce, A. T., Ikeda, H., Old, L. J. & Schreiber, R. D. Cancer immunoediting: from immunosurveillance to tumor escape. *Nat Immunol* **3**, 991-998, doi:10.1038/ni1102-991 (2002).
59 Schreiber, R. D., Old, L. J. & Smyth, M. J. Cancer immunoediting: integrating immunity's roles in cancer suppression and promotion. *Science* **331**, 1565-1570, doi:10.1126/science.1203486 (2011).
60 Vesely, M. D., Kershaw, M. H., Schreiber, R. D. & Smyth, M. J. Natural innate and adaptive immunity to cancer. *Annu Rev Immunol* **29**, 235-271, doi:10.1146/annurev-immunol-031210-101324 (2011).
61 Guerra, N. *et al.* NKG2D-deficient mice are defective in tumor surveillance in models of spontaneous malignancy. *Immunity* **28**, 571-580, doi:10.1016/j.immuni.2008.02.016 (2008).
62 Girardi, M. *et al.* Regulation of cutaneous malignancy by gammadelta T cells. *Science* **294**, 605-609, doi:10.1126/science.1063916 (2001).
63 Girardi, M. *et al.* The distinct contributions of murine T cell receptor (TCR)gammadelta+ and TCRalphabeta+ T cells to different stages of chemically induced skin cancer. *J Exp Med* **198**, 747-755, doi:10.1084/jem.20021282 (2003).
64 Aguirre-Ghiso, J. A. Models, mechanisms and clinical evidence for cancer dormancy. *Nat Rev Cancer* **7**, 834-846, doi:10.1038/nrc2256 (2007).
65 Koebel, C. M. *et al.* Adaptive immunity maintains occult cancer in an equilibrium state. *Nature* **450**, 903-907, doi:10.1038/nature06309 (2007).
66 Farrar, J. D. *et al.* Cancer dormancy. VII. A regulatory role for CD8+ T cells and IFN-gamma in establishing and maintaining the tumor-dormant state. *J Immunol* **162**, 2842-2849 (1999).
67 Khong, H. T. & Restifo, N. P. Natural selection of tumor variants in the generation of "tumor escape" phenotypes. *Nat Immunol* **3**, 999-1005, doi:10.1038/ni1102-999 (2002).
68 Nagarajan, D. & McArdle, S. E. B. Immune Landscape of Breast Cancers. *Biomedicines* **6**, doi:10.3390/biomedicines6010020 (2018).
69 Barriga, V., Kuol, N., Nurgali, K. & Apostolopoulos, V. The Complex Interaction between the Tumor Micro-Environment and Immune Checkpoints in Breast Cancer. *Cancers (Basel)* **11**, doi:10.3390/cancers11081205 (2019).
70 Whiteside, T. L. The tumor microenvironment and its role in promoting tumor growth. *Oncogene* **27**, 5904-5912, doi:10.1038/onc.2008.271 (2008).
71 Yuan, Y., Jiang, Y. C., Sun, C. K. & Chen, Q. M. Role of the tumor microenvironment in tumor progression and the clinical applications (Review). *Oncol Rep* **35**, 2499-2515, doi:10.3892/or.2016.4660 (2016).
72 Cirri, P. & Chiarugi, P. Cancer associated fibroblasts: the dark side of the coin. *Am J Cancer Res* **1**, 482-497 (2011).
73 Gabrilovich, D. I., Ostrand-Rosenberg, S. & Bronte, V. Coordinated regulation of myeloid cells by tumours. *Nat Rev Immunol* **12**, 253-268, doi:10.1038/nri3175 (2012).
74 Wang, Z. *et al.* Low mutation and neoantigen burden and fewer effector tumor infiltrating lymphocytes correlate with breast cancer metastasization to lymph nodes. *Sci Rep* **9**, 253, doi:10.1038/s41598-018-36319-x (2019).

75 Luen, S., Virassamy, B., Savas, P., Salgado, R. & Loi, S. The genomic landscape of breast cancer and its interaction with host immunity. *Breast* **29**, 241-250, doi:10.1016/j.breast.2016.07.015 (2016).
76 DeNardo, D. G. & Coussens, L. M. Inflammation and breast cancer. Balancing immune response: crosstalk between adaptive and innate immune cells during breast cancer progression. *Breast Cancer Res* **9**, 212, doi:10.1186/bcr1746 (2007).
77 Campbell, M. J., Scott, J., Maecker, H. T., Park, J. W. & Esserman, L. J. Immune dysfunction and micrometastases in women with breast cancer. *Breast Cancer Res Treat* **91**, 163-171, doi:10.1007/s10549-004-7048-0 (2005).
78 Tsavaris, N., Kosmas, C., Vadiaka, M., Kanelopoulos, P. & Boulamatsis, D. Immune changes in patients with advanced breast cancer undergoing chemotherapy with taxanes. *Br J Cancer* **87**, 21-27, doi:10.1038/sj.bjc.6600347 (2002).
79 Dewan, M. Z. *et al.* Role of natural killer cells in hormone-independent rapid tumor formation and spontaneous metastasis of breast cancer cells in vivo. *Breast Cancer Res Treat* **104**, 267-275, doi:10.1007/s10549-006-9416-4 (2007).
80 Abel, A. M., Yang, C., Thakar, M. S. & Malarkannan, S. Natural Killer Cells: Development, Maturation, and Clinical Utilization. *Front Immunol* **9**, 1869, doi:10.3389/fimmu.2018.01869 (2018).
81 Mamessier, E. *et al.* Human breast cancer cells enhance self tolerance by promoting evasion from NK cell antitumor immunity. *J Clin Invest* **121**, 3609-3622, doi:10.1172/JCI45816 (2011).
82 Fainaru, O. *et al.* Tumor growth and angiogenesis are dependent on the presence of immature dendritic cells. *FASEB J* **24**, 1411-1418, doi:10.1096/fj.09-147025 (2010).
83 Syed Khaja, A. S. *et al.* Preferential accumulation of regulatory T cells with highly immunosuppressive characteristics in breast tumor microenvironment. *Oncotarget* **8**, 33159-33171, doi:10.18632/oncotarget.16565 (2017).
84 Toor, S. M. *et al.* Myeloid cells in circulation and tumor microenvironment of breast cancer patients. *Cancer Immunol Immunother* **66**, 753-764, doi:10.1007/s00262-017-1977-z (2017).
85 Law, A. M. K., Lim, E., Ormandy, C. J. & Gallego-Ortega, D. The innate and adaptive infiltrating immune systems as targets for breast cancer immunotherapy. *Endocr Relat Cancer* **24**, X1, doi:10.1530/ERC-16-0404e (2017).
86 Garrido, F., Aptsiauri, N., Doorduijn, E. M., Garcia Lora, A. M. & van Hall, T. The urgent need to recover MHC class I in cancers for effective immunotherapy. *Curr Opin Immunol* **39**, 44-51, doi:10.1016/j.coi.2015.12.007 (2016).
87 Noske, A. *et al.* Relevance of tumour-infiltrating lymphocytes, PD-1 and PD-L1 in patients with high-risk, nodal-metastasised breast cancer of the German Adjuvant Intergroup Node-positive study. *Eur J Cancer* **114**, 76-88, doi:10.1016/j.ejca.2019.04.010 (2019).
88 Ma, W., Gilligan, B. M., Yuan, J. & Li, T. Current status and perspectives in translational biomarker research for PD-1/PD-L1 immune checkpoint blockade therapy. *J Hematol Oncol* **9**, 47, doi:10.1186/s13045-016-0277-y (2016).
89 Bertucci, F., Finetti, P., Birnbaum, D. & Mamessier, E. The PD1/PDL1 axis, a promising therapeutic target in aggressive breast cancers. *Oncoimmunology* **5**, e1085148, doi:10.1080/2162402X.2015.1085148 (2016).
90 Zhang, H., Xiang, R., Wu, B., Li, J. & Luo, G. T-cell immunoglobulin mucin-3 expression in invasive ductal breast carcinoma: Clinicopathological correlations and association with

tumor infiltration by cytotoxic lymphocytes. *Mol Clin Oncol* **7**, 557-563, doi:10.3892/mco.2017.1360 (2017).
91 Burugu, S., Gao, D., Leung, S., Chia, S. K. & Nielsen, T. O. LAG-3+ tumor infiltrating lymphocytes in breast cancer: clinical correlates and association with PD-1/PD-L1+ tumors. *Ann Oncol* **28**, 2977-2984, doi:10.1093/annonc/mdx557 (2017).
92 Korkaya, H., Liu, S. & Wicha, M. S. Breast cancer stem cells, cytokine networks, and the tumor microenvironment. *J Clin Invest* **121**, 3804-3809, doi:10.1172/JCI57099 (2011).
93 Soysal, S. D., Tzankov, A. & Muenst, S. E. Role of the Tumor Microenvironment in Breast Cancer. *Pathobiology* **82**, 142-152, doi:10.1159/000430499 (2015).
94 Loi, S. Tumor-infiltrating lymphocytes, breast cancer subtypes and therapeutic efficacy. *Oncoimmunology* **2**, e24720, doi:10.4161/onci.24720 (2013).
95 Adams, S. *et al.* Prognostic value of tumor-infiltrating lymphocytes in triple-negative breast cancers from two phase III randomized adjuvant breast cancer trials: ECOG 2197 and ECOG 1199. *J Clin Oncol* **32**, 2959-2966, doi:10.1200/JCO.2013.55.0491 (2014).
96 Ali, H. R., Chlon, L., Pharoah, P. D., Markowetz, F. & Caldas, C. Patterns of Immune Infiltration in Breast Cancer and Their Clinical Implications: A Gene-Expression-Based Retrospective Study. *PLoS Med* **13**, e1002194, doi:10.1371/journal.pmed.1002194 (2016).
97 Lotze, M. T. Getting to the source: dendritic cells as therapeutic reagents for the treatment of patients with cancer. *Ann Surg* **226**, 1-5, doi:10.1097/00000658-199707000-00001 (1997).
98 Klingen, T. A., Chen, Y., Aas, H., Wik, E. & Akslen, L. A. Tumor-associated macrophages are strongly related to vascular invasion, non-luminal subtypes, and interval breast cancer. *Hum Pathol* **69**, 72-80, doi:10.1016/j.humpath.2017.09.001 (2017).
99 Ono, M. *et al.* Tumor-infiltrating lymphocytes are correlated with response to neoadjuvant chemotherapy in triple-negative breast cancer. *Breast Cancer Res Treat* **132**, 793-805, doi:10.1007/s10549-011-1554-7 (2012).
100 Kareva, I. A Combination of Immune Checkpoint Inhibition with Metronomic Chemotherapy as a Way of Targeting Therapy-Resistant Cancer Cells. *Int J Mol Sci* **18**, doi:10.3390/ijms18102134 (2017).
101 Verma, C. *et al.* Natural killer (NK) cell profiles in blood and tumour in women with large and locally advanced breast cancer (LLABC) and their contribution to a pathological complete response (PCR) in the tumour following neoadjuvant chemotherapy (NAC): differential restoration of blood profiles by NAC and surgery. *J Transl Med* **13**, 180, doi:10.1186/s12967-015-0535-8 (2015).
102 Weiss, S. A., Wolchok, J. D. & Sznol, M. Immunotherapy of Melanoma: Facts and Hopes. *Clin Cancer Res* **25**, 5191-5201, doi:10.1158/1078-0432.CCR-18-1550 (2019).
103 Anagnostou, V. K. & Brahmer, J. R. Cancer immunotherapy: a future paradigm shift in the treatment of non-small cell lung cancer. *Clin Cancer Res* **21**, 976-984, doi:10.1158/1078-0432.CCR-14-1187 (2015).
104 Wang, J. & Zhou, P. New Approaches in CAR-T Cell Immunotherapy for Breast Cancer. *Adv Exp Med Biol* **1026**, 371-381, doi:10.1007/978-981-10-6020-5_17 (2017).
105 Jackson, H. J., Rafiq, S. & Brentjens, R. J. Driving CAR T-cells forward. *Nat Rev Clin Oncol* **13**, 370-383, doi:10.1038/nrclinonc.2016.36 (2016).
106 Yuetao Xie, Y. H., Nawu Zhou, Cuicui Yao, Lixin Wu, Lin Liu, Fang Chen. CAR T-cell therapy for triple-negative breast cancer: Where we are. *Cancer Letters* **491**, 121-131 (2020).

107 Mittendorf, E. A. *et al.* Clinical trial results of the HER-2/neu (E75) vaccine to prevent breast cancer recurrence in high-risk patients: from US Military Cancer Institute Clinical Trials Group Study I-01 and I-02. *Cancer* **118**, 2594-2602, doi:10.1002/cncr.26574 (2012).
108 *Efficacy and Safety Study of NeuVax™ (Nelipepimut-S or E75) Vaccine to Prevent Breast Cancer Recurrence*, <https://clinicaltrials.gov/ct2/show/NCT01479244
109 *MUC1 Vaccine for Triple-negative Breast Cancer*, <https://clinicaltrials.gov/ct2/show/record/NCT00986609
110 Gheybi, E. *et al.* Immunogenicity of chimeric MUC1-HER2 vaccine against breast cancer in mice. *Iran J Basic Med Sci* **21**, 26-32, doi:10.22038/IJBMS.2017.25686.6335 (2018).
111 Meraviglia, S. *et al.* In vivo manipulation of Vgamma9Vdelta2 T cells with zoledronate and low-dose interleukin-2 for immunotherapy of advanced breast cancer patients. *Clin Exp Immunol* **161**, 290-297, doi:10.1111/j.1365-2249.2010.04167.x (2010).
112 Silva-Santos, B., Serre, K. & Norell, H. gammadelta T cells in cancer. *Nat Rev Immunol* **15**, 683-691, doi:10.1038/nri3904 (2015).
113 Born, W. *et al.* Peptide sequences of T-cell receptor delta and gamma chains are identical to predicted X and gamma proteins. *Nature* **330**, 572-574, doi:10.1038/330572a0 (1987).
114 Hayday, A. C. *et al.* Structure, organization, and somatic rearrangement of T cell gamma genes. *Cell* **40**, 259-269, doi:10.1016/0092-8674(85)90140-0 (1985).
115 Vantourout, P. & Hayday, A. Six-of-the-best: unique contributions of gammadelta T cells to immunology. *Nat Rev Immunol* **13**, 88-100, doi:10.1038/nri3384 (2013).
116 Kabelitz, D., Wesch, D. & He, W. Perspectives of gammadelta T cells in tumor immunology. *Cancer Res* **67**, 5-8, doi:10.1158/0008-5472.CAN-06-3069 (2007).
117 Born, W. K., Kemal Aydintug, M. & O'Brien, R. L. Diversity of gammadelta T-cell antigens. *Cell Mol Immunol* **10**, 13-20, doi:10.1038/cmi.2012.45 (2013).
118 Willcox, B. E. & Willcox, C. R. gammadelta TCR ligands: the quest to solve a 500-million-year-old mystery. *Nat Immunol* **20**, 121-128, doi:10.1038/s41590-018-0304-y (2019).
119 Benveniste, P. M. *et al.* Generation and molecular recognition of melanoma-associated antigen-specific human gammadelta T cells. *Sci Immunol* **3**, doi:10.1126/sciimmunol.aav4036 (2018).
120 Chien, Y. H., Meyer, C. & Bonneville, M. gammadelta T cells: first line of defense and beyond. *Annu Rev Immunol* **32**, 121-155, doi:10.1146/annurev-immunol-032713-120216 (2014).
121 Pennington, D. J. *et al.* The integration of conventional and unconventional T cells that characterizes cell-mediated responses. *Adv Immunol* **87**, 27-59, doi:10.1016/S0065-2776(05)87002-6 (2005).
122 Couzi, L. *et al.* Antibody-dependent anti-cytomegalovirus activity of human gammadelta T cells expressing CD16 (FcgammaRIIIa). *Blood* **119**, 1418-1427, doi:10.1182/blood-2011-06-363655 (2012).
123 Gao, Y. *et al.* Gamma delta T cells provide an early source of interferon gamma in tumor immunity. *J Exp Med* **198**, 433-442, doi:10.1084/jem.20030584 (2003).
124 Nedellec, S., Bonneville, M. & Scotet, E. Human Vgamma9Vdelta2 T cells: from signals to functions. *Semin Immunol* **22**, 199-206, doi:10.1016/j.smim.2010.04.004 (2010).
125 Rincon-Orozco, B. *et al.* Activation of V gamma 9V delta 2 T cells by NKG2D. *J Immunol* **175**, 2144-2151 (2005).
126 Gogoi, D. & Chiplunkar, S. V. Targeting gamma delta T cells for cancer immunotherapy: bench to bedside. *Indian J Med Res* **138**, 755-761 (2013).

127 Bonneville, M., O'Brien, R. L. & Born, W. K. Gammadelta T cell effector functions: a blend of innate programming and acquired plasticity. *Nat Rev Immunol* **10**, 467-478, doi:10.1038/nri2781 (2010).
128 Kabelitz, D. & He, W. The multifunctionality of human Vgamma9Vdelta2 gammadelta T cells: clonal plasticity or distinct subsets? *Scand J Immunol* **76**, 213-222, doi:10.1111/j.1365-3083.2012.02727.x (2012).
129 Brandes, M., Willimann, K. & Moser, B. Professional antigen-presentation function by human gammadelta T Cells. *Science* **309**, 264-268, doi:10.1126/science.1110267 (2005).
130 Correia, D. V., Lopes, A. & Silva-Santos, B. Tumor cell recognition by gammadelta T lymphocytes: T-cell receptor vs. NK-cell receptors. *Oncoimmunology* **2**, e22892, doi:10.4161/onci.22892 (2013).
131 Wesch, D., Peters, C. & Siegers, G. M. Human gamma delta T regulatory cells in cancer: fact or fiction? *Front Immunol* **5**, 598, doi:10.3389/fimmu.2014.00598 (2014).
132 Paul, S., Shilpi & Lal, G. Role of gamma-delta (gammadelta) T cells in autoimmunity. *J Leukoc Biol* **97**, 259-271, doi:10.1189/jlb.3RU0914-443R (2015).
133 Zheng, R. & Yang, Q. The role of the gamma delta T cell in allergic diseases. *J Immunol Res* **2014**, 963484, doi:10.1155/2014/963484 (2014).
134 Riganti, C., Massaia, M., Davey, M. S. & Eberl, M. Human gammadelta T-cell responses in infection and immunotherapy: common mechanisms, common mediators? *Eur J Immunol* **42**, 1668-1676, doi:10.1002/eji.201242492 (2012).
135 Bottino, C. *et al.* Two subsets of human T lymphocytes expressing gamma/delta antigen receptor are identifiable by monoclonal antibodies directed to two distinct molecular forms of the receptor. *J Exp Med* **168**, 491-505, doi:10.1084/jem.168.2.491 (1988).
136 Wu, D., Wu, P., Qiu, F., Wei, Q. & Huang, J. Human gammadeltaT-cell subsets and their involvement in tumor immunity. *Cell Mol Immunol* **14**, 245-253, doi:10.1038/cmi.2016.55 (2017).
137 Siegers, G. M. *et al.* Human Vdelta1 gammadelta T cells expanded from peripheral blood exhibit specific cytotoxicity against B-cell chronic lymphocytic leukemia-derived cells. *Cytotherapy* **13**, 753-764, doi:10.3109/14653249.2011.553595 (2011).
138 Freed-Pastor, W. A. *et al.* Mutant p53 disrupts mammary tissue architecture via the mevalonate pathway. *Cell* **148**, 244-258, doi:10.1016/j.cell.2011.12.017 (2012).
139 Hintz, M. *et al.* Identification of (E)-4-hydroxy-3-methyl-but-2-enyl pyrophosphate as a major activator for human gammadelta T cells in Escherichia coli. *FEBS Lett* **509**, 317-322, doi:10.1016/s0014-5793(01)03191-x (2001).
140 Gober, H. J. *et al.* Human T cell receptor gammadelta cells recognize endogenous mevalonate metabolites in tumor cells. *J Exp Med* **197**, 163-168, doi:10.1084/jem.20021500 (2003).
141 Kondo, M. *et al.* Expansion of human peripheral blood gammadelta T cells using zoledronate. *J Vis Exp*, doi:10.3791/3182 (2011).
142 Scotet, E. *et al.* Tumor recognition following Vgamma9Vdelta2 T cell receptor interactions with a surface F1-ATPase-related structure and apolipoprotein A-I. *Immunity* **22**, 71-80, doi:10.1016/j.immuni.2004.11.012 (2005).
143 Vavassori, S. *et al.* Butyrophilin 3A1 binds phosphorylated antigens and stimulates human gammadelta T cells. *Nat Immunol* **14**, 908-916, doi:10.1038/ni.2665 (2013).
144 Boutin, L. & Scotet, E. Towards Deciphering the Hidden Mechanisms That Contribute to the Antigenic Activation Process of Human Vgamma9Vdelta2 T Cells. *Front Immunol* **9**, 828, doi:10.3389/fimmu.2018.00828 (2018).

145 Harly, C. *et al.* Key implication of CD277/butyrophilin-3 (BTN3A) in cellular stress sensing by a major human gammadelta T-cell subset. *Blood* **120**, 2269-2279, doi:10.1182/blood-2012-05-430470 (2012).
146 Das, H. *et al.* MICA engagement by human Vgamma2Vdelta2 T cells enhances their antigen-dependent effector function. *Immunity* **15**, 83-93 (2001).
147 Wrobel, P. *et al.* Lysis of a broad range of epithelial tumour cells by human gamma delta T cells: involvement of NKG2D ligands and T-cell receptor- versus NKG2D-dependent recognition. *Scand J Immunol* **66**, 320-328, doi:10.1111/j.1365-3083.2007.01963.x (2007).
148 Kong, Y. *et al.* The NKG2D ligand ULBP4 binds to TCRgamma9/delta2 and induces cytotoxicity to tumor cells through both TCRgammadelta and NKG2D. *Blood* **114**, 310-317, doi:10.1182/blood-2008-12-196287 (2009).
149 Nausch, N. & Cerwenka, A. NKG2D ligands in tumor immunity. *Oncogene* **27**, 5944-5958, doi:10.1038/onc.2008.272 (2008).
150 Pietschmann, K. *et al.* Toll-like receptor expression and function in subsets of human gammadelta T lymphocytes. *Scand J Immunol* **70**, 245-255, doi:10.1111/j.1365-3083.2009.02290.x (2009).
151 Mo, C., Dai, Y., Kang, N., Cui, L. & He, W. Ectopic expression of human MutS homologue 2 on renal carcinoma cells is induced by oxidative stress with interleukin-18 promotion via p38 mitogen-activated protein kinase (MAPK) and c-Jun N-terminal kinase (JNK) signaling pathways. *J Biol Chem* **287**, 19242-19254, doi:10.1074/jbc.M112.349936 (2012).
152 Siegers, G. M. & Lamb, L. S., Jr. Cytotoxic and regulatory properties of circulating Vdelta1+ gammadelta T cells: a new player on the cell therapy field? *Mol Ther* **22**, 1416-1422, doi:10.1038/mt.2014.104 (2014).
153 Poggi, A. *et al.* Vdelta1 T lymphocytes from B-CLL patients recognize ULBP3 expressed on leukemic B cells and up-regulated by trans-retinoic acid. *Cancer Res* **64**, 9172-9179, doi:10.1158/0008-5472.CAN-04-2417 (2004).
154 Catellani, S. *et al.* Expansion of Vdelta1 T lymphocytes producing IL-4 in low-grade non-Hodgkin lymphomas expressing UL-16-binding proteins. *Blood* **109**, 2078-2085, doi:10.1182/blood-2006-06-028985 (2007).
155 Correia, D. V. *et al.* Differentiation of human peripheral blood Vdelta1+ T cells expressing the natural cytotoxicity receptor NKp30 for recognition of lymphoid leukemia cells. *Blood* **118**, 992-1001, doi:10.1182/blood-2011-02-339135 (2011).
156 Adams, E. J., Gu, S. & Luoma, A. M. Human gamma delta T cells: Evolution and ligand recognition. *Cell Immunol* **296**, 31-40, doi:10.1016/j.cellimm.2015.04.008 (2015).
157 Lamb, L. S., Jr. *et al.* Increased frequency of TCR gamma delta + T cells in disease-free survivors following T cell-depleted, partially mismatched, related donor bone marrow transplantation for leukemia. *J Hematother* **5**, 503-509, doi:10.1089/scd.1.1996.5.503 (1996).
158 Godder, K. T. *et al.* Long term disease-free survival in acute leukemia patients recovering with increased gammadelta T cells after partially mismatched related donor bone marrow transplantation. *Bone Marrow Transplant* **39**, 751-757, doi:10.1038/sj.bmt.1705650 (2007).
159 Shafi, S. *et al.* An NKG2D-mediated human lymphoid stress surveillance response with high interindividual variation. *Sci Transl Med* **3**, 113ra124, doi:10.1126/scitranslmed.3002922 (2011).
160 Bauer, S. *et al.* Activation of NK cells and T cells by NKG2D, a receptor for stress-inducible MICA. *Science* **285**, 727-729, doi:10.1126/science.285.5428.727 (1999).

161 Groh, V. *et al.* Broad tumor-associated expression and recognition by tumor-derived gamma delta T cells of MICA and MICB. *Proc Natl Acad Sci U S A* **96**, 6879-6884, doi:10.1073/pnas.96.12.6879 (1999).
162 Zingoni, A. *et al.* NKG2D and Its Ligands: "One for All, All for One". *Front Immunol* **9**, 476, doi:10.3389/fimmu.2018.00476 (2018).
163 Paczulla, A. M. *et al.* Absence of NKG2D ligands defines leukaemia stem cells and mediates their immune evasion. *Nature* **572**, 254-259, doi:10.1038/s41586-019-1410-1 (2019).
164 Wang, B. *et al.* Metastatic consequences of immune escape from NK cell cytotoxicity by human breast cancer stem cells. *Cancer Res* **74**, 5746-5757, doi:10.1158/0008-5472.CAN-13-2563 (2014).
165 Siegers, G. M. *et al.* Aberrantly Expressed Embryonic Protein NODAL Alters Breast Cancer Cell Susceptibility to gammadelta T Cell Cytotoxicity. *Front Immunol* **11**, 1287, doi:10.3389/fimmu.2020.01287 (2020).
166 Siegers, G. M., Dutta, I., Lai, R. & Postovit, L. M. Functional Plasticity of Gamma Delta T Cells and Breast Tumor Targets in Hypoxia. *Front Immunol* **9**, 1367, doi:10.3389/fimmu.2018.01367 (2018).
167 Groh, V., Wu, J., Yee, C. & Spies, T. Tumour-derived soluble MIC ligands impair expression of NKG2D and T-cell activation. *Nature* **419**, 734-738, doi:10.1038/nature01112 (2002).
168 Fernandez-Messina, L. *et al.* Differential mechanisms of shedding of the glycosylphosphatidylinositol (GPI)-anchored NKG2D ligands. *J Biol Chem* **285**, 8543-8551, doi:10.1074/jbc.M109.045906 (2010).
169 Waldhauer, I. *et al.* Tumor-associated MICA is shed by ADAM proteases. *Cancer Res* **68**, 6368-6376, doi:10.1158/0008-5472.CAN-07-6768 (2008).
170 Boutet, P. *et al.* Cutting edge: the metalloproteinase ADAM17/TNF-alpha-converting enzyme regulates proteolytic shedding of the MHC class I-related chain B protein. *J Immunol* **182**, 49-53, doi:10.4049/jimmunol.182.1.49 (2009).
171 Beck, B. H. *et al.* Adoptively transferred ex vivo expanded gammadelta-T cells mediate in vivo antitumor activity in preclinical mouse models of breast cancer. *Breast Cancer Res Treat* **122**, 135-144, doi:10.1007/s10549-009-0527-6 (2010).
172 Chitadze, G. *et al.* Shedding of endogenous MHC class I-related chain molecules A and B from different human tumor entities: heterogeneous involvement of the "a disintegrin and metalloproteases" 10 and 17. *Int J Cancer* **133**, 1557-1566, doi:10.1002/ijc.28174 (2013).
173 Silva-Santos, B., Mensurado, S. & Coffelt, S. B. gammadelta T cells: pleiotropic immune effectors with therapeutic potential in cancer. *Nat Rev Cancer* **19**, 392-404, doi:10.1038/s41568-019-0153-5 (2019).
174 Cordova, A. *et al.* Characterization of human gammadelta T lymphocytes infiltrating primary malignant melanomas. *PLoS One* **7**, e49878, doi:10.1371/journal.pone.0049878 (2012).
175 Ma, C. *et al.* Tumor-infiltrating gammadelta T lymphocytes predict clinical outcome in human breast cancer. *J Immunol* **189**, 5029-5036, doi:10.4049/jimmunol.1201892 (2012).
176 Raspollini, M. R. *et al.* Tumour-infiltrating gamma/delta T-lymphocytes are correlated with a brief disease-free interval in advanced ovarian serous carcinoma. *Ann Oncol* **16**, 590-596, doi:10.1093/annonc/mdi112 (2005).
177 Bao, Y., Guo, L. & Mo, J. Characterization of gammadelta T cells in patients with non-small cell lung cancer. *Oncol Lett* **14**, 1133-1140, doi:10.3892/ol.2017.6191 (2017).

178 Gentles, A. J. *et al.* The prognostic landscape of genes and infiltrating immune cells across human cancers. *Nat Med* **21**, 938-945, doi:10.1038/nm.3909 (2015).
179 Tosolini, M. *et al.* Assessment of tumor-infiltrating TCRVgamma9Vdelta2 gammadelta lymphocyte abundance by deconvolution of human cancers microarrays. *Oncoimmunology* **6**, e1284723, doi:10.1080/2162402X.2017.1284723 (2017).
180 Kabelitz, D., Serrano, R., Kouakanou, L., Peters, C. & Kalyan, S. Cancer immunotherapy with gammadelta T cells: many paths ahead of us. *Cell Mol Immunol*, doi:10.1038/s41423-020-0504-x (2020).
181 Bouet-Toussaint, F. *et al.* Vgamma9Vdelta2 T cell-mediated recognition of human solid tumors. Potential for immunotherapy of hepatocellular and colorectal carcinomas. *Cancer Immunol Immunother* **57**, 531-539, doi:10.1007/s00262-007-0391-3 (2008).
182 Kang, N. *et al.* Adoptive immunotherapy of lung cancer with immobilized anti-TCRgammadelta antibody-expanded human gammadelta T-cells in peripheral blood. *Cancer Biol Ther* **8**, 1540-1549 (2009).
183 Kunzmann, V. *et al.* Stimulation of gammadelta T cells by aminobisphosphonates and induction of antiplasma cell activity in multiple myeloma. *Blood* **96**, 384-392 (2000).
184 Wilhelm, M. *et al.* Gammadelta T cells for immune therapy of patients with lymphoid malignancies. *Blood* **102**, 200-206, doi:10.1182/blood-2002-12-3665 (2003).
185 Zou, C. *et al.* gammadelta T cells in cancer immunotherapy. *Oncotarget* **8**, 8900-8909, doi:10.18632/oncotarget.13051 (2017).
186 Zhao, Y., Niu, C. & Cui, J. Gamma-delta (gammadelta) T cells: friend or foe in cancer development? *J Transl Med* **16**, 3, doi:10.1186/s12967-017-1378-2 (2018).
187 Bank, I. *et al.* V delta 2+ gamma delta T lymphocytes are cytotoxic to the MCF 7 breast carcinoma cell line and can be detected among the T cells that infiltrate breast tumors. *Clin Immunol Immunopathol* **67**, 17-24, doi:10.1006/clin.1993.1040 (1993).
188 Guo, B. L., Liu, Z., Aldrich, W. A. & Lopez, R. D. Innate anti-breast cancer immunity of apoptosis-resistant human gammadelta-T cells. *Breast Cancer Res Treat* **93**, 169-175, doi:10.1007/s10549-005-4792-8 (2005).
189 Aggarwal, R. *et al.* Human Vgamma2Vdelta2 T cells limit breast cancer growth by modulating cell survival-, apoptosis-related molecules and microenvironment in tumors. *Int J Cancer* **133**, 2133-2144, doi:10.1002/ijc.28217 (2013).
190 Nicol, A. J. *et al.* Clinical evaluation of autologous gamma delta T cell-based immunotherapy for metastatic solid tumours. *Br J Cancer* **105**, 778-786, doi:10.1038/bjc.2011.293 (2011).
191 Dhar, S. & Chiplunkar, S. V. Lysis of aminobisphosphonate-sensitized MCF-7 breast tumor cells by Vgamma9Vdelta2 T cells. *Cancer Immun* **10**, 10 (2010).
192 Peng, G. *et al.* Tumor-infiltrating gammadelta T cells suppress T and dendritic cell function via mechanisms controlled by a unique toll-like receptor signaling pathway. *Immunity* **27**, 334-348, doi:10.1016/j.immuni.2007.05.020 (2007).
193 Coffelt, S. B. *et al.* IL-17-producing gammadelta T cells and neutrophils conspire to promote breast cancer metastasis. *Nature* **522**, 345-348, doi:10.1038/nature14282 (2015).
194 Welte, T. & Zhang, X. H. Interleukin-17 Could Promote Breast Cancer Progression at Several Stages of the Disease. *Mediators Inflamm* **2015**, 804347, doi:10.1155/2015/804347 (2015).
195 McKenzie, D. R., Comerford, I., Silva-Santos, B. & McColl, S. R. The Emerging Complexity of gammadeltaT17 Cells. *Front Immunol* **9**, 796, doi:10.3389/fimmu.2018.00796 (2018).

196 Sugie, T. *et al.* Zoledronic acid-induced expansion of gammadelta T cells from early-stage breast cancer patients: effect of IL-18 on helper NK cells. *Cancer Immunol Immunother* **62**, 677-687, doi:10.1007/s00262-012-1368-4 (2013).
197 Gaafar, A. *et al.* Defective gammadelta T-cell function and granzyme B gene polymorphism in a cohort of newly diagnosed breast cancer patients. *Exp Hematol* **37**, 838-848, doi:10.1016/j.exphem.2009.04.003 (2009).
198 Chabab, G. *et al.* Identification of a regulatory Vdelta1 gamma delta T cell subpopulation expressing CD73 in human breast cancer. *J Leukoc Biol* **107**, 1057-1067, doi:10.1002/JLB.3MA0420-278RR (2020).
199 Hidalgo, J. V. *et al.* Histological Analysis of gammadelta T Lymphocytes Infiltrating Human Triple-Negative Breast Carcinomas. *Frontiers in immunology* **5**, 632, doi:10.3389/fimmu.2014.00632 (2014).
200 Wu, Y. *et al.* An innate-like Vdelta1(+) gammadelta T cell compartment in the human breast is associated with remission in triple-negative breast cancer. *Sci Transl Med* **11**, doi:10.1126/scitranslmed.aax9364 (2019).
201 Bense, R. D. *et al.* Relevance of Tumor-Infiltrating Immune Cell Composition and Functionality for Disease Outcome in Breast Cancer. *J Natl Cancer Inst* **109**, doi:10.1093/jnci/djw192 (2017).
202 Janssen, A. *et al.* gammadelta T-cell Receptors Derived from Breast Cancer-Infiltrating T Lymphocytes Mediate Antitumor Reactivity. *Cancer Immunol Res* **8**, 530-543, doi:10.1158/2326-6066.CIR-19-0513 (2020).
203 Fisher, J. P., Heuijerjans, J., Yan, M., Gustafsson, K. & Anderson, J. gammadelta T cells for cancer immunotherapy: A systematic review of clinical trials. *Oncoimmunology* **3**, e27572, doi:10.4161/onci.27572 (2014).
204 Jiang, X. *et al.* Adoptive CD8(+) T cell therapy against cancer:Challenges and opportunities. *Cancer Lett* **462**, 23-32, doi:10.1016/j.canlet.2019.07.017 (2019).
205 Brandes, M. *et al.* Cross-presenting human gammadelta T cells induce robust CD8+ alphabeta T cell responses. *Proc Natl Acad Sci U S A* **106**, 2307-2312, doi:10.1073/pnas.0810059106 (2009).
206 Siegers, G. M. *et al.* Anti-leukemia activity of in vitro-expanded human gamma delta T cells in a xenogeneic Ph+ leukemia model. *PLoS One* **6**, e16700, doi:10.1371/journal.pone.0016700 (2011).
207 Siegers, G. M., Ribot, E. J., Keating, A. & Foster, P. J. Extensive expansion of primary human gamma delta T cells generates cytotoxic effector memory cells that can be labeled with Feraheme for cellular MRI. *Cancer Immunol Immunother* **62**, 571-583, doi:10.1007/s00262-012-1353-y (2013).
208 Polito, V. A. *et al.* Universal Ready-to-Use Immunotherapeutic Approach for the Treatment of Cancer: Expanded and Activated Polyclonal gammadelta Memory T Cells. *Front Immunol* **10**, 2717, doi:10.3389/fimmu.2019.02717 (2019).
209 Almeida, A. R. *et al.* Delta One T Cells for Immunotherapy of Chronic Lymphocytic Leukemia: Clinical-Grade Expansion/Differentiation and Preclinical Proof of Concept. *Clin Cancer Res* **22**, 5795-5804, doi:10.1158/1078-0432.CCR-16-0597 (2016).
210 Deniger, D. C. *et al.* Activating and propagating polyclonal gamma delta T cells with broad specificity for malignancies. *Clinical cancer research : an official journal of the American Association for Cancer Research* **20**, 5708-5719, doi:10.1158/1078-0432.CCR-13-3451 (2014).

211 Kondo, M. *et al.* Zoledronate facilitates large-scale ex vivo expansion of functional gammadelta T cells from cancer patients for use in adoptive immunotherapy. *Cytotherapy* **10**, 842-856, doi:10.1080/14653240802419328 (2008).
212 Sumi, E. *et al.* Effects of zoledronic acid and the association between its efficacy and gammadeltaT cells in postmenopausal women with breast cancer treated with preoperative hormonal therapy: a study protocol. *J Transl Med* **12**, 310, doi:10.1186/s12967-014-0310-2 (2014).
213 Gnant, M. *et al.* Adjuvant endocrine therapy plus zoledronic acid in premenopausal women with early-stage breast cancer: 62-month follow-up from the ABCSG-12 randomised trial. *Lancet Oncol* **12**, 631-641, doi:10.1016/S1470-2045(11)70122-X (2011).
214 Coscia, M. *et al.* Dysfunctional Vgamma9Vdelta2 T cells are negative prognosticators and markers of dysregulated mevalonate pathway activity in chronic lymphocytic leukemia cells. *Blood* **120**, 3271-3279, doi:10.1182/blood-2012-03-417519 (2012).
215 Morgan, G. J. *et al.* First-line treatment with zoledronic acid as compared with clodronic acid in multiple myeloma (MRC Myeloma IX): a randomised controlled trial. *Lancet* **376**, 1989-1999, doi:10.1016/S0140-6736(10)62051-X (2010).
216 Oliver Nussbaumer, M. K. The emerging role of γδ T cells in cancer immunotherapy. *Immuno-Oncology Technology* **1**, 3-10 (2019).
217 Marten, A., von Lilienfeld-Toal, M., Buchler, M. W. & Schmidt, J. Soluble MIC is elevated in the serum of patients with pancreatic carcinoma diminishing gammadelta T cell cytotoxicity. *Int J Cancer* **119**, 2359-2365, doi:10.1002/ijc.22186 (2006).
218 Lo Presti, E. *et al.* Current Advances in gammadelta T Cell-Based Tumor Immunotherapy. *Front Immunol* **8**, 1401, doi:10.3389/fimmu.2017.01401 (2017).
219 Lo Presti, E. *et al.* Squamous Cell Tumors Recruit gammadelta T Cells Producing either IL17 or IFNgamma Depending on the Tumor Stage. *Cancer Immunol Res* **5**, 397-407, doi:10.1158/2326-6066.CIR-16-0348 (2017).
220 Kalyan, S., Chandrasekaran, V., Quabius, E. S., Lindhorst, T. K. & Kabelitz, D. Neutrophil uptake of nitrogen-bisphosphonates leads to the suppression of human peripheral blood gammadelta T cells. *Cell Mol Life Sci* **71**, 2335-2346, doi:10.1007/s00018-013-1495-x (2014).
221 Kunzmann, V. *et al.* Tumor-promoting versus tumor-antagonizing roles of gammadelta T cells in cancer immunotherapy: results from a prospective phase I/II trial. *J Immunother* **35**, 205-213, doi:10.1097/CJI.0b013e318245bb1e (2012).
222 Lin, J. H., Russell, G. & Gertz, B. Pharmacokinetics of alendronate: an overview. *Int J Clin Pract Suppl* **101**, 18-26 (1999).
223 Hoh, A. *et al.* The activity of gammadelta T cells against paediatric liver tumour cells and spheroids in cell culture. *Liver Int* **33**, 127-136, doi:10.1111/liv.12011 (2013).
224 Oberg, H. H. *et al.* gammadelta T cell activation by bispecific antibodies. *Cell Immunol* **296**, 41-49, doi:10.1016/j.cellimm.2015.04.009 (2015).
225 Oberg, H. H. *et al.* Tribody [(HER2)2xCD16] Is More Effective Than Trastuzumab in Enhancing gammadelta T Cell and Natural Killer Cell Cytotoxicity Against HER2-Expressing Cancer Cells. *Front Immunol* **9**, 814, doi:10.3389/fimmu.2018.00814 (2018).
226 Peipp, M. *et al.* CD20-Specific Immunoligands Engaging NKG2D Enhance gammadelta T Cell-Mediated Lysis of Lymphoma Cells. *Scand J Immunol* **86**, 196-206, doi:10.1111/sji.12581 (2017).

227 Deniger, D. C. *et al.* Bispecific T-cells expressing polyclonal repertoire of endogenous gammadelta T-cell receptors and introduced CD19-specific chimeric antigen receptor. *Mol Ther* **21**, 638-647, doi:10.1038/mt.2012.267 (2013).
228 Marcu-Malina, V. *et al.* Redirecting alphabeta T cells against cancer cells by transfer of a broadly tumor-reactive gammadeltaT-cell receptor. *Blood* **118**, 50-59, doi:10.1182/blood-2010-12-325993 (2011).
229 Straetemans, T. *et al.* GMP-Grade Manufacturing of T Cells Engineered to Express a Defined gammadeltaTCR. *Front Immunol* **9**, 1062, doi:10.3389/fimmu.2018.01062 (2018).
230 *Netherlands Trial Register. Trial NL6357 (NTR6541)*, https://www.trialregister.nl/trial/6357 (2017).
231 Capietto, A. H., Martinet, L. & Fournie, J. J. Stimulated gammadelta T cells increase the in vivo efficacy of trastuzumab in HER-2+ breast cancer. *J Immunol* **187**, 1031-1038, doi:10.4049/jimmunol.1100681 (2011).
232 Wu, D. *et al.* Ex vivo expanded human circulating Vdelta1 gammadeltaT cells exhibit favorable therapeutic potential for colon cancer. *Oncoimmunology* **4**, e992749, doi:10.4161/2162402X.2014.992749 (2015).
233 Schilbach, K., Frommer, K., Meier, S., Handgretinger, R. & Eyrich, M. Immune response of human propagated gammadelta-T-cells to neuroblastoma recommend the Vdelta1+ subset for gammadelta-T-cell-based immunotherapy. *J Immunother* **31**, 896-905, doi:10.1097/CJI.0b013e31818955ad (2008).
234 Nussbaumer, O. W., R.; Beatson, R.; Hayday, A. C.;. in *Gamma Delta Conference 2016* (King's College, London, 2016).
235 Rosenberg, S. A. *et al.* Durable complete responses in heavily pretreated patients with metastatic melanoma using T-cell transfer immunotherapy. *Clin Cancer Res* **17**, 4550-4557, doi:10.1158/1078-0432.CCR-11-0116 (2011).
236 Besser, M. J. *et al.* Adoptive transfer of tumor-infiltrating lymphocytes in patients with metastatic melanoma: intent-to-treat analysis and efficacy after failure to prior immunotherapies. *Clin Cancer Res* **19**, 4792-4800, doi:10.1158/1078-0432.CCR-13-0380 (2013).
237 Todaro, M. *et al.* Efficient killing of human colon cancer stem cells by gammadelta T lymphocytes. *J Immunol* **182**, 7287-7296, doi:10.4049/jimmunol.0804288 (2009).
238 Lai, D. *et al.* Human ovarian cancer stem-like cells can be efficiently killed by gammadelta T lymphocytes. *Cancer Immunol Immunother* **61**, 979-989, doi:10.1007/s00262-011-1166-4 (2012).
239 Nishio, N. *et al.* Zoledronate sensitizes neuroblastoma-derived tumor-initiating cells to cytolysis mediated by human gammadelta T cells. *J Immunother* **35**, 598-606, doi:10.1097/CJI.0b013e31826a745a (2012).
240 Dong, H. *et al.* Tumor-associated B7-H1 promotes T-cell apoptosis: a potential mechanism of immune evasion. *Nat Med* **8**, 793-800, doi:10.1038/nm730 (2002).
241 Lin, L. & Du, L. The role of secreted factors in stem cells-mediated immune regulation. *Cell Immunol* **326**, 24-32, doi:10.1016/j.cellimm.2017.07.010 (2018).
242 Soslow, R. A. *et al.* COX-2 is expressed in human pulmonary, colonic, and mammary tumors. *Cancer* **89**, 2637-2645 (2000).
243 Wang, D., Fu, L., Sun, H., Guo, L. & DuBois, R. N. Prostaglandin E2 Promotes Colorectal Cancer Stem Cell Expansion and Metastasis in Mice. *Gastroenterology* **149**, 1884-1895 e1884, doi:10.1053/j.gastro.2015.07.064 (2015).

244 Pang, L. Y., Hurst, E. A. & Argyle, D. J. Cyclooxygenase-2: A Role in Cancer Stem Cell Survival and Repopulation of Cancer Cells during Therapy. *Stem Cells Int* **2016**, 2048731, doi:10.1155/2016/2048731 (2016).
245 Martinet, L. *et al.* A regulatory cross-talk between Vgamma9Vdelta2 T lymphocytes and mesenchymal stem cells. *Eur J Immunol* **39**, 752-762, doi:10.1002/eji.200838812 (2009).
246 Lo Presti, E. *et al.* gammadelta T Cells and Tumor Microenvironment: From Immunosurveillance to Tumor Evasion. *Front Immunol* **9**, 1395, doi:10.3389/fimmu.2018.01395 (2018).
247 Sitkovsky, M. V. *et al.* Physiological control of immune response and inflammatory tissue damage by hypoxia-inducible factors and adenosine A2A receptors. *Annu Rev Immunol* **22**, 657-682, doi:10.1146/annurev.immunol.22.012703.104731 (2004).
248 Ohta, A. *et al.* A2A adenosine receptor protects tumors from antitumor T cells. *Proc Natl Acad Sci U S A* **103**, 13132-13137, doi:10.1073/pnas.0605251103 (2006).
249 Martinet, L., Poupot, R. & Fournie, J. J. Pitfalls on the roadmap to gammadelta T cell-based cancer immunotherapies. *Immunol Lett* **124**, 1-8, doi:10.1016/j.imlet.2009.03.011 (2009).
250 Liu, F. T. & Rabinovich, G. A. Galectins as modulators of tumour progression. *Nat Rev Cancer* **5**, 29-41, doi:10.1038/nrc1527 (2005).
251 Zhou, X. *et al.* Galectin-1 is overexpressed in CD133+ human lung adenocarcinoma cells and promotes their growth and invasiveness. *Oncotarget* **6**, 3111-3122, doi:10.18632/oncotarget.3076 (2015).
252 Gonnermann, D. *et al.* Galectin-3 Released by Pancreatic Ductal Adenocarcinoma Suppresses gammadelta T Cell Proliferation but Not Their Cytotoxicity. *Front Immunol* **11**, 1328, doi:10.3389/fimmu.2020.01328 (2020).
253 Lee, K. M. *et al.* MYC and MCL1 Cooperatively Promote Chemotherapy-Resistant Breast Cancer Stem Cells via Regulation of Mitochondrial Oxidative Phosphorylation. *Cell Metab* **26**, 633-647 e637, doi:10.1016/j.cmet.2017.09.009 (2017).
254 Konopleva, M. *et al.* The anti-apoptotic genes Bcl-X(L) and Bcl-2 are over-expressed and contribute to chemoresistance of non-proliferating leukaemic CD34+ cells. *Br J Haematol* **118**, 521-534, doi:10.1046/j.1365-2141.2002.03637.x (2002).
255 Tagscherer, K. E. *et al.* Apoptosis-based treatment of glioblastomas with ABT-737, a novel small molecule inhibitor of Bcl-2 family proteins. *Oncogene* **27**, 6646-6656, doi:10.1038/onc.2008.259 (2008).
256 Schwickart, M. *et al.* Deubiquitinase USP9X stabilizes MCL1 and promotes tumour cell survival. *Nature* **463**, 103-107, doi:10.1038/nature08646 (2010).
257 Siddharth, S., Das, S., Nayak, A. & Kundu, C. N. SURVIVIN as a marker for quiescent-breast cancer stem cells-An intermediate, adherent, pre-requisite phase of breast cancer metastasis. *Clin Exp Metastasis* **33**, 661-675, doi:10.1007/s10585-016-9809-7 (2016).
258 Lee, M. R., Ji, S. Y., Mia-Jan, K. & Cho, M. Y. Chemoresistance of CD133(+) colon cancer may be related with increased survivin expression. *Biochem Biophys Res Commun* **463**, 229-234, doi:10.1016/j.bbrc.2015.05.031 (2015).
259 Chen, H. C. *et al.* An interconnected hierarchical model of cell death regulation by the BCL-2 family. *Nat Cell Biol* **17**, 1270-1281, doi:10.1038/ncb3236 (2015).
260 Xiang, W., Yang, C. Y. & Bai, L. MCL-1 inhibition in cancer treatment. *Onco Targets Ther* **11**, 7301-7314, doi:10.2147/OTT.S146228 (2018).
261 Krajewski, S. *et al.* Immunohistochemical analysis of Mcl-1 protein in human tissues. Differential regulation of Mcl-1 and Bcl-2 protein production suggests a unique role for Mcl-1 in control of programmed cell death in vivo. *Am J Pathol* **146**, 1309-1319 (1995).

262 Perciavalle, R. M. & Opferman, J. T. Delving deeper: MCL-1's contributions to normal and cancer biology. *Trends Cell Biol* **23**, 22-29, doi:10.1016/j.tcb.2012.08.011 (2013).
263 Merino, D. *et al.* Synergistic action of the MCL-1 inhibitor S63845 with current therapies in preclinical models of triple-negative and HER2-amplified breast cancer. *Sci Transl Med* **9**, doi:10.1126/scitranslmed.aam7049 (2017).
264 Campbell, K. J. *et al.* MCL-1 is a prognostic indicator and drug target in breast cancer. *Cell Death Dis* **9**, 19, doi:10.1038/s41419-017-0035-2 (2018).
265 Ding, Q. *et al.* Myeloid cell leukemia-1 inversely correlates with glycogen synthase kinase-3beta activity and associates with poor prognosis in human breast cancer. *Cancer Res* **67**, 4564-4571, doi:10.1158/0008-5472.CAN-06-1788 (2007).
266 Hird, A. W. & Tron, A. E. Recent advances in the development of Mcl-1 inhibitors for cancer therapy. *Pharmacol Ther* **198**, 59-67, doi:10.1016/j.pharmthera.2019.02.007 (2019).
267 Kozopas, K. M., Yang, T., Buchan, H. L., Zhou, P. & Craig, R. W. MCL1, a gene expressed in programmed myeloid cell differentiation, has sequence similarity to BCL2. *Proc Natl Acad Sci U S A* **90**, 3516-3520, doi:10.1073/pnas.90.8.3516 (1993).
268 Papatzimas, J. W. *et al.* From Inhibition to Degradation: Targeting the Antiapoptotic Protein Myeloid Cell Leukemia 1 (MCL1). *J Med Chem* **62**, 5522-5540, doi:10.1021/acs.jmedchem.9b00455 (2019).
269 Caenepeel, S. *et al.* AMG 176, a Selective MCL1 Inhibitor, Is Effective in Hematologic Cancer Models Alone and in Combination with Established Therapies. *Cancer Discov* **8**, 1582-1597, doi:10.1158/2159-8290.CD-18-0387 (2018).
270 Koch, R. *et al.* Biomarker-driven strategy for MCL1 inhibition in T-cell lymphomas. *Blood* **133**, 566-575, doi:10.1182/blood-2018-07-865527 (2019).
271 Moujalled, D. M. *et al.* Combining BH3-mimetics to target both BCL-2 and MCL1 has potent activity in pre-clinical models of acute myeloid leukemia. *Leukemia* **33**, 905-917, doi:10.1038/s41375-018-0261-3 (2019).
272 Ramsey, H. E. *et al.* A Novel MCL1 Inhibitor Combined with Venetoclax Rescues Venetoclax-Resistant Acute Myelogenous Leukemia. *Cancer Discov* **8**, 1566-1581, doi:10.1158/2159-8290.CD-18-0140 (2018).
273 Tron, A. E. *et al.* Discovery of Mcl-1-specific inhibitor AZD5991 and preclinical activity in multiple myeloma and acute myeloid leukemia. *Nat Commun* **9**, 5341, doi:10.1038/s41467-018-07551-w (2018).
274 Wolfsberg, T. G. *et al.* The precursor region of a protein active in sperm-egg fusion contains a metalloprotease and a disintegrin domain: structural, functional, and evolutionary implications. *Proc Natl Acad Sci U S A* **90**, 10783-10787, doi:10.1073/pnas.90.22.10783 (1993).
275 Wolfsberg, T. G., Primakoff, P., Myles, D. G. & White, J. M. ADAM, a novel family of membrane proteins containing A Disintegrin And Metalloprotease domain: multipotential functions in cell-cell and cell-matrix interactions. *J Cell Biol* **131**, 275-278, doi:10.1083/jcb.131.2.275 (1995).
276 Black, R. A. *et al.* A metalloproteinase disintegrin that releases tumour-necrosis factor-alpha from cells. *Nature* **385**, 729-733, doi:10.1038/385729a0 (1997).
277 Schumacher, N. *et al.* Shedding of Endogenous Interleukin-6 Receptor (IL-6R) Is Governed by A Disintegrin and Metalloproteinase (ADAM) Proteases while a Full-length IL-6R Isoform Localizes to Circulating Microvesicles. *J Biol Chem* **290**, 26059-26071, doi:10.1074/jbc.M115.649509 (2015).

278 Clayton, K. L. *et al.* Soluble T cell immunoglobulin mucin domain 3 is shed from CD8+ T cells by the sheddase ADAM10, is increased in plasma during untreated HIV infection, and correlates with HIV disease progression. *J Virol* **89**, 3723-3736, doi:10.1128/JVI.00006-15 (2015).
279 Zheng, H. *et al.* Elevated serum HER-2 predicts poor prognosis in breast cancer and is correlated to ADAM10 expression. *Cancer Med* **8**, 679-685, doi:10.1002/cam4.1859 (2019).
280 Nagano, O. & Saya, H. Mechanism and biological significance of CD44 cleavage. *Cancer Sci* **95**, 930-935, doi:10.1111/j.1349-7006.2004.tb03179.x (2004).
281 Tian, L. *et al.* ADAM10 is essential for proteolytic activation of Notch during thymocyte development. *Int Immunol* **20**, 1181-1187, doi:10.1093/intimm/dxn076 (2008).
282 Romero, Y., Wise, R. & Zolkiewska, A. Proteolytic processing of PD-L1 by ADAM proteases in breast cancer cells. *Cancer Immunol Immunother* **69**, 43-55, doi:10.1007/s00262-019-02437-2 (2020).
283 Schulte, M. *et al.* ADAM10 regulates FasL cell surface expression and modulates FasL-induced cytotoxicity and activation-induced cell death. *Cell Death Differ* **14**, 1040-1049, doi:10.1038/sj.cdd.4402101 (2007).
284 Duffy, M. J., McKiernan, E., O'Donovan, N. & McGowan, P. M. The role of ADAMs in disease pathophysiology. *Clin Chim Acta* **403**, 31-36, doi:10.1016/j.cca.2009.01.007 (2009).
285 Duffy, M. J., McKiernan, E., O'Donovan, N. & McGowan, P. M. Role of ADAMs in cancer formation and progression. *Clin Cancer Res* **15**, 1140-1144, doi:10.1158/1078-0432.CCR-08-1585 (2009).
286 Mochizuki, S. & Okada, Y. ADAMs in cancer cell proliferation and progression. *Cancer Sci* **98**, 621-628, doi:10.1111/j.1349-7006.2007.00434.x (2007).
287 Mullooly, M., McGowan, P. M., Crown, J. & Duffy, M. J. The ADAMs family of proteases as targets for the treatment of cancer. *Cancer Biol Ther* **17**, 870-880, doi:10.1080/15384047.2016.1177684 (2016).
288 Le Gall, S. M. *et al.* ADAMs 10 and 17 represent differentially regulated components of a general shedding machinery for membrane proteins such as transforming growth factor alpha, L-selectin, and tumor necrosis factor alpha. *Mol Biol Cell* **20**, 1785-1794, doi:10.1091/mbc.E08-11-1135 (2009).
289 Smith, T. M., Jr., Tharakan, A. & Martin, R. K. Targeting ADAM10 in Cancer and Autoimmunity. *Front Immunol* **11**, 499, doi:10.3389/fimmu.2020.00499 (2020).
290 Baumeister, S. H., Freeman, G. J., Dranoff, G. & Sharpe, A. H. Coinhibitory Pathways in Immunotherapy for Cancer. *Annu Rev Immunol* **34**, 539-573, doi:10.1146/annurev-immunol-032414-112049 (2016).
291 Okazaki, T., Chikuma, S., Iwai, Y., Fagarasan, S. & Honjo, T. A rheostat for immune responses: the unique properties of PD-1 and their advantages for clinical application. *Nat Immunol* **14**, 1212-1218, doi:10.1038/ni.2762 (2013).
292 Chemnitz, J. M., Parry, R. V., Nichols, K. E., June, C. H. & Riley, J. L. SHP-1 and SHP-2 associate with immunoreceptor tyrosine-based switch motif of programmed death 1 upon primary human T cell stimulation, but only receptor ligation prevents T cell activation. *J Immunol* **173**, 945-954, doi:10.4049/jimmunol.173.2.945 (2004).
293 Arasanz, H. *et al.* PD1 signal transduction pathways in T cells. *Oncotarget* **8**, 51936-51945, doi:10.18632/oncotarget.17232 (2017).

294 Keir, M. E., Butte, M. J., Freeman, G. J. & Sharpe, A. H. PD-1 and its ligands in tolerance and immunity. *Annu Rev Immunol* **26**, 677-704, doi:10.1146/annurev.immunol.26.021607.090331 (2008).
295 Sanmamed, M. F. & Chen, L. Inducible expression of B7-H1 (PD-L1) and its selective role in tumor site immune modulation. *Cancer J* **20**, 256-261, doi:10.1097/PPO.0000000000000061 (2014).
296 Ishida, Y., Agata, Y., Shibahara, K. & Honjo, T. Induced expression of PD-1, a novel member of the immunoglobulin gene superfamily, upon programmed cell death. *EMBO J* **11**, 3887-3895 (1992).
297 Xiao, G., Deng, A., Liu, H., Ge, G. & Liu, X. Activator protein 1 suppresses antitumor T-cell function via the induction of programmed death 1. *Proc Natl Acad Sci U S A* **109**, 15419-15424, doi:10.1073/pnas.1206370109 (2012).
298 Bally, A. P. *et al.* NF-kappaB regulates PD-1 expression in macrophages. *J Immunol* **194**, 4545-4554, doi:10.4049/jimmunol.1402550 (2015).
299 Austin, J. W., Lu, P., Majumder, P., Ahmed, R. & Boss, J. M. STAT3, STAT4, NFATc1, and CTCF regulate PD-1 through multiple novel regulatory regions in murine T cells. *J Immunol* **192**, 4876-4886, doi:10.4049/jimmunol.1302750 (2014).
300 Voron, T. *et al.* VEGF-A modulates expression of inhibitory checkpoints on CD8+ T cells in tumors. *J Exp Med* **212**, 139-148, doi:10.1084/jem.20140559 (2015).
301 Chen, J., Jiang, C. C., Jin, L. & Zhang, X. D. Regulation of PD-L1: a novel role of pro-survival signalling in cancer. *Ann Oncol* **27**, 409-416, doi:10.1093/annonc/mdv615 (2016).
302 Noman, M. Z. *et al.* PD-L1 is a novel direct target of HIF-1alpha, and its blockade under hypoxia enhanced MDSC-mediated T cell activation. *J Exp Med* **211**, 781-790, doi:10.1084/jem.20131916 (2014).
303 Cheng, X. *et al.* Structure and interactions of the human programmed cell death 1 receptor. *J Biol Chem* **288**, 11771-11785, doi:10.1074/jbc.M112.448126 (2013).
304 Xu-Monette, Z. Y., Zhang, M., Li, J. & Young, K. H. PD-1/PD-L1 Blockade: Have We Found the Key to Unleash the Antitumor Immune Response? *Front Immunol* **8**, 1597, doi:10.3389/fimmu.2017.01597 (2017).
305 Sobral-Leite, M. *et al.* Assessment of PD-L1 expression across breast cancer molecular subtypes, in relation to mutation rate, BRCA1-like status, tumor-infiltrating immune cells and survival. *Oncoimmunology* **7**, e1509820, doi:10.1080/2162402X.2018.1509820 (2018).
306 Thompson, R. H. *et al.* Costimulatory B7-H1 in renal cell carcinoma patients: Indicator of tumor aggressiveness and potential therapeutic target. *Proc Natl Acad Sci U S A* **101**, 17174-17179, doi:10.1073/pnas.0406351101 (2004).
307 Hamanishi, J. *et al.* Programmed cell death 1 ligand 1 and tumor-infiltrating CD8+ T lymphocytes are prognostic factors of human ovarian cancer. *Proc Natl Acad Sci U S A* **104**, 3360-3365, doi:10.1073/pnas.0611533104 (2007).
308 Teixido, C., Vilarino, N., Reyes, R. & Reguart, N. PD-L1 expression testing in non-small cell lung cancer. *Ther Adv Med Oncol* **10**, 1758835918763493, doi:10.1177/1758835918763493 (2018).
309 Obeid, J. M. *et al.* PD-L1, PD-L2 and PD-1 expression in metastatic melanoma: Correlation with tumor-infiltrating immune cells and clinical outcome. *Oncoimmunology* **5**, e1235107, doi:10.1080/2162402X.2016.1235107 (2016).

310 Shen, Z., Gu, L., Mao, D., Chen, M. & Jin, R. Clinicopathological and prognostic significance of PD-L1 expression in colorectal cancer: a systematic review and meta-analysis. *World J Surg Oncol* **17**, 4, doi:10.1186/s12957-018-1544-x (2019).
311 Chen, R. Q., Liu, F., Qiu, X. Y. & Chen, X. Q. The Prognostic and Therapeutic Value of PD-L1 in Glioma. *Front Pharmacol* **9**, 1503, doi:10.3389/fphar.2018.01503 (2018).
312 Zhao, Y. J. *et al.* Expression of PD-1 on CD4(+) Tumor-Infiltrating Lymphocytes in Tumor Microenvironment Associated with Pathological Characteristics of Breast Cancer. *J Immunol Res* **2018**, 5690258, doi:10.1155/2018/5690258 (2018).
313 Ren, X. *et al.* PD1 protein expression in tumor infiltrated lymphocytes rather than PDL1 in tumor cells predicts survival in triple-negative breast cancer. *Cancer Biol Ther* **19**, 373-380, doi:10.1080/15384047.2018.1423919 (2018).
314 Myklebust, J. H. *et al.* High PD-1 expression and suppressed cytokine signaling distinguish T cells infiltrating follicular lymphoma tumors from peripheral T cells. *Blood* **121**, 1367-1376, doi:10.1182/blood-2012-04-421826 (2013).
315 Muenst, S. *et al.* The presence of programmed death 1 (PD-1)-positive tumor-infiltrating lymphocytes is associated with poor prognosis in human breast cancer. *Breast Cancer Res Treat* **139**, 667-676, doi:10.1007/s10549-013-2581-3 (2013).
316 Zhang, Y. *et al.* Prognostic significance of programmed cell death 1 (PD-1) or PD-1 ligand 1 (PD-L1) Expression in epithelial-originated cancer: a meta-analysis. *Medicine (Baltimore)* **94**, e515, doi:10.1097/MD.0000000000000515 (2015).
317 Muenst, S. *et al.* Expression of programmed death ligand 1 (PD-L1) is associated with poor prognosis in human breast cancer. *Breast Cancer Res Treat* **146**, 15-24, doi:10.1007/s10549-014-2988-5 (2014).
318 Wu, P., Wu, D., Li, L., Chai, Y. & Huang, J. PD-L1 and Survival in Solid Tumors: A Meta-Analysis. *PLoS One* **10**, e0131403, doi:10.1371/journal.pone.0131403 (2015).
319 Zhang, M. *et al.* Expression of PD-L1 and prognosis in breast cancer: a meta-analysis. *Oncotarget* **8**, 31347-31354, doi:10.18632/oncotarget.15532 (2017).
320 Salmaninejad, A. *et al.* PD-1/PD-L1 pathway: Basic biology and role in cancer immunotherapy. *J Cell Physiol* **234**, 16824-16837, doi:10.1002/jcp.28358 (2019).
321 Chen, Y. *et al.* Looking for the Optimal PD-1/PD-L1 Inhibitor in Cancer Treatment: A Comparison in Basic Structure, Function, and Clinical Practice. *Front Immunol* **11**, 1088, doi:10.3389/fimmu.2020.01088 (2020).
322 Atezolizumab, T. IMpassion130 Efficacy Results in First-Line PD-L1+ Metastatic Triple-Negative Breast Cancer.
323 Phan, G. Q. *et al.* Cancer regression and autoimmunity induced by cytotoxic T lymphocyte-associated antigen 4 blockade in patients with metastatic melanoma. *Proc Natl Acad Sci U S A* **100**, 8372-8377, doi:10.1073/pnas.1533209100 (2003).
324 Brunner, M. C. *et al.* CTLA-4-Mediated inhibition of early events of T cell proliferation. *J Immunol* **162**, 5813-5820 (1999).
325 Krummel, M. F. & Allison, J. P. CTLA-4 engagement inhibits IL-2 accumulation and cell cycle progression upon activation of resting T cells. *J Exp Med* **183**, 2533-2540, doi:10.1084/jem.183.6.2533 (1996).
326 Chambers, C. A., Kuhns, M. S., Egen, J. G. & Allison, J. P. CTLA-4-mediated inhibition in regulation of T cell responses: mechanisms and manipulation in tumor immunotherapy. *Annu Rev Immunol* **19**, 565-594, doi:10.1146/annurev.immunol.19.1.565 (2001).
327 Lee, K. M. *et al.* Molecular basis of T cell inactivation by CTLA-4. *Science* **282**, 2263-2266, doi:10.1126/science.282.5397.2263 (1998).

328 Walunas, T. L. *et al.* CTLA-4 can function as a negative regulator of T cell activation. *Immunity* **1**, 405-413 (1994).
329 Kassardjian, A., Shintaku, P. I. & Moatamed, N. A. Expression of immune checkpoint regulators, cytotoxic T lymphocyte antigen 4 (CTLA-4) and programmed death-ligand 1 (PD-L1), in female breast carcinomas. *PLoS One* **13**, e0195958, doi:10.1371/journal.pone.0195958 (2018).
330 Bu, X., Yao, Y. & Li, X. in *Translational Research in Breast Cancer: Biomarker Diagnosis, Targeted Therapies and Approaches to Precision Medicine* (eds Erwei Song & Hai Hu) 383-402 (Springer Singapore, 2017).
331 Rotte, A. Combination of CTLA-4 and PD-1 blockers for treatment of cancer. *J Exp Clin Cancer Res* **38**, 255, doi:10.1186/s13046-019-1259-z (2019).
332 Li, Z., Ju, Z. & Frieri, M. The T-cell immunoglobulin and mucin domain (Tim) gene family in asthma, allergy, and autoimmunity. *Allergy Asthma Proc* **34**, e21-26, doi:10.2500/aap.2013.34.3646 (2013).
333 He, Y. *et al.* TIM-3, a promising target for cancer immunotherapy. *Onco Targets Ther* **11**, 7005-7009, doi:10.2147/OTT.S170385 (2018).
334 de Mingo Pulido, A. *et al.* TIM-3 Regulates CD103(+) Dendritic Cell Function and Response to Chemotherapy in Breast Cancer. *Cancer Cell* **33**, 60-74 e66, doi:10.1016/j.ccell.2017.11.019 (2018).
335 Sakuishi, K. *et al.* Targeting Tim-3 and PD-1 pathways to reverse T cell exhaustion and restore anti-tumor immunity. *J Exp Med* **207**, 2187-2194, doi:10.1084/jem.20100643 (2010).
336 Takano, S., Saito, H. & Ikeguchi, M. An increased number of PD-1+ and Tim-3+ CD8+ T cells is involved in immune evasion in gastric cancer. *Surg Today* **46**, 1341-1347, doi:10.1007/s00595-016-1305-9 (2016).
337 Zhou, Q. *et al.* Coexpression of Tim-3 and PD-1 identifies a CD8+ T-cell exhaustion phenotype in mice with disseminated acute myelogenous leukemia. *Blood* **117**, 4501-4510, doi:10.1182/blood-2010-10-310425 (2011).
338 Wu, J., Liu, C., Qian, S. & Hou, H. The expression of Tim-3 in peripheral blood of ovarian cancer. *DNA Cell Biol* **32**, 648-653, doi:10.1089/dna.2013.2116 (2013).
339 Koyama, S. *et al.* Adaptive resistance to therapeutic PD-1 blockade is associated with upregulation of alternative immune checkpoints. *Nat Commun* **7**, 10501, doi:10.1038/ncomms10501 (2016).
340 Fourcade, J. *et al.* Upregulation of Tim-3 and PD-1 expression is associated with tumor antigen-specific CD8+ T cell dysfunction in melanoma patients. *J Exp Med* **207**, 2175-2186, doi:10.1084/jem.20100637 (2010).
341 Ngiow, S. F. *et al.* Anti-TIM3 antibody promotes T cell IFN-gamma-mediated antitumor immunity and suppresses established tumors. *Cancer Res* **71**, 3540-3551, doi:10.1158/0008-5472.CAN-11-0096 (2011).
342 Fourcade, J. *et al.* PD-1 and Tim-3 regulate the expansion of tumor antigen-specific CD8(+) T cells induced by melanoma vaccines. *Cancer Res* **74**, 1045-1055, doi:10.1158/0008-5472.CAN-13-2908 (2014).
343 Zhou, G. *et al.* Antibodies Against Immune Checkpoint Molecules Restore Functions of Tumor-Infiltrating T Cells in Hepatocellular Carcinomas. *Gastroenterology* **153**, 1107-1119 e1110, doi:10.1053/j.gastro.2017.06.017 (2017).

344 Huard, B., Gaulard, P., Faure, F., Hercend, T. & Triebel, F. Cellular expression and tissue distribution of the human LAG-3-encoded protein, an MHC class II ligand. *Immunogenetics* **39**, 213-217 (1994).
345 Workman, C. J., Dugger, K. J. & Vignali, D. A. Cutting edge: molecular analysis of the negative regulatory function of lymphocyte activation gene-3. *J Immunol* **169**, 5392-5395, doi:10.4049/jimmunol.169.10.5392 (2002).
346 Huard, B., Prigent, P., Tournier, M., Bruniquel, D. & Triebel, F. CD4/major histocompatibility complex class II interaction analyzed with CD4- and lymphocyte activation gene-3 (LAG-3)-Ig fusion proteins. *Eur J Immunol* **25**, 2718-2721, doi:10.1002/eji.1830250949 (1995).
347 Macon-Lemaitre, L. & Triebel, F. The negative regulatory function of the lymphocyte-activation gene-3 co-receptor (CD223) on human T cells. *Immunology* **115**, 170-178, doi:10.1111/j.1365-2567.2005.02145.x (2005).
348 Long, L. *et al.* The promising immune checkpoint LAG-3: from tumor microenvironment to cancer immunotherapy. *Genes Cancer* **9**, 176-189, doi:10.18632/genesandcancer.180 (2018).
349 Scala, E. *et al.* Lymphocyte activation gene-3 (LAG-3) expression and IFN-gamma production are variably coregulated in different human T lymphocyte subpopulations. *J Immunol* **161**, 489-493 (1998).
350 Tundo, G. R., Sbardella, D., Lacal, P. M., Graziani, G. & Marini, S. On the Horizon: Targeting Next-Generation Immune Checkpoints for Cancer Treatment. *Chemotherapy*, 1-19, doi:10.1159/000500902 (2019).
351 Blackburn, S. D. *et al.* Coregulation of CD8+ T cell exhaustion by multiple inhibitory receptors during chronic viral infection. *Nat Immunol* **10**, 29-37, doi:10.1038/ni.1679 (2009).
352 Woo, S. R. *et al.* Immune inhibitory molecules LAG-3 and PD-1 synergistically regulate T-cell function to promote tumoral immune escape. *Cancer Res* **72**, 917-927, doi:10.1158/0008-5472.CAN-11-1620 (2012).
353 Matsuzaki, J. *et al.* Tumor-infiltrating NY-ESO-1-specific CD8+ T cells are negatively regulated by LAG-3 and PD-1 in human ovarian cancer. *Proc Natl Acad Sci U S A* **107**, 7875-7880, doi:10.1073/pnas.1003345107 (2010).
354 Iwasaki, M. *et al.* Expression and function of PD-1 in human gammadelta T cells that recognize phosphoantigens. *Eur J Immunol* **41**, 345-355, doi:10.1002/eji.201040959 (2011).
355 Castella, B. *et al.* Anergic bone marrow Vgamma9Vdelta2 T cells as early and long-lasting markers of PD-1-targetable microenvironment-induced immune suppression in human myeloma. *Oncoimmunology* **4**, e1047580, doi:10.1080/2162402X.2015.1047580 (2015).
356 Hsu, H. *et al.* Prolonged PD1 Expression on Neonatal Vdelta2 Lymphocytes Dampens Proinflammatory Responses: Role of Epigenetic Regulation. *J Immunol* **197**, 1884-1892, doi:10.4049/jimmunol.1600284 (2016).
357 Hoeres, T., Holzmann, E., Smetak, M., Birkmann, J. & Wilhelm, M. PD-1 signaling modulates interferon-gamma production by Gamma Delta (gammadelta) T-Cells in response to leukemia. *Oncoimmunology* **8**, 1550618, doi:10.1080/2162402X.2018.1550618 (2019).
358 Casetti, R. *et al.* Cutting edge: TGF-beta1 and IL-15 Induce FOXP3+ gammadelta regulatory T cells in the presence of antigen stimulation. *J Immunol* **183**, 3574-3577, doi:10.4049/jimmunol.0901334 (2009).

359 Gogoi, D., Biswas, D., Borkakoty, B. & Mahanta, J. Exposure to Plasmodium vivax is associated with the increased expression of exhaustion markers on gammadelta T lymphocytes. *Parasite Immunol* **40**, e12594, doi:10.1111/pim.12594 (2018).
360 Belkina, A. C. *et al.* Multivariate Computational Analysis of Gamma Delta T Cell Inhibitory Receptor Signatures Reveals the Divergence of Healthy and ART-Suppressed HIV+ Aging. *Front Immunol* **9**, 2783, doi:10.3389/fimmu.2018.02783 (2018).
361 Maxwell, P. H. *et al.* The tumour suppressor protein VHL targets hypoxia-inducible factors for oxygen-dependent proteolysis. *Nature* **399**, 271-275, doi:10.1038/20459 (1999).
362 Semenza, G. L. Hydroxylation of HIF-1: oxygen sensing at the molecular level. *Physiology (Bethesda)* **19**, 176-182, doi:10.1152/physiol.00001.2004 (2004).
363 Vaupel, P., Briest, S. & Hockel, M. Hypoxia in breast cancer: pathogenesis, characterization and biological/therapeutic implications. *Wien Med Wochenschr* **152**, 334-342, doi:10.1046/j.1563-258x.2002.02032.x (2002).
364 Ye, I. C. *et al.* Molecular Portrait of Hypoxia in Breast Cancer: A Prognostic Signature and Novel HIF-Regulated Genes. *Mol Cancer Res* **16**, 1889-1901, doi:10.1158/1541-7786.MCR-18-0345 (2018).
365 Pescador, N. *et al.* Hypoxia promotes glycogen accumulation through hypoxia inducible factor (HIF)-mediated induction of glycogen synthase 1. *PLoS One* **5**, e9644, doi:10.1371/journal.pone.0009644 (2010).
366 Iyer, N. V. *et al.* Cellular and developmental control of O2 homeostasis by hypoxia-inducible factor 1 alpha. *Genes Dev* **12**, 149-162, doi:10.1101/gad.12.2.149 (1998).
367 Jing, X. *et al.* Role of hypoxia in cancer therapy by regulating the tumor microenvironment. *Mol Cancer* **18**, 157, doi:10.1186/s12943-019-1089-9 (2019).
368 Walsh, J. C. *et al.* The clinical importance of assessing tumor hypoxia: relationship of tumor hypoxia to prognosis and therapeutic opportunities. *Antioxid Redox Signal* **21**, 1516-1554, doi:10.1089/ars.2013.5378 (2014).
369 Du, R. *et al.* HIF1alpha induces the recruitment of bone marrow-derived vascular modulatory cells to regulate tumor angiogenesis and invasion. *Cancer Cell* **13**, 206-220, doi:10.1016/j.ccr.2008.01.034 (2008).
370 Lyden, D. *et al.* Impaired recruitment of bone-marrow-derived endothelial and hematopoietic precursor cells blocks tumor angiogenesis and growth. *Nat Med* **7**, 1194-1201, doi:10.1038/nm1101-1194 (2001).
371 Muz, B., de la Puente, P., Azab, F., Luderer, M. & Azab, A. K. Hypoxia promotes stem cell-like phenotype in multiple myeloma cells. *Blood Cancer J* **4**, e262, doi:10.1038/bcj.2014.82 (2014).
372 Hill, R. P., Marie-Egyptienne, D. T. & Hedley, D. W. Cancer stem cells, hypoxia and metastasis. *Semin Radiat Oncol* **19**, 106-111, doi:10.1016/j.semradonc.2008.12.002 (2009).
373 Semenza, G. L. Hypoxia-inducible factors: mediators of cancer progression and targets for cancer therapy. *Trends Pharmacol Sci* **33**, 207-214, doi:10.1016/j.tips.2012.01.005 (2012).
374 Frame, F. M. & Maitland, N. J. Cancer stem cells, models of study and implications of therapy resistance mechanisms. *Adv Exp Med Biol* **720**, 105-118, doi:10.1007/978-1-4614-0254-1_9 (2011).
375 Vaupel, P., Thews, O. & Hoeckel, M. Treatment resistance of solid tumors: role of hypoxia and anemia. *Med Oncol* **18**, 243-259, doi:10.1385/MO:18:4:243 (2001).
376 Brown, J. M. Tumor hypoxia in cancer therapy. *Methods Enzymol* **435**, 297-321, doi:10.1016/S0076-6879(07)35015-5 (2007).

377 Multhoff, G. & Vaupel, P. Hypoxia Compromises Anti-Cancer Immune Responses. *Adv Exp Med Biol* **1232**, 131-143, doi:10.1007/978-3-030-34461-0_18 (2020).
378 Tamura, R. *et al.* The role of vascular endothelial growth factor in the hypoxic and immunosuppressive tumor microenvironment: perspectives for therapeutic implications. *Med Oncol* **37**, 2, doi:10.1007/s12032-019-1329-2 (2019).
379 Kumar, V. & Gabrilovich, D. I. Hypoxia-inducible factors in regulation of immune responses in tumour microenvironment. *Immunology* **143**, 512-519, doi:10.1111/imm.12380 (2014).
380 Palazon, A., Aragones, J., Morales-Kastresana, A., de Landazuri, M. O. & Melero, I. Molecular pathways: hypoxia response in immune cells fighting or promoting cancer. *Clin Cancer Res* **18**, 1207-1213, doi:10.1158/1078-0432.CCR-11-1591 (2012).
381 Noman, M. Z., Messai, Y., Muret, J., Hasmim, M. & Chouaib, S. Crosstalk between CTC, Immune System and Hypoxic Tumor Microenvironment. *Cancer Microenviron* **7**, 153-160, doi:10.1007/s12307-014-0157-3 (2014).
382 Kim, H. *et al.* Engineering human tumor-specific cytotoxic T cells to function in a hypoxic environment. *Mol Ther* **16**, 599-606, doi:10.1038/sj.mt.6300391 (2008).
383 Atkuri, K. R., Herzenberg, L. A. & Herzenberg, L. A. Culturing at atmospheric oxygen levels impacts lymphocyte function. *Proc Natl Acad Sci U S A* **102**, 3756-3759, doi:10.1073/pnas.0409910102 (2005).
384 Neumann, A. K. *et al.* Hypoxia inducible factor 1 alpha regulates T cell receptor signal transduction. *Proc Natl Acad Sci U S A* **102**, 17071-17076, doi:10.1073/pnas.0506070102 (2005).
385 Chang, C. H. *et al.* Metabolic Competition in the Tumor Microenvironment Is a Driver of Cancer Progression. *Cell* **162**, 1229-1241, doi:10.1016/j.cell.2015.08.016 (2015).
386 Ho, P. C. *et al.* Phosphoenolpyruvate Is a Metabolic Checkpoint of Anti-tumor T Cell Responses. *Cell* **162**, 1217-1228, doi:10.1016/j.cell.2015.08.012 (2015).
387 Frauwirth, K. A. & Thompson, C. B. Regulation of T lymphocyte metabolism. *J Immunol* **172**, 4661-4665, doi:10.4049/jimmunol.172.8.4661 (2004).
388 Pauken, K. E. & Wherry, E. J. Overcoming T cell exhaustion in infection and cancer. *Trends Immunol* **36**, 265-276, doi:10.1016/j.it.2015.02.008 (2015).
389 Doedens, A. L. *et al.* Hypoxia-inducible factors enhance the effector responses of CD8(+) T cells to persistent antigen. *Nat Immunol* **14**, 1173-1182, doi:10.1038/ni.2714 (2013).
390 Caldwell, C. C. *et al.* Differential effects of physiologically relevant hypoxic conditions on T lymphocyte development and effector functions. *J Immunol* **167**, 6140-6149, doi:10.4049/jimmunol.167.11.6140 (2001).
391 Sukumar, M. *et al.* Inhibiting glycolytic metabolism enhances CD8+ T cell memory and antitumor function. *J Clin Invest* **123**, 4479-4488, doi:10.1172/JCI69589 (2013).
392 Sureshbabu, S. K., Chaukar, D. & Chiplunkar, S. V. Hypoxia regulates the differentiation and anti-tumor effector functions of gammadeltaT cells in oral cancer. *Clin Exp Immunol* **201**, 40-57, doi:10.1111/cei.13436 (2020).
393 Elia, A. R. *et al.* Human dendritic cells differentiated in hypoxia down-modulate antigen uptake and change their chemokine expression profile. *J Leukoc Biol* **84**, 1472-1482, doi:10.1189/jlb.0208082 (2008).
394 Mancino, A. *et al.* Divergent effects of hypoxia on dendritic cell functions. *Blood* **112**, 3723-3734, doi:10.1182/blood-2008-02-142091 (2008).

395 Balsamo, M. *et al.* Hypoxia downregulates the expression of activating receptors involved in NK-cell-mediated target cell killing without affecting ADCC. *Eur J Immunol* **43**, 2756-2764, doi:10.1002/eji.201343448 (2013).
396 Hughes, R. *et al.* Perivascular M2 Macrophages Stimulate Tumor Relapse after Chemotherapy. *Cancer Res* **75**, 3479-3491, doi:10.1158/0008-5472.CAN-14-3587 (2015).
397 Ohno, S. *et al.* Correlation of histological localization of tumor-associated macrophages with clinicopathological features in endometrial cancer. *Anticancer Res* **24**, 3335-3342 (2004).
398 Gabrilovich, D. Mechanisms and functional significance of tumour-induced dendritic-cell defects. *Nat Rev Immunol* **4**, 941-952, doi:10.1038/nri1498 (2004).
399 Serafini, P., Mgebroff, S., Noonan, K. & Borrello, I. Myeloid-derived suppressor cells promote cross-tolerance in B-cell lymphoma by expanding regulatory T cells. *Cancer Res* **68**, 5439-5449, doi:10.1158/0008-5472.CAN-07-6621 (2008).
400 Barsoum, I. B., Koti, M., Siemens, D. R. & Graham, C. H. Mechanisms of hypoxia-mediated immune escape in cancer. *Cancer Res* **74**, 7185-7190, doi:10.1158/0008-5472.CAN-14-2598 (2014).
401 Wrzesinski, S. H., Wan, Y. Y. & Flavell, R. A. Transforming growth factor-beta and the immune response: implications for anticancer therapy. *Clin Cancer Res* **13**, 5262-5270, doi:10.1158/1078-0432.CCR-07-1157 (2007).
402 Sethumadhavan, S. *et al.* Hypoxia and hypoxia-inducible factor (HIF) downregulate antigen-presenting MHC class I molecules limiting tumor cell recognition by T cells. *PLoS One* **12**, e0187314, doi:10.1371/journal.pone.0187314 (2017).
403 Murthy, A., Gerber, S. A., Koch, C. J. & Lord, E. M. Intratumoral Hypoxia Reduces IFN-gamma-Mediated Immunity and MHC Class I Induction in a Preclinical Tumor Model. *Immunohorizons* **3**, 149-160, doi:10.4049/immunohorizons.1900017 (2019).
404 Siemens, D. R. *et al.* Hypoxia increases tumor cell shedding of MHC class I chain-related molecule: role of nitric oxide. *Cancer Res* **68**, 4746-4753, doi:10.1158/0008-5472.CAN-08-0054 (2008).
405 Tawadros, A. I. F. & Khalafalla, M. M. M. Expression of programmed death-ligand 1 and hypoxia-inducible factor-1alpha proteins in endometrial carcinoma. *J Cancer Res Ther* **14**, S1063-S1069, doi:10.4103/0973-1482.202891 (2018).
406 Allan, I. M., Lunec, J., Salmon, M. & Bacon, P. A. Reactive oxygen species selectively deplete normal T lymphocytes via a hydroxyl radical dependent mechanism. *Scand J Immunol* **26**, 47-53 (1987).
407 Sitkovsky, M. & Lukashev, D. Regulation of immune cells by local-tissue oxygen tension: HIF1 alpha and adenosine receptors. *Nat Rev Immunol* **5**, 712-721, doi:10.1038/nri1685 (2005).
408 Dang, E. V. *et al.* Control of T(H)17/T(reg) balance by hypoxia-inducible factor 1. *Cell* **146**, 772-784, doi:10.1016/j.cell.2011.07.033 (2011).
409 Siegers, G. M. & Lamb, L. S., Jr. Cytotoxic and regulatory properties of circulating Vdelta1+ gammadelta T cells: a new player on the cell therapy field? *Molecular therapy : the journal of the American Society of Gene Therapy* **22**, 1416-1422, doi:10.1038/mt.2014.104 (2014).
410 Dieli, F. *et al.* Targeting human {gamma}delta} T cells with zoledronate and interleukin-2 for immunotherapy of hormone-refractory prostate cancer. *Cancer Res* **67**, 7450-7457, doi:10.1158/0008-5472.CAN-07-0199 (2007).

411 Lang, J. M. *et al.* Pilot trial of interleukin-2 and zoledronic acid to augment gammadelta T cells as treatment for patients with refractory renal cell carcinoma. *Cancer Immunol Immunother* **60**, 1447-1460, doi:10.1007/s00262-011-1049-8 (2011).
412 Siegers, G. M., Ribot, E. J., Keating, A. & Foster, P. J. Extensive expansion of primary human gamma delta T cells generates cytotoxic effector memory cells that can be labeled with Feraheme for cellular MRI. *Cancer Immunol Immunother* **62**, 571-583, doi:10.1007/s00262-012-1353-y (2013).
413 von Lilienfeld-Toal, M. *et al.* Activated gammadelta T cells express the natural cytotoxicity receptor natural killer p 44 and show cytotoxic activity against myeloma cells. *Clin Exp Immunol* **144**, 528-533, doi:10.1111/j.1365-2249.2006.03078.x (2006).
414 Rivas, A., Koide, J., Cleary, M. L. & Engleman, E. G. Evidence for involvement of the gamma, delta T cell antigen receptor in cytotoxicity mediated by human alloantigen-specific T cell clones. *J Immunol* **142**, 1840-1846 (1989).
415 Liu, Z., Guo, B. L., Gehrs, B. C., Nan, L. & Lopez, R. D. Ex vivo expanded human Vgamma9Vdelta2+ gammadelta-T cells mediate innate antitumor activity against human prostate cancer cells in vitro. *The Journal of urology* **173**, 1552-1556 (2005).
416 Chitadze, G. *et al.* NKG2D- and T-cell receptor-dependent lysis of malignant glioma cell lines by human gammadelta T cells: Modulation by temozolomide and A disintegrin and metalloproteases 10 and 17 inhibitors. *Oncoimmunology* **5** (2015).
417 Fisch, P. *et al.* Gamma/delta T cell clones and natural killer cell clones mediate distinct patterns of non-major histocompatibility complex-restricted cytolysis. *The Journal of experimental medicine* **171**, 1567-1579 (1990).
418 Lanca, T. *et al.* The MHC class Ib protein ULBP1 is a nonredundant determinant of leukemia/lymphoma susceptibility to gammadelta T-cell cytotoxicity. *Blood* **115**, 2407-2411, doi:10.1182/blood-2009-08-237123 (2010).
419 Maeurer, M. J. *et al.* Human intestinal Vdelta1+ lymphocytes recognize tumor cells of epithelial origin. *The Journal of experimental medicine* **183**, 1681-1696 (1996).
420 Dai, Y., Chen, H., Mo, C., Cui, L. & He, W. Ectopically expressed human tumor biomarker MutS homologue 2 is a novel endogenous ligand that is recognized by human gammadelta T cells to induce innate anti-tumor/virus immunity. *The Journal of biological chemistry* **287**, 16812-16819, doi:10.1074/jbc.M111.327650 (2012).
421 Janssen, O. *et al.* T cell receptor/CD3-signaling induces death by apoptosis in human T cell receptor gamma delta + T cells. *J Immunol* **146**, 35-39 (1991).
422 Fotedar, A. *et al.* Fine specificity of antigen recognition by T cell hybridoma clones specific for poly-18: a synthetic polypeptide antigen of defined sequence and conformation. *J Immunol* **135**, 3028-3033 (1985).
423 Band, H. *et al.* Immunochemical proof that a novel rearranging gene encodes the T cell receptor delta subunit. *Science* **238**, 682-684 (1987).
424 Borst, J. *et al.* Distinct molecular forms of human T cell receptor gamma/delta detected on viable T cells by a monoclonal antibody. *The Journal of experimental medicine* **167**, 1625-1644 (1988).
425 Koopman, G. *et al.* Annexin V for flow cytometric detection of phosphatidylserine expression on B cells undergoing apoptosis. *Blood* **84**, 1415-1420 (1994).
426 Russell, J. H., Rush, B., Weaver, C. & Wang, R. Mature T cells of autoimmune lpr/lpr mice have a defect in antigen-stimulated suicide. *Proc Natl Acad Sci U S A* **90**, 4409-4413 (1993).

427 Gan, Y. H., Lui, S. S. & Malkovsky, M. Differential susceptibility of naive and activated human gammadelta T cells to activation-induced cell death by T-cell receptor cross-linking. *Mol Med* **7**, 636-643 (2001).
428 Li, H. & David Pauza, C. Interplay of T-cell receptor and interleukin-2 signalling in Vgamma2Vdelta2 T-cell cytotoxicity. *Immunology* **132**, 96-103, doi:10.1111/j.1365-2567.2010.03343.x (2010).
429 Lenardo, M. J. Interleukin-2 programs mouse alpha beta T lymphocytes for apoptosis. *Nature* **353**, 858-861, doi:10.1038/353858a0 (1991).
430 Guo, B., Hollmig, K. & Lopez, R. D. In vitro activity of apoptosis-resistant human gd-T cells against solid malignances. *Journal of Clinical Oncology* **20**, 267 (abstract) (2001).
431 Koenecke, C. *et al.* In vivo application of mAb directed against the gammadelta TCR does not deplete but generates "invisible" gammadelta T cells. *European journal of immunology* **39**, 372-379, doi:10.1002/eji.200838741 (2009).
432 Bryant, N. L. *et al.* Characterization and Immunotherapeutic Potential of γδ T Cells in Patients with Glioblastoma *Neuro-Oncology* **In press** (2009).
433 Argentati, K. *et al.* Reduced number and impaired function of circulating gamma delta T cells in patients with cutaneous primary melanoma. *Journal of Investigative Dermatology.* **120**, 829-834 (2003).
434 Kabelitz, D. *et al.* Activation and activation-driven death of human gamma/delta T cells. *Immunol Rev* **120**, 71-88 (1991).
435 Vaupel, P., Hockel, M. & Mayer, A. Detection and characterization of tumor hypoxia using pO2 histography. *Antioxid Redox Signal* **9**, 1221-1235, doi:10.1089/ars.2007.1628 (2007).
436 Le, Q. T., Denko, N. C. & Giaccia, A. J. Hypoxic gene expression and metastasis. *Cancer Metastasis Rev* **23**, 293-310, doi:10.1023/B:CANC.0000031768.89246.d7 (2004).
437 Postovit, L. M., Adams, M. A., Lash, G. E., Heaton, J. P. & Graham, C. H. Oxygen-mediated regulation of tumor cell invasiveness. Involvement of a nitric oxide signaling pathway. *The Journal of biological chemistry* **277**, 35730-35737, doi:10.1074/jbc.M204529200 (2002).
438 Subarsky, P. & Hill, R. P. The hypoxic tumour microenvironment and metastatic progression. *Clin Exp Metastasis* **20**, 237-250 (2003).
439 Brizel, D. M. *et al.* Tumor oxygenation predicts for the likelihood of distant metastases in human soft tissue sarcoma. *Cancer Res* **56**, 941-943 (1996).
440 Brizel, D. M., Sibley, G. S., Prosnitz, L. R., Scher, R. L. & Dewhirst, M. W. Tumor hypoxia adversely affects the prognosis of carcinoma of the head and neck. *Int J Radiat Oncol Biol Phys* **38**, 285-289 (1997).
441 Semenza, G. L. Defining the role of hypoxia-inducible factor 1 in cancer biology and therapeutics. *Oncogene* **29**, 625-634, doi:10.1038/onc.2009.441 (2010).
442 Noman, M. Z. *et al.* Hypoxia: a key player in antitumor immune response. A Review in the Theme: Cellular Responses to Hypoxia. *Am J Physiol Cell Physiol* **309**, C569-579, doi:10.1152/ajpcell.00207.2015 (2015).
443 Barsoum, I. B. *et al.* Hypoxia induces escape from innate immunity in cancer cells via increased expression of ADAM10: role of nitric oxide. *Cancer Res* **71**, 7433-7441, doi:10.1158/0008-5472.CAN-11-2104 (2011).
444 Lo Presti, E., Dieli, F. & Meraviglia, S. Tumor-Infiltrating gammadelta T Lymphocytes: Pathogenic Role, Clinical Significance, and Differential Programing in the Tumor Microenvironment. *Front Immunol* **5**, 607, doi:10.3389/fimmu.2014.00607 (2014).

445 Chitadze, G., Oberg, H. H., Wesch, D. & Kabelitz, D. The Ambiguous Role of gammadelta T Lymphocytes in Antitumor Immunity. *Trends Immunol* **38**, 668-678, doi:10.1016/j.it.2017.06.004 (2017).
446 Dutta, I., Postovit, L. M. & Siegers, G. M. Apoptosis Induced via Gamma Delta T Cell Antigen Receptor "Blocking" Antibodies: A Cautionary Tale. *Front Immunol* **8**, 776, doi:10.3389/fimmu.2017.00776 (2017).
447 Tafreshi, N. K. *et al.* Evaluation of CAIX and CAXII Expression in Breast Cancer at Varied O2 Levels: CAIX is the Superior Surrogate Imaging Biomarker of Tumor Hypoxia. *Mol Imaging Biol* **18**, 219-231, doi:10.1007/s11307-015-0885-x (2016).
448 Jin, M. S. *et al.* Overexpression of HIF1alpha and CAXI predicts poor outcome in early-stage triple negative breast cancer. *Virchows Arch* **469**, 183-190, doi:10.1007/s00428-016-1953-6 (2016).
449 Tan, E. Y. *et al.* The key hypoxia regulated gene CAIX is upregulated in basal-like breast tumours and is associated with resistance to chemotherapy. *British journal of cancer* **100**, 405-411, doi:10.1038/sj.bjc.6604844 (2009).
450 Chia, S. K. *et al.* Prognostic significance of a novel hypoxia-regulated marker, carbonic anhydrase IX, in invasive breast carcinoma. *Journal of clinical oncology : official journal of the American Society of Clinical Oncology* **19**, 3660-3668, doi:10.1200/JCO.2001.19.16.3660 (2001).
451 Lu, J. *et al.* Human ovarian tumor cells escape gammadelta T cell recognition partly by down regulating surface expression of MICA and limiting cell cycle related molecules. *PloS one* **6**, e23348, doi:10.1371/journal.pone.0023348 (2011).
452 Lamb, L. S., Jr. & Lopez, R. D. gammadelta T cells: a new frontier for immunotherapy? *Biol Blood Marrow Transplant* **11**, 161-168, doi:10.1016/j.bbmt.2004.11.015 (2005).
453 Gomes, A. Q., Martins, D. S. & Silva-Santos, B. Targeting gammadelta T lymphocytes for cancer immunotherapy: from novel mechanistic insight to clinical application. *Cancer Res* **70**, 10024-10027, doi:10.1158/0008-5472.CAN-10-3236 (2010).
454 Hannani, D. *et al.* Harnessing gammadelta T cells in anticancer immunotherapy. *Trends in immunology* **33**, 199-206, doi:10.1016/j.it.2012.01.006 (2012).
455 Kabelitz, D., Wesch, D., Pitters, E. & Zoller, M. Potential of human gammadelta T lymphocytes for immunotherapy of cancer. *International journal of cancer. Journal international du cancer* **112**, 727-732, doi:10.1002/ijc.20445 (2004).
456 Scheper, W., Sebestyen, Z. & Kuball, J. Cancer Immunotherapy Using gammadeltaT Cells: Dealing with Diversity. *Frontiers in immunology* **5**, 601, doi:10.3389/fimmu.2014.00601 (2014).
457 Jungbluth, A. A. *et al.* Immunohistochemical Detection of γ/δ T Lymphocytes in Formalin-fixed Paraffin-embedded Tissues. *Applied Immunohistochemistry & Molecular Morphology* **Publish Ahead of Print**, doi:10.1097/pai.0000000000000650 (2018).
458 Holliday, D. L. & Speirs, V. Choosing the right cell line for breast cancer research. *Breast cancer research : BCR* **13**, 215, doi:10.1186/bcr2889 (2011).
459 Lafont, V. *et al.* Plasticity of gammadelta T Cells: Impact on the Anti-Tumor Response. *Frontiers in immunology* **5**, 622, doi:10.3389/fimmu.2014.00622 (2014).
460 Carding, S. R. & Egan, P. J. Gammadelta T cells: functional plasticity and heterogeneity. *Nature reviews. Immunology* **2**, 336-345, doi:10.1038/nri797 (2002).
461 Trastour, C. *et al.* HIF-1alpha and CA IX staining in invasive breast carcinomas: prognosis and treatment outcome. *International journal of cancer. Journal international du cancer* **120**, 1451-1458, doi:10.1002/ijc.22436 (2007).

462 Ma, C. *et al.* Tumor-Infiltrating gammadelta T Lymphocytes Predict Clinical Outcome in Human Breast Cancer. *J Immunol*, doi:10.4049/jimmunol.1201892 (2012).
463 Choi, J., Jung, W. H. & Koo, J. S. Metabolism-related proteins are differentially expressed according to the molecular subtype of invasive breast cancer defined by surrogate immunohistochemistry. *Pathobiology* **80**, 41-52, doi:10.1159/000339513 (2013).
464 Dieli, F. *et al.* Differentiation of effector/memory Vdelta2 T cells and migratory routes in lymph nodes or inflammatory sites. *The Journal of experimental medicine* **198**, 391-397, doi:10.1084/jem.20030235 (2003).
465 Naldini, A., Carraro, F., Silvestri, S. & Bocci, V. Hypoxia affects cytokine production and proliferative responses by human peripheral mononuclear cells. *J Cell Physiol* **173**, 335-342, doi:10.1002/(SICI)1097-4652(199712)173:3<335::AID-JCP5>3.0.CO;2-O (1997).
466 Dyugovskaya, L., Lavie, P. & Lavie, L. Phenotypic and functional characterization of blood gammadelta T cells in sleep apnea. *Am J Respir Crit Care Med* **168**, 242-249, doi:10.1164/rccm.200210-1226OC (2003).
467 Tikhonov, I. *et al.* Human Vgamma2Vdelta2 T cells contain cytoplasmic RANTES. *Int Immunol* **18**, 1243-1251, doi:10.1093/intimm/dxl055 (2006).
468 Caux, C. *et al.* Dendritic cell biology and regulation of dendritic cell trafficking by chemokines. *Springer Semin Immunopathol* **22**, 345-369 (2000).
469 Sozzani, S., Allavena, P., Vecchi, A. & Mantovani, A. Chemokines and dendritic cell traffic. *J Clin Immunol* **20**, 151-160 (2000).
470 Soria, G. & Ben-Baruch, A. The inflammatory chemokines CCL2 and CCL5 in breast cancer. *Cancer Lett* **267**, 271-285, doi:10.1016/j.canlet.2008.03.018 (2008).
471 Hudspeth, K. *et al.* Engagement of NKp30 on Vdelta1 T cells induces the production of CCL3, CCL4, and CCL5 and suppresses HIV-1 replication. *Blood* **119**, 4013-4016, doi:10.1182/blood-2011-11-390153 (2012).
472 Yamada, M. *et al.* CD40-CD40 ligand (CD154) engagement is required but not sufficient for modulating MHC class I, ICAM-1 and Fas expression and proliferation of human non-small cell lung tumors. *International journal of cancer. Journal international du cancer* **92**, 589-599 (2001).
473 Alexandroff, A. B. *et al.* Role for CD40-CD40 ligand interactions in the immune response to solid tumours. *Mol Immunol* **37**, 515-526 (2000).
474 Tong, A. W. *et al.* Growth-inhibitory effects of CD40 ligand (CD154) and its endogenous expression in human breast cancer. *Clinical cancer research : an official journal of the American Association for Cancer Research* **7**, 691-703 (2001).
475 Hirano, A. *et al.* Inhibition of human breast carcinoma growth by a soluble recombinant human CD40 ligand. *Blood* **93**, 2999-3007 (1999).
476 Deng, W. *et al.* Antitumor immunity. A shed NKG2D ligand that promotes natural killer cell activation and tumor rejection. *Science* **348**, 136-139, doi:10.1126/science.1258867 (2015).
477 Ye, J. *et al.* Tumor-derived gammadelta regulatory T cells suppress innate and adaptive immunity through the induction of immunosenescence. *J Immunol* **190**, 2403-2414, doi:10.4049/jimmunol.1202369 (2013).
478 Ye, J. *et al.* Specific recruitment of gammadelta regulatory T cells in human breast cancer. *Cancer Res* **73**, 6137-6148, doi:10.1158/0008-5472.CAN-13-0348 (2013).
479 Siegel, R. L., Miller, K. D. & Jemal, A. Cancer statistics, 2019. *CA Cancer J Clin* **69**, 7-34, doi:10.3322/caac.21551 (2019).

480 Velasco-Velazquez, M. A., Popov, V. M., Lisanti, M. P. & Pestell, R. G. The role of breast cancer stem cells in metastasis and therapeutic implications. *Am J Pathol* **179**, 2-11, doi:10.1016/j.ajpath.2011.03.005 (2011).
481 Wang, H. *et al.* CD44(+)/CD24(-) phenotype predicts a poor prognosis in triple-negative breast cancer. *Oncol Lett* **14**, 5890-5898, doi:10.3892/ol.2017.6959 (2017).
482 Dhar, P. & Wu, J. D. NKG2D and its ligands in cancer. *Curr Opin Immunol* **51**, 55-61, doi:10.1016/j.coi.2018.02.004 (2018).
483 Peters, C. *et al.* TGF-beta enhances the cytotoxic activity of Vdelta2 T cells. *Oncoimmunology* **8**, e1522471, doi:10.1080/2162402X.2018.1522471 (2019).
484 Wexler, H. Accurate identification of experimental pulmonary metastases. *J Natl Cancer Inst* **36**, 641-645, doi:10.1093/jnci/36.4.641 (1966).
485 Dieters-Castator, D. Z. *et al.* Proteomics-Derived Biomarker Panel Improves Diagnostic Precision to Classify Endometrioid and High-grade Serous Ovarian Carcinoma. *Clin Cancer Res* **25**, 4309-4319, doi:10.1158/1078-0432.CCR-18-3818 (2019).
486 Cox, J. & Mann, M. MaxQuant enables high peptide identification rates, individualized p.p.b.-range mass accuracies and proteome-wide protein quantification. *Nat Biotechnol* **26**, 1367-1372, doi:10.1038/nbt.1511 (2008).
487 Safa, A. R. Resistance to Cell Death and Its Modulation in Cancer Stem Cells. *Crit Rev Oncog* **21**, 203-219, doi:10.1615/CritRevOncog.2016016976 (2016).
488 Fournie, J. J. *et al.* What lessons can be learned from gammadelta T cell-based cancer immunotherapy trials? *Cell Mol Immunol* **10**, 35-41, doi:10.1038/cmi.2012.39 (2013).
489 Chen, H. C. *et al.* Synergistic targeting of breast cancer stem-like cells by human gammadelta T cells and CD8(+) T cells. *Immunol Cell Biol* **95**, 620-629, doi:10.1038/icb.2017.21 (2017).
490 Meraviglia, S. *et al.* Distinctive features of tumor-infiltrating gammadelta T lymphocytes in human colorectal cancer. *Oncoimmunology* **6**, e1347742, doi:10.1080/2162402X.2017.1347742 (2017).
491 Stovgaard, E. S., Dyhl-Polk, A., Roslind, A., Balslev, E. & Nielsen, D. PD-L1 expression in breast cancer: expression in subtypes and prognostic significance: a systematic review. *Breast Cancer Res Treat* **174**, 571-584, doi:10.1007/s10549-019-05130-1 (2019).
492 Dondero, A. *et al.* PD-L1 expression in metastatic neuroblastoma as an additional mechanism for limiting immune surveillance. *Oncoimmunology* **5**, e1064578, doi:10.1080/2162402X.2015.1064578 (2016).
493 Hermanson, D. L., Das, S. G., Li, Y. & Xing, C. Overexpression of Mcl-1 confers multidrug resistance, whereas topoisomerase IIbeta downregulation introduces mitoxantrone-specific drug resistance in acute myeloid leukemia. *Mol Pharmacol* **84**, 236-243, doi:10.1124/mol.113.086140 (2013).
494 Senichkin, V. V., Streletskaia, A. Y., Gorbunova, A. S., Zhivotovsky, B. & Kopeina, G. S. Saga of Mcl-1: regulation from transcription to degradation. *Cell Death Differ* **27**, 405-419, doi:10.1038/s41418-019-0486-3 (2020).
495 Ness-Schwickerath, K. J., Jin, C. & Morita, C. T. Cytokine requirements for the differentiation and expansion of IL-17A- and IL-22-producing human Vgamma2Vdelta2 T cells. *J Immunol* **184**, 7268-7280, doi:10.4049/jimmunol.1000600 (2010).
496 Zhang, J., Basher, F. & Wu, J. D. NKG2D Ligands in Tumor Immunity: Two Sides of a Coin. *Front Immunol* **6**, 97, doi:10.3389/fimmu.2015.00097 (2015).
497 Smith, K. A. Interleukin-2: inception, impact, and implications. *Science* **240**, 1169-1176, doi:10.1126/science.3131876 (1988).

498 Powell, J. D., Ragheb, J. A., Kitagawa-Sakakida, S. & Schwartz, R. H. Molecular regulation of interleukin-2 expression by CD28 co-stimulation and anergy. *Immunol Rev* **165**, 287-300, doi:10.1111/j.1600-065x.1998.tb01246.x (1998).
499 Arenas-Ramirez, N., Woytschak, J. & Boyman, O. Interleukin-2: Biology, Design and Application. *Trends Immunol* **36**, 763-777, doi:10.1016/j.it.2015.10.003 (2015).
500 Dai, Z., Arakelov, A., Wagener, M., Konieczny, B. T. & Lakkis, F. G. The role of the common cytokine receptor gamma-chain in regulating IL-2-dependent, activation-induced CD8+ T cell death. *J Immunol* **163**, 3131-3137 (1999).
501 Refaeli, Y., Van Parijs, L., London, C. A., Tschopp, J. & Abbas, A. K. Biochemical mechanisms of IL-2-regulated Fas-mediated T cell apoptosis. *Immunity* **8**, 615-623, doi:10.1016/s1074-7613(00)80566-x (1998).
502 Zheng, L., Trageser, C. L., Willerford, D. M. & Lenardo, M. J. T cell growth cytokines cause the superinduction of molecules mediating antigen-induced T lymphocyte death. *J Immunol* **160**, 763-769 (1998).
503 Kim, H., Lin, Q., Glazer, P. M. & Yun, Z. The hypoxic tumor microenvironment in vivo selects the cancer stem cell fate of breast cancer cells. *Breast Cancer Res* **20**, 16, doi:10.1186/s13058-018-0944-8 (2018).
504 Muz, B., de la Puente, P., Azab, F. & Azab, A. K. The role of hypoxia in cancer progression, angiogenesis, metastasis, and resistance to therapy. *Hypoxia (Auckl)* **3**, 83-92, doi:10.2147/HP.S93413 (2015).
505 Ou, Z. L. *et al.* Hypoxia-induced shedding of MICA and HIF1A-mediated immune escape of pancreatic cancer cells from NK cells: role of circ_0000977/miR-153 axis. *RNA Biol* **16**, 1592-1603, doi:10.1080/15476286.2019.1649585 (2019).
506 Chen, J. Y., Lin, C. H. & Chen, B. C. Hypoxia-induced ADAM 17 expression is mediated by RSK1-dependent C/EBPbeta activation in human lung fibroblasts. *Mol Immunol* **88**, 155-163, doi:10.1016/j.molimm.2017.06.029 (2017).
507 Nakagawa, Y. *et al.* Effects of extracellular pH and hypoxia on the function and development of antigen-specific cytotoxic T lymphocytes. *Immunol Lett* **167**, 72-86, doi:10.1016/j.imlet.2015.07.003 (2015).
508 Vuillefroy de Silly, R. *et al.* Phenotypic switch of CD8(+) T cells reactivated under hypoxia toward IL-10 secreting, poorly proliferative effector cells. *Eur J Immunol* **45**, 2263-2275, doi:10.1002/eji.201445284 (2015).
509 Gropper, Y. *et al.* Culturing CTLs under Hypoxic Conditions Enhances Their Cytolysis and Improves Their Anti-tumor Function. *Cell Rep* **20**, 2547-2555, doi:10.1016/j.celrep.2017.08.071 (2017).
510 Wowk, M. E. & Trapani, J. A. Cytotoxic activity of the lymphocyte toxin granzyme B. *Microbes Infect* **6**, 752-758, doi:10.1016/j.micinf.2004.03.008 (2004).
511 Palomeras, S., Ruiz-Martinez, S. & Puig, T. Targeting Breast Cancer Stem Cells to Overcome Treatment Resistance. *Molecules* **23**, doi:10.3390/molecules23092193 (2018).
512 Yang, L. *et al.* Targeting cancer stem cell pathways for cancer therapy. *Signal Transduct Target Ther* **5**, 8, doi:10.1038/s41392-020-0110-5 (2020).
513 Sun, H. R. *et al.* Therapeutic Strategies Targeting Cancer Stem Cells and Their Microenvironment. *Front Oncol* **9**, 1104, doi:10.3389/fonc.2019.01104 (2019).
514 Hu, J., Li, G., Zhang, P., Zhuang, X. & Hu, G. A CD44v(+) subpopulation of breast cancer stem-like cells with enhanced lung metastasis capacity. *Cell Death Dis* **8**, e2679, doi:10.1038/cddis.2017.72 (2017).

515 Kassim, S. K. *et al.* Vascular endothelial growth factor and interleukin-8 are associated with poor prognosis in epithelial ovarian cancer patients. *Clin Biochem* **37**, 363-369, doi:10.1016/j.clinbiochem.2004.01.014 (2004).
516 Waugh, D. J. & Wilson, C. The interleukin-8 pathway in cancer. *Clin Cancer Res* **14**, 6735-6741, doi:10.1158/1078-0432.CCR-07-4843 (2008).
517 Toia, F. *et al.* Gammadelta T Cell-Based Immunotherapy in Melanoma: State of the Art. *J Oncol* **2019**, 9014607, doi:10.1155/2019/9014607 (2019).
518 Zumwalde, N. A. *et al.* Adoptively transferred Vgamma9Vdelta2 T cells show potent antitumor effects in a preclinical B cell lymphomagenesis model. *JCI Insight* **2**, doi:10.1172/jci.insight.93179 (2017).
519 Chikuma, S. *et al.* PD-1-mediated suppression of IL-2 production induces CD8+ T cell anergy in vivo. *J Immunol* **182**, 6682-6689, doi:10.4049/jimmunol.0900080 (2009).
520 Jubel, J. M., Barbati, Z. R., Burger, C., Wirtz, D. C. & Schildberg, F. A. The Role of PD-1 in Acute and Chronic Infection. *Front Immunol* **11**, 487, doi:10.3389/fimmu.2020.00487 (2020).
521 Agata, Y. *et al.* Expression of the PD-1 antigen on the surface of stimulated mouse T and B lymphocytes. *Int Immunol* **8**, 765-772, doi:10.1093/intimm/8.5.765 (1996).
522 Mognol, G. P. *et al.* Exhaustion-associated regulatory regions in CD8(+) tumor-infiltrating T cells. *Proc Natl Acad Sci U S A* **114**, E2776-E2785, doi:10.1073/pnas.1620498114 (2017).
523 Fernandez-Poma, S. M. *et al.* Expansion of Tumor-Infiltrating CD8(+) T cells Expressing PD-1 Improves the Efficacy of Adoptive T-cell Therapy. *Cancer Res* **77**, 3672-3684, doi:10.1158/0008-5472.CAN-17-0236 (2017).
524 Zhou, Q. *et al.* Blockade of programmed death-1 pathway rescues the effector function of tumor-infiltrating T cells and enhances the antitumor efficacy of lentivector immunization. *J Immunol* **185**, 5082-5092, doi:10.4049/jimmunol.1001821 (2010).
525 Ngiow, S. F. *et al.* A Threshold Level of Intratumor CD8+ T-cell PD1 Expression Dictates Therapeutic Response to Anti-PD1. *Cancer Res* **75**, 3800-3811, doi:10.1158/0008-5472.CAN-15-1082 (2015).
526 Thomas, L. W., Lam, C. & Edwards, S. W. Mcl-1; the molecular regulation of protein function. *FEBS Lett* **584**, 2981-2989, doi:10.1016/j.febslet.2010.05.061 (2010).
527 Raina, K. *et al.* PROTAC-induced BET protein degradation as a therapy for castration-resistant prostate cancer. *Proc Natl Acad Sci U S A* **113**, 7124-7129, doi:10.1073/pnas.1521738113 (2016).
528 Nabet, B. *et al.* The dTAG system for immediate and target-specific protein degradation. *Nat Chem Biol* **14**, 431-441, doi:10.1038/s41589-018-0021-8 (2018).
529 Holdenrieder, S. *et al.* Soluble MICB in malignant diseases: analysis of diagnostic significance and correlation with soluble MICA. *Cancer Immunol Immunother* **55**, 1584-1589, doi:10.1007/s00262-006-0167-1 (2006).
530 Skov, S. *et al.* Cancer cells become susceptible to natural killer cell killing after exposure to histone deacetylase inhibitors due to glycogen synthase kinase-3-dependent expression of MHC class I-related chain A and B. *Cancer Res* **65**, 11136-11145, doi:10.1158/0008-5472.CAN-05-0599 (2005).
531 Armeanu, S. *et al.* Natural killer cell-mediated lysis of hepatoma cells via specific induction of NKG2D ligands by the histone deacetylase inhibitor sodium valproate. *Cancer Res* **65**, 6321-6329, doi:10.1158/0008-5472.CAN-04-4252 (2005).

532 Huang, B., Sikorski, R., Sampath, P. & Thorne, S. H. Modulation of NKG2D-ligand cell surface expression enhances immune cell therapy of cancer. *J Immunother* **34**, 289-296, doi:10.1097/CJI.0b013e31820e1b0d (2011).
533 Kaiser, B. K. *et al.* Disulphide-isomerase-enabled shedding of tumour-associated NKG2D ligands. *Nature* **447**, 482-486, doi:10.1038/nature05768 (2007).
534 Ferrari de Andrade, L. *et al.* Antibody-mediated inhibition of MICA and MICB shedding promotes NK cell-driven tumor immunity. *Science* **359**, 1537-1542, doi:10.1126/science.aao0505 (2018).
535 Ludwig, A. *et al.* Metalloproteinase inhibitors for the disintegrin-like metalloproteinases ADAM10 and ADAM17 that differentially block constitutive and phorbol ester-inducible shedding of cell surface molecules. *Comb Chem High Throughput Screen* **8**, 161-171, doi:10.2174/1386207053258488 (2005).
536 Dreymueller, D., Uhlig, S. & Ludwig, A. ADAM-family metalloproteinases in lung inflammation: potential therapeutic targets. *Am J Physiol Lung Cell Mol Physiol* **308**, L325-343, doi:10.1152/ajplung.00294.2014 (2015).
537 Witters, L. *et al.* Synergistic inhibition with a dual epidermal growth factor receptor/HER-2/neu tyrosine kinase inhibitor and a disintegrin and metalloprotease inhibitor. *Cancer Res* **68**, 7083-7089, doi:10.1158/0008-5472.CAN-08-0739 (2008).
538 Newton, R. C. *et al.* Clinical benefit of INCB7839, a potent and selective ADAM inhibitor, in combination with trastuzumab in patients with metastatic HER2+ breast cancer. *Journal of Clinical Oncology* **28**, 3025-3025, doi:10.1200/jco.2010.28.15_suppl.3025 (2010).
539 Wetzel, S., Seipold, L. & Saftig, P. The metalloproteinase ADAM10: A useful therapeutic target? *Biochim Biophys Acta Mol Cell Res* **1864**, 2071-2081, doi:10.1016/j.bbamcr.2017.06.005 (2017).
540 Moss, M. L. & Minond, D. Recent Advances in ADAM17 Research: A Promising Target for Cancer and Inflammation. *Mediators Inflamm* **2017**, 9673537, doi:10.1155/2017/9673537 (2017).
541 Wolpert, F., Tritschler, I., Steinle, A., Weller, M. & Eisele, G. A disintegrin and metalloproteinases 10 and 17 modulate the immunogenicity of glioblastoma-initiating cells. *Neuro Oncol* **16**, 382-391, doi:10.1093/neuonc/not232 (2014).
542 Barsoum, I. B., Smallwood, C. A., Siemens, D. R. & Graham, C. H. A mechanism of hypoxia-mediated escape from adaptive immunity in cancer cells. *Cancer Res* **74**, 665-674, doi:10.1158/0008-5472.CAN-13-0992 (2014).

Chapter 7 Appendix

Appendix Table 1.1. Subset percentages and purities of donor-derived γδ T cell cultures used in chapter 4. Donors are listed in order of appearance of the first γδ T cell culture from that donor in the figures. Flow refers to the day cells were harvested, stained with fixable viability dye followed by the following antibodies: pan γδ TCR, Vδ1 TCR and Vδ2 TCR, after which they were washed and fixed; samples were acquired by flow cytometry within one week. The purity is calculated as the sum of %Vδ1, %Vδ2 and %γδTCR+Vδ1-Vδ2-. Day 0 percentages are for γδ T cell subsets within the mononuclear cell fraction isolated from peripheral blood. Day indicates the day on which the experiment(s) listed in the figure panel ended and cells were harvested for analysis. Their use in experiments for figures in this manuscript are listed in the order in which they appear.

ID	Flow	%Vδ1	%Vδ2	% γδ+Vδ1-Vδ2-	% Purity	Day	Figure(s)
1-1	0	0.9	1.1	1.6	3.6		
	19	24.1	34.1	7.2	65.4	20	1A, S1M-1
						21	5A-C, S5G
1-2	0	0.8	0.9	0.8	2.5		
	19	28.5	50.5	6.0	85.0	21	1D, S1P-2, S3L, S8J
1-3	0	0.6	0.6	0.9	2.1		
	21	43.3	43.6	7.3	94.3	18	1E
1-4	21	69.4	12.8	8.4	90.6	19	S3M
						21	5I, S5W
1-5	0	0.9	1.1	1.5	3.5		
	22	69.0	6.6	16.9	92.5	20	S8H
1-6	0	1.0	1.0	1.2	3.2		
	21	26.3	50.6	3.5	80.4	19	S8Q,R
2-1	0	0.8	4.7	0.3	5.8		
	22	1.8	92.4	1.6	95.8	22	1A, S1M-2
2-2	0	0.2	2.7	0.5	3.4		
	21	0.9	94.3	1.4	96.6	19	S1Q-1
						20	S5C
2-3	0	0.2	1.0	0.2	1.4		
	21	0.8	94	1.6	96.4	18	2A,B, S2C, S2G, S8F,G
						21	3E-H, S3E,H,J,P,S, S8I, L,M
2-4	0	0.1	1.0	0.1	1.2		
	21	1.3	88.1	2.7	92.1	21	3I,J, 5D, S3T,U,S5K
						20	4E-J, S4O,S, S5H
2-5	0	0.2	4.6	0.1	4.9		
	21	1.1	94.4	1.3	96.8	21	S8H
3-1	0	1.3	2.3	0.1	3.7		
	21	11.0	77.9	3.7	92.6	20	1A, S1M-3
3-2	0	1.3	2.0	2.7	6.0		
	21	53.5	23.8	13.2	90.5	21	1D, S1P-1
3-3	0	1.2	1.9	5.2	8.3		
	24	29.0	50.5	13.4	92.9	20	2B, S2D
						21	S3F,I,J, S8I
						19	S5C
4-1	0	0.4	7.2	0.6	8.2		
	21	52.2	4.0	14.7	70.9	21	1B, S1N-1, S8Q,R
4-2	0	1.7	1.9	2.3	5.9		
	21	8.0	77.1	1.5	86.6	21	2C,E,F
						20	S8H
						22	S8J
4-3	0	1.9	2.4	1.9	6.2		
	21	30.0	29.8	22.0	81.8	20	2E,F, S2I
5-1	0	1.2	2.3	0.7	4.2		
	22	41.2	47.1	7.0	95.3	22	1B, S1N-2

ID	Flow	%Vδ1	%Vδ2	% γδ+Vδ1-Vδ2-	% Purity	Day	Figure(s)
5-2	0	1.0	1.9	0.5	3.4		
	21	23.2	69.4	5.5	98.1	20	5A,B, S5A,B
						21	5A-C, S5E
6-1	0	0.5	1.4	0.7	2.6		
	21	29.2	56.4	6.1	91.7	20	1B,C, S1N-3,O-1, S8C
6-2	22	13.4	71.5	5.2	90.1	22	S3L
7-1	0	0.6	3.0	0.4	4.0		
	21	21.9	73.4	4.2	99.5	20	1B, S1N-4, S8Q,R
						18	1C, S1O-2
7-2	0	0.6	2.1	0.9	3.6		
	21	40.0	44.2	7.7	91.9	18	S1Q-2
7-3	0	0.7	1.3	1.0	3.0		
	21	4.9	1.2	91.1	97.2	19	2E,F, S2H, S8H
7-4	0	0.6	2.2	0.4	3.2		
	21	0.6	81.3	8.6	90.5	18	3K,L, S3V,AA, S8N
						21	4I,J, 5F,G, S4M,Q, S5N-3,O-2
7-5	0	0.5	3.3	0.7	4.5		
	20	14.0	74.4	2.1	90.5	21	S5A
7-6	0	0.6	3.3	1.1	5.0		
	18	14.8	67.8	2.4	85.0	22	S8B
8-1	0	2.4	0.6	0.8	3.8		
	20	28.0	52.3	7.2	87.5	20	1C, S1O-3
8-2	0	2.3	0.5	1.1	3.9		
	19	16.4	74.6	2.3	93.3	20	S3K-M, S8J
						21	1D, S1P-4
8-3	0	2.1	0.6	1.8	4.5		
	20	32.3	27.4	12.3	72.0	22	4J, S4P
8-4	20	45.1	33.3	6.9	85.3	19	7J,K, S7L,O
9-1	0	0.2	1.7	2.1	4.0		
	20	17.4	71.7	2.3	91.4	20	1D, S1P-3, S3L, S8J
9-2	21	1.6	87.2	9.0	97.8	20	1F
9-3	22	8.4	85.2	3.7	97.3	19	2D, 5D, S5H,I
						22	4F, S4I, S8P, S8T
9-4	0	0.1	1.8	3.6	5.5		
	21	7.0	84.5	5.1	96.6	18	3C-H, S3O,R, S8K-M
						20	S5C
						22	S5U
9-5	0	0.3	1.6	0.2	2.1		
	22	4.0	87.2	2.8	94.0	22	4L, S4Y
9-6	0	2.5	0.3	2.0	4.8		
	21	2.5	92.4	3.3	98.2	20	7J,K, S7K,N
10-1	0	0.5	1.0	0.3	1.8		
	21	1.9	94.1	1.7	97.7	21	2A,B, S2A, S2E, S8D,G
11-1	0	1.7	2.0	0.2	3.9		
	21	10.3	75.9	3.3	89.5	21	2A,B, S2B, S2F, S8E,G
11-2	18	11.1	76.9	2.5	90.5	20	4K,L, S2J, S4V,X, S5T
11-3	21	16.5	60.8	11.3	88.6	20	5D, S5H,J

ID	Flow	%Vδ1	%Vδ2	% γδ+Vδ1-Vδ2-	% Purity	Day	Figure(s)
12	0	3.1	0.9	1.4	5.4		
	21	60.2	6.0	20.3	86.5	19	S2K
13-1	0	0.6	1.0	2.4	4.0		
	21	9.4	81.7	4.8	95.9	21	3A-H, S3A-D,G,J,N S8I,K-M
13-2	0	0.6	1.5	0.3	2.4		
	20	17.6	72.0	2.1	91.7	19	S3M
						21	5H
13-3	0	0.7	1.0	0.5	2.2		
	21	4.0	87.6	3.5	95.1	18	3K,L, S3X,Z, S8N
						20	4F,H-L, 5F,G, S4J,L,N,R,U,W, S5O-2,O-1,R
13-4	0	0.6	0.9	0.4	1.9		
	21	21.1	64.3	1.8	87.2	20	4H, S4K
13-5	0	2.0	0.5	1.0	3.5		
	21	46.0	42.2	7.4	95.6	20	S5S
13-6	0	0.8	1.1	0.8	2.7		
	20	16.2	79.2	2.2	97.6	20	7J,K, S7M,P
14	0	2.0	0.9	0.2	3.1		
	20	4.5	88.0	3.9	96.4	20	3I,J, 5E-G, S3T,U, S5P
15	0	0.1	1.9	0.3	2.3		
	21	0.1	87.9	2.6	90.6	20	3I,J, 5F,I, S3T,U, S5O-1
						21	S5V
16	0	0.5	1.1	0.3	1.9		
	20	17.8	68.5	3.4	89.7	20	5A-C, S5A,B,D
17	0	0.2	1.3	0.1	1.6		
	20	16.4	62.5	4.8	83.7	19	5A-C, S5B,F
						20	S8C
18	23	9.9	65.9	9.4	85.2	20	5I, S5X
19-1	0	1.4	3.2	0.9	5.5		
	20	70.0	14.9	11.5	96.4	21	S8B
19-2	0	2.8	4.8	0.1	7.7		
	21	49.1	32.2	8.7	90.0	20	S8B
20-1	0	4.3	1.2	1.0	6.5		
	21	49.4	32.0	7.3	88.7	21	S8B
20-2	0	5.3	1.6	1.2	8.1		
	20	24.4	64.6	7.5	96.5	19	S8C

Appendix Table 1.2.Statistical tests employed and resulting p-values for experiments shown in Figures 4.1-7. Bonf=Bonferroni's multiple comparisons test; E:T=effector:target ratio; F=failed; L=left panel; R=right panel; RM=repeated measures; S-W=Shapiro-Wilk Normality test; Tukey=Tukey's multiple comparisons test.

Figure	S-W	Test	Sample Comparison	p-value
1A	All passed	Two-way ANOVA	CD24-/CD24+	0.0054
1B	All passed	Two-way ANOVA, Sidak	3D/2D 10:1	0.0261
1C	All passed	Simple Linear Regression	γδTc vs. SUM149/SUM149	0.0093
1D	All passed	Two-way ANOVA, Sidak	3D/2D 20:1	0.0666
1E	All failed	Simple Linear Regression	γδTc vs. PDX401/PDX401	<0.0001
1F	All passed	Unpaired 1-tailed t-test	SUM149 post-γδTc/SUM149	0.0110
2A	All passed	Paired 2-tailed t-test	CD24-/CD24+	0.0361
2B	F: 2D	Wilcoxon	3D/2D	0.1250
2C	n=2, too small	One-way ANOVA, Tukey	γδTc + CD24-/γδTc, a-a	0.6871
			γδTc + CD24+/γδTc, a-b	<0.0001
			γδTc + CD24-/ γδTc + CD24+, a-b	<0.0001
2D	n=2, too small	One-way ANOVA, Tukey	γδTc + 3D/γδTc, a-a	0.9994
			γδTc + 2D/γδTc, a-b	0.0011
			γδTc + 3D/ γδTc + 2D, a-b	0.0010
2E	All passed	1-tail ratio paired t-test	γδTc + CD24-/ γδTc + CD24+	0.0071
2F	F: γδTc + 3D	Wilcoxon	γδTc + 3D/ γδTc + 2D	0.1250
3B	All passed	One-way ANOVA, Sidak	CD24-/CD24+	0.7216
			3D/2D	0.9414
3C	n=2, too small	No test performed		
3D	n=2, too small	No test performed		
3E	All passed	Paired 1-tailed t-test	CD24-/CD24+	0.2105
3F	All passed	Paired 1-tailed t-test	3D/2D	0.0371
3G	All passed	Paired 1-tailed t-test	CD24-/CD24+	0.0797
3H	All passed	Paired 1-tailed t-test	3D/2D	0.0282
3I	All passed	Two-way ANOVA, Sidak	CD24-/CD24+ at 1:1	0.1865
			CD24-/CD24+ at 10:1	0.2411
			CD24-/CD24+ at 20:1	0.0043
3J	All passed	Two-way ANOVA, Sidak	3D/2D at 1:1	0.3949
			3D/2D at 10:1	0.3165
			3D/2D at 20:1	0.0022
3K	All passed	1-tail ratio paired t-test	CD24- stim/CD24- unstim, a-b	0.0482
			CD24+ stim/CD24+ unstim, a-c	0.0107
			CD24- stim/CD24+ stim, b-c	0.0255
3L	All passed	1-tail ratio paired t-test	3D stim/3D unstim, a-b	0.0094
			2D stim/2D unstim, a-c	0.0079
			3D stim/2D stim, b-c	0.0085
4C	All passed		3D/2D	0.0288

Figure	S-W	Test	Sample Comparison	p-value
4D	n=2, too small	No test performed		
4F	All passed	1-tail ratio paired t-test	γδTc + SUM149/SUM149	0.0310
4H	All passed	1-tail ratio paired t-test	γδTc + PDX401/ PDX401	0.0939
4I	All passed	1-tail ratio paired t-test	γδTc + SUM149/SUM149	0.2808
4J	All passed	1-tail ratio paired t-test	γδTc + PDX401/ PDX401	0.0809
4K	All passed	One-way ANOVA, Tukey	CD24- αPD-1 vs. IgG	0.0222
			CD24+ αPD-1 vs. IgG	0.1847
4L	All passed	One-way ANOVA, Tukey	αPD-1 3D vs. IgG	0.3405
			αPD-1 2D vs. IgG	0.3032
5A	All passed	RM 1-way ANOVA, Bonf	NKG2D, FasL vs. IgG	>0.05
			sTRAIL vs. IgG	0.0216
			MICA/B vs. IgG	0.0006
			CD54 vs. IgG	<0.0001
5B	F: NKG2D	RM 1-way ANOVA, Bonf	NKG2D vs. IgG	0.0004
			FasL vs. IgG	<0.0001
			sTRAIL vs. IgG	0.0002
			MICA/B, CD54 vs. IgG	<0.0001
5C	All passed	Paired 1-tailed t-test	CD24-/CD24+	0.0591
5D	All passed	Paired 1-tailed t-test	3D/2D	0.0037
5F	All passed	Paired 1-tailed t-test	γδTc + SUM149/SUM149	0.0950
5G	All passed	Paired 1-tailed t-test	γδTc + PDX401/ PDX401	0.2722
5H	All passed	One-way ANOVA, Sidak	3D dMCL1-2 vs. DMSO	0.0003
			3D A-121 vs. DMSO	0.5805
			3D dMCL1-2 vs. A-121	<0.0001
			2D dMCL1-2 vs. DMSO	0.0073
			2D A-121 vs. DMSO	0.9886
			2D dMCL1-2 vs. A-121	0.0237
5I	All passed	Two-way ANOVA, Tukey	CD24- αPD-1 vs. IgG	0.0086
			CD24- DMSO vs. dMCL1-2	0.7553
			CD24- αPD-1 vs. dMCL1-2	0.0728
			CD24- αPD-1 vs. Combination	0.8545
			CD24- dMCL1-2 vs. Combination	0.0088
			CD24+ αPD-1 vs. IgG	0.0096
			CD24+ DMSO vs. dMCL1-2	0.8346
			CD24+ αPD-1 vs. dMCL1-2	0.0430
			CD24+ αPD-1 vs. Combination	>0.9999
			CD24+ dMCL1-2 vs. Combination	0.0347
5J	All passed	Two-way ANOVA, Tukey	3D αPD-1 vs. IgG	<0.0001
			3D DMSO vs. dMCL1-2	0.4344
			3D αPD-1 vs. dMCL1-2	<0.0001

Figure	S-W	Test	Sample Comparison	p-value
5J			3D αPD-1 vs. Combination	>0.9999
			3D dMCL1-2 vs. Combination	<0.0001
			2D αPD-1 vs. IgG	0.0024
			2D DMSO vs. dMCL1-2	0.9352
			2D αPD-1 vs. dMCL1-2	0.0088
			2D αPD-1 vs. Combination	0.6505
			2D dMCL1-2 vs. Combination	0.0004
6B	All passed	Paired 1-tailed t-test	CD24-/CD24+ MICA/B	0.0428
	All passed	Paired 1-tailed t-test	CD24-/CD24+ ULBP-2,5,6	0.0518
	All passed	Paired 1-tailed t-test	CD24-/CD24+ ULBP-3	0.0467
	All passed	Paired 1-tailed t-test	CD24-/CD24+ ULBP-4	0.0430
6D	All passed	Paired 1-tailed t-test	3D/2D MICA/B	0.0088
	All passed	Paired 1-tailed t-test	3D/2D ULBP-2,5,6	0.2084
	All passed	Paired 1-tailed t-test	3D/2D ULBP-3	0.3923
	All passed	Paired 1-tailed t-test	3D/2D ULBP-4	0.3388
7C	All passed	Paired 1-tailed t-test	CD24-/CD24+	0.0033
7D	All passed	Paired 1-tailed t-test	3D/2D	0.0038
7F	All passed	Paired 1-tailed t-test	ADAMi vs. DMSO	0.0008
7G	All passed	Paired 1-tailed t-test	ADAMi vs. DMSO	0.0011
7H	F: ADAMi	Ratio paired t-test	ADAMi vs. DMSO	0.0332
7I	All passed	Paired 1-tailed t-test	ADAMi vs. DMSO	0.0058
7J	All passed	Two-way ANOVA, Tukey	CD24- ADAMi vs. DMSO	<0.0001
			CD24+ ADAMi vs. DMSO	0.0007
			CD24- ADAMi vs. CD24+ DMSO	0.6781
			CD24- DMSO vs. CD24+ DMSO	<0.0001
7K	All passed	Two-way ANOVA, Tukey	3D ADAMi vs. DMSO	<0.0001
			2D ADAMi vs. DMSO	<0.0001
			3D ADAMi vs. 2D DMSO	0.2139
			3D DMSO vs. 2D DMSO	<0.0001

Appendix Table 1.3. Statistical tests employed and resulting p-values for experiments shown in Supplemental Figures S4.1-S4.8. Biological replicates are listed in order from left to right as indicated by numbers 1-4; Bonf=Bonferroni's multiple comparisons test; E:T=effector:target ratio; F=failed; L=left panel; R=right panel; S-W=Shapiro-Wilk Normality test; Tukey=Tukey's multiple comparisons test.

Figure	S-W	Test	Sample Comparison	p-value
S1K-1	CD24- passed	Simple Linear Regression	CD24-/CD24+	<0.0001
S1K-2	CD24- passed	Simple Linear Regression	CD24-/CD24+	<0.0001
S1M-1	All passed	Two-way ANOVA	CD24-/CD24+ at all E:T	<0.0001
S1M-2	F: CD24+ 20:1	Two-way ANOVA	CD24-/CD24+ at 10:1	0.0349
S1M-3	All passed	Two-way ANOVA	CD24-/CD24+ at 10:1	0.0433
S1N-1	All passed	Two-way ANOVA	3D/2D at all E:T	>0.05
S1N-2	All passed	Two-way ANOVA	3D/2D at 10:1	0.0001
S1N-3	All passed	Two-way ANOVA	3D/2D at 1:1	0.0007
			3D/2D at 10:1	0.0003
			3D/2D at 20:1	<0.0001
S1N-4	All passed	Two-way ANOVA	3D/2D at all E:T	<0.0001
S1O-1	All passed	Simple Linear Regression	γδTc vs. SUM149/SUM149	<0.0001
S1O-2	All passed	Simple Linear Regression	γδTc vs. SUM149/SUM149	0.0197
S1O-3	F:SUM149	Simple Linear Regression	γδTc vs. SUM149/SUM149	0.0025
S1P-1	All passed	Two-way ANOVA	3D/2D at 20:1	<0.0001
S1P-2	All passed	Two-way ANOVA	3D/2D at 10:1	0.0045
			3D/2D at 20:1	0.0011
S1P-3	All passed	Two-way ANOVA	3D/2D at 10:1	0.0026
			3D/2D at 20:1	0.0004
S1P-4	All passed	Two-way ANOVA	3D/2D at 10:1	0.0066
S1Q-1	F:PDX401	Simple Linear Regression	γδTc vs. PDX401/PDX401	<0.0001
S1Q-2	All passed	Simple Linear Regression	γδTc vs. PDX401/PDX401	0.0140
S2H	n=2, too small	One-way ANOVA, Tukey	γδTc + CD24-/γδTc, a-a	0.7916
			γδTc + CD24+/γδTc, a-b	0.0043
			γδTc/CD24- or CD24+, a-c	<0.05
			γδTc + CD24-/CD24- or CD24+, a-c	<0.05
			γδTc + CD24+/CD24- or CD24+, b-c	<0.001
			γδTc + CD24-/ γδTc vs. CD24+, a-b	0.0022
S2I	n=2, too small	One-way ANOVA, Tukey	γδTc + CD24-/γδTc, a-b	0.0011
			γδTc + CD24+/γδTc, a-c	<0.0001
			γδTc/CD24- or CD24+, a-d	<0.0001
			γδTc + CD24-/CD24- or CD24+, b-d	<0.0001
			γδTc + CD24+/CD24- or CD24+, c-d	<0.0001
			γδTc + CD24-/ γδTc + CD24+, b-c	<0.0001
S2J	n=2, too small	One-way ANOVA, Tukey	γδTc + 3D/γδTc, a-b	0.9011
			γδTc + 2D/γδTc, a-c	<0.0001

Figure	S-W	Test	Sample Comparison	p-value
S2J			γδTc/3D a-d	0.0009
			γδTc/2D a-e	0.0005
			γδTc + 3D/3D b-d	0.0014
			γδTc + 3D/2D b-e	0.0007
			γδTc + 2D/3D, c-d	<0.0001
			γδTc + 2D/2D, c-e	<0.0001
			γδTc + 3D/ γδTc + 2D, b-c	<0.0001
S2K	n=2, too small	One-way ANOVA, Tukey	γδTc + 3D/γδTc, a-b	0.5693
			γδTc + 2D/γδTc, a-c	0.0016
			γδTc/3D a-d	<0.0001
			γδTc/2D a-e	0.0007
			γδTc + 3D/3D b-d	<0.0001
			γδTc + 3D/2D b-e	0.0004
			γδTc + 2D/3D, c-d	<0.0001
			γδTc + 2D/2D, c-e	<0.0001
			γδTc + 3D/ γδTc + 2D, b-c	0.0038
S3J	All passed	One-way ANOVA, Sidak	CD24-/CD24+	0.2247
			3D/2D	0.1750
S3L	All passed	Two-way ANOVA, Sidak	CD24-/CD24+ all time points	>0.05
S3M	All passed	Two-way ANOVA, Sidak	3D/2D	>0.05
S3T-1	All passed	Two-way ANOVA, Sidak	CD24-/CD24+ at 20:1	0.0227
S3T-2	All passed	Two-way ANOVA, Sidak	CD24-/CD24+ at 10:1	0.0170
			CD24-/CD24+ at 20:1	<0.0001
S3T-3	All passed	Two-way ANOVA, Sidak	CD24-/CD24+ at 20:1	0.0089
S3U-1	All passed	Two-way ANOVA, Sidak	3D/2D at 20:1	0.0355
S3U-2	All passed	Two-way ANOVA, Sidak	3D/2D at 1:1	0.0100
		Two-way ANOVA, Sidak	3D/2D at 10:1	0.0060
		Two-way ANOVA, Sidak	3D/2D at 20:1	<0.0001
S3U-3	All passed	Two-way ANOVA, Sidak	3D/2D at 1:1	0.0003
			3D/2D at 10:1	0.0063
			3D/2D at 20:1	<0.0001
S4T	All passed	One-way ANOVA, Tukey	CD24- αPD-1 vs. IgG	0.0051
			CD24+ αPD-1 vs. IgG	0.0838
S4U	All passed	One-way ANOVA, Tukey	CD24- αPD-1 vs. IgG	0.0003
			CD24+ αPD-1 vs. IgG	0.1317
S4V	All passed	One-way ANOVA, Tukey	CD24- αPD-1 vs. IgG	0.0172
			CD24+ αPD-1 vs. IgG	0.0045
S4W	All passed	One-way ANOVA, Tukey	3D αPD-1 vs. IgG	0.4082

Figure	S-W	Test	Sample Comparison	p-value
S4W			2D αPD-1 vs. IgG	0.0570
S4X	All passed	One-way ANOVA, Tukey	3D αPD-1 vs. IgG	0.0141
			2D αPD-1 vs. IgG	0.7328
S4Y	All passed	One-way ANOVA, Tukey	3D αPD-1 vs. IgG	0.0267
			2D αPD-1 vs. IgG	0.0033
S5A	All passed	One-way ANOVA, Sidak	NKG2D vs. IgG	0.0472
			FasL, sTRAIL vs. IgG	>0.05
S5B	All passed	One-way ANOVA, Sidak	CD54 vs. IgG	0.0240
			MICA/B vs. IgG	0.0286
S5C	All passed	One-way ANOVA, Sidak	NKG2D vs. IgG	0.0117
			FasL vs. IgG	0.0042
			sTRAIL, MICA/B, CD54 vs. IgG	>0.05
S5D(L)	All passed	One-way ANOVA, Sidak	NKG2D vs. IgG	0.0059
			FasL vs. IgG	>0.05
			sTRAIL vs. IgG	0.0035
			MICA/B vs. IgG	0.0003
			CD54 vs. IgG	<0.0001
S5D(R)	All passed	One-way ANOVA, Sidak	NKG2D, FasL, sTRAIL, CD54 vs. IgG	<0.0001
			MICA/B vs. IgG	0.0001
S5E(L)	All passed	One-way ANOVA, Sidak	NKG2D, FasL, m or sTRAIL vs. IgG	>0.05
			MICA/B vs. IgG	0.0002
			CD54 vs. IgG	0.0007
S5E(R)	All passed	One-way ANOVA, Sidak	NKG2D vs. IgG	0.0072
			FasL vs. IgG	0.0097
			mTRAIL vs. IgG	0.1311
			sTRAIL vs. IgG	0.0002
			MICA/B, CD54 vs. IgG	<0.0001
S5F(L)	All passed	One-way ANOVA, Sidak	NKG2D, FasL, sTRAIL vs. IgG	>0.05
			MICA/B vs. IgG	0.4403
			CD54 vs. IgG	0.0016
S5F(R)	All passed	One-way ANOVA, Sidak	NKG2D, FasL vs. IgG	>0.05
			sTRAIL vs. IgG	0.0273
			MICA/B vs. IgG	0.0005
			CD54 vs. IgG	<0.0001
S5G(L)	All passed	One-way ANOVA, Sidak	NKG2D, FasL, sTRAIL vs. IgG	>0.05
			MICA/B vs. IgG	0.0022
			CD54 vs. IgG	0.0086
			TRAIL R1 vs. IgG	0.0001
			TRAIL R2 vs. IgG	0.0004
S5G(R)	F: TRAIL R2	One-way ANOVA, Sidak	NKG2D vs. IgG	0.0014

Figure	S-W	Test	Sample Comparison	p-value
S5G(R)			FasL, CD54, TRAILR1 vs. IgG	<0.0001
			sTRAIL, MICA/B vs. IgG	0.0002
			TRAIL R2 vs. IgG	0.0058
S5H(L)	All passed	RM 1-way ANOVA, Bonf	Any vs. IgG	>0.9999
S5H(R)	All passed	RM 1-way ANOVA, Bonf	NKG2D vs. IgG	0.0001
			FasL, sTRAIL, MICA/B	<0.0001
			CD54 vs. IgG	0.0008
S5I(L)	F: FasL	One-way ANOVA, Sidak	NKG2D, FasL, m or sTRAIL vs. IgG	>0.05
			MICA/B vs. IgG	>0.05
			CD54 vs. IgG	<0.0001
			TRAIL R1 vs. IgG	0.0002
			TRAIL R2 vs. IgG	0.0320
			Fas vs. IgG	0.1606
S5I(R)	F: MICA/B	One-way ANOVA, Sidak	NKG2D vs. IgG	0.0038
			FasL, sTRAIL, Fas vs. IgG	<0.0001
			mTRAIL vs. IgG	0.0007
			MICA/B vs. IgG	0.0004
			CD54 vs. IgG	0.0100
			TRAIL R1, TRAIL R2 vs. IgG	<0.0001
S5J(L)	All passed	One-way ANOVA, Sidak	NKG2D vs. IgG	0.0092
			FasL, sTRAIL vs. IgG	>0.05
			MICA/B, CD54 vs. IgG	<0.0001
			TRAIL R1, TRAIL R2 vs. IgG	<0.0001
S5J(R)	All passed	One-way ANOVA, Sidak	NKG2D, FasL, sTRAIL vs. IgG	<0.0001
			MICA/B, CD54, TRAILR1/R2 vs. IgG	<0.0001
S5K(L)	All passed	One-way ANOVA, Sidak	NKG2D, FasL, sTRAIL vs. IgG	>0.05
			MICA/B, CD54 vs. IgG	>0.05
			Fas, TRAIL R1, TRAIL R2 vs. IgG	>0.05
S5K(R)	F: MICA/B, Fas	One-way ANOVA, Sidak	NKG2D vs. IgG	0.0255
			FasL vs. IgG	0.0275
			sTRAIL vs. IgG	0.0119
			MICA/B vs. IgG	0.0016
			CD54 vs. IgG	0.0366
			Fas vs. IgG	0.0059
			TRAIL R1 vs. IgG	0.0028
			TRAIL R2 vs. IgG	0.6449
S5R(L)	All passed	One-way ANOVA, Sidak	CD24- dMCL1-2 vs. DMSO	0.0254
			CD24+ dMCL1-2 vs. DMSO	0.7828
S5R(R)	All passed	One-way ANOVA, Sidak	CD24- dMCL1-2 vs. DMSO	0.2639
			CD24+ dMCL1-2 vs. DMSO	0.2875
S5S(L)	F:CD24-DMSO	One-way ANOVA, Sidak	CD24- dMCL1-2 vs. DMSO	0.0239

Figure	S-W	Test	Sample Comparison	p-value
			CD24- A-121 vs. DMSO	0.7440
			CD24- dMCL1-2 vs. A-121	0.0022
			CD24+ dMCL1-2 vs. DMSO	0.2884
			CD24+ A-121 vs. DMSO	0.0824
			CD24+ dMCL1-2 vs. A-121	0.0019
S5S(R)	All passed	One-way ANOVA, Bonf	3D dMCL1-2 vs. DMSO	0.0971
			3D A-121 vs. DMSO	>0.9999
			3D dMCL1-2 vs. A-121	0.0161
			2D dMCL1-2 vs. DMSO	>0.9999
			2D A-121 vs. DMSO	0.0034
			2D dMCL1-2 vs. A-121	0.0060
S5T(L)	All passed	One-way ANOVA, Sidak	CD24- dMCL1-2 vs. DMSO	0.9681
			CD24+ dMCL1-2 vs. DMSO	0.9934
S5T(R)	All passed	One-way ANOVA, Sidak	3D dMCL1-2 vs. DMSO	0.1065
			2D dMCL1-2 vs. DMSO	0.1669
S5U	All passed	One-way ANOVA, Sidak	3D dMCL1-2 vs. DMSO	0.9782
			2D dMCL1-2 vs. DMSO	0.1526
S5V(L)	All passed	Two-way ANOVA, Tukey	CD24- αPD-1 vs. IgG	<0.0001
			CD24- αPD-1 vs. dMCL1-2	<0.0001
			CD24- αPD-1 vs. Combination	>0.9999
			CD24- DMSO vs. dMCL1-2	0.7125
			CD24- DMSO vs. A-121	0.8731
			CD24- dMCL1-2 vs. A-121	0.0845
			CD24- dMCL1-2 vs. Combination	<0.0001
			CD24- dMCL1-2 only vs. A-121 only	>0.9999
			CD24+ αPD-1 vs. IgG	<0.0001
			CD24+ αPD-1 vs. dMCL1-2	<0.0001
			CD24+ αPD-1 vs. Combination	0.3429
			CD24+ DMSO vs. dMCL1-2	0.1558
			CD24+ DMSO vs. A-121	0.4577
			CD24+ dMCL1-2 vs. A-121	0.0009
			CD24+ dMCL1-2 vs. Combination	<0.0001
			CD24+ dMCL1-2 only vs. A-121only	0.5036
S5V(R)	All passed	Two-way ANOVA, Tukey	3D αPD-1 vs. IgG	<0.0001
			3D αPD-1 vs. dMCL1-2	0.0005
			3D αPD-1 vs. Combination	0.9792
			3D DMSO vs. dMCL1-2	>0.9999
			3D DMSO vs. A-121	0.9549
			3D dMCL1-2 vs. A-121	0.8200
			3D dMCL1-2 vs. Combination	0.0065
			3D dMCL1-2 only vs. A-121 only	>0.9999

Figure	S-W	Test	Sample Comparison	p-value
S5V(R)			2D αPD-1 vs. IgG	0.0057
			2D αPD-1 vs. dMCL1-2	0.0293
			2D αPD-1 vs. Combination	0.9962
			2D DMSO vs. dMCL1-2	0.6859
			2D DMSO vs. A-121	0.9891
			2D dMCL1-2 vs. A-121	0.2141
			2D dMCL1-2 vs. Combination	0.0047
			2D dMCL1-2 only vs. A-121 only	0.3152
S5W(L)	All passed	Two-way ANOVA, Tukey	CD24- αPD-1 vs. IgG	<0.0001
			CD24- αPD-1 vs. dMCL1-2	0.0761
			CD24- αPD-1 vs. Combination	0.0248
			CD24- DMSO vs. dMCL1-2	0.1365
			CD24- DMSO vs. A-121	0.6204
			CD24- dMCL1-2 vs. A-121	0.9754
			CD24- dMCL1-2 vs. Combination	<0.0001
			CD24- dMCL1-2 only vs. A-121 only	>0.9999
			CD24+ αPD-1 vs. IgG	0.0007
			CD24+ αPD-1 vs. dMCL1-2	0.0199
			CD24+ αPD-1 vs. Combination	>0.9999
			CD24+ DMSO vs. dMCL1-2	0.6657
			CD24+ DMSO vs. A-121	>0.9999
			CD24+ dMCL1-2 vs. A-121	0.7131
			CD24+ dMCL1-2 vs. Combination	0.0129
			CD24+ dMCL1-2 only vs. A-121only	0.7111
S5W(R)	All passed	Two-way ANOVA, Tukey	3D αPD-1 vs. IgG	<0.0001
			3D αPD-1 vs. dMCL1-2	0.0008
			3D αPD-1 vs. Combination	0.6862
			3D DMSO vs. dMCL1-2	0.3164
			3D DMSO vs. A-121	0.9841
			3D dMCL1-2 vs. A-121	0.8425
			3D dMCL1-2 vs. Combination	<0.0001
			3D dMCL1-2 only vs. A-121 only	0.2801
			2D αPD-1 vs. IgG	0.0022
			2D αPD-1 vs. dMCL1-2	0.0200
			2D αPD-1 vs. Combination	0.0721
			2D DMSO vs. dMCL1-2	0.9989
			2D DMSO vs. A-121	0.4506
			2D dMCL1-2 vs. A-121	0.8059
			2D dMCL1-2 vs. Combination	<0.0001
			2D dMCL1-2 only vs. A-121 only	0.4860
S5X(L)	All passed	Two-way ANOVA, Tukey	CD24- αPD-1 vs. IgG	<0.0001

Figure	S-W	Test	Sample Comparison	p-value
S5X(L)			CD24- αPD-1 vs. dMCL1-2	<0.0001
			CD24- αPD-1 vs. Combination	>0.9999
			CD24- DMSO vs. dMCL1-2	0.7247
			CD24- DMSO vs. A-121	0.7564
			CD24- dMCL1-2 vs. A-121	0.0522
			CD24- dMCL1-2 vs. Combination	<0.0001
			CD24- dMCL1-2 only vs. A-121 only	0.2634
			CD24+ αPD-1 vs. IgG	<0.0001
			CD24+ αPD-1 vs. dMCL1-2	0.0006
			CD24+ αPD-1 vs. Combination	0.6840
			CD24+ DMSO vs. dMCL1-2	0.8042
			CD24+ DMSO vs. A-121	>0.9999
			CD24+ dMCL1-2 vs. A-121	0.9258
			CD24+ dMCL1-2 vs. Combination	0.0521
			CD24+ dMCL1-2 only vs. A-121only	0.9998
S5X(R)	All passed	Two-way ANOVA, Tukey	3D αPD-1 vs. IgG	<0.0001
			3D αPD-1 vs. dMCL1-2	<0.0001
			3D αPD-1 vs. Combination	0.7728
			3D DMSO vs. dMCL1-2	0.0929
			3D DMSO vs. A-121	>0.9999
			3D dMCL1-2 vs. A-121	0.1101
			3D dMCL1-2 vs. Combination	<0.0001
			3D dMCL1-2 only vs. A-121 only	0.9983
			2D αPD-1 vs. IgG	0.0017
			2D αPD-1 vs. dMCL1-2	0.0017
			2D αPD-1 vs. Combination	0.9995
			2D DMSO vs. dMCL1-2	0.7790
			2D DMSO vs. A-121	0.4842
			2D dMCL1-2 vs. A-121	0.0229
			2D dMCL1-2 vs. Combination	0.0067
			2D dMCL1-2 only vs. A-121 only	>0.9999
S7E	All passed	Two-way ANOVA, Bonf	Replicate 1 CD24- vs. CD24+	0.0004
			Replicate 2 CD24- vs. CD24+	0.0019
			Replicate 3 CD24- vs. CD24+	0.0420
			Replicate 4 CD24- vs. CD24+	0.0011
S7F	All passed	Two-way ANOVA, Bonf	Replicate 1 3D vs. 2D	0.0041
			Replicate 2 3D vs. 2D	<0.0001
			Replicate 3 3D vs. 2D	<0.0001
			Replicate 4 3D vs. 2D	<0.0001
S7I	DMSO passed	Two-way ANOVA, Bonf	Replicate 1 ADAMi vs. DMSO	0.0069
			Replicate 2 ADAMi vs. DMSO	0.0007

Figure	S-W	Test	Sample Comparison	p-value
S7I			Replicate 3 ADAMi vs. DMSO	0.0143
S7J	All passed	Two-way ANOVA, Bonf	Replicate 1 ADAMi vs. DMSO	0.0010
			Replicate 2 ADAMi vs. DMSO	0.0007
			Replicate 3 ADAMi vs. DMSO	0.0053
S7K	F: 24+ ADAMi	Two-way ANOVA, Tukey	CD24- ADAMi vs. DMSO	0.0002
			CD24- ADAMi vs. CD24+ DMSO	>0.9999
			CD24+ ADAMi vs. DMSO	0.0054
S7L	All passed	Two-way ANOVA, Tukey	CD24- ADAMi vs. DMSO	0.0010
			CD24- ADAMi vs. CD24+ DMSO	0.6988
			CD24+ ADAMi vs. DMSO	0.0009
S7M	All passed	Two-way ANOVA, Tukey	CD24- ADAMi vs. DMSO	<0.0001
			CD24- ADAMi vs. CD24+ DMSO	0.9998
			CD24+ ADAMi vs. DMSO	0.0208
S7N	F:2D Control	Two-way ANOVA, Tukey	3D ADAMi vs. DMSO	<0.0001
			3D ADAMi vs. 2D DMSO	0.7278
			2D ADAMi vs. DMSO	0.0025
S7O	All passed	Two-way ANOVA, Tukey	3D ADAMi vs. DMSO	0.0024
			3D ADAMi vs. 2D DMSO	0.8584
			2D ADAMi vs. DMSO	0.0501
S7P	All passed	Two-way ANOVA, Tukey	3D ADAMi vs. DMSO	0.0035
			3D ADAMi vs. 2D DMSO	>0.9999
			2D ADAMi vs. DMSO	0.0226
S8B	All passed	Two-way ANOVA, Sidak	3D/2D at 1:1	0.3845
			3D/2D at 10:1	0.0532
			3D/2D at 20:1	0.0239
S8C	F: MCF-7	Simple Linear Regression	γδTc vs. MCF-7/MCF-7	0.0016
S8G	F: 3D	Wilcoxon	3D vs. 2D	0.2500
S8H	All passed	2-tail ratio paired t-test	γδTc + 3D/ γδTc + 2D	0.0262
S8I(L)	All passed	2-tailed paired t-test	3D vs. 2D	0.0216
S8I(R)	All passed	2-tailed paired t-test	3D vs. 2D	0.0020
S8J	All passed	Two-way ANOVA, Sidak	3D vs. 2D, all time points	>0.05
S8K	n=2, too small	No test performed		
S8L	F: 2D	Wilcoxon	3D vs. 2D	0.2500
S8M	All passed	1-tailed paired t-test	3D vs. 2D	0.0282
S8N	All passed	1-tail ratio paired t-test	3D stim vs. 2D stim, b-c	0.0452
S8Q	F:2D CD54	One-way ANOVA, Sidak	3D NKG2D, FasL vs. IgG	>0.05
			3D sTRAIL vs. IgG	0.0115
			3D CD54 vs. IgG	0.0033
			3D MICA/B vs. IgG	0.0021

Figure	S-W	Test	Sample Comparison	p-value
S8Q			2D NKG2D vs. IgG	0.0003
			2D FasL vs. IgG	0.0005
			2D sTRAIL vs. IgG	<0.0001
			2D CD54 vs. IgG	0.0002
			2D MICA/B vs. IgG	0.0003
S8R	All passed	1-tailed paired t-test	3D vs. 2D	0.1614

Appendix Table 1.4. Flow cytometry, western blot and blocking assays antibodies used in chapter 4.

Flow Cytometry Antibody	Dilution or Concentration	Clone	Company
CD107a AlexaFluor (AF) 647	1:40	H4A3	BioLegend
CD24 APC	1:50	REA832	Miltenyi
CD44 PerCP Cy5.5	1:50	BJ18	BioLegend
CD44 Vioblue	1:20	REA690	Miltenyi
CTLA-4(CD152) APC	1:10	L3D10	BioLegend
Fas (CD95) APC	1:100	DX2	BioLegend
IFN-γ VioBlue	1:50	REA600	Miltenyi
LAG-3 FITC	1:20	11C3C65	BioLegend
MCL-1 AF488	1:20	22	Santa Cruz
MICA/B PE	0.1µg	6D4,	BioLegend
PD-1(CD279) BV421	1:10	EH12.2H7	BioLegend
PD-L1 APC	1:10	29E.2A3	BioLegend
PD-L2 PE	1:10	24F.10C12	BioLegend
TCR Vδ1 FITC	1:10	REA173	Miltenyi
TCR Vδ2 PerCP	1:25	B6	BioLegend
TCRγδ PE	1:25	B1	BioLegend
TIM-3 APC/Fire750	1:20	F38-2E2	BioLegend
TRAIL R1 APC	1:20	DJR1	BioLegend
TRAIL R2 APC	1:5	DJR2-4	BioLegend
ULBP-2,5,6 PE	0.2µg	165903	R&D systems
ULBP-3 APC	0.04µg	166510	R&D systems
ULBP-4 APC	0.1µg	709116	R&D systems
Western Blot Antibodies	**Dilution or Concentration**	**Clone**	**Company**
rabbit anti-human ADAM10	1:500	ab1997	Abcam
rabbit anti-human ADAM17	1:1000	ab39162	Abcam
mouse anti-human BCL-2	1:1000	C2	Santa Cruz
mouse anti-human BCL-XL	1:1000	H5	Santa Cruz
mouse anti-human MCL-1	1:1000	22	Santa Cruz
rabbit anti-human Survivin	1:1000	71G4B7E	Cell Signaling
mouse anti-human XIAP	1:500	48/hILP/XIAP(RUO)	BD Biosciences
mouse anti-human β-Actin	1:3000	C4	Santa Cruz
rabbit anti-human β-Actin	1:2000	13E5	Cell Signaling

Blocking Antibodies	Concentration	Clone	Company
CD54	1µg/100ul	HCD54	BioLegend
Fas	1µg/100ul	A16086F	BioLegend
FasL	1µg/100ul	NOK-1	BioLegend
IgG1k	1µg/100ul	MOPC-21	BioLegend
MICA/B	1µg/100ul	6D4	BioLegend
NKG2D	1µg/100ul	1D11	BioLegend
PD-1	1µg/100ul	A17188B	BioLegend
TRAIL	1µg/100ul	RIK-2	BioLegend
TRAIL R1	1µg/100ul	DJR1	BioLegend
TRAIL R2	1µg/100ul	DJR2-4	BioLegend